TECHNISCHE UNIVERSITÄT WIEN
Vienna University of Technology

Dissertation

Comparative Studies of Conventional and Cross-linked Implants and Explants

ausgeführt zum Zwecke der Erlangung des akademischen Grades einer Doktorin
der technischen Wissenschaften
unter der Leitung von

Ao.Univ.Prof. Dipl.Ing. Dr.mont. Vasiliki-Maria Archodoulaki
Institut für Werkstoffwissenschaft und Werkstofftechnologie - E 308
Arbeitsgruppe Nichtmetallische Werkstoffe

Eingereicht an der Technischen Universität Wien
Fakultät für Maschinenwesen und Betriebswissenschaften
Von

MSc. Aysenur Örs-Ünsal
1329733
Seyringer Strasse 1/1/38, 1210 Wien, Österreich

Wien, June, 2020
Reviewed by

……. …….

Die approbierte gedruckte Originalversion dieser Dissertation ist an der TU Wien Bibliothek verfügbar.
The approved original version of this doctoral thesis is available in print at TU Wien Bibliothek.
TU WIEN Bibliothek Your knowledge hub

Acknowledgements

I thank particularly my supervisor, Prof. Vasiliki-Maria Archodoulaki, who guided and supported me in every step from the beginning till the end.

I would like to thank cordially all colleagues in the Structural Polymer Group who encouraged and supported me through the course of completing my dissertation study. I believe that we have a shared a great learning experience at the Vienna Technical University. I particularly would like to mention Dr. Bernadette Duscher, Dr. Thomas Koch for their help especially explaining evaluation of my data. To my colleague; Dr. Marcela Petrica, Dr. Florian Kamleitner and DI. Erdal Karaagac.

I would also like to thank the team of technical staff, especially Stefan Zellhofer, Gerhard Kern, Roman Stoiber and Edith Asiemo who helped me a lot and provided me suitable equipment whatever and whenever I needed.

My final acknowledgment is, of course, for my beloved family who gave me endless support, motivation and encouragement to complete my studies.

Die approbierte gedruckte Originalversion dieser Dissertation ist an der TU Wien Bibliothek verfügbar.
The approved original version of this doctoral thesis is available in print at TU Wien Bibliothek.
TU Bibliothek Your knowledge hub WIEN

Die approbierte gedruckte Originalversion dieser Dissertation ist an der TU Wien Bibliothek verfügbar.
The approved original version of this doctoral thesis is available in print at TU Wien Bibliothek.
TU Bibliothek Your knowledge hub WIEN

Abstract

Total Hip Replacement (THR) is a surgical technique to treat patients suffering from severe musculoskeletal disorders or injury of the hip. In this technique, the bearing surfaces of the femur (thigh bone) and hip are replaced by prostheses that renew functioning of the hip.

Ultra High Molecular Weight Polyethylene (UHMWPE) has been extensively used since 1960's to manufacture hip replacement components such as acetabular liners. Wear and oxidative degradation are major reasons of failure of UHMWPE components or may hinder the in-vivo performance of the components. Therefore, it is important to investigate the surface and subsurface chemical, physical and mechanical properties of retrieved UHMWPE acetabular liners. In this study, we aimed to reveal different aspects of the effects of combined chemical, physical and mechanical properties on in-vivo time.

A total number of 20 explants, 2 conventional and 18 cross-linked have been tested for their chemical, morphological and micromechanical properties. Two commercial engineering polymer blocks GUR 1050, GUR 1020 and GUR 1020 doped with Vitamin E (Vit. E) were also investigated. For comparison reasons, results from former studies carried out at TU-Wien were included and discussed. Additionally, the accelerated aging was examined to better understand the in-vivo structural, physical, mechanical and tribological properties.

Stereomicroscope, Fourier Transform Infrared Spectroscopy (FTIR), Differential Scanning Calorimetry (DSC), Depth Sensing Indentation (DSI), Small Punch Test (SPT), and Ball-on-Plate (BOP) equipment and techniques for tests and measurements were used.

OI increases with increasing in-vivo time and the value of OI is higher in conventional explants than all different types of cross-linked explants. In the conventional explants (in-vivo time > 15 years), the higher the oxidation index (OI > 2) correlates with increasing the degree of crystallinity. Increasing the chain scission via oxidation leads to increasing degree of crystallinity and results in increasing E- modulus in conventional explants.

The first generation cross-linked remelted explants show the lowest degree of crystallinity, but they are better stabilized against oxidative degradation. The second-generation cross-linked explants show higher degree of crystallinity than the first-generation remelted and annealed explants.

FTIR and DSI results show that, with aging, the OI and E-Modulus substantially increases for GUR 1050 and GUR 1020 type bulk materials and higher OI makes material susceptible to severe wear. The more oxidized conventional explants have less toughness than their bulk material. As Vit E. hinders oxidation, GUR 1020 Vit. E samples' wear rate does not change dramatically. Furthermore, cross-linked implants are far more wear resistant than bulk material but less tough. For all materials abrasive wear is the dominant wear mechanism.

The relatively higher work to failure i.e. toughness values of DePuy (cross-linked, remelted) and second generation (cross-linked, sequentially annealed or using high pressure to form) explants is a result of the irradiation dose and thermal treatment after cross-linking. Moreover, DePuy explants have higher toughness values than other second-generation explants which is believed to be a result of moderate irradiation dose exposure of the explant during cross-linking. Cross-linked and remelted explants showed lower ultimate tensile strength and toughness.

In this work an attempt was taken to correlate stiffness values obtained from DSI and SPT methods. E-modulus values obtained from SPT method are lower than the ones from DSI method.

Kurzfassung

Totalhüftprothesen (engl. Total Hip Replacement (THR)) ist eine Operationstechnik zur Behandlung von Patienten mit Muskel-Skelett-Erkrankungen oder einer Hüftverletzung. Bei dieser Technik werden die Auflageflächen des Femurs (Oberschenkelknochen) und der Hüfte durch Prothesen ersetzt.

Polyethylen mit ultrahohem Molekulargewicht (UHMWPE) wird seit den 1960er Jahren in großem Umfang zur Herstellung von Hüftersatzkomponenten wie Hüftgelenkpfannen verwendet. Verschleiß und oxidativer Abbau sind die Hauptgründe für die Schaden von UHMWPE-Komponenten. Daher ist es wichtig, die chemischen, physikalischen und mechanischen Eigenschaften von UHMWPE aus Hüftgelenkpfannenauskleidungen. Das Ziel dieser Studie ist es, verschiedene Aspekte der Auswirkungen kombinierter chemischer, physikalischer und mechanischer Eigenschaften auf die In-vivo-Zeit aufzuzeigen.

Insgesamt 20 Explantate, 2 konventionelle und 18 vernetzte, wurden auf ihre chemischen, morphologischen und mikromechanischen Eigenschaften getestet. Zwei kommerzielle technische Polymerblöcke GUR 1050, GUR 1020 und GUR 1020, die mit Vitamin E (Vit. E) dotiert waren, wurden ebenfalls untersucht. Zu Vergleichszwecken wurden Ergebnisse früherer Studien an der TU-Wien aufgenommen und diskutiert. Zusätzlich wurde die beschleunigte Alterung untersucht, um die in- vivo strukturellen, physikalischen, mechanischen und tribologischen Eigenschaften besser zu verstehen.

Stereomikroskop, Fourier-Transform-Infrarotspektroskopie (FTIR), Differential Scanning Calorimetry (DSC), Depth Sensing Indentation (DSI), Small Punch Test (SPT) und Ball-on-Plate (BOP) Geräte und Techniken wurden für die Tests und Messungen verwendet.

Bei herkömmlichen Explantaten steigt der OI mit zunehmender In-vivo-Zeit und der OI-Wert ist höher als bei vernetzten Explantaten. Bei den herkömmlichen Explantaten (In-vivo-Zeit> 15 Jahre) wird gezeigt, dass der Kristallinitätsgrad umso höher ist, je höher der Oxidationsindex (OI> 2) ist. Das Erhöhen der Kettenspaltung durch Oxidation führt zu einem zunehmenden Kristallinitätsgrad und daraus folgt bei herkömmlichen Explantaten zu einem zunehmenden E-Modul.

Die vernetzten umgeschmolzenen Explantate der ersten Generation weisen den niedrigsten Kristallinitätsgrad auf, sind jedoch besser gegen oxidativen Abbau stabilisiert. Die vernetzten Explantate der zweiten Generation zeigen einen höheren Kristallinitätsgrad als die umgeschmolzenen und getemperten Explantate der ersten Generation.

FTIR- und DSI-Ergebnisse zeigen, dass mit zunehmendem In-vivo-Zeit der OI- und E-Modul für das Grundmaterial vom Typ GUR 1050 und GUR 1020 erheblich ansteigt und ein höherer OI das Material anfällig für starken Verschleiß macht. Die stärker oxidierten konventionellen Explantate haben eine geringere Zähigkeit als ihr Schüttgut. Da Vitamin E die Oxidation behindert, ändert sich die Verschleißrate der GUR 1020 Vitamin E-Proben nicht dramatisch. Darüber hinaus sind vernetzte Implantate weitaus verschleißfester als Schüttgut, jedoch weniger zäh. Bei allen Materialiendominiert der abrasiver Verschleiß.

Die relativ hohe Zätigkeit bis zum Bruch, d.h. die Zähigkeitswerte von DePuy-Explantaten (vernetzt, umgeschmolzen) und Explantaten der zweiten Generation (vernetzt, nacheinander getempert oder unter Verwendung von Hochdruck), sind ein Ergebnis der Bestrahlungsdosis und der Wärmebehandlung nach der Vernetzung. Darüber hinaus weisen DePuy-Explantate höhere Zähigkeitswerte als andere Explantate der zweiten Generation auf, was vermutlich auf eine mäßige

Die approbierte gedruckte Originalversion dieser Dissertation ist an der TU Wien Bibliothek verfügbar.
The approved original version of this doctoral thesis is available in print at TU Wien Bibliothek.
TU Bibliothek Your knowledge hub WIEN

Bestrahlungsdosis des Explantats während der Vernetzung zurückzuführen ist. Vernetzte und umgeschmolzene Explantate zeigten eine geringere Zugfestigkeit und Zähigkeit.

In dieser Arbeit wurde versucht, Steifigkeitswerte zu korrelieren, die mit der DSI- und SPT-Methoden erzielten wurden. Die mit der SPT-Methode erhaltenen E-Modul-Werte sind niedriger als die mit der DSI-Methode erhaltenen E-Modul-Werte.

Die approbierte gedruckte Originalversion dieser Dissertation ist an der TU Wien Bibliothek verfügbar.
The approved original version of this doctoral thesis is available in print at TU Wien Bibliothek.
TU Bibliothek Your knowledge hub WIEN

Table of Contents

Acknowledgements ..... *i*

Abstract ..... *ii*

Kurzfassung ..... *iii*

List of Tables ..... *v*

List of Figures ..... *vi*

Abbreviations ..... *ix*

Chapter 1: Introduction *1*

Chapter 2: Human Hip Joint *3*

2.2 Hip Joint Diseases 4

2.3 Failure of Hip Joint Replacement 5

2.3.1 Aseptic loosening 5

2.3.2 Bone cement damage 6

2.3.3 Other complications 7

2.4 Hip Joint Replacement 7

2.5 THR Procedure 8

2.6 History of Total Hip Replacement 10

2.7 Gender 12

Chapter 3: UHMWPE *15*

3.1 History 15

3.2 Structure 15

3.3 UHMWPE Consolidation 17

3.4 Fabrication of UHMWPE Implants 19

3.5 Sterilization 19

3.6 Oxidation 21

3.7 Crosslinked UHMWPE 22

3.8 Additive Stabilized UHMWPE 28

3.9 Mechanical Properties of UHMWPE 29

Stress-Strain Behavior 29

Plastic Deformation 31

Chapter 4: Tribology and Its Influence on Hip Replacement *34*

4.1 Tribology Behavior of UHMWPE 34

4.1.1 Abrasive Wear 35

4.1.2 Adhesive Wear 36

4.1.3 Fatigue Wear 37

4.2 Hip Joint Motion 38

Die approbierte gedruckte Originalversion dieser Dissertation ist an der TU Wien Bibliothek verfügbar.
The approved original version of this doctoral thesis is available in print at TU Wien Bibliothek.
TU Bibliothek Your knowledge hub WIEN

4.3 Contact Mechanics 39
Chapter 5: Samples & Experimental Techniques *41*
5.1 Optical Damage Scoring 45
5.2 Structural and Physical Properties 46
5.2.1 Fourier Transform Infrared Spectroscopy 47
5.2.2 Differential Scanning Calorimetry 49
5.2.3 Swelling of Crosslinked Networks 51
5.3 Mechanical Properties 53
5.3.1 Depth Sensing Indentation of Polymers 53
5.3.2 Small Punch Testing 55
5.4 Testing of Tribological Properties 58
5.4.1 Ball on Plate Test 59
5.5 Accelerated Aging 62
Chapter 6: Results and Assessment *63*
6.1 Optical Damage Scoring 63
6.2 Gender Influence on Age, BMI and UCLA Activity 69
6.3 FTIR Results 72
6.4 DSC Results 83
6.5 Depth Sensing Indentation Results 89
6.6 Small-punch Results 91
6.7 Tribological results 96
6.7.1 Wear results 97
Chapter 7: General Discussion *103*
Chapter 8: References *114*
APPENDIX *130*

Die approbierte gedruckte Originalversion dieser Dissertation ist an der TU Wien Bibliothek verfügbar.
The approved original version of this doctoral thesis is available in print at TU Wien Bibliothek.
TU WIEN Bibliothek Your knowledge hub

List of Tables

Table 3. 1 A summary of properties of UHMWPE along with other polymeric materials.....19

Table 5. 1 Investigated conventional and cross-linked explants.....42
Table 5. 2 Absolute values by complications.....43
Table 5. 3 Scoring system for assessing damage mechanisms on explant bearing surfaces and rims.....46
Table 5. 4: Chemical composition of SS440 steel ball as given in technical data sheet.....60
Table 5. 5 Tribological testing conditions used 60

Table 7. 1 E-modulus values were obtained from DSI and SPT.....108

Die approbierte gedruckte Originalversion dieser Dissertation ist an der TU Wien Bibliothek verfügbar.
The approved original version of this doctoral thesis is available in print at TU Wien Bibliothek.
TU Bibliothek Your knowledge hub WIEN

List of Figures

Figure 2. 1 The hip joint. (a) dissected joint, (b) hip joint with synovial capsule [18] 3
Figure 2. 2 THR surgery process [58] 9
Figure 2. 3 Pink dental cement 11
Figure 2. 4 OECD report of knee and hip replacement in 2015 13
Figure 3. 1 A schematic of (A) Ethylene and (B) UHMWPE Chemical Structures [74] 16
Figure 3. 2 A Schematic of the Morphology of UHMWPE [74] 17
Figure 3. 3 Ongoing gamma radiation of UHMWPE 20
Figure 3. 4 Molecular structure of conventional UHMWPE and cross-linked UHMWPE [92] 22
Figure 3. 5 Schematic to outline the trade-offs in wear resistance, fatigue crack propagation resistance and oxidation resistance 27
Figure 3. 6 α-tocopherol free radical 28
Figure 3. 7 Stress vs. strain curve for PE [121] 30
Figure 3. 8 Schematic diagrams of the deformation in semi-crystalline polymers in different stress directions [132] 33
Figure 4. 1 Schematic of wear types that is important for hip implants 35
Figure 4. 2 Four types of abrasive wear; (a) low stress abrasion, (b) high-stress abrasion, (c) gouging abrasion, and (d) polishing abrasion [140] 36
Figure 4. 3 Anatomic movements for the hip joints 38
Figure 4. 4 Effected loads and movements on the ball in socket geometry 39
Figure 5. 1 a) hip explant; b) explant cut into three pieces; c) cross-sectional view of explant; d) sample preparation of rim and center parts for tests 46
Figure 5. 2 A schematic plot of load vs. depth curves of nanoindentation experiment [183] 53
Figure 5. 3 View of grid of indents 55
Figure 5. 4 Load-displacement curve for GUR 1020 UHMWPE [198] 56
Figure 5. 5 Picture of SPT 57
Figure 5. 6 An upper die of SPT 57
Figure 5. 7 Zwick Roell Z050 testing maschine 58
Figure 5. 8 Ball on Plate Tribometer with schematic configuration 60
Figure 6. 1 a) AUMA displaying crack on the rim, b) Delamination on BUC sample 63
Figure 6. 2 a) Scratch on the AUMA sample, b) Grooves on VOST sample 64
Figure 6. 3 Color change on LUIN sample 65
Figure 6. 4 a) Machining marks on STEL, b) Pitting on GOKA sample 65
Figure 6. 5 Burnishing on WIRU sample 66
Figure 6. 6 AUMA displaying a) worn surface at articulating part and b) bone ingrowth 67
Figure 6. 7 Damage score as a function of in-vivo time (r =0.74) 69
Figure 6. 8 a) BMI versus patient age, b) BMI as a function of gender 70

Die approbierte gedruckte Originalversion dieser Dissertation ist an der TU Wien Bibliothek verfügbar.
The approved original version of this doctoral thesis is available in print at TU Wien Bibliothek.
TU Bibliothek Your knowledge hub WIEN

Figure 6. 9 Scatterplot of UCLA activity and patient age 71
Figure 6. 10 AUMA OI profile as a function of distance 73
Figure 6. 11 AUMA KOR and REOP rim OI profile as a function of distance 74
Figure 6. 12 AUMA, KOR and REOP degree of crystallinity profile as a function of distance ... 75
Figure 6. 13 Sandwich types of explant OI profile as a function of distance 75
Figure 6. 14 Sandwich type explants degree of crystallinity profile as a function of distance 76
Figure 6. 15 Durasul® OI profile as a function of distance 77
Figure 6. 16 Durasul® degree of crystallinity profile as a function of distance 77
Figure 6. 17 X3™ OI profile as a function of distance 78
Figure 6. 18 X3™ degree of crystallinity profile as a function of distance 79
Figure 6. 19 DePuy OI profile as a function of distance 80
Figure 6. 20 DePuy degree of crystallinity profile as a function of distance 80
Figure 6. 21 AUMA degree of crystallinity profile as a function of distance 84
Figure 6. 22 AUMA degree of crystallinity and thermal data profile as a function of distance 84
Figure 6. 23 PLWI degree of crystallinity and thermal data profile as a function of distance. 85
Figure 6. 24 MAWO degree of crystallinity profile as a function of distance 85
Figure 6. 25 MAWO degree of crystallinity and thermal data profile as a function of distance. .. 86
Figure 6. 26 Lamellar thickness distribution (LTD) of explants rim IO as a function of depth 87
Figure 6. 27 a) Hardness profile as a function of depth b) Indentation modulus profile as a function of depth 89
Figure 6. 28 a) H_{IT} profiles as a function of depth for all cross-linked explants b) E_{IT} profiles as a function of depth for all cross-linked explants 90
Figure 6. 29 The load-displacement curve of GUR 1020 and GUR 1050 92
Figure 6. 30 The load displacement curve of A) GUR 1020 and X3™ and B) GUR 1020 and cross-linked explant 93
Figure 6. 31 The load displacement curve of A) conventional and B) cross-linked explants 94
Figure 6. 32 The load displacement curve of A) GUR 1050 and Dsa 3weeks aged implant and B) Different aging time of Dsa implants 95
Figure 6. 33 Comparison of the specific volumetric wear rates of three UHMWPE types. Working load: 30 N 97
Figure 6. 34 Comparison of the specific volumetric wear rates of two UHMWPE types. Working load: 2N 98
Figure 6. 35 Comparison of the specific volumetric wear rates of cross-linked implants. Working load: 30 N 98

Die approbierte gedruckte Originalversion dieser Dissertation ist an der TU Wien Bibliothek verfügbar.
The approved original version of this doctoral thesis is available in print at TU Wien Bibliothek.
TU Bibliothek Your knowledge hub WIEN

Figure 6. 36 Wear tracks for GUR 1050; GUR 1020 and GUR 1020 Vit. E. Working load: 30 N 100
Figure 6. 37 Wear tracks for GUR 1050; GUR 1020. Working load: 2N 100
Figure 7. 1 Oxidation index versus in-vivo time. 104
Figure 7. 2 Degree of crystallinity as a function of OI 105
Figure 7. 3 E-modulus and micro hardness as a function of degree of crystallinity 106
Figure 7. 4 E-modulus as a function of OI. 106
Figure 7. 5 Comparison of the wear rates of three UHMWPE types under 30N 107
Figure 7. 6 Total damage score versus work to failure of the explants (r =-0.61) 109
Figure 7. 7 Work to failure of conventional and cross-linked explants and implants 110
Figure 7. 8 Work to failure versus wear rate of a bulk material and conventional implants 111

Die approbierte gedruckte Originalversion dieser Dissertation ist an der TU Wien Bibliothek verfügbar.
The approved original version of this doctoral thesis is available in print at TU Wien Bibliothek.
TU Bibliothek Your knowledge hub WIEN

Abbreviations

AO: Outer surface

ASTM: American Society for Testing and Materials

BOP: Ball on plate

BMI: Body mass index

CoC: Ceramic on ceramic

CoP: Ceramic on polymer

DSC: Differential scanning calorimetry

DSI: Depth sensing indentation

E_{eff}: Effective elastic modulus

E_{IT}: Indentation elastic modulus

EtO: Ethylene oxide

FTIR: Fourier transform infrared spectroscopy

H_{IT}: Indentation hardness

ICI: Imperial chemical industries

IO: Inner surface

LFA: Low friction arthroplasty

MoM: Metal on metal

MoP: Metal on polymer

OI: Oxidation index

PAA: Progressive accelerated aging

PMMA: Poly-methyl methacrylate

PTFE: Polytetrafluoroethylene

SPT: Small punch test

TermVI: Terminal-vinyl-group

THR: Total hip replacement

TVI: Trans vinylene index

UHMWPE: Ultra High Molecular Weight Polyethylene

Die approbierte gedruckte Originalversion dieser Dissertation ist an der TU Wien Bibliothek verfügbar.
The approved original version of this doctoral thesis is available in print at TU Wien Bibliothek.
TU Bibliothek Your knowledge hub WIEN

Chapter 1: Introduction

Ultra High Molecular Weight Polyethylene (UHMWPE) has been used as a bearing surface in joint arthroplasty against a metallic or ceramic part over the past 40 years. It has been demonstrated that the major factor responsible for failures in arthroplasty is due to decrease in mechanical properties caused by oxidative degradation [1-3]. UHMWPE is a chemically inert and stable material. However, fabrication and post fabrication sterilization processes cause free radicals. These free radicals react with oxygen leading to oxidative degradation and induce decrease in UHMWPE molecular mass[4]. To prevent oxidation degradation of UHMWPE, Vitamin E is mostly used as a stabilizer agent [5-7]. It is an effective biological antioxidant and incorporation of Vitamin E favorably influences the mechanical properties after accelerated aging [8].

Wear debris plays important role of starting osteolysis, hence researchers focused on decreasing wear rate and improving implants life span [9-14] in particular for young active patients.

The primary objective of this research was to assess the structural, physical, mechanical and tribological performance of conventional and cross-linked explants and commercial engineering polymer blocks in order to investigate the material's response to in-vivo service. The results of the accelerated aging were examined to better understand the in-vivo structural, physical, mechanical and tribological properties. Additional objectives of this study included assessing the gender factors and the variation of the structural or mechanical properties with in-vivo time.

The below tests were conducted to reach the above objectives:

- Examination of the articulating inner and outer surfaces of explants to investigate surface features generated in-vivo by using stereomicroscope.
- Measurement of the oxidation index and degree of crystallinity as a function of distance from the bearing surface using Fourier Transform Infrared Spectroscopy (FTIR).
- Measurement of the melting point, crystallization temperature, onset crystallization temperature and degree of crystallinity of UHMWPE by using Differential Scanning Calorimetry (DSC).
- Investigation of the distribution of micro-hardness and indentation modulus through thickness of samples by using Depth Sensing Indentation (DSI).
- Investigation and assessment of relationships between DSI and small punch test (SPT) data.

Die approbierte gedruckte Originalversion dieser Dissertation ist an der TU Wien Bibliothek verfügbar.
The approved original version of this doctoral thesis is available in print at TU Wien Bibliothek.
TU Bibliothek Your knowledge hub WIEN

- Assessment of wear response and wear mechanisms using different loads and 2-body tribological test by using a tribometer.

Chapter 2 discusses the details of a total hip replacement and the use of UHMWPE as a bearing surface in joint arthroplasty. Chapter 3 presents general information about UHMWPE. Chapter 4 discusses the theoretical background of tribology. Chapter 5 details the samples and experimental techniques used in this study. Chapter 6 discusses the results and the assessments of each individual test. Finally, Chapter 7 presents the discussion and conclusion of all results.

Die approbierte gedruckte Originalversion dieser Dissertation ist an der TU Wien Bibliothek verfügbar.
The approved original version of this doctoral thesis is available in print at TU Wien Bibliothek.
TU Bibliothek Your knowledge hub WIEN

Chapter 2: Human Hip Joint

2.1 Hip Joint

In the human body, a joint is the location where two or more bones make contact. The most common type of joint in the human body is the synovial joint [15]. In a synovial joint, the end part of the articulating surface is covered with the articular cartilage. The articulating bones are separated by a space called the joint cavity but held together by the synovial membrane, which forms a synovial capsule and secretes synovial fluid into the joint cavity for lubrication and also provides a source of nutrition [16].

The hip joint is a typical ball and socket type of synovial joint that connects the lower extremities of the body to the pelvis and axial skeleton and it allows various movements and provide mechanical support. The hip joint is formed by the head of the femur (thigh bone) and the acetabulum of the pelvis (Figure 2.1 a), and it conforms to a wide range of movements, as well as bears high dynamic loads (7-8 times the body weight) [17]. The hip joint is covered in a capsule that contains the synovial fluid (Figure 2.1 b). The stability of the hip joint is mainly ensured by the strong ligaments, the joint capsule that surrounds the hip joint and the muscles that surround the hip.

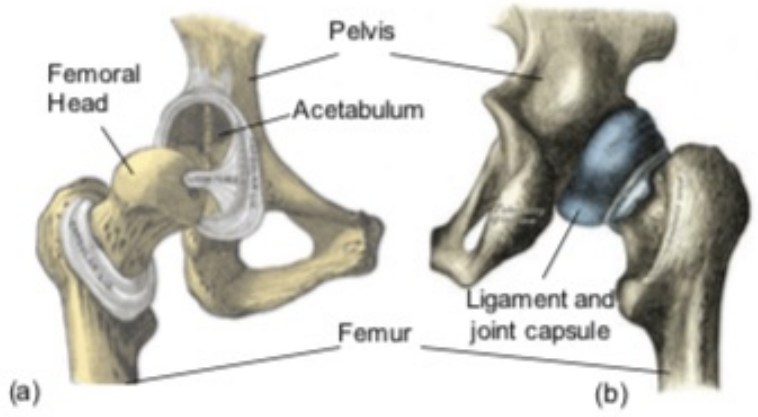

Figure 2. 1 The hip joint. (a) dissected joint, (b) hip joint with synovial capsule [18]

Die approbierte gedruckte Originalversion dieser Dissertation ist an der TU Wien Bibliothek verfügbar.
The approved original version of this doctoral thesis is available in print at TU Wien Bibliothek.

2.2 Hip Joint Diseases

The hip joint is one of the strongest and most long-lasting joints. There are many reasons for disruption of hip mobility. Many of them like occurs from disease or trauma, leading to pain, inflammation and even loss of function [19]. Arthritis is a painful, degenerative joint disease that can affect any joint in the body, with the hip joint being the most affected. Many factors can play a part of the cause of osteoarthritis. It occurs when the balance between the breakdown and repair of the joint tissues becomes unstable. It is a slow, progressive, ultimately degenerative disorder. Osteoarthritis can range from mild to severe conditions and mostly affects older people. Apart from age-related reasons, it is also believed to be induced by high levels of stress in the joint causing structural and biomechanical changes [20]. The end state of osteoarthritis is the state under which the cartilage is completely worn out, the femoral and acetabular subchondral bones are exposed and are directly in contact with each other.

Rheumatoid arthritis is a systemic inflammatory disease that affects the lining of all joints in the body. It causes an inflammatory response in the joint lining which destroys the articular cartilage and surrounding tissues [19]. This disease is more common in women. Rheumatoid arthritis has a mirror image, meaning that it will usually involve the same joints on both sides of the body. In contrast to osteoarthritis, rheumatoid arthritis may also affect the heart, lungs and eyes of some patients and can cause an overall feeling of sickness and fatigue as well as weight loss and fever. Rheumatoid Arthritis is created by the body's own immune system attacking the synovial lining of the hip joint causing it to become inflamed. Inflammation of the synovium leads to chemicals to be released that thickens the synovium and damages the cartilage and bone of the affected joint. In the process of time, the femoral head is gradually worn off and can break down suddenly resulting in true shortening of the leg. Symptoms of rheumatoid arthritis are joint pain, swelling and the skin over the joint may appear swollen and red, and feel hot when touched [21, 22].

Avascular necrosis happens when blood supplying to the head of the femur is interrupted. Due to the lack of nutrition and oxygen, the joint will destroy gradually. The end result of this disease is the collapse and complete deterioration of the femoral head, commonly referred to as the “ball” of the hip joint [19].

Die approbierte gedruckte Originalversion dieser Dissertation ist an der TU Wien Bibliothek verfügbar.
The approved original version of this doctoral thesis is available in print at TU Wien Bibliothek.
TU Bibliothek Your knowledge hub WIEN

2.3 Failure of Hip Joint Replacement

Hip implant failure occurs and can be caused by several reasons. This section tries to outline the causes of failure of hip implants.

2.3.1 Aseptic loosening

Aseptic loosening is the most common cause of failure and revision of hip implants. It is defined that the loosening of arthroplasty in the absence of infection and can be the result of poor initial fixation and mechanical or biological loss of fixation [23]. Among these, the biological loss of fixation caused by the resorption of periprosthetic bone or osteolysis induced by the particulate debris is increasingly accepted as the main reason [24].

Clinically, the particulate debris can be accumulated due to implant interface wear, micromotion, minor pathogen contaminations, and oxidative reactions [25, 26]. It can be started at the prosthetic joint articulations, or at non-bearing surfaces that rub together such as the backside of the acetabular liner, the modular interface, the bone-cement and cement-implant interfaces. However, wear debris caused by the articulating surface wear is considered as the main contributor, particularly the polyethylene debris in metal on polyethylene hip joint replacement [27, 28]. In time, particulate debris form and accumulate after THR and can be different shapes and sizes [29, 30]. Accumulated particulate debris results in a tissue response and local osteolysis and bone resorption at the bone-implant interface.

An interaction of mechanical and biological processes affects the mechanisms of bone resorption of hip arthroplasty [23]. As a mechanic response, joint forces and kinematics joined with contact surface geometries and material properties describe the cyclic stresses that lead to the generation of particulate debris. As a biologic response, the entrance of accumulated particle debris to the bone-implant interface stimulates a foreign-body response. These phenomena cause the release of bone resorption mediators and formation of a periprosthetic membrane with an abundance of macrophages, giant cells and particulate debris around the hip prosthesis [24, 31, 32]. Following this, resultant bone loss occurs due to the phagocytosis of particulate debris by macrophages and other cells capable of phagocytosis at the bone-implant interface, which then causes the limiting and removal of the hip prosthesis [24, 33, 34].

Die approbierte gedruckte Originalversion dieser Dissertation ist an der TU Wien Bibliothek verfügbar.
The approved original version of this doctoral thesis is available in print at TU Wien Bibliothek.
TU Bibliothek Your knowledge hub WIEN

The main factor of the failure in THR is started with bone resorption or osteolysis events. This process is a more complex and multifactorial event than it is thought. It is defined as a series of "failure scenarios", which were useful to classify the potential failure processes for the cemented THR. These "failure scenarios" included:

(a) the "implant reaction scenario", which is related to the particulate-induced bone resorption;

(b) the "accumulated damage scenario", which is related to the bone-cement interface failure due to the mechanical stresses upon it;

(c) the "bone- adaptation scenario", where the bone responds to the uneven stress patterns caused bone hypertrophy in high stress areas and bone resorption in low stress areas;

(d) the "destructive wear scenario", which involves the mechanical wear and eventually loss of continuity of the bearing surface [35].

2.3.2 Bone cement damage

One of the main factors that cause the aseptic loosening and failure of the hip implants is bone cement damage [23, 36]. Bone cement damage to loosening can be two different main mechanisms: the fatigue failure and defects of the cement mantle causes the release of cement particles. These particles would attack the articulating surface and act as third-body particles, causing severe articulating surface wear. It would also cause a foreign body reaction, promoting the osteolysis and loosening of the hip arthroplasty [37, 38]. Moreover, the bone-cement limitation or the crack of cement mantle, either by mechanical overload or due to the cement mantle damage, provided a way for the particulate debris to enter the bone- cement interface directly. Hence, it leads to the spreading of inflammatory and osteolytic events [39]. The accumulated damage of the cement mantle is affected by the mechanical behavior in the cement material and at the bone-cement or cement-implant interfaces [40, 41]. It is supported by two factors - the stresses in the cement mantle and at the bone-cement or cement-implant interfaces, and the strength at these interfaces. If the stress levels in the materials or at the interfaces exceed the corresponding strength, cement damage or mechanical failure would be triggered. As a result, reducing stresses and/or increasing strength of the interfaces can make a decrease a failure of the cement mantle. [42].

Die approbierte gedruckte Originalversion dieser Dissertation ist an der TU Wien Bibliothek verfügbar.
The approved original version of this doctoral thesis is available in print at TU Wien Bibliothek.
TU Bibliothek Your knowledge hub WIEN

2.3.3 Other complications

The second major cause of failure in total hip arthroplasty is dislocation. [43]. The contributing factors to dislocation include insufficient pseudo- capsular tissue, muscle weakness and imbalance due to inappropriate implant placement [44, 45]. Dislocation usually occurs along with impingement which is caused by excessive joint motion. Impingement means that the center of rotation moves from head center to the rim of the cup. The repeated impingement can result in material failure of the implant components, such as plastic damage of the polyethylene liner and fracture of the ceramic components [46]. Additional motion causes subluxation of the femoral head and lever-out [44]. Also a dislocation occurs via unsteadiness of hip implant and improper motions [47, 48]. Advanced design and proper implant positioning are necessary to avoid impingement and dislocation. Soft-tissue treatments such as posterior tissue or capsular repair are surgical treatments for avoiding repeated dislocation. Also, some advanced designs are used against dislocation such as dual-head cups, larger heads, modular cups, high offset femoral necks [49-51].

There are other determinants lead to the failure of the hip implant include avascular necrosis or osteonecrosis that will cause the collapse of the bone and periprosthetic fractures such as the infection and fracture of the stem. These determinants can occur at the early stage of the operation.

2.4 Hip Joint Replacement

THR is the process of completely removing the existing joint and replacing it with an artificial hip. When the hip joint is blocked because of diseases which are mentioned above, implant is implanted in place of injured joint part to perform function of hip joint.

THR is currently the most successful surgical treatment for hip joint disease, and the outcomes are excellent with a long-term survival rate [52, 53]. After hip replacements, most of the patients have no pain and improved functioning to perform their daily activities.

The materials for the components and fixation methods for the prostheses should be considered carefully when a hip joint replacement is attempted. The most popular and favorite material combinations for the hip joint replacement are metal on polymer (MoP), metal on metal (MoM) and ceramic on ceramic (CoC). They are usually categorized into hard-on-soft combinations (e.g. MoP) and hard- on-hard combinations (e.g. MoM and CoC). Fixation of the implants can be done by using bone cement (referred as cemented hip replacement) or a porous sintered coating which

Die approbierte gedruckte Originalversion dieser Dissertation ist an der TU Wien Bibliothek verfügbar.
The approved original version of this doctoral thesis is available in print at TU Wien Bibliothek.
TU Bibliothek Your knowledge hub WIEN

allows bone in-growth (referred as non- cemented or cementless hip replacement) or combination of them (hybrid hip prostheses). Several factors affect the choice of the material combination and fixation method for the hip joint replacements. These factors can be such as patient age, patient activity level and the surgeon's choice.

Metal on UHMWPE is the most implanted bearing combination followed by ceramic on UHMWPE (CoP). However, UHMWPE is susceptible to high wear rates.

Ceramic on UHMWPE bearings have been shown to wear less that metal on UHMWPE bearings, which is thought to be due to a higher resistance to scratching and damage [54, 55].

CoC bearings have good wear resistance but can be susceptible to fracture [56]. Furthermore, mal-positioning of these components can lead to edge loading of the acetabular rim and an increase in wear [57].

It is possible to combine the best mechanical properties of all the materials described and good engineering design needed in order to produce an implant with the optimum chance of long-term clinical survival.

Therefore, UHMWPE is desired to use for total hip replacement due to its optimum material properties and low cost.

2.5 THR Procedure

The surgery starts with general anesthesia or with the spinal anesthesia when the spinal cord receives the substance through injection. In the spinal anesthesia, the medication is delivered to the spinal cord of the patient which numbs the lower leg. Therefore, the patient does not have any sense during surgery. In addition to spinal anesthesia, sedation is delivered to the patient to enable the patient not to listen to the surgery process.

After having anesthesia effects, the intended region for the incision is cleaned with an antiseptic substance. The fluoroscope is used during the surgery to show the position of the instruments and the joint. The incision is done over the side of the hip joint, as shown in Figure 2.2. The muscles and ligaments are split to the extent that eventually hip joint is exposed. The femur of the patient is bent for dislocation of the femoral head from acetabulum. The femoral head is cut off from the end of the femur with a saw and the acetabulum socket is reamed with a special reamer to form a

Die approbierte gedruckte Originalversion dieser Dissertation ist an der TU Wien Bibliothek verfügbar.
The approved original version of this doctoral thesis is available in print at TU Wien Bibliothek.
TU Bibliothek Your knowledge hub WIEN

hemispherical shape for accepting the metal shell by screws, bone cement or by pressing which is fitted tightly and held in place by friction.

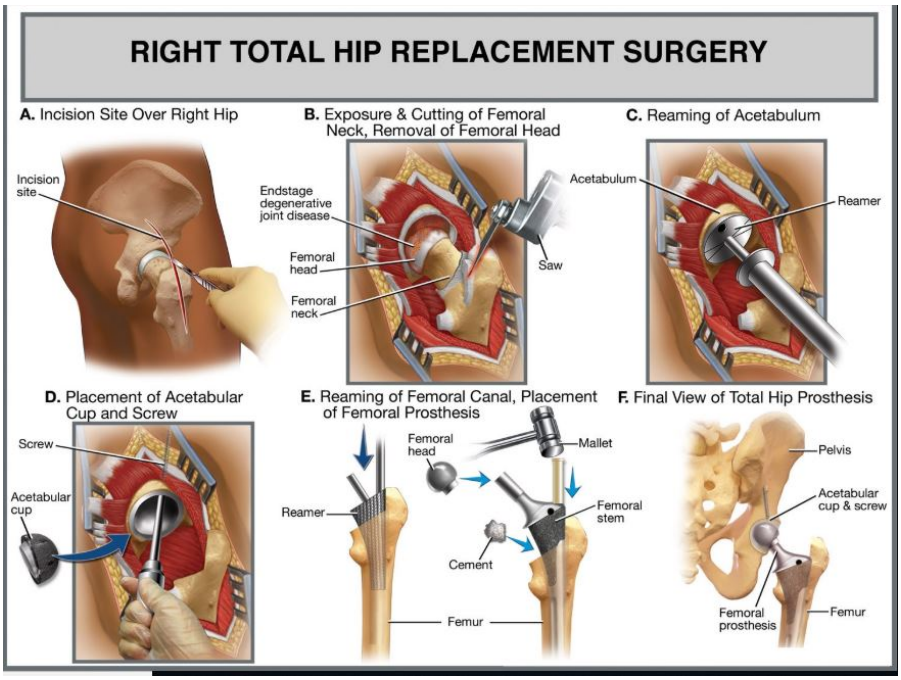

Figure 2. 2 THR surgery process [58]

Femur formed with a ball and a stem. The ball fits into the socket and the stem runs through the femur. The objective is that the head of the femur is removed by power saw and other special instruments are utilized to rasp the shaft of the femur. While the spongy bone is removed from inside of the canal, it is shaped to accept the stem. The stem should be fixed into the femur as well as the socket to the acetabulum either with cement or without cement which depends on the condition of the patient's bone, age and the implant type. Sometimes the combination of these two is suitable which is called a Hybrid total hip implant. When the stem is secured inside of the femur canal, trial balls fit into the socket to assess the proper size of the ball for each patient. Some patients order the customized implant, which is made particularly according to the hip anatomy of the patient. Modularity is another option for the patient which enables the surgeon to use different sizes of the ball in different angles with different lengths of the stem associated with his/her anatomic feature.

After having chosen the appropriate ball, it is pressed on the top of the stem and locked with friction. This forms the artificial femoral head while it gets bound with the socket and tested again

Die approbierte gedruckte Originalversion dieser Dissertation ist an der TU Wien Bibliothek verfügbar.
The approved original version of this doctoral thesis is available in print at TU Wien Bibliothek.
TU Bibliothek Your knowledge hub WIEN

for its stability and the leg length of the patient. The incisions are sutured with two to three non-dissolvable sutures and swaddled with the bandage. The surgery takes from one hour to two hours.

The patient after surgery is advised to use walking stick for several days. The full recovery depends on the patients' condition.

2.6 History of Total Hip Replacement

Operators have been trying to find a successful technique to overcome the adverse effect of arthritis resulting from a total hip replacement.

The term arthroplasty can be defined as "surgery to relieve pain and restore range of motion by change or reconstructing a joint" [21]. The term arthroplasty originally exists in the presence of joints that had stiffened after pyrogenic or tuberculosis infection or by serious injury. Before the advent of joint replacement, attempts to treat arthritic hips included arthrodesis (fusion of femur and acetabulum), osteotomy (re-alignment of femoral head or hip bone), nerve division, and joint debridements (removal of arthritic spurs, calcium deposits, and irregular cartilage in an attempt to smooth the surfaces of the joint) [21, 59].

The earliest attempt on the hip joint replacement was in 1891 when a technique termed 'interpositional hip arthroplasty' was introduced [60]. This technique was composed of a spacer being placed between the femoral and acetabular bearing surfaces of the hip. A series of different materials was examined that included zinc, tin, rubber, celluloid and gold leaf [21, 60]. Little success was observed when biological materials such as muscle, ivory, fascia and chromatised pig's bladder were used [60, 61].

Dr. Marius Smith-Peterson progressed the idea of hip intervention and in the mid of 1920s introduced the 'mould arthroplasty' [62]. The principle was to stimulate cartilage regeneration on both sides of the glass and then remove the glass once the cartilage has been restored. However, the glass was too fragile and fractured. In 1937, he selected cobalt- chrome alloy named Vitallium (60% Co I 20% Cr I 5% Mo and traces of other substances [21] for his mould arthroplasties [63]. The introduction of cobalt-chrome proved sufficiently successful to allow the widespread use of mould arthroplasties [15]. After cup arthroplasty, there was no pain relief and hip movement was

Die approbierte gedruckte Originalversion dieser Dissertation ist an der TU Wien Bibliothek verfügbar.
The approved original version of this doctoral thesis is available in print at TU Wien Bibliothek.
TU Bibliothek Your knowledge hub WIEN

limited. Besides, the technique didn't allow surgeons to treat a range of arthritic deformities of the hip [59].

Philip Wiles first used stainless steel in total hip arthroplasty at the end of the 1930s. The all-metal implant consisted of a cup that screwed into the acetabulum and a femoral stem bolted to the outside of the femur. In 1938, Wiles carried out the first total hip replacement. The technique was offered to patients who mostly had young chronic arthritis and were confined to bad or just able to walk. Results were noted as being 'only tolerable' in 25% of cases although exact results were not explained [59].

In 1946, the Judet brothers carried out a 'resection-reconstruction' using a poly-methyl methacrylate (PMMA) femoral stem that passed axially down the neck of the femur. The prothesis failed due to creation of wear debris [60, 64].

Dr. Haboush successfully used an acrylic fast-setting dental cement to anchor hip prostheses in the 1950s. In the 1960s Charnley used a pink dental acrylic cement called 'Nu-Fix' to anchor THR components in position (Figure 2.3).

Figure 2. 3 Pink dental cement

At present, the application of acrylic has been using as bone cement in the orthopedic fixation technique successfully.

Several operators began regularly installing stainless steel THR in the 1950s. Charnley had noted the 'squeaking' noise emanating from these early metal-metal arthroplasties [64]. He performed experiments [65, 66] to show that metal-metal joints had high frictional torque and postulated that this might lead to loosening of the implant. As a result, in 1958 he developed a low friction arthroplasty consisting of a polytetrafluoroethylene (PTFE, Teflon^{TM}) acetabular cup and a Moore stainless-steel Charnley used this combination till 1963 when the use of Teflon was stopped.

Die approbierte gedruckte Originalversion dieser Dissertation ist an der TU Wien Bibliothek verfügbar.
The approved original version of this doctoral thesis is available in print at TU Wien Bibliothek.
TU Bibliothek Your knowledge hub WIEN

Although the joint articulation was successful in the first one to two years after surgery, over 99% had to be revised within two to three years of implantation due to severe wear and the inflammatory response provoked by the PTFE wear debris.

Charley experimented with a glass filled PTFE called 'Fluorosint' [67]. Having used this material on acetabular components showed an improvement in wear resistance over PTFE. Components fabricated from Fluorosint were implanted but they had severe wear rates. Following the clinical failure of filled PTFE Charnley has quit the development of his THR system for a short time. In 1960's, Charnley was introduced to a new polymer called Ultra-High Molecular Weight Polyethylene (UHMWPE). Charnley felt uneasy about this new material and handled its wear behavior. After three weeks of wear testing, the UHMWPE had showed an identical degree of wear as was seen for PTFE components after only 24 hours of testing. After having these wear results he continued to use of UHMWPE for acetabular components [64]. The material used by Charnley was compression moulded RCH-l000 UHMWPE manufactured by Ruhrchemie (later merged into Hoechst) [68]. In November 1962, he achieved the first THR using an UHMWPE cemented acetabular cup in conjunction with a stainless steel 316L femoral head 22.25 mm diameter [68]. The combination of UHMWPE cup and stainless-steel femoral component was termed the 'low friction arthroplasty' (LFA) and proved to be a great success in terms of component function and longevity. A plenty of designs have been studied since the discovery of Charnley's LFA concept but the LFA is still regarded as the 'gold standard' worldwide.

2.7 Gender

All over the world, it is estimated that 10% of men and 18% of women aged over 60 years have moderate and severe symptomatic osteoarthritis [69]. Age is the most important indicator for progressing of osteoarthritis. Joint replacement is seen commonly in women who are age 50 and above, but it can also be performed at younger ages.

In the OECD report expresses that Switzerland, Germany, Austria and Belgium had the highest rates for both of hip and knee replacement in 2015 (See in Figure 2.4) [70]. In Austria between 2009 and 2015 nearly continuous increase in the number of hip and knee arthroplasties was found. In detail, the number of primary THA increased by 14% (n = 15,834 in 2009 and n = 18,052 in 2015) via this period. This represents 210 primary THA per 100.000 inhabitants in 2015. Ninety-two percent of THA was performed in the age group 50-90 between 2009 and 2015. Between 2009

Die approbierte gedruckte Originalversion dieser Dissertation ist an der TU Wien Bibliothek verfügbar.
The approved original version of this doctoral thesis is available in print at TU Wien Bibliothek.
TU Bibliothek Your knowledge hub WIEN

and 2015 the population aged 50-90 increased only by 1.1% to 3.3 million people, the population older than 65 years in Austria increased by 9.3%, and the population older than 70 years increased the strongest by 19.8%. The mean age of patients receiving THA (67.1 to 67.4 years) sustained relatively constant between 2009 and 2015, whereas the comparable mean age in the Austrian general population increased during this period (41.2 to 42.3 years)[71].

1290 THA re-implantations (7.1% of primary hip arthroplasties, increase of 34.7% between 2009 and 2015) were performed in 2015. For THA the calculated of patients receiving re-implantation surgery in Austria was 70.8 years old for the same year.

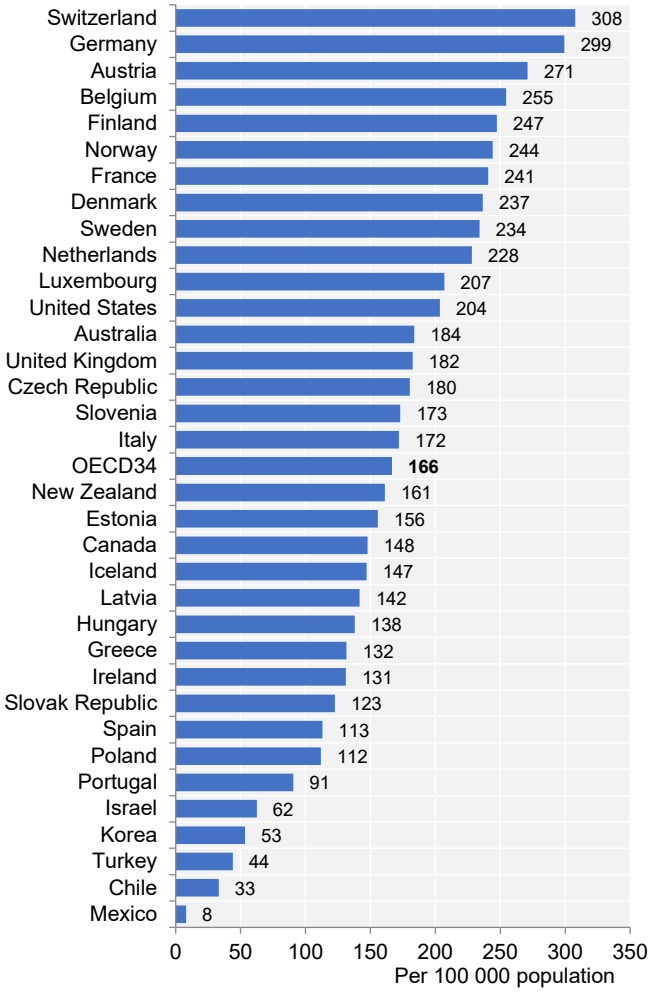

Figure 2. 4 OECD report of knee and hip replacement in 2015

The retrieved explants investigated in this thesis were sent by Universitätsklinik in Innsbruck. In this study, there wasn't a special selection standard for inclusion of patients. Twenty patients were

Die approbierte gedruckte Originalversion dieser Dissertation ist an der TU Wien Bibliothek verfügbar.
The approved original version of this doctoral thesis is available in print at TU Wien Bibliothek.
TU Bibliothek Your knowledge hub WIEN

taken of their consent before they underwent revision hip surgery. Having obtained their consent to take part in the study, patients were assessed using a study specific information collection form. Their medical notes were also consulted to identify certain pieces of information such as the reason for primary hip replacement, reason for revision, UCLA activity etc. A full summary of patient information is contained in APPENDIX A.

Die approbierte gedruckte Originalversion dieser Dissertation ist an der TU Wien Bibliothek verfügbar.
The approved original version of this doctoral thesis is available in print at TU Wien Bibliothek.
TU Bibliothek Your knowledge hub WIEN

Chapter 3: UHMWPE

3.1 History

The Nobel Prize for Chemistry in 1963 was won by organic chemist Karl Ziegler and Giulio Natta. In 1953, they found a family of stereo-specific catalysts able to introduce an exact and regular structure to various polymers. This finding led to improve the fundamental techniques of new materials such as synthetic plastics, fibers, rubbers, and films derived from such olefins as ethylene (ethene) and butadiene (but- 1,2,3,4-diene).

In the 1930s, Imperial Chemical Industries (ICI) started a research program to develop new high-pressure reaction materials. Polyethylene was discovered accidentally after circa 50 different reactions have been tried. One of the mixtures included ethylene, a very light gas prepared from petroleum and the high-pressure reaction left a white waxy solid on the walls of the reaction vessel that was later called to be polyethylene.

Karl Ziegler made a crucial invention in 1953. The molecules of ethylene combine in a more disciplined manner on the surface of particles of "Ziegler catalyst" without the high pressures and temperatures previously required. The production of polyethylene is successful however, it does not have low cost. It was much more rigid and could handle boiling water.

Ziegler shared the Nobel Prize for his invention with Giulio Natta, who simultaneously found how to control other monomers to produce other plastics. Therefore, in general, these methods are referred to as Ziegler-Natta catalysts [72].

3.2 Structure

Ultra-high molecular weight polyethylene continues the most commonly implanted bearing material and can reasonably be expected to perform well clinically for 10-15 years [73]. However, beyond 10 years the survival of UHMWPE total hip replacements becomes limited by wear of the UHMWPE primarily at the articulating surface. Ultra-high molecular weight polyethylene for orthopedic components is made up of ethylene monomer units joined together by covalent bonds to form a linear homopolymer, an un-branched chain of identical repeated units (Figure 3.1). A UHMWPE chain can have between 71,000 and 214,000 repeated units being equal to a molecular weight of between 2 and 6 million g mol^{-1} [74].

Die approbierte gedruckte Originalversion dieser Dissertation ist an der TU Wien Bibliothek verfügbar.
The approved original version of this doctoral thesis is available in print at TU Wien Bibliothek.
TU Bibliothek Your knowledge hub WIEN

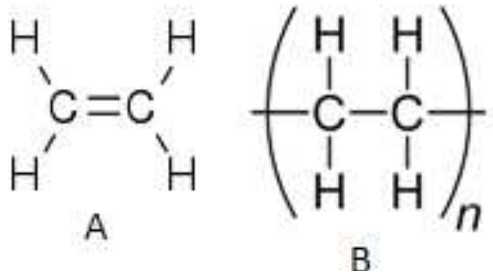

Figure 3. 1 A schematic of (A) Ethylene and (B) UHMWPE Chemical Structures [74]

UHMWPE is a semi crystalline polymer and fundamentally, contains crystalline lamellae embedded in amorphous regions. The crystalline phase is arranged as a series of folds generating lamellae located randomly amongst the amorphous phase, and tie molecules link individual lamellae together, adding crystallinity. Figure 3.2 shows the structure of UHMWPE [74-76]. The degree and orientation of crystalline regions within UHMWPE depends on several such as molecular weight, processing conditions, and environmental conditions (i.e. in-vivo loading). In UHMWPE material, the percentage of crystallization is normally between 50-55% [74]. The mechanical properties of UHMWPE are determined by the ratio and distribution of crystalline and amorphous regions (crystallinity), the number of connections between the crystalline regions (number of tie molecules, which is inversely proportional to the thickness of the crystallite), the number and nature of connections within the amorphous regions (the degree of mechanical entanglements and crosslinks) and the presence or absence of orientation of the crystallites [77].

Changes in crystallinity and crystalline orientation lead to affect the elastic modulus of UHMWPE. An increase in elastic modulus is nearly proportional to the increase in the degree of crystallinity. If the elastic modulus increases without a proportional increase in yield strength the probability of plastic contact in the UHMWPE may increase leading to an increase in the wear rate [78].

Die approbierte gedruckte Originalversion dieser Dissertation ist an der TU Wien Bibliothek verfügbar.
The approved original version of this doctoral thesis is available in print at TU Wien Bibliothek.
TU Bibliothek Your knowledge hub WIEN

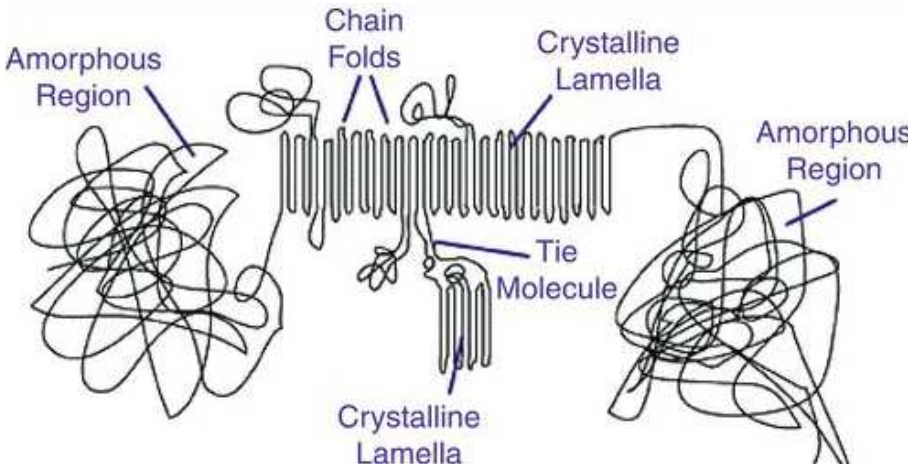

Figure 3. 2 A Schematic of the Morphology of UHMWPE [74]

Two medical grades of UHMWPE currently use as a bearing material in THR, GUR 1020 and GUR 1050, which the main difference is the average molecular weight (3-3.5 and 5.5-6 x 10^6 g/mol, respectively).

3.3 UHMWPE Consolidation

UHMWPE has high melt viscosity that leads to consolidated under elevated temperatures and pressures. There are three processing methods for consolidation polymers. These are injection moulding, blow moulding and ram extrusion. Due to high melt viscosity of UHMWPE, compression moulding and ram extrusion are mainly used.

The process conditions of producing UHMWPE are being kept secret by manufacturers however the fundamental scientific basis for the consolidation of UHMWPE powder has been discussed in some degree [79, 80]. The fundamental mechanism included the consolidation of UHMWPE is diffusion. The temperature and pressure are important factors for controlling the rate of diffusion and affect adjacent resin particles at a molecular level. High temperatures and pressures are used to enhance the mobility of polymer chains and reduce the distance between interfaces. Because the process is diffusion-dependent, the material must be in steady-state at the processing temperature and pressure for the identified amount of time. This enables the molecular chains enough time to migrate across grain boundaries.

Since the 1950s compression moulding has been used to produce UHMWPE and the material was initially sold under the trade name RCH1000/Hostalen GUR 412.

Die approbierte gedruckte Originalversion dieser Dissertation ist an der TU Wien Bibliothek verfügbar.
The approved original version of this doctoral thesis is available in print at TU Wien Bibliothek.
TU Bibliothek Your knowledge hub WIEN

The process involves a hydraulic press with a mould containing heating and cooling system. Processing can hold on 24 hours of large sheets of material (2m x 4m x 80mm). RCH 1000 was used by Sir John Charnley to fabricate acetabular components in the 1960s. The material was also distributed under the name CHIRULEN and is very similar to contemporary GUR 1020. It is important to say that GUR412 contained calcium stearate whereas GUR1020 does not. There are currently two companies that produce compression moulded GUR 1020 and GUR 1050 UHMWPE, Perplas Medical and Poly Hi Solidur Meditech.

In the 1970s ram extrusion was improved in the United States as another consolidation method. The UHMWPE powder is fed into a cylinder i.e heating chamber where the powder becomes molten. Molten UHMWPE is pushed through a heated die and the shaped rod exits the extruder through an outlet. The rod then slowly passes through a series of heated mantles to cool it. They are fabricated for medical applications and diameters varying from 20-80 nm. As in compression moulding, the production rate can be quite slow depending on the dimensions of the consolidated form and production rates of the order mm/min are common.

Despite the variances in processing paths, there is no big difference between the properties of GUR 1020 and GUR1050 produced via ram extrusion and compression moulding. It was found that the material density was sensitive to the type of resin but not the conversion method. However, the impact strength and the tensile mechanical properties were sensitive to the type of resin and conversion method [81].

A summary of the chemical, physical and mechanical properties of UHMWPE along with other polymeric materials is given in Table 3.1 [82].

Die approbierte gedruckte Originalversion dieser Dissertation ist an der TU Wien Bibliothek verfügbar.
The approved original version of this doctoral thesis is available in print at TU Wien Bibliothek.
TU Bibliothek Your knowledge hub WIEN

Table 3. 1 A summary of properties of UHMWPE along with other polymeric materials

	ASTM Standard	LDPE	HDPE	UHMWPE
Molar mass [g/mol]	na	50.000-200.000	50.000-300.000	> 2.000.000
Crystallinity [%]	Density data	40 - 55	60 - 75	50 – 60
Density [g/cm³]	D-792	0,91-0,930	0,945-0,965	0,927-0,944
Melting Point [°C]	na	105-115	128-137	125-145
Tensile yield strength [MPa]	D 638	6-11	15-35	> 19 (19-23)
Elastic modulus [MPa]	D 638	100-500	400-1500	Na
Ultimate tensile strength [MPa]	D 638	7-16	18-40	> 27
Elongation to breakpoint	D 638	50-800	40-1000	> 300%
Shore D hardness	D 2240	na	60-70	60

na: not available

3.4 Fabrication of UHMWPE Implants

There are two steps, which are initial rough machining and a finishing phase, for machining polymers. Feed rate, tool cutting force, and spindle speed are the machining parameters of UHMWPE and these parameters must be carefully controlled due to heat sensitivity of UHMWPE. However, particulars of machining variables are registered and therefore few information is available about the effect of machining parameters on the properties of UHMWPE. The machining process is demonstrated to produce a modified surface layer with polymer molecules oriented in the direction of machining. Hereby, this preferred orientation of the surface layer leads to increase crystallinity [83].

3.5 Sterilization

A sterilization method must be carefully selected due to an effect on the chemical and mechanical properties of the polymer that can influence polymer long term performance. Formerly, orthopedic components were sterilized by gamma radiation in the presence of air and then packaged in air permeable packaging. Gamma irradiation causes cross-linking, which improves the wear resistance of the material but also generates free radicals. Free radicals can react with oxygen in the air or in-

Die approbierte gedruckte Originalversion dieser Dissertation ist an der TU Wien Bibliothek verfügbar.
The approved original version of this doctoral thesis is available in print at TU Wien Bibliothek.
TU WIEN Bibliothek Your knowledge hub

vivo to cause oxidative degradation of the component. A diagram explaining how gamma radiation can break carbon-carbon or carbon-hydrogen bonds, leading to chain scission or immediate oxidation in the presence of oxygen is shown in Figure 3.3 [84].

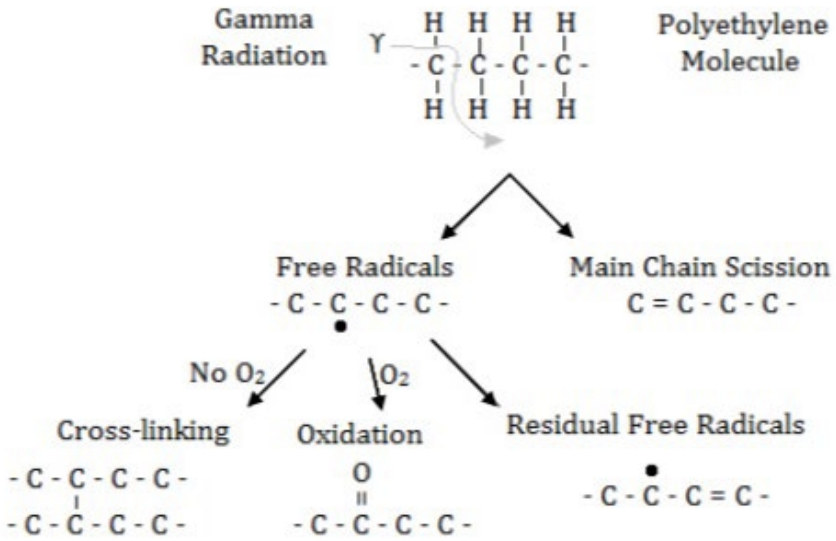

Figure 3. 3 Ongoing gamma radiation of UHMWPE

It was reported that these air sterilized components were subjected to oxidative degradation or shelf aging, resulting in an increase in density and crystallinity and a decrease in ductility and toughness. Oxidative damage was observed as a white band below the surface of these implants and was responsible for fatigue damage and increased wear of the material [85, 86]. Accordingly, gamma sterilization in the air has been stopped and a range of other methods are used instead.

Using gamma irradiation in an inert environment causes to eliminate the availability of oxygen which can react with free radicals. These inert environments are argon, nitrogen and vacuum conditions. Effectivity of packaging methods (inert environment in conjunction with barrier packaging) and oxidation again becomes a problem once the packaging has been opened. Additionally, the degree of effectiveness in terms of preventing oxidation during shelf aging can be affected by the type of packaging used, as defined in a survey by Costa et al. [87] on contemporary packaging.

Ethylene oxide (EtO) sterilization nor affects the physical structure of the UHMWPE neither generates free radicals. Collier et al. [86] studied on oxidation levels after EtO sterilization and found that damage modes such as rim cracking and delamination observed in components that had

Die approbierte gedruckte Originalversion dieser Dissertation ist an der TU Wien Bibliothek verfügbar.
The approved original version of this doctoral thesis is available in print at TU Wien Bibliothek.
TU Bibliothek Your knowledge hub WIEN

been gamma radiated were not observed in EtO sterilized components. EtO sterilization does not develop cross-linking of the UHMWPE and therefore does not offer the improvement to wear resistance of gamma radiation.

Clinically, it is too early to observe outcomes of the gas plasma sterilization technique. Nevertheless, it is a cheap and quick sterilization method and does not generate free radicals or make a change in material properties.

3.6 Oxidation

Chain scission is a process leads to break chemical bonds within the material when UHMWPE is subjected to gamma radiation for either the reasons of sterilization or crosslinking. Thus, free radicals are generated within the polymer. The more mobile free radicals will recombine to form crosslinks. Residual free radicals, that do not recombine, will react with oxygen to form unstable hydroperoxides. That decay causing embrittlement of the material through chain scission and recrystallization [42]. This embrittlement of the material reduces wear resistance and fatigue resistance and can lead to failure of the material through the fracture.

Edidin et al. [88] compared the surface and subsurface mechanical properties of shelf aged and naturally aged UHMWPE test specimens using the small punch technique and compared them with non-aged controls. It is reported that an increase in elastic modulus and a decrease in ductility, ultimate strength and toughness resulting from post-irradiation aging that was consistent with a progressive embrittlement process. The accelerated aging process used in the study (4 weeks at 80 ^{0}C in an atmospheric oven) induced mechanical degradation at the surface but not the subsurface. It shows the difficulty to mimic the natural aging process in these materials. Collier et al. [86] found that gamma induced oxidation from sterilization in air had a significant correlation with component cracking and delamination and resulted in reductions in ultimate tensile strength and elongation. Oxidation can be seen when UHMWPE is exposed to oxygen in-vivo (i.e existence oxygen in synovial fluid) or shelf storage time (i.e. existence oxygen in the air).

The same in-vivo oxidation mechanisms were seen on components sterilized in air and components sterilized in barrier packaging with gamma radiation The long term results were expected to be a loss of mechanical properties leaving the components susceptible to fatigue failure with increasing time and loading cycles [89].

Die approbierte gedruckte Originalversion dieser Dissertation ist an der TU Wien Bibliothek verfügbar.
The approved original version of this doctoral thesis is available in print at TU Wien Bibliothek.
TU Bibliothek Your knowledge hub WIEN

20 gamma sterilized acetabular liners are retrieved and measured the oxidation index and wear. All liners showed oxidation and crystallization but the liners with a shelf life of more than 3 years exhibited significantly higher wear rates [90]. Using scanning electron microscopy, extensive abrasive wear on the component surface is observed.

3.7 Crosslinked UHMWPE

Wear is the major reason for the failure of implant material and hinders the ideal performance of total hip prosthesis. Another problem is the susceptibility of UHMWPE to oxidative degradation. Both problems degrade the implant's mechanical properties. For that reason, formerly first-generation cross-linked explants latter second-generation cross-linked implants were launched to the medical market. So-called first-generation cross-linked UHMWPE, which is considered to be exposed to radiation doses of 50 kGy and above and then stabilized with thermal treatments, was launched clinically for THR in 1998 to improve the wear resistance of the polymer. Since that day it has been widely used increasingly all over the world, with all major manufacturers offering a registered version of the material. The advantage of cross-linked UHMWPE is reducing wear rate which plays an important role of starting osteolysis.

Chain scission is a process when UHMWPE is exposed to ionizing radiation subsequently is being cleaved the C-C and C-H bonds. Free radicals are generated in this process and two free radicals may then go on to combine forming cross-links (Figure 3.4). Crosslinking is harmful to the mechanical properties such as strength, ductility, toughness, elastic modulus and fatigue crack propagation resistance [91].

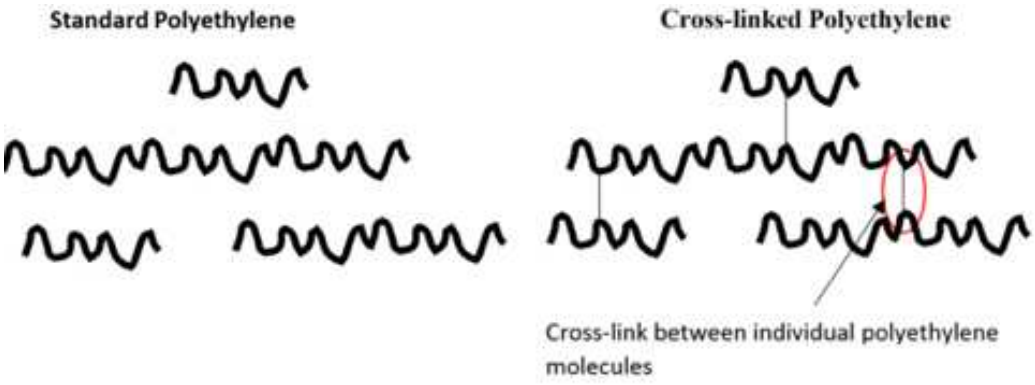

Figure 3. 4 Molecular structure of conventional UHMWPE and cross-linked UHMWPE [92]

Die approbierte gedruckte Originalversion dieser Dissertation ist an der TU Wien Bibliothek verfügbar.
The approved original version of this doctoral thesis is available in print at TU Wien Bibliothek.
TU Bibliothek Your knowledge hub WIEN

The crosslinks between the polymer chains prevent slippage and make the UHMWPE more resistant to surface orientation. This reduces the wear debris generation which occurs when conventional UHMWPE is subjected to cross shear during multidirectional movement [93].

During the cross-linking process, most of the free radicals are produced. These free radicals are not mobile enough to recombine and cause an oxidation risk to the material as they can go on to react with oxygen in the environment. The radiation dose and post-irradiation thermal treatment must be carefully selected due to oxidation risk. Increasing the radiation dose will increase the cross-link density up to a dose of around 100 kGy, after which the cross-linking begins to saturate [94]. Increasing the radiation dose up to this threshold will increase the wear resistance and free radicals and results in reducing mechanical properties. A post-irradiation thermal treatment is required to quench these free radicals and stop the oxidation of the material. This can be done by heating the polymer to above its melting temperature i.e. remelting or heating the polymer to below the melting temperature i.e. annealing. Post-irradiation remelting reduces the crystallinity of the material allowing the free radicals to mobilize and recombine but deteriorates the strength of the material. Annealing tolerates the microstructure to be maintained but is less efficient at eliminating free radicals. Performing a cross-linked UHMWPE that will allow implant longevity requires a balance to be achieved between the wear resistance, mechanical properties, free radicals and crystallinity of the material.

In [91] a review of the mechanical properties of conventional and highly crosslinked UHMWPE is performed. It is reported that the improved resistance to plastic deformation and corresponding improvement in wear result in by reductions in ultimate tensile stress, ductility, modulus, toughness and crack propagation resistance. Several in vitro studies have been conducted on the wear resistance of cross-linked UHMWPE [55, 95-97]. The results have showed a significant decrease in wear when compared to conventional UHMWPE and these findings are beginning to be confirmed by clinical experience [98-103].

The study [95] was conducted the wear of cross-linked UHMWPE cups for a range of radiation doses. It was found that the wear rate decreased remarkably for increasing radiation dose. Wear rates for gamma radiation doses above 200 kGy were extremely low and machining marks still visible in the main contact zone. Radiation doses of 200 kGy lead to deterioration of the mechanical properties of the polymer. Nevertheless, it would be a balance between wear and material properties are essential. The wear rates in above study at more clinically relevant radiation doses were

Die approbierte gedruckte Originalversion dieser Dissertation ist an der TU Wien Bibliothek verfügbar.
The approved original version of this doctoral thesis is available in print at TU Wien Bibliothek.
TU Bibliothek Your knowledge hub WIEN

9.3 ± 0.9 mm^3/yr and 2.2 ± 0.2 mm^3/yr (for 45 kGy and 95 kGy, respectively). UHMWPE materials crosslinked at 75 kGy and 100 kGy and then remelted have significantly lower wear rates compared to a control material subjected to a radiation dose of 25 kGy in air (conventional UHMWPE) [104].The steady state wear rate for the highly crosslinked material (100kGy) was 4.6 mm^3/million cycles compared to over 40 mm^3/million cycles for the conventional UHMWPE.

Gravimetric wear rates of ethylene oxide sterilized UHMWPE, gamma inert sterilized UHMWPE and two crosslinked UHMWPEs exposed to clinically relevant radiation doses (50 kGy and 100 kGy) and aged materials were tested in hip simulator. Both crosslinked materials had lower wear rate than conventional materials [96]. It was found negative wear rates for the 100 kGy crosslinked UHMWPE. However, it was recorded that fluid absorption of the UHMWPE material would make it difficult to correctly measure very low wear rates gravimetrically. Moreover, these tests were done with ISO standard which recommends that hip simulator tests must be done with 100% bovine serum rather than 25%. It was reported that the temperature at the bearing is higher than 37°C and at these higher temperatures, increased protein precipitation may occur [95, 105]. Protein concentration and precipitation influence the wear of UHMWPE and may explain the slight amount wear reported in the above study [78, 106]. Clinically, any wear has not been observed for these materials.

Medium-term clinical results for crosslinked materials have been released. Engh et al. performed a 10 year of highly crosslinked acetabular cups (50 kGy and heat treated) and conventional cups of the same design (DePuy, Duraloc® cups). They reported an 83% reduction in the wear rate of the crosslinked cup compared to the non- crosslinked cup (0.04 mm/yr and 0.22 mm/yr, respectively) and this corresponded with a clinically significant reduction in occurrences of osteolysis for the crosslinked group [101].

Another similar study was done using the results of the mean yearly linear penetration rates measured on radiographs. After 10 to 12 years, it was reported that a highly crosslinked UHMWPE and a nitrogen sterilized UHMWPE showed significantly lower rates for a highly crosslinked UHMWPE compared to a conventional UHMWPE (a 64% reduction; 0.08mm/yr and 0.16mm/yr respectively) [102].

Further study is that 50 patients who were younger than the age of 50 were examined. 100% survival and a very low head penetration rate (0.02 mm/yr) were found after a 10-year in-vivo time.

Die approbierte gedruckte Originalversion dieser Dissertation ist an der TU Wien Bibliothek verfügbar.
The approved original version of this doctoral thesis is available in print at TU Wien Bibliothek.
TU Bibliothek Your knowledge hub WIEN

In that study concluded that the crosslinked material had excellent long-term potential considering the younger patients who would be more active and therefore place higher demand in terms of wear on the materials [107].

The linear penetration rate was calculated in the above studies which include creep and wear. Creep varies the type of UHMWPE and the material properties such as the degree of crystallinity which depends on factors such as radiation dose, thermal processing, and oxidative degradation. Wear debris depends on osteolysis and it is therefore important to distinguish wear from creep, which cannot be supposed to be the same for all UHMWPE materials. Within the first 6 months to 2 years of implantation is important for creep occurrence.

The volumetric wear between 1 and 10 years, excluding the first year of implantation, in a study of a crosslinked UHMWPE and a conventional UHMWPE of the same design was reported [103]. These authors observed lower wear volumes for the crosslinked liners (98 mm^3 and 14^3 mm, respectively). The limitation of the above studies is the measurement of wear and penetration using radiographs. The error of measurements occurs due to patient positioning, poor quality images and observer variation, rather than direct wear measurement on an explanted liner. Besides, backside wear could be a source of wear debris that is not measurable using radiographs.

Several factors should be taken into consideration when explaining the wear rates of UHMWPE. These factors are component design, radiation dose, thermal processing, material degradation, and adverse loading. The results of wear studies are encouraging considering the medium-term performance of crosslinked UHMWPE. Despite many studies have reported lower wear rates for crosslinked UHMWPE than conventional UHMWPE, there is currently limited evidence on clinical outcomes in the long term.

Cross-linked UHMWPE shows better wear resistance than conventional UHMWPE but there are concerns about the effect of the change to mechanical properties on the clinical performance. Baker et al. performed a study on the degree of cross-linking and its effect on the fatigue crack initiation and propagation resistance [108]. It was found that although cross- linking can be useful in preventing the initiation of defects within the material, the resistance to crack propagation is reduced as a result of the decrease in plasticity at the crack tip. Crack propagation resistance is crucial for the lifespan of the implant. Cyclic loading in the body results in some failures or defects capable of spreading on clinically available components. It was found in this study that a lower

Die approbierte gedruckte Originalversion dieser Dissertation ist an der TU Wien Bibliothek verfügbar.
The approved original version of this doctoral thesis is available in print at TU Wien Bibliothek.
TU Bibliothek Your knowledge hub WIEN

degree of crosslinking is ideal when modeling for both wear resistance and fatigue crack propagation resistance. Further study by Bradford et al. with 21 retrieved acetabular cups demonstrated surface cracking, abrasions, pitting and scratching after only 10 months in-vivo time [109]. On the contrary of in vitro studies of cross-linked UHMWPE cups still have machining marks after simulation of long-term implantation. It can be said that increasing the ductility of material increasing the creep occurrence at the articulating surface.

Selection of thermal treatment method is important, as it influences not only oxidative stability but also microstructure and mechanical properties. The common believe is that irradiated and annealed UHMWPE is at risk of in-vivo oxidation as a result of residual free radicals.

Increased crystallinity and unexpected levels of in-vivo oxidation of irradiated and annealed components after 3 years of implantation was found [110]. Subsurface white bands and embrittlement were observed as in conventional UHMWPE components sterilized in air. Additionally, these results were compared to components that were irradiated and remelted to remove all free radicals. No oxidation was observed and no change in crystallinity occurred in-vivo. Besides, retrieved Crossfire® liners, which were annealed, have oxidized significantly and been susceptible to fatigue damage after 3 years of implantation [89].

In another study, traditional gamma air sterilized liners, conventional gamma inert sterilized liners and annealed highly cross-linked liners for in-vivo degradation were analyzed [111]. It was found that all three groups of liners had subjected to in-vivo degradation. However, it was also found that the most severe oxidation occurs at the liner rim where normally the lowest amount of wear is seen. This is due to the bearing itself being protected against exposure to oxidizing body fluids. As a result, it was reported that during the first 5 years of implantation, in-vivo degradation of annealed highly cross-linked UHMWPE was not clinically relevant without impingement and on condition that the locking mechanism was not exposed to large volumes of oxidizing fluid.

Free radicals are fully quenched during the remelting process. Therefore, irradiated and remelted UHMWPE is used against the problem of in-vivo oxidation. However, this process results in the degradation of mechanical properties as mentioned before.

The clinical trade-offs were examined between fatigue, wear and oxidation of highly crosslinked and thermally processed materials [112]. It is built a diagrammatic that effectively showed the

Die approbierte gedruckte Originalversion dieser Dissertation ist an der TU Wien Bibliothek verfügbar.
The approved original version of this doctoral thesis is available in print at TU Wien Bibliothek.
TU Bibliothek Your knowledge hub WIEN

correlation between these properties for untreated controls, a moderately crosslinked and remelted UHMWPE, a highly crosslinked and remelted UHMWPE and a highly crosslinked and annealed UHMWPE (Figure 3.5). The untreated controls display good oxidation and fatigue crack propagation resistance but poor wear resistance. The moderately crosslinked and remelted UHMWPE displays good oxidation resistance but moderate fatigue crack propagation and wear resistance. The highly crosslinked remelted UHMWPE shows good oxidation resistance and wear resistance but poor fatigue crack propagation resistance. Finally, the highly cross linked and annealed UHMWPE shows good wear resistance and fatigue crack propagation resistance but poor oxidation resistance.

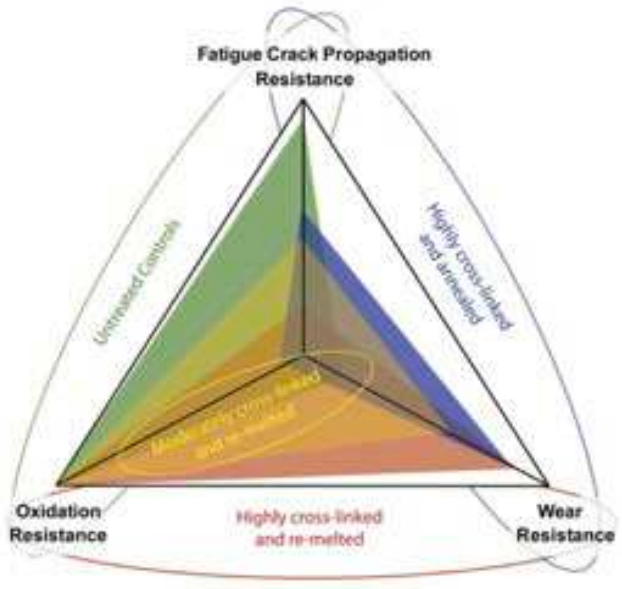

Figure 3. 5 Schematic to outline the trade-offs in wear resistance, fatigue crack propagation resistance and oxidation resistance developed by [112]

Alternative methods have been searched for to stabilize UHMWPE due to the inconclusive nature of the best post-irradiation thermal treatment. Thus, the need of the second-generation of UHMWPE is emerged due to maintain the microstructure and mechanical properties, which is linked wear resistance, and the same time oxidative stability. There are several methods of second-generation cross-linked UHMWPEs that have been developed since 2005. Some of them: sequentially irradiated and annealed, sintering at high pressure, incorporation of Vitamin E, and high pressure crystallization after melting cross-linked UHMWPE [113-117].

Die approbierte gedruckte Originalversion dieser Dissertation ist an der TU Wien Bibliothek verfügbar.
The approved original version of this doctoral thesis is available in print at TU Wien Bibliothek.
TU Bibliothek Your knowledge hub WIEN

3.8 Additive Stabilized UHMWPE

Vitamin E (α-tocopherol) is the most common antioxidant that has been added to crosslinked UHMWPE to stabilize residual free radicals and improve the materials resistance to oxidation, is shown in Figure 3.6 [118]. This terminated the requirement for post-irradiation thermal treatments of varying effectiveness or that are harmful to the mechanical properties of the material.

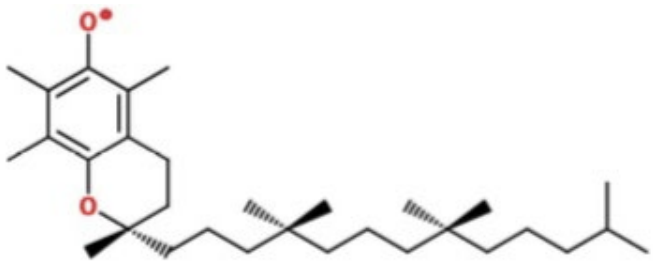

Figure 3. 6 α-tocopherol free radical

Vitamin E is a biocompatible free radical scavenger. It can be used instead of remelting and annealing thermal treatments and preserves mechanical properties of polymer. Clinically, Vitamin E stabilized polymers' performance has not been proved yet. Similar wear performance was observed for Vitamin E stabilized UHMPWE acetabular liners when compared to highly crosslinked and remelted UHMWPE in hip simulator tests. It is also reported higher strength and fatigue crack propagation resistance of the material, which they attributed to the higher crystallinity of the base material [119].

Under extended aging conditions, the wear performance of Vitamin-E stabilized UHMWPE acetabular liners were examined in hip simulator tests. It was compared with standard and highly crosslinked remelted UHMWPE. The standard UHMWPE started to oxidize after two weeks of accelerated aging, the crosslinked UHMWPE after 5 weeks and the Vitamin-E stabilized UHMWPE was oxidation resistant after 6 weeks of accelerated aging. In this study, wear also correlated with oxidation [120].

Aside from Vitamin E, other antioxidants have been studied for use as a stabilizing agent in UHMWPE. These agents are such as nitroxide tempo, anthocyanin extracts and hindered phenol antioxidants. UHMWPE stabilized with hindered phenol antioxidants (HPAOs) has been less widely studied than Vitamin E stabilized UHMWPE.

Die approbierte gedruckte Originalversion dieser Dissertation ist an der TU Wien Bibliothek verfügbar.
The approved original version of this doctoral thesis is available in print at TU Wien Bibliothek.
TU Bibliothek Your knowledge hub WIEN

3.9 Mechanical Properties of UHMWPE

To be sure whether a material is appropriate for a specific use several mechanical properties should be evaluated. The mechanical properties can be figured out by testing the deformation mechanisms of the material. The stress-strain relationship of a material will provide valuable information about its mechanical properties.

Stress-Strain Behavior

The most common measurement of the mechanical properties is testing a relation between stress and strain behavior. It is used to obtain fundamental models of the material's mechanical behavior. In a tensile test, the specimen is subjected to a tensile force that causes deformation in the direction of loading. Engineering stress (σ_E) is defined as the force (F) divided by the original cross-sectional area (A_O), as shown in the following equation:

$$\sigma_E = \frac{F}{A_0} \tag{3.1}$$

Engineering strain (ε, dimensionless) is defined as the change in the length of the sample divided by the original length of the sample, as shown in Equation (3.2):

$$\varepsilon_E = \frac{\delta L}{L_0} \tag{3.2}$$

Engineering stress and strain are applicable when the extension that the material undergoes is very much less than the original length of the sample ($\delta L << L_0$). When this not the case, true stress and strain should be used.

The true stress (σ_T) is defined as the instantaneous load (F(t)) divided by instantaneous cross-sectional area (A(t)). The true strain (ε_T) is defined as the rate of instantaneous increase divided by the instantaneous gauge length.

Figure 3.7 shows a typical engineering-stress vs. engineering-strain curve for a semi- crystalline polymer under tensile loading, with images of the sample at different stages [121]. Elastic modulus can be obtained from the slope of the elastic part, however, in polymeric materials viscoelastic i.e. rate dependent deformation takes place, which often controlled by the amorphous phase [122]. The yield stress is the stress at which plastic deformation occurs. Plastic deformation occurs due to the failure of the weak bonds between the molecular chains in thermoplastic materials. In most semi-

Die approbierte gedruckte Originalversion dieser Dissertation ist an der TU Wien Bibliothek verfügbar.
The approved original version of this doctoral thesis is available in print at TU Wien Bibliothek.
TU Bibliothek Your knowledge hub WIEN

crystalline polymers whitening can be observed during the plastic deformation, which is caused by the reflection of light during the formation of gaps, cracks and failure. Yielding can be affected by temperature and physical properties such as crystallinity, molecular weight and cross-linking [123]. Beyond the yield point, necking occurs, parts (b and c) in Figure 3.7, where the spherulitic structure transforms to a fibril structure [124]. At the end of the neck forming phase (d), neck propagation, or cold drawing, occurs where the molecules align in the direction of loading. Once necking is complete (e), strain hardening starts, where the stress increases until fracture. Polyethylene is a viscoelastic material, and therefore test conditions such as temperature and strain rate can cause significant variations in the mechanical properties [125].

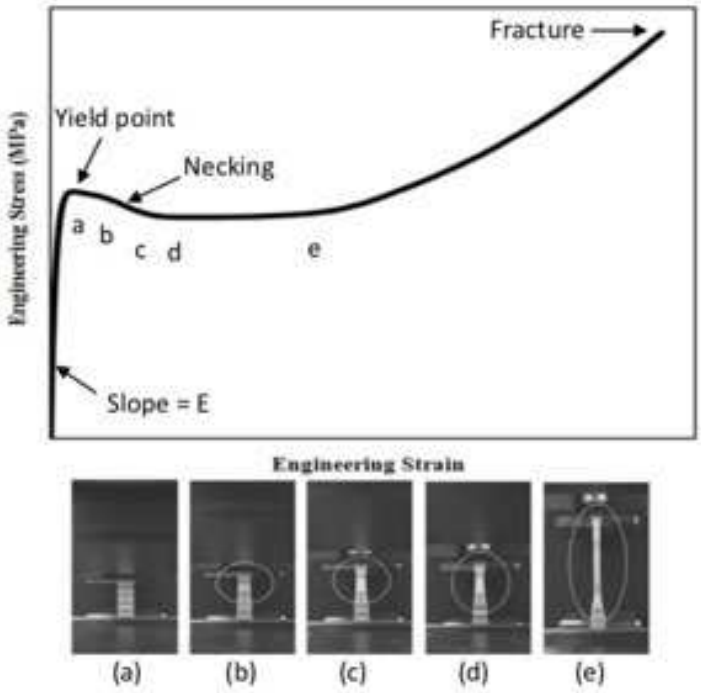

Figure 3. 7 Stress vs. strain curve for PE [121]

Mechanical Deformation of UHMWPE

The mechanical deformation of polymers can occur when external forces applied. After the deforming stress is removed the response of the material can be either elastic or plastic. Elastic behavior is defined when the material returns to its original size and shape. On the contrary, plastic behavior occurs when the material does not return to its original size and shape when the external force is removed [126]. Similarly, the time dependent behavior can be either viscoelastic or

Die approbierte gedruckte Originalversion dieser Dissertation ist an der TU Wien Bibliothek verfügbar.
The approved original version of this doctoral thesis is available in print at TU Wien Bibliothek.
TU Bibliothek Your knowledge hub WIEN

viscoplastic. Viscoelastic deformation is a combination of elastic and viscous behavior, while viscoplastic is a rate dependent plastic deformation. Viscoplastic deformation is a combination of permanent plastic deformation and creep, it is known also as viscoelastic-plastic deformation [127].

Elastic Behavior

After having removed applied load, if the material can be returned to their original size and shape, this is called elastic deformation. In thermosetting polymers show this behavior up to fracture. The elastic modulus can be obtained from the slope of the elastic curve, which is described by Hooke's law ($\sigma = E\ \varepsilon$).

Fundamentally, the mechanism of elastic deformation in polymers is an elongation of chains in the direction of the applied load. In semi-crystalline polymers, elastic behavior occurs when the stress is applied to two adjacent chain-folded lamellae with an amorphous interlamellar phase between them. The material exhibits elongation of the tie chain and slide of the lamellas. The elastic modulus is obtained from the elastic properties of both crystal and amorphous phases. This deformation is reversible when the load is removed [128-130].

Plastic Deformation

Modeling the plastic deformation in semi-crystalline polymers is difficult due to the complexity of the microstructure. To understand the plastic deformation in such polymers, the deformation mechanisms should be categorized at three different scale levels: micro, meso and macro-scale [131]. Tensile and creep tests are generally used to obtain deformation mechanisms such as deformation of crystalline and amorphous phases at the micro-level, deformation of spherulites, bending, rotation and fragmentation of lamellar bulk at the meso-level and the overall polymer deformation at the macro-level.

To better understand polymer plasticity, it is important to know its macromolecular nature. As explained in Chapter 3.2, UHMWPE is a semi crystalline polymer and fundamentally, contains crystalline lamellae embedded in amorphous regions. Tie molecules are parts of the polymer chain that link amorphous and crystalline areas. It is impossible to separate lamella from the adjacent amorphous layer. Thus, concurrently and steady deformation is occurring for lamellae and adjacent amorphous layers and the influence of each deformation on the other cannot be ignored, which increases the complexity of the deformation.

Die approbierte gedruckte Originalversion dieser Dissertation ist an der TU Wien Bibliothek verfügbar.
The approved original version of this doctoral thesis is available in print at TU Wien Bibliothek.
TU Bibliothek Your knowledge hub WIEN

A basic description of the deformation of a semi- crystalline polymer was explained in two stress directions, towards the lamella side and towards the lamella surface, as seen in Figure 3.8 [132]. For the former, the figure shows two adjacent chain-folded lamellae with an amorphous interlamellar phase between them. When the stress is applied, elongation of the tie chain and stretch and slide of the lamellas occur, which is an elastic deformation, as seen in Figure 3.8-1B. At higher stress, plastic deformation begins with the unfolding of lamellas and separation of crystal block segments, as shown in Figure 3.8-1C. This is followed by the orientation of the segments and tie chains in the direction of the tensile stress, Figure 3.8-1D. Similar deformation occurs when the load is applied toward the lamella surface; however, in the elastic region the elongation of the tie chains is combined with contraction of the lamella segments, as seen in Figure 3.8-2B. The plastic deformation starts with separation of crystalline lamella block segments, as shown in Figure 3.8-2C. This is followed by elongation of crystalline lamella to form an aligned morphology, as seen in Figure 3.8-2D.

1) Toward lamellae side:

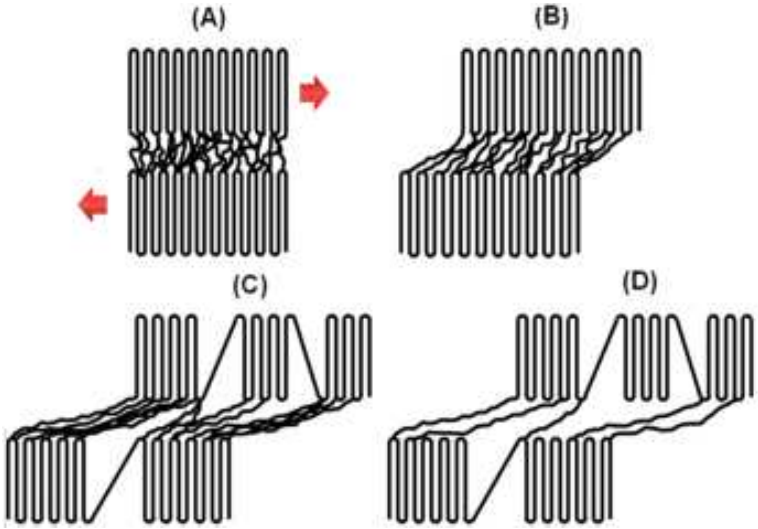

Die approbierte gedruckte Originalversion dieser Dissertation ist an der TU Wien Bibliothek verfügbar.
The approved original version of this doctoral thesis is available in print at TU Wien Bibliothek.

2) Toward lamellae surface:

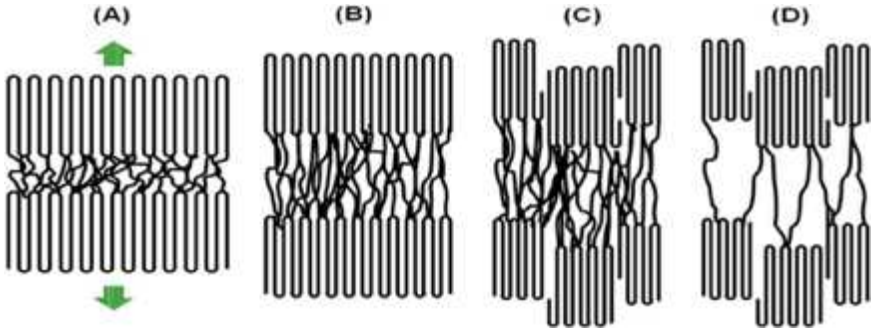

Figure 3. 8 Schematic diagrams of the deformation in semi-crystalline polymers in different stress directions [132]

Although numerous studies have been executed to better understand the plastic deformation of semi-crystalline polymers, a comprehensible explanation has not been found yet.

Die approbierte gedruckte Originalversion dieser Dissertation ist an der TU Wien Bibliothek verfügbar.
The approved original version of this doctoral thesis is available in print at TU Wien Bibliothek.
TU Bibliothek Your knowledge hub WIEN

Chapter 4: Tribology and Its Influence on Hip Replacement

4.1 Tribology Behavior of UHMWPE

Tribology is important concepts for the development of UHMWPE as a bearing material in THR. The word tribology, originated from the Greek word "tribos" meaning rubbing, can be defined as interdisciplinary science and technology related to friction, wear and lubrication. The tribology part is related to developing and improving surfaces that have low friction and high wear resistance for engineering applications. In 1960s, tribological behavior of polymers has been studied. Much research has been carried out on the tribology of polymers and its application in various industries with the application of polymers for tribological purposes increasing and extending into even more new areas [133]. Wear is the process of material loss from two contacting bodies. As being mentioned before, wear of UHMWPE is the major cause of failure in joint replacements.

Historically in-vitro wear test was carried out by Charnley in 1960 with metal-on-UHMWPE. After that, wear tests have been used to better understand the wear and wear mechanisms. Primitive wear simulators were various in their method of motion, however, these simulators only used unidirectional motion on the test components. Thus, yielding wear rates significantly lower than the rates observed in-vivo [83, 134, 135]. From these results emerged the importance of multidirectional motion in the wear of UHMWPE in-vivo, with the addition of multidirectional motion to wear tests delivering wear rates comparable to those observed in-vivo [136]. The importance of multidirectional motion in the wear of UHMWPE is related to the cross shear and aspect ratio values of the wear track. Turell et.al indicated if using UHMWPE as a bearing material in-vivo, differences in gait patterns of an individual could produce different wear factors as a result of the cross shear and aspect ratio values of the resulting wear track [137]. The increasing aspect ratio is shown to increasing wear rates of virgin UHMWPE up to a critical value. It was found the wear rate of highly crosslinked UHMWPE (90 kGy) to be unaffected by increasing aspect ratio [138]. The effect of the crosslinking of UHMWPE is expressed before in chapter 3.7.

There are several types of wear that are important in hip replacements. These are abrasive wear, adhesive wear and fatigue wear, is seen in Figure 4.1 [139]. Wear mechanisms are the processes that cause wear and damage to the UHMWPE.

Die approbierte gedruckte Originalversion dieser Dissertation ist an der TU Wien Bibliothek verfügbar.
The approved original version of this doctoral thesis is available in print at TU Wien Bibliothek.
TU Bibliothek Your knowledge hub WIEN

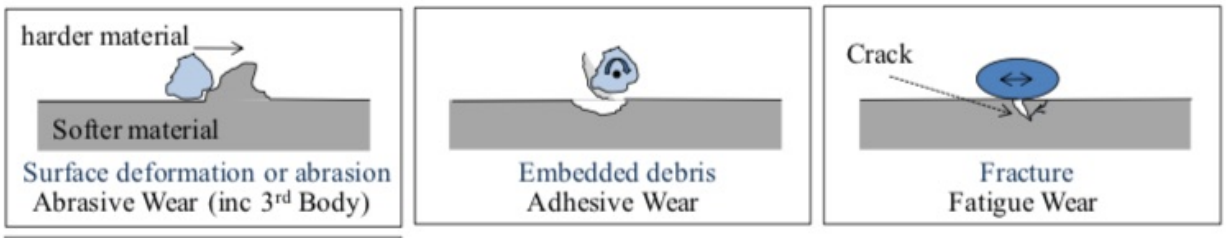

Figure 4. 1 Schematic of wear types that is important for hip implants

4.1.1 Abrasive Wear

Abrasive wear occurs where one‘s asperities or a third body particle forced against and move along a solid surface contact. Due to hardness differences between surfaces, abrasive wear is observed on both surfaces (this means, both surfaces are being subjected to abrasive wear). The surface abrade rate depends on the characteristics of each surface, the presence of abrasives between the first and second surfaces, the speed of contact and other environmental conditions. Abrasive wear results in the softer material being removed from the track traces by the asperity during the motion of the harder surface.

Abrasion is typically classified according to types of contact, as well as contact environment. There are two types of contact which includes two-body and three-body wear. The former occurs when an abrasive slide along a surface, and the latter, when an abrasive is caught between one surface and another. Two-body systems typically experience from 10 to 1000 times as much loss as three-body systems for a given load and path length of wear. Abrasion is often further categorized as being low stress abrasion, high-stress abrasion, gouging abrasion, and polishing abrasion, which are shown in Figure 4.2. Each of these forms of abrasion is characterized by varying amounts of surface or subsurface damage [140].

Die approbierte gedruckte Originalversion dieser Dissertation ist an der TU Wien Bibliothek verfügbar.
The approved original version of this doctoral thesis is available in print at TU Wien Bibliothek.

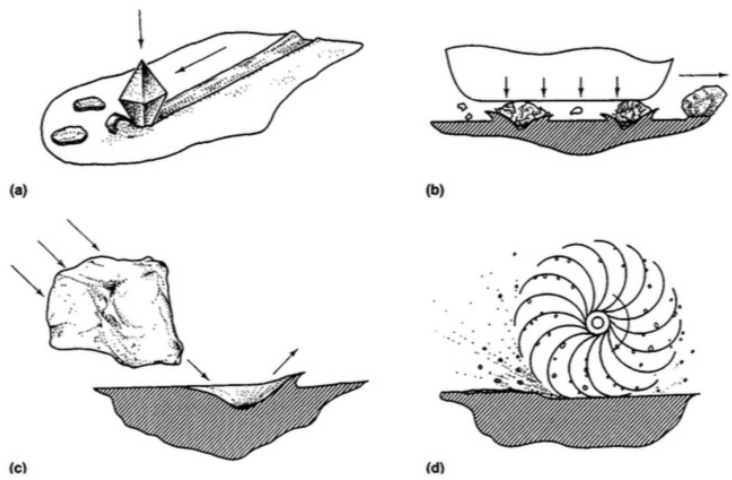

Figure 4. 2 Four types of abrasive wear; (a) low stress abrasion, (b) high-stress abrasion, (c) gouging abrasion, and (d) polishing abrasion [140]

Scratching i.e. low-stress abrasion, is defined as wear that takes place an indicator to relatively light rubbing contact of abrasive particles with the metal. The criteria constructed for low-stress abrasion is that the forces must be low enough to prevent crushing of the abradant. Wear scars usually show scratches, and the amount of subsurface deformation is minimal. Consequently, the surface does not work harden significantly.

High-stress abrasion is a wear under a level of stress that is high enough to crush the abrasive. Considerably more strain hardening of the metal surface occurs.

The gouging abrasion is used to describe the high-stress abrasion that results in great grooves or gouges on the worn surface. Strain hardening and plastic deformation are the dominant factors.

Polishing wear is an extremely mild form of wear for which the mechanism has not been clearly identified, but that may involve extremely fine-scale abrasion, plastic smearing of micro-asperities, and/or chemical corrosion. Surfaces that have been subjected to polishing wear are usually smoothed and brightened, but this smoothing or brightening requires material removal [140].

4.1.2 Adhesive Wear

Adhesive wear is when asperities in a contact form a bond, known as an adhesive junction; as the surfaces slide apart the adhering material may be pulled away from its main surface [141]. The removed material may stay attached to the second surface or be released as a wear particle. In

Die approbierte gedruckte Originalversion dieser Dissertation ist an der TU Wien Bibliothek verfügbar.
The approved original version of this doctoral thesis is available in print at TU Wien Bibliothek.
TU Bibliothek Your knowledge hub WIEN

severe cases of adhesion, extremely large volumes of material may become unattached, creating macroscopic sized wear debris [142, 143].

Adhesive wear process progresses in formation of adhesion junction, its growth and fracture. A distinguishing feature of this wear is that transfer of material from one surface to another occurs due to localized bonding between the contacting solid surfaces. Adhesive wear shows a wearing action in which no specific agency can be identified as the cause of the wear. Adhesion was accepted in the 1930s to be a major contributor to sliding resistance (friction). Adhesion is not the cause of wear, but only the consequence of contact. Wearing occurs when interfaces in contact are made to slide and the locally adhered regions must separate. This separation may occur by one or two of the failure modes of solids, resulting in a very wide range of wear rate. The reason of defining and studying specific wear modes is to find ways to make longer the wear life of sliding systems. Each mode of wear can be resisted by the proper choice of material, lubricant, and method of operation [140].

The phenomenon of friction transfer is observed for nearly all materials (metals, ceramics, and polymers) and their combinations. A significant thing is whether the transfer produces an influence on the tribological behavior of the friction couple. At this stage, the consequences of material transfer may be more visible. If small particles of micrometer size are transferred from one surface to the other, then the wear rate varies only a small extent. Under certain conditions, the situations occur when thin film of soft material is transferred onto the hard-mating surface, e.g., MoP. The transfer of polymer is the most important characteristic of adhesive wear for polymers. The transferred polymer fragment may exhibit a wide variety of forms depending on polymer properties and friction conditions or changes in roughness of both surfaces in contact [144]. Within the majority of polymers-on-polymer and polymer-on- metal interactions, the attractive forces that create these adhesive junctions are hydrogen bonds and Van der Walls forces [144].

4.1.3 Fatigue Wear

Fatigue wear is caused by the cyclic loading when a local stress exceeds the fatigue strength of the material. The cyclic stressing of material causes small cracks to propagate and accumulate [144]. A similar process occurs at friction accompanying nearly all the wear modes. A friction contact undergoes the cyclic stressing at rolling and reciprocal sliding. In addition, each asperity of friction surface experiences sequential loading from the asperities of the counter surface. In consequence,

Die approbierte gedruckte Originalversion dieser Dissertation ist an der TU Wien Bibliothek verfügbar.
The approved original version of this doctoral thesis is available in print at TU Wien Bibliothek.
TU Bibliothek Your knowledge hub WIEN

two varying stress fields are produced in surface and sub-surface regions with different scales. These fields are responsible for material fatigue in these regions that lead to the generation and propagation of cracks and the formation of wear particles. This process is named friction fatigue. Unlike the bulk fatigue, it extends only surface and sub-surface regions. The loss of material from solid surfaces due to friction fatigue, is referred to as fatigue wear. It has been known that the fatigue cracks are initiated at the points where the maximum tangential stress or the tensile strain takes place. The theoretical and experimental studies show that under contact loading the maximum tangential stress position is dependent on friction of coefficient [144]

If the stress field exceeds the yield stress and fatigue limit of the material it can cause structural fatigue after relatively few cycles. This wear process otherwise known as delamination can produce large amounts of wear debris but is much more common in total knee replacements than total hip replacements [145, 146].

The understanding of the tribology of UHMWPE is important for the development of a low-wearing, longer lasting bearing material in total hip replacements. The tribology of two contacting surfaces is highly based on the surfaces microscopic structure and properties, texture, and the lubricant between them.

4.2 Hip Joint Motion

The "ball in socket design" of the hip joint allows the head of the femur to rotate inside the socket of the acetabulum, resulting in three degrees of freedom movement in three planes: flexion-extension in the sagittal plane, abduction-adduction in the coronal plane, and inward-outward rotation in the transverse plane, is shown in Figure 4.3.

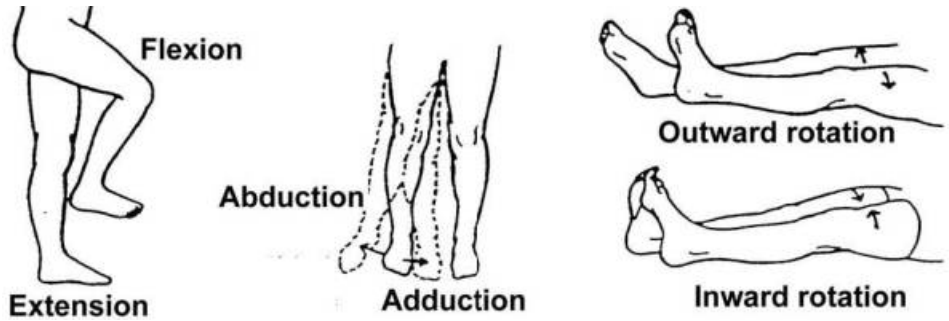

Figure 4. 3 Anatomic movements for the hip joints

Die approbierte gedruckte Originalversion dieser Dissertation ist an der TU Wien Bibliothek verfügbar.
The approved original version of this doctoral thesis is available in print at TU Wien Bibliothek.
TU Bibliothek Your knowledge hub WIEN

The hip joint could carry seven to eight times more weight by the help of the ball in socket design and could move extensively [147]. The hip joint has three degrees of freedom i.e. flexion-extension (ω_x), lateral-medial rotation (ω_y) and abduction-adduction (ω_z) and is loaded in three axes during its movement, W_x, W_y, W_z (Figure 4.4). These loads could reach up to 2 to 5 times of the body weight during gait cycle [148].

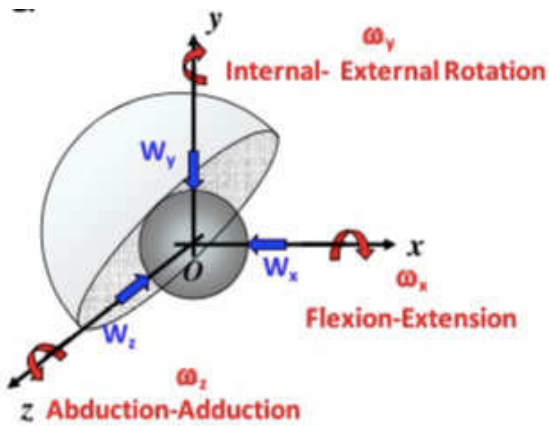

Figure 4. 4 Effected loads and movements on the ball in socket geometry

Genda et. al. has calculated the pressure on hip joint as 1.67 MPa for women and 1.38 MPa for men. Genda attributes the difference in pressure to different femur head diameters in women and men. the femur head diameter was measured as 23.8 mm for women and 26.0 mm for men in the same study. Daily activities such as walking, climbing up the stairs and running also changes the pressure on the hip joint [149].

4.3 Contact Mechanics

A contact area is evolved when two bodies contact each other, under load. Contact area and contact stress are important to solve the contact problems. This is an important factor to design the hip implant because the contact stress should not exceed the strength of the contact area to prevent rapid fatigue failure. Bartel et. al. reported by using the finite element method that the maximum principal stress within the UHMWPE during normal walking less than 10 MPa for hip replacement and 45 MPa for knee replacement [150]. The yield strength of UHMWPE is 21-28 MPa [151] and when the UHMWPE materials are subjected to high contact stresses then it can exceed its yield strength.

Die approbierte gedruckte Originalversion dieser Dissertation ist an der TU Wien Bibliothek verfügbar.
The approved original version of this doctoral thesis is available in print at TU Wien Bibliothek.
TU Bibliothek Your knowledge hub WIEN

It has been found for UHMWPE; an increase in thickness and conformity leads to a decrease in the stress [150]. This was an important criterion in designing the rim sleeve with polyethylene however failing of UHMWPE due to the oxidation and reduction of fatigue strength rather than contact stress. In this regard, recent studies show the less contact and conformity in polyethylene can result in a reduction of the wear rate if the polyethylene has enough strength and stress is not excessive [152].

Hertz contact theory is an analytic method to solve the contact mechanics problems in the hip implant. Theoretically, the nominal contact area is considered to be the smooth surface of the bearing. While the real contact area includes roughness and asperity of the contact area that should be measured with sensor or pressure sensitive film [153]. When any two curved surfaces contact each other, the contact initiates with a point or along a line. With a small load, elastic deformation spreads these into contact areas and the load is distributed as a pressure. This is first explained by Hertz in 1881 [154] based on four assumptions, which are:

- Material should be homogeneous, isotropic and linear elastic
- Contact surfaces should be smooth and frictionless
- Contact surfaces should be continues and non-conformed
- Contact radius should be much smaller than radius of the surfaces is in contact.

Die approbierte gedruckte Originalversion dieser Dissertation ist an der TU Wien Bibliothek verfügbar.
The approved original version of this doctoral thesis is available in print at TU Wien Bibliothek.
TU Bibliothek Your knowledge hub WIEN

Chapter 5: Samples & Experimental Techniques

A total 20 explants (2 conventional, 18 cross-linked) and commercial engineering polymers blocks (GUR 1020, GUR 1020 Vit. E and GUR 1050) are investigated. The explants were provided by the Universitätsklinik in Innsbruck. Additionally, the data of eighteen more explants which were subjected to same measurement methods by our colleagues [155] and received from the same clinic were included for a better comparison. All available information including retrieval reasons of explants as declared by surgeons is shown in 5.1. Each explant has its own acronym like KOR, ZAW etc. for ease of identification.

Die approbierte gedruckte Originalversion dieser Dissertation ist an der TU Wien Bibliothek verfügbar.
The approved original version of this doctoral thesis is available in print at TU Wien Bibliothek.
TU Bibliothek Your knowledge hub WIEN

Table 5. 1 Investigated conventional and cross-linked explants

Explant number	Acronym	Type	In-vivo time (months)	Producer	Gender F/M	Age	BMI	Reason of retrieval
Formerly Studied								
1	KIR/XLBiomet Arcom	Conv.	19	unknown	F	53	-	Infection
2	GIE/sandwich	Conv.	120	unknown	F	53	-	Infection
3	BUC/sandwich	Conv.	132	unknown	F	74	-	Wear
4	KOR	Conv.	276	unknown	M	56	-	Loosening
5	ZAW	Conv.	58	unknown	F	85	-	Loosening
6	REOP	Conv.	204	unknown	M	-	-	Eccentricity
7	MAS	Conv.	unknown	unknown	F		-	unknown
8	BIN	Conv.	unknown	unknown	M	86	-	Infection
9	BAS	Conv.	unknown	unknown	M	-	-	unknown
10	TSCH	Cross-linked (XL)	0.3	Zimmer	F	62	-	Fracture
11	KLOI	XL	0.5	Zimmer	F	66	-	Infection
12	WEG	XL	0.6	Zimmer	M	77	-	Malposition
13	BEH	XL	1	Zimmer	F	62	-	Infection
14	GAN	XL	10	Zimmer	F	84	-	Infection
15	FIN	XL	12	Stryker	F	64	-	Loosening
16	RIE	XL	16	Zimmer	M	54	-	Infection
17	LAP	XL	58	unknown	F	-	-	Loosening
18	STE	XL	84	S&N	M	-	-	Loosening
New Explants								
1	AUMA	Conv.	372	unknown	F	-	-	Fracture
2	GOKA/sandwich	Conv.	204	unknown	M	-	-	Wear
3	PLWI	XL	1.5	Stryker	F	76	24.80	Infection
4	TRCH	XL	12	Stryker	F	72	38.10	Infection
5	LAMA1	XL	36	Stryker	F	73	27.30	Infection
6	LAMA2	XL	1.07	Stryker	F	73	27.30	Infection
7	LOPE	XL	6.36	Medacta	M	66	22.10	Infection
8	JEJO	XL	24	Zimmer	M	67	31.40	Sepsis
9	WIRU	XL	60	DePuy	M	68	-	Infection
10	STEL	XL	172	DePuy	M	70	24.40	unknown
11	LUIN	XL	180	DePuy	F	73	32.60	Wear
12	KOEV	XL	156	Link	F	79	-	Wear
13	MAWO	XL	288	DePuy	M	78	26.37	unknown
14	MÜCL	XL	156	DePuy	F	59	-	Wear
15	VOST	XL	252	DePuy	M	63	27.08	Wear
16	GIWA	XL	192	DePuy	F	82	22.43	Wear
17	GLFR	XL	180	DePuy	M	71	33.69	Wear
18	SCME	XL	168	DePuy	F	65	31.83	Wear
19	FADA	XL	7	unknown	F	65	28.70	Infection
20	GRMA	XL	24	unknown	F	68	21.72	Infection

Die approbierte gedruckte Originalversion dieser Dissertation ist an der TU Wien Bibliothek verfügbar.
The approved original version of this doctoral thesis is available in print at TU Wien Bibliothek.
TU Bibliothek Your knowledge hub WIEN

Table 5.2 shows the number of retrieved explants per reasons of retrieval. Infection has the most share of early retrieval reasons (9 days to 2 years) and is mostly attributed to hygienic conditions during surgery [156, 157]. Among other retrieval reasons, loosening, wear, and fracture can be attributed to material properties. The reason of including explants which have short in-vivo times, up to a year, is to have a better comparison of the morphological and micromechanical properties of the same implant type and model during short and long term in-vivo performance.

Table 5. 2 Absolute values by complications

Reasons of retrieval	**Number of retrieved explants**
Infection	15
Wear	9
Loosening	5
Eccentricity	1
Fracture	2
Malposition	1
Sepsis	1
Unknown	4

The samples used in the tests can be grouped into two. The first group is the explants which could also be sub-grouped as conventional and first- and second- generation cross-linked (XL) types. The second group of materials is the virgin commercially available engineered polymers which are GUR 1050, GUR 1020 and GUR 1020 with Vitamin E from the company Ticona (Oberhausen, Germany). Table 5.3 summarizes the commercial brand names, resin types, thermal treatment methods, sterilization methods, crosslinking types and the irradiation doses of the cross-linked explant samples. Similar data is not available for the conventional samples.

Die approbierte gedruckte Originalversion dieser Dissertation ist an der TU Wien Bibliothek verfügbar.
The approved original version of this doctoral thesis is available in print at TU Wien Bibliothek.
TU Bibliothek Your knowledge hub WIEN

Table 5. 3 Manufacturing properties of cross-linked UHMWPE explants

Brand Name of the explants	# of samples	Resin Type	Thermal Treatment	Sterilization Method	Generation	Irradiation Dose (kGy)
Durasul®(Dsa)/ Zimmer	7	GUR 1050	Remelted (150 ^{0}C for 2 h)	Ethylen oxide (EtO)	1st generation	95
Marathon™/ DePuy	9	GUR 1050	Remelted (155 ^{0}C for 24h)	Gas plasma	1st generation	50
XLPE™/S&N	1	GUR 1050	Remelted (147 ^{0}C at least 5 h)	EtO	1st generation	100
Mpact/Medacta	1	GUR 1020	Remelted (150 ^{0}C)	EtO	1st generation	100
Crossfire/Stryker	1	GUR 1050	Annealed (130 ^{0}C)	Gamma	1st generation	75
X3™/Stryker*	4	GUR 1020	Annealed	Gamma	2nd generation	90
X-LINKed/Link**	1	GUR 1020	-	EtO	2nd generation	75

*: X3™/Stryker, 30 kGy of gamma irradiation followed by annealing. Each step is repeated three times. The cumulative radiation dose is 90 kGy.

**: X-LINKed is sintered at high pressure to form sheets then turn into rods, which are finally gamma irradiated. A 5 mm layer is then shaved off the entire surface to remove the oxidized outer skin. Hence, its mechanical properties are maintained.

The lack of component specific information, in particular the conventional explant details (producer, resin type, sterilization method, atmospheric conditions used, etc.) is a limitation of the study. Despite the lack of information regarding specific components, it is known that the use of calcium stearate reduced significantly by 1998 due to improved processing techniques. On the market the most employed UHMWPE powder grades are produced by Ticona (Oberhausen, Germany) and they stopped using it in 2002. In our study AUMA, GOKA, KOR and REOP were produced before the year of 1998.

Die approbierte gedruckte Originalversion dieser Dissertation ist an der TU Wien Bibliothek verfügbar.
The approved original version of this doctoral thesis is available in print at TU Wien Bibliothek.
TU Bibliothek Your knowledge hub WIEN

The methodology in which the components were sterilized (gamma irradiation in air or reduced/inert atmosphere) is important but unknown. However, orthopedic companies stopped gamma irradiating UHMWPE components in air in 1998 at the latest [83]. Analysis of the time components have been implanted for indicates that there are only 4 explants (AUMA, GOKA, KOR and REOP) in this study that might have been gamma irradiated in air. For all the explants, the amount of time that they were stored on the shelf prior to implant is unknown. Shelf life is defined as the period of time between when the implant is sterilized and packaged and when it is inserted into the patient [158]. UHMWPE acetabular components generally have a five-year shelf life following sterilization [83]. Based on the amount of time components AUMA, GOKA, KOR and REOP had been implanted for (31, 17, 23 and 17 years respectively).

5.1 Optical Damage Scoring

Optical evaluation on all retrieved acetabular cups was performed, and the total damage score was obtained as proposed by Hood et al. [159]. The articulating (inner) and backside (outer) surfaces of explants were sub-divided into four regions and damage scores were observed for each region using a stereomicroscope (Zeiss Stemi 2000-C, Germany). Total damage scores of surface degradation were obtained by observing scratching, pitting, burnishing, embedding debris, abrasion, deformation and delamination [159] and summing up scores of inner and outer surfaces. The highly burnished zones were designated as the highly loaded zones and further used in this study. A sample of damage score analyze data sheet is in APPENDIX B.

The presence and degree of each damage mechanism was graded on a scale of 0 to 3 depending on the percentage coverage of the quadrant (Table 5.3). Then points were summed up, the final results for the inner and the outer one are presented.

Die approbierte gedruckte Originalversion dieser Dissertation ist an der TU Wien Bibliothek verfügbar.
The approved original version of this doctoral thesis is available in print at TU Wien Bibliothek.
TU Bibliothek Your knowledge hub WIEN

Table 5. 3 Scoring system for assessing damage mechanisms on explant bearing surfaces and rims

Damage Score	Extend of Damage
0	No sign of damage
1	Covered less than 20% of surface
2	Between 20-50%
3	More than 50% of investigated area

The evaluator's perception of severity was also taken into account in the final score. For example, if the damage mechanism only covered 10% of the surface but was considered to be particularly severe, this may have scored as highly as small scratches over more than 50% of the surface. The total possible score for each subdivision was 24, which equates to 48 for each quadrant and 192 for the whole acetabular liner.

5.2 Structural and Physical Properties

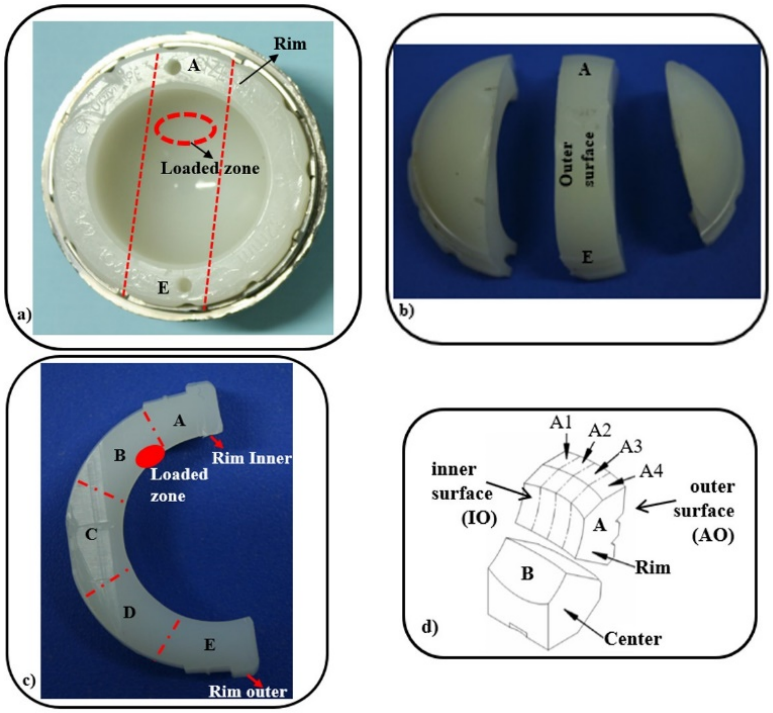

Figure 5. 1 a) hip explant; b) explant cut into three pieces; c) cross-sectional view of explant; d) sample preparation of rim and center parts for tests

Die approbierte gedruckte Originalversion dieser Dissertation ist an der TU Wien Bibliothek verfügbar.
The approved original version of this doctoral thesis is available in print at TU Wien Bibliothek.
TU Bibliothek Your knowledge hub WIEN

The results of optical damage scoring were used to determine the highly loaded zones because highly loaded zones manifest themselves as the most burnished and worn zones (Figure 5.1 (a)). The explants were first vertically cut into pieces by using an electrical or manual saw as shown in Figure 5.1 (b) with the preselection of the highly loaded zone piece to use for FTIR and DSC tests. Cross-sectional view of explant after cutting is shown in Figure 5.1 (c). Before establishing the above standard procedure, all pieces i.e. without preselection of a piece (from A,B,D and E parts) were microtomed and further subjected to the FTIR test to check if non-selected pieces are as oxidized as the highly loaded piece. The results showed that highly loaded pieces were more oxidized.

The selected piece was then cut into two pieces as shown in Figure 5.1 (d) so called rim and center by using a stanley knife. Each rim and center pieces were cut into four equal final pieces. One of these pieces was microtomed from inner to outer surface and one other piece was microtomed from outer to inner surface as for some explants the contact zones could be closer to the outward surface. These two sub-pieces of both from rim and center parts were used for FTIR and DSC measurements. The other two remaining pieces were used for DSI testing. All results of FTIR and DSC measurements were reported in this study, however rim inner i.e. Rim IO results were mostly used for comparison purposes because more oxidation was observed in these regions.

5.2.1 Fourier Transform Infrared Spectroscopy

It is a well-known technique that has commonly been used to investigate chemical changes in UHMWPE [111, 160-163]. FTIR imaging differs from conventional equipment in a number of ways but the important one is that it is fitted with a precise sample positioning stage. This enables the user to accurately map the chemical properties of a sample at high resolution. Changes to UHMWPE specimen chemistry are analyzed using FTIR spectroscopy. IR uses molecule absorption at specific wavenumbers. Various vibrational modes are IR active, such as symmetrical and anti-symmetrical stretching, rocking, wagging and scissoring of the bond between two atoms. The absorption data for UHMWPE specimens is collected in transmission mode through a thin film of the material.

A Tensor 27 (Brucker Optics, Ettlingen, Germany) was used to carry out FTIR imaging on specimens from retrieved UHMWPE components. Samples used for FTIR analysis are microtomed

Die approbierte gedruckte Originalversion dieser Dissertation ist an der TU Wien Bibliothek verfügbar.
The approved original version of this doctoral thesis is available in print at TU Wien Bibliothek.
TU Bibliothek Your knowledge hub WIEN

by trimming material with a 180 µm thickness from the surface through the bulk material. It was therefore, obtained a depth profile of approximately 5 mm. The UHMWPE slices were moved using tweezers in order to prevent contamination. They were then placed in individual labelled bags for storage. Specimens were held in a magnetic slide with a pinhole of sample holder that slotted into a sample holder on the machine. Before conducting each test, an assessment of background absorption was carried out. Background IR data was subtracted from the spectra obtained from the sample and the resulting spectra were normalized to the reference peaks known to be non-sensitive to the effects of radiation are 1370 cm^{-1} and 2022 cm^{-1} in order to standardize against thickness variations [164].

A transmission with 16 scans is collected a resolution of 4 cm^{-1} and with data collection from 4000 cm^{-1} to 400 cm^{-1}.

Analysis of the intensity of the carbonyl groups such as ester (1738 cm^{-1}), carbonacid (1713 cm^{-1}) and ketones (1720 cm^{-1}) have been shown to give a good indication of the post-irradiation oxidation of UHMWPE [160, 162, 165, 166].

The FTIR absorbance data are processed by the OPUS 6.0 software. Every FTIR transmission data point for specific bands of interest; 1305 cm^{-1}, 1370 cm^{-1}, 1720 cm^{-1}, 1740 cm-$^{-1}$and 1896 cm^{-1}, was exported to MS Excel in order to calculate oxidation values and hence generate graphs of the variation in properties with depth. The integration limits were checked in each spectrum.

According to ASTM F 2102 the oxidation index and is defined as the ratio of the area of the carbonyl absorption peak centered near 1720 cm^{-1} (A_{1720}) to the area of the absorption peak centered near 1370 cm^{-1} (A_{1370}) [167].

$$OI = \frac{A_{1720}}{A_{1370}} \tag{5.1}$$

The degree of crystallinity was determined according to Costa et al. and Dalborg et.al [165, 168] by relating the area of the crystalline band at 1896 cm^{-1} (A_{1896}) with the area of the amorphous band at 1305 cm^{-1} (A_{1305}) using the following formula

$$X_{FTIR} = \left(\frac{\left(\frac{A_{1896}}{A_{1305}}\right)}{\left(\frac{A_{1896}}{A_{1305}}\right)+0{,}25} \right) . 100 \tag{5.2}$$

Die approbierte gedruckte Originalversion dieser Dissertation ist an der TU Wien Bibliothek verfügbar.
The approved original version of this doctoral thesis is available in print at TU Wien Bibliothek.
TU Bibliothek Your knowledge hub WIEN

According to ASTM F 238 the trans-vinylene index TVI was calculated. The concentration of vinylene double bonds in UHMWPE is a function of the absorbed radiation dose [48]. Therefore, TVI can be used to confirm that components had been irradiated and furthermore to control the irradiation process. The number of trans-vinylene-groups in UHMWPE is expressed by the trans-vinylene-index which can be calculated as the ratio of the absorption area at 965 cm^{-1} (A_{965}) to the absorption peak area at 1370 cm^{-1} (A_{1370}).

$$TVI = \frac{A_{965}}{A_{1370}} \tag{5.3}$$

Terminal-Vinyl-Index (TV) The terminal-vinyl-group is a double bond at the end of a polymer chain which absorption peak can be seen at a wavenumber of 909 cm^{-1} in the spectra. Terminal-vinyl-group concentration decreases with irradiation. Moreover, this decrease is associated with the formation of Y-crosslinks [74].

The calculation can be done according to formula 3.4.

$$TermVI = \frac{A_{909}}{A_{1370}} \tag{5.4}$$

5.2.2 Differential Scanning Calorimetry

DSC is a technique used to study the thermal transition properties of a material by measuring the difference in energy input into a sample and a reference material over a specified temperature range. DSC is markedly more popular in both research and industry than other comparable thermal analysis techniques, although it is not the oldest technique. The popularity of the DSC method is derived from the almost universal interest of the technique to applications where the characterization of any physical or chemical change that takes place with an exchange of energy as heat [169].

The thermal properties and crystallinity of UHMWPE are measured by DSC according to ASTM 2625 [170]. The crystallinity of a polymer sample is measured by the difference in heat flow between the sample and an empty reference pan as the temperature is increased or decreased across the sample's melting point, T_m, or the glass transition temperature, T_g. For UHMWPE, the T_g is -122 ± 2°C [171] hence, the polymer exhibits plastic flow rather than being glassy (as below the T_g). A typical DSC experiment measures the melting of UHMWPE crystals the T_m (for first and

Die approbierte gedruckte Originalversion dieser Dissertation ist an der TU Wien Bibliothek verfügbar.
The approved original version of this doctoral thesis is available in print at TU Wien Bibliothek.
TU Bibliothek Your knowledge hub WIEN

second heating run) and then cooling to measure the crystallization temperature T_c, onset crystallization temperature $T_{c,\ onset}$ and enthalpy of melting $\Delta H_{endotherm}$ for both heating runs.

Each run of heating and cooling cycles identifies different polymer properties. The first melt determines crystallinity and T_m due to thermal processing of the specimen. Cooling from the melt at a standard rate recrystallizes the polymer. A second melting cycle measures the structural polymer properties by erasing the thermal history.

A DSC Q2000 Differential Scanning Calorimeter is used. Having measured the samples by FTIR means, the same samples were then used for DSC investigations. Each sample had a mass of between 1 and 2 mg and crimped in a standard aluminum DSC pan and lid. This sample pan is placed in the DSC with an empty reference pan. Nitrogen (50 ml/min) is used to purge the system before and during measurements. The following thermal cycles are used:

First heat: 0°C to 200°C at 10 K /min, held at 200°C 5 minutes

Cool: 200°C to 0°C cooled at 10 K /min, held at 0°C 5 minutes

Second heat: Repeat first heat and then quench to room temperature

To measure the $\Delta H_{endotherm}$, a flat baseline is extrapolated from 60°C to 180°C and the area under the curve is integrated and ΔH_f, 100 % crystalline UHMWPE, is 291 J/g [74]. The degree of crystallinity, X_{DSC} (%), is calculated using the formula:

$$X_{DSC} = \frac{\Delta H_{endotherm}}{\Delta H_f} . 100 \tag{5.5}$$

Statistical analysis is performed with a TA analysis software.

The lamellar thickness distribution in crystalline polymers is an important factor when interpreting macroscopic properties. Differences in lamellar size distribution may explain remarkable differences in thermal and mechanical properties. Lamellar thickness was calculated via Thomson-Gibbs equation.

$$T_m = T_m{}^o (1 - \frac{2\sigma_e}{L_c \Delta H_f}) \tag{5.6}$$

The thickness distribution is expressed by the following equation [172, 173]

Die approbierte gedruckte Originalversion dieser Dissertation ist an der TU Wien Bibliothek verfügbar.
The approved original version of this doctoral thesis is available in print at TU Wien Bibliothek.
TU Bibliothek Your knowledge hub WIEN

$$\frac{1}{M}\frac{dM}{dL} = \frac{dE}{dT}\frac{(Tm^0 - Tm)^2 \rho_c}{2\sigma_e T_m^o M} \tag{5.7}$$

Sample dependent parameters are:

T_m: observed melting temperature of the sample [K]; L: lamellar thickness [nm]; dM: mass of crystalline phase that has a lamellar thickness between L and L+dL and melts between T and T+dT [kg]; dE/dT: the energy necessary to melt the crystalline mass dM in the temperature range between T and T+dT

Constant parameters for polyethylene are:

T_m^o: equilibrium melting temperature of an infinitely thick crystal, T_m^o = 418,15 K [173]

σ_e – surface-free energy per unit area of the basal face, σ_e = 90 mJ/m²

ρ_c– crystalline density, ρ_c = 967 kg/m³ [172]

ΔH_f - theoretical heat of fusion of an ideal polyethylene crystal by unit volume, ΔH_f = 291 J/g [174].

5.2.3 Swelling of Crosslinked Networks

To calculate degree of cross-linking in polymer networks, the swell ratio analysis is used. We applied this method to make sure if examined samples are crosslinked or not. This method was used to understand whether some explants (there was no information in patient report form) cross-linked or not. Tabulated data is shown in APPENDIX C.

Swelling is a thermodynamic phenomenon, which can be considered as the mixing of a polymer and solvent, resulting in deformation of the polymer network [175]. The thermodynamics of liquid mixtures can therefore be extended to swollen polymers.

On immersion, such a crosslinked structure should not dissolve completely in the solvent but may absorb a large quantity of it. Swelling occurs through the interaction of the solvent with the polymer chains, similar to linear polymers forming an ordinary polymer solution, to form an elastic solution (or swollen gel) rather than a viscous one. The added volume of the polymer throughout which the solvent may spread affords an opportunity for increases in entropy, termed the entropy of dilution, which may be increased or decreased by the heat of dilution. As swelling proceeds, the chains between network junctions become elongated and an opposing force develops similar to the elastic retractive force in rubber. A state of equilibrium is eventually reached when both these forces are

Die approbierte gedruckte Originalversion dieser Dissertation ist an der TU Wien Bibliothek verfügbar.
The approved original version of this doctoral thesis is available in print at TU Wien Bibliothek.
TU Bibliothek Your knowledge hub WIEN

balanced. According to Kurtz et al. [74] steady state is achieved after approximately 1 hour in o-xylene at 135 °C. In this study calculation was done according to ASTM D2765-01 [176].

Samples were cut into cube pieces using a Stanley knife and a razor blade, usually of approximately 2.5 x 2.5 x 2.5 mm^3 and an approximate mass of 15 mg. Moreover, vials were prepared with a Polytetrafluorethene PTFE gasket in the cover of each vial. The PTFE is solvent resistance and has an impermeability. The mass of the empty vials and the mass of the cubes was determined by using an accurate microbalance (±0.01 mg). The masses were recorded and summed up for each sample to obtain the mass of unswollen state sample. The swelling experiments were performed using o-xylene as a solvent mixed with 0.8 mass % of 2,2'-Mehtylene-Bis (4-methyl-6-tertiary butyl phenol) (Irganox 1010, Fa. Ciba), added as an antioxidant. After weighing, the cubes were put into labeled glass (pyrex) tubes and filled with 2.5 ml of xylene. Afterwards the tubes containing the solvent and sample were placed in a preheated silicone oil bath and kept at 135 °C for two hours to allow each sample to swell in the hot xylene. After two hours the swollen samples were removed from the glass tubes. Having dried cubes, they were placed in the pre-weighted vial. The vials containing the swollen sample were reweighted on an accurate microbalance.

Using the densities of UHMWPE and xylene, the volumes of both components of the swollen sample were determined ($\rho_{xylene} = 0.75$ g/cm^3, $\rho_{UHMWPE} = 0.99$ g/cm^3).

The swell ratio q is calculated as the ratio of the sum of the volume of the unswollen sample V_i and the volume of the swollen sample V_q to the volume of the unswollen sample V_i

$$q = \frac{(Vi+Vq)}{Vi} \tag{5.8}$$

From the swell ratio, the crosslink density was determined using following formula. νd is given in mol / dm^3 and is defined according to [94]:

$$\nu d = \left(\frac{-\ln\left(1-\frac{1}{q}\right)+\frac{1}{q}+\left(\frac{1}{3}+\frac{\frac{5}{9q}}{q^2}\right)}{\frac{\frac{136}{1}}{q^{\frac{1}{3}}}} \right) . 1000 \tag{5.9}$$

Die approbierte gedruckte Originalversion dieser Dissertation ist an der TU Wien Bibliothek verfügbar.
The approved original version of this doctoral thesis is available in print at TU Wien Bibliothek.
TU Bibliothek Your knowledge hub WIEN

5.3 Mechanical Properties

5.3.1 Depth Sensing Indentation of Polymers

Depth sensing indentation (DSI), instrumented indentation tests have been widely used as a powerful way to evaluate the near surface properties of UHMWPE in an extremely small area, using various loading and unloading pressures and loading and unloading rates [177-180]. The indentation hardness and elastic modulus are two important material properties that can be obtained using this technique [181, 182].

The basic idea of the DSI test is the application of an indenter into the surface of a material while measuring force and displacement, with control over loading parameters and indenter shape. The force can be precisely applied down to a few milli-Newtons over an area in the micro to nanometer scale. In this study a sharp triangular based pyramid indenter (Berkovich) was used. Figure 5.2 shows schematic curves for a nanoindentation test using a Berkovich indenter. The load (P) is applied at a specific loading rate until it reaches the pre-defined maximum load at point (A). During the unloading part, the behavior of the material can be classified; Elastic behavior at (A-O) when the deformation is fully recovered; Elastic-plastic (time independent) behavior for the unloading curve (A-B); Viscoelastic (time dependent) behavior for the unloading curve (A-C); Plastic behavior for the unloading curve (A-D).

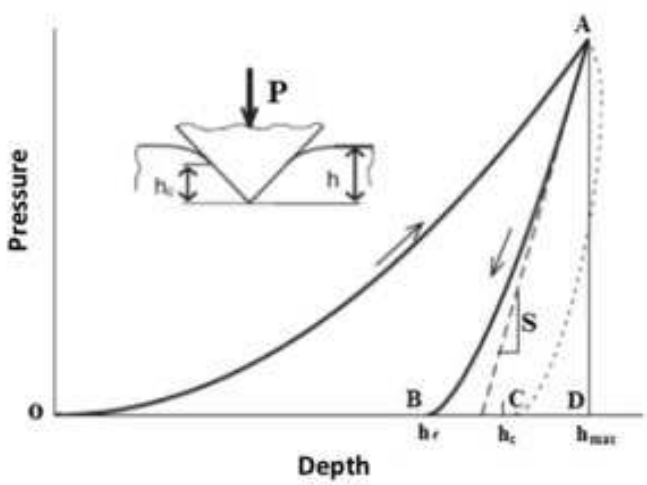

Figure 5. 2 A schematic plot of load vs. depth curves of nanoindentation experiment, where h_{max} is the depth at the maximum load, h_f is the final depth after unloading, h_c is the contact depth and S is the stiffness [183]

Die approbierte gedruckte Originalversion dieser Dissertation ist an der TU Wien Bibliothek verfügbar.
The approved original version of this doctoral thesis is available in print at TU Wien Bibliothek.
TU Bibliothek Your knowledge hub WIEN

Hardness H_{IT} is calculated using to following formula [184]:

$$H_{IT} = \frac{\mathrm{Fmax}}{A} \tag{5.10}$$

with F_{max} being the load at maximal displacement and A the projected area under the indenter. The effective elastic modulus (E_{eff}) can be calculated by using the contact stiffness S. β is a constant based on the indenter geometry.

$$E_{eff} = \frac{S\sqrt{\pi}}{2\beta\sqrt{A}} \tag{5.11}$$

The elastic modulus determined by indentation testing E_{IT} is calculated from:

$$\frac{1}{E_{eff}} = \frac{(1-\nu^2)}{E_{IT}} + \frac{(1-\nu_i^2)}{E_i} \tag{5.12}$$

where E_{IT} and the Poisson's ratio ν are properties of the sample and E_i and ν_i the according properties of the indenter material.

5.3.3.1 Standard Load-Unload Test for Polymers

The use of the DSI technique is hard to apply in UHMWPE due to the complex structure and deformation mechanisms involved. Both elastic-plastic behavior and viscoelastic behavior can be seen in the indentation. The calculation of the indentation hardness and the indentation elastic modulus in the DSI technique depends on the assumption that the initial unloading part is elastic. The viscoelastic curve (A-C) that is shown in Figure 5.2 is the most common behavior for polymers in nanoindentation tests [185-187]. This results in a negative slope, which invalidates the assumption of elastic unloading, and leads to a major error in the calculation of contact depth and contact stiffness. Hence, applying appropriate loading and unloading rates and holding times at maximum load are important factors that should be considered to minimize the effect of viscoelastic behavior in the unloading curve when testing polymers [188]. Therefore, it is common practice to eliminate or minimize the creep effect through a long holding time at maximum load [186, 189].

In this study, hardness and E-Modulus were calculated with a Berkovich indenter test device (NHT, CSM Switzerland). Samples from center and rim area were cut and embedded in epoxy resin,

Die approbierte gedruckte Originalversion dieser Dissertation ist an der TU Wien Bibliothek verfügbar.
The approved original version of this doctoral thesis is available in print at TU Wien Bibliothek.
TU Bibliothek Your knowledge hub WIEN

grinded (water cooled) and polished (with a polishing paste diamond particle) to provide a smooth surface. The prepared surface must be perfect parallel to the ground. The depth profiles from inner surface and outer surface towards the center of the component were measured on the same sample.

A Berkovich indenter was used to make a grid of 15x5 indents, as shown in Figure 5.3 using 5 µm maximum depth, 30s holding time and 120 mN/min loading and unloading rates. The results were analyzed by Indentation 4.12 software. The Poisson's ratio of the UHMWPE it is 0.43 [190].

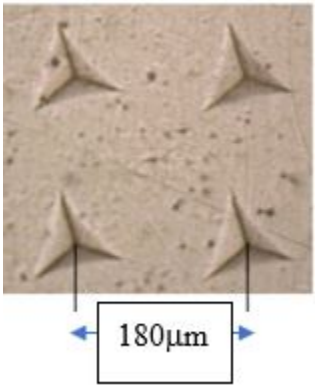

Figure 5. 3 View of grid of indents

5.3.2 Small Punch Testing

The small punch test (SPT) is a semi-destructive technique because it uses a very limited amount of material. The technique was adapted from the nuclear industry particularly for testing UHMWPE. ASTM F2183-02 "Small Punch Testing of Ultra-High Molecular Weight Polyethylene Used in Surgical Implants" was first published in June 2002 and defines detailed the test method [191].

SPT is a valuable tool for investigating the influence of different factors on the mechanical properties of UHMWPE such as different sterilization techniques [192-194], accelerated aging [193, 194] and cross-linking [2, 195]. Edidin et al. used the technique to investigate the properties of nine retrieved UHMWPE components and found a significant correlation between patient weight and the toughness (work to failure) of components. The heaviest patient was also the one with the shortest longevity in-situ. However, the authors themselves emphasized that further testing was required due to the low number of components evaluated [196]. Kurtz et al. also used the technique

Die approbierte gedruckte Originalversion dieser Dissertation ist an der TU Wien Bibliothek verfügbar.
The approved original version of this doctoral thesis is available in print at TU Wien Bibliothek.
TU Bibliothek Your knowledge hub WIEN

in a retrieval study and found that the peak load, ultimate load and work to failure were all significantly lower at the worn and unworn surfaces (< 25 µm from articulating surface) compared to values obtained at subsurface locations (1.5-2 mm from the articulating surface) [197].

From a load-displacement curve four basic gauges are obtained of a material subjected to the SPT. These include the initial stiffness, peak load, ultimate load, and the maximum displacement at failure. Work to failure, which is fifth derived gauge, is obtained by integrating the area under the load displacement curve. It shows the total energy required to fail the specimen. A typical load-displacement curve for GUR 1020 UHMWPE is shown in Figure 5.4 [198].

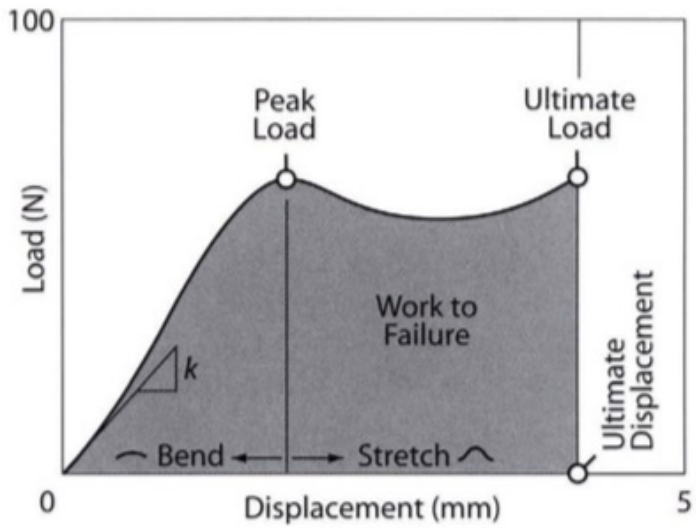

Figure 5. 4 Load-displacement curve for GUR 1020 UHMWPE [198]

According to literature [198] initial stiffness of the load -displacement curve is proportional to elastic modulus of UHMWPE.

$$E = 13.5k \tag{5.13}$$

k is the initial stiffness of the load-displacement curve in N/mm and E-modulus is in MPa.

A custom built SPT (a master's degree study was supervised by our team) is shown in Figure 5.5 A specimen is clamped between an upper and lower die and the load is applied to the specimen through a hemispherical punch head. SPT was conducted at ambient temperature.

Die approbierte gedruckte Originalversion dieser Dissertation ist an der TU Wien Bibliothek verfügbar.
The approved original version of this doctoral thesis is available in print at TU Wien Bibliothek.
TU Bibliothek Your knowledge hub WIEN

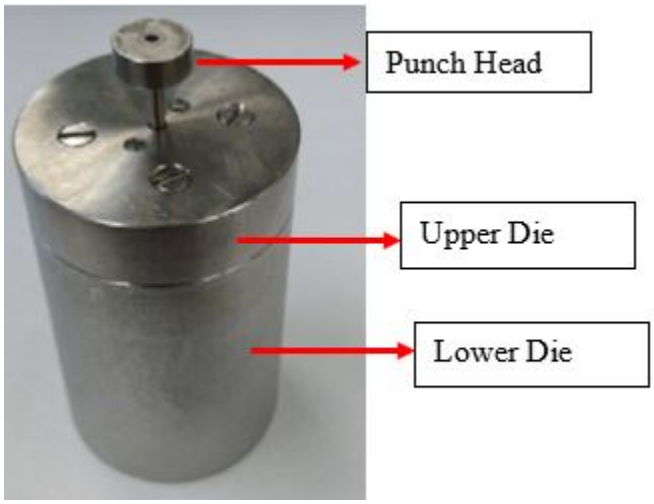

Figure 5. 5 Picture of SPT

Mechanical behavior was examined in commercial engineering polymers blocks (GUR 1020, GUR 1020 Vit. E and GUR 1050), conventional, cross-linked and accelerated aged explants. In the beginning the specimens for the SPT are produced by the compression molding process. In this study hydraulic hot press (Collin P 200 P) was used. During that process the material was cut from the blocks and explants and heated above its melting point (175ºC) compressed to a thickness of 0.5 mm, kept at this temperature for 5 min and then cooled with a rate of 10 K/min to the room temperature. A 6.4 mm punch was used to extract the disk-shaped sample. Samples were put into the nut as shown in Figure 5.6.

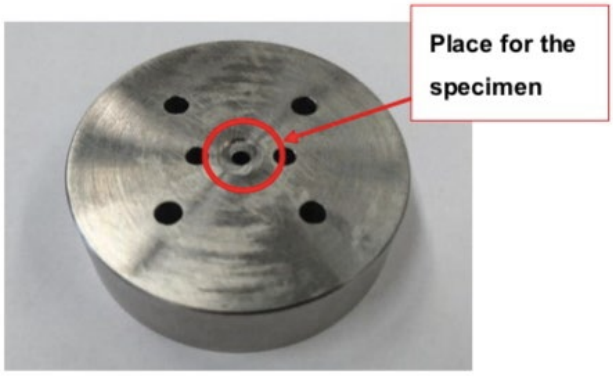

Figure 5. 6 An upper die of SPT

The load on the punch bearing was applied by Zwick Roell Z050 shown in Figure 5.7 and interfaced with a computer showed force and displacement. The machine stopped after the punch got through the sample. The force displacement curve during the small punch test was observed by the lab view in the computer. The ball between punch and force measurement unit, shown in Figure 5.7, is

Die approbierte gedruckte Originalversion dieser Dissertation ist an der TU Wien Bibliothek verfügbar.
The approved original version of this doctoral thesis is available in print at TU Wien Bibliothek.
TU Bibliothek Your knowledge hub WIEN

necessary to create an ideal vertical force on the punch without any side forces which would be responsible for disruptive friction forced between punch and die.

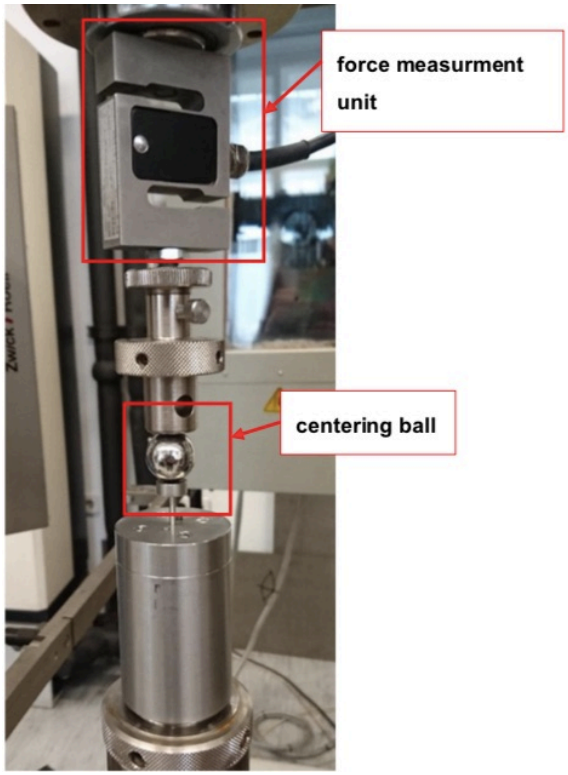

Figure 5. 7 Zwick Roell Z050 testing maschine

Peak load, ultimate load, and work to failure were so high comparing to literature results. Then the sample preparation method was changed. At first, from the block and explant's articulating surface 0.5 mm thick specimens were cut by using a microtome and subsequently punched as a disc shape. The most important part is that the thermal pressing method was not applied. Secondly, the velocity of cross head was set at 0.5 mm/min. Before applying these tests, the samples were cyclically loaded 10 times in a range from 0.2 to 2.7 N to show the stabilization (saturation) of the slope of the initial linear portion of the curve as was mentioned in the study [199]. The aforementioned properties were tested again and compared with literature.

5.4 Testing of Tribological Properties

The specimens for the tribology tests are produced by the compression molding process in order to reduce physical-aging effects and to exhibit the same surface roughness. During that process the

Die approbierte gedruckte Originalversion dieser Dissertation ist an der TU Wien Bibliothek verfügbar.
The approved original version of this doctoral thesis is available in print at TU Wien Bibliothek.
TU Bibliothek Your knowledge hub WIEN

material is heated above its melting point with a specified heating rate and pressure. The material was cut from the blocks, heated above its melting point (175°C) and compressed to a thickness of 3 mm. The heating rate of 10 K/min was applied and the specimen was held at that temperature for 5 minutes to homogenize the temperature distribution in the material. After this stage, the material is cooled down to room temperature at same heating rate. The samples were then cut into dimensions of 20×20×3 mm^3 and put in the oven in air atmosphere at 80°C for aging. The aging durations are 3, 6 and 9 weeks.

Tribological tests could only be applied to two implants as the test requires suitable rim width and enough material for aging. Two shelf aged implants were aged up to 9 weeks. Specimens were embedded into epoxy resin and were then burnished and polished.

5.4.1 Ball on Plate Test

The tribological tests were performed on a ball on plate (BOP) device represented in Figure 5.8 in a 2-body dry sliding environment. The tribometer operates according to ASTM G99 [200] and has the following testing principle: a 6 mm steel ball– the chemical composition is given in Table 5.4- is loaded against the tested specimen with the help of the pin support that keeps the ball in a fixed position as the specimen rotates. This creates a circular wear track with a well-defined diameter. The load cycle was checked using an independent load and used to be the minimum 2 N and maximum 30 N. For 2N at the 1 million cycle and for 30 N, at the 85000 cycle were used then the simulator automatically turned itself off.

During the tests, the friction coefficient was automatically measured by the Nanovea Software. The surface temperature was monitored throughout the tests using a thermocouple which was attached to the tribometer and allowed to save the temperature values for the entire testing period.

Die approbierte gedruckte Originalversion dieser Dissertation ist an der TU Wien Bibliothek verfügbar.
The approved original version of this doctoral thesis is available in print at TU Wien Bibliothek.
TU Bibliothek Your knowledge hub WIEN

Table 5. 4: Chemical composition of SS440 steel ball as given in technical data sheet

Material	Chemical Composition (%)				
	C	**Si**	**Mn**	**Cr**	**Mo**
X105CrMo17	1.08	1	1	17	0.6

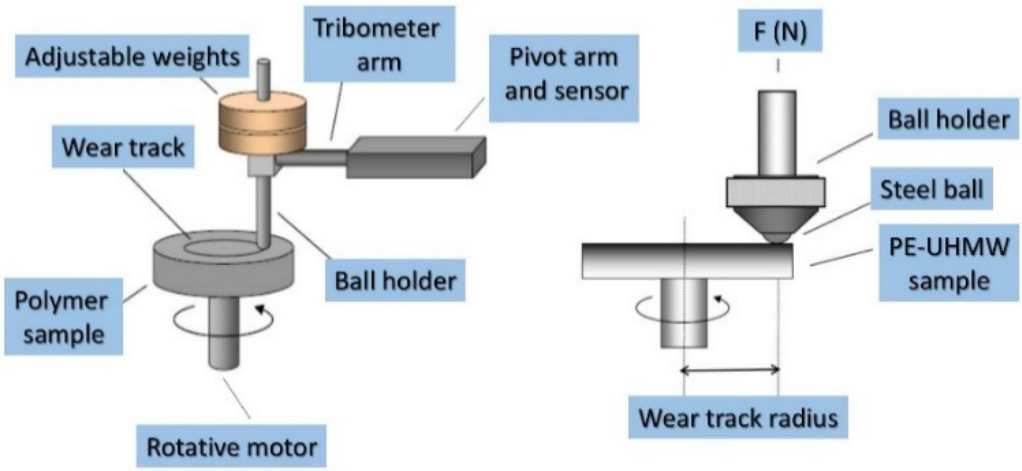

Figure 5. 8 Ball on Plate Tribometer with schematic configuration

The tribological testing conditions are given in Table 5.5.

Table 5. 5 Tribological testing conditions used

Sample	Value	Unit
Loads	2 and 30	N
Speed	2250 and 4500	mm/min
Temperature	25 ± 2	°C
Revolutions	238.1	Rpm
Wear track diameter	3 and 6	Mm
Total testing revolutions	1000000 and 85000	rev.

The profilometer uses as Axial Chromatism as a measuring principle which has a white light source that passes through an objective lens with a high degree of chromatic aberration. When the sample is in the measurable range a single monochromatic point is focused to form the image. Additionally, information about surface topography is collected using the same measurement principle. Another

Die approbierte gedruckte Originalversion dieser Dissertation ist an der TU Wien Bibliothek verfügbar.
The approved original version of this doctoral thesis is available in print at TU Wien Bibliothek.
TU Bibliothek Your knowledge hub WIEN

method to characterize the wear is a qualitative method that uses a Light Microscope (LM) in order to identify the wear mechanisms that occur on the surface after the tribological tests.

The wear characterization was conducted using a quantitative method based on measuring the volumetric wear loss by using the 3D Profilometer (Nanovea PS50). By scanning the wear track precise values for the area and the volume can be calculated (Eq. 5.14).

Volume loss is calculated according to Eq. (5.14), where the area (A) is measured by the profilometer and r is the radius of the wear track:

$$V = A * 2\pi r \tag{5.14}$$

Wear rate is calculated from:

$$W_r = \mathrm{V/number\ of\ cycles} \tag{5.15}$$

The BOP test was performed beyond the elastic limit in this thesis but according to [96, 201, 202] average contact pressure was calculated roughly by using Hertz contact theory. Hertz contact theory is used only if there is an elastic contact. Using this theory, it is seen that working condition is how much higher than the yield strength. If the contact is assumed to be fully plastic, the hardness is the average contact pressure [203, 204].

The theory of a contact between a sphere and a plane sample. In that case the contact pressure was calculated from

$$P = \frac{F}{\pi a^2} \tag{5.16}$$

where P is the average contact pressure, F is the normal force

and a is the radius of the contact area given by:

$$a = \sqrt[3]{\frac{3WR^*}{4E^*}} \tag{5.17}$$

Die approbierte gedruckte Originalversion dieser Dissertation ist an der TU Wien Bibliothek verfügbar.
The approved original version of this doctoral thesis is available in print at TU Wien Bibliothek.
TU Bibliothek Your knowledge hub WIEN

The equivalent elastic modulus was calculated from:

$$\frac{1}{E^*} = \frac{1-v_1^2}{E_1} + \frac{1-v_2^2}{E_2} \tag{5.18}$$

where, E_1, E_2 are the elastic moduli of the materials, E^* is the combined modulus and ν_1, ν_2 are the Poisson's ratios of the materials. The equivalent radius was calculated from:

$$\frac{1}{R_*} = \frac{1}{R_1} + \frac{1}{R_2} \tag{5.19}$$

where, R_1 represents the radius of the sphere and R_2 is infinitive due to plane sample.

5.5 Accelerated Aging

An accelerated aging method is developed to imitate long term oxidative effects without needing a long time of periods. Therefore, the oxidation of the polymer is mostly carried out at elevated temperature and pressure of oxygen. An increase in temperature and pressure leads to an increase in the relative rates of degradation reactions. Accelerated aging has been studied extensively with a combination of elevated temperatures and oxygen partial pressures [2, 205-207]. In accelerated aging studies, the temperature has ranged from 60 to 127ºC, the oxygen pressure has been varied from pure oxygen to 102 atmospheres [2] and the aging duration is typically from 1 to 28 days. A study [208] provided with an accelerated aging protocol where specimens were thermally aged at 80ºC for up to 23 days with a slow initial heating rate of 0.6 ºC/min Results are compared with up to 10 years of shelf-aged components irradiated in air. It is observed that maximum oxidation index for accelerated aging for above protocol compared well with seven to nine years of shelf aging. It is suggested that either a surface or subsurface peak in oxidation can be achieved depending on the time period between gamma sterilization and accelerated aging. An alternative accelerated aging method has been proposed by Sanford et al. [209]. This involves use of a pressurized vessel. Using this technique, with a pressure of 5 atmospheres oxygen and temperature of 70°C, 5 to 10 years of shelf aging could be simulated in as little as one week. Another study [210] compared the accelerated aging oxidation index profiles with four-year old explant. It is found that the results obtained for accelerated aging would be reasonably similar to the explant. An ASTM standard for accelerated aging of UHMWPE published (ASTM F2003-00) [211]. It incorporates both method A (21 days at 80°C in air) and method B (14 days at 70°C in 5 bar oxygen). In this study, method A was used and followed by an extension up to 9 weeks.

Die approbierte gedruckte Originalversion dieser Dissertation ist an der TU Wien Bibliothek verfügbar.
The approved original version of this doctoral thesis is available in print at TU Wien Bibliothek.
TU Bibliothek Your knowledge hub WIEN

Chapter 6: Results and Assessment

This study investigated optical damage scoring, structural properties such as: oxidation index, crystallinity, cross-linked density; mechanical properties such as: indentation hardness and modulus, ultimate stress, work to failure, and tribological properties such as volumetric wear rate and wear mechanisms.

6.1 Optical Damage Scoring

The observable surface properties that are used for optical damage scoring calculation are: cracks, delamination, scratches and groves, color change, machining marks, pitting and burnishing.

Cracks:

Generally, polymer surface cracks can be caused by exposure to mechanical and thermal stresses at microscopic and macroscopic level.

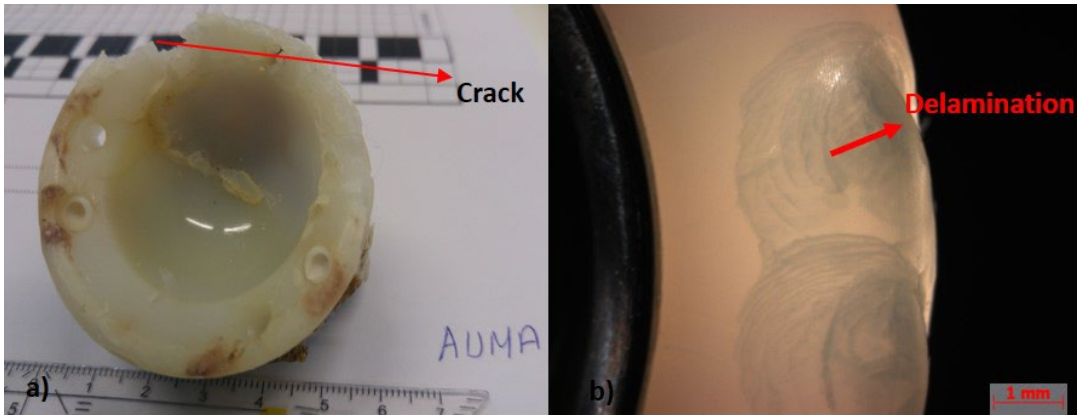

Figure 6. 1 a) AUMA displaying crack on the rim, b) Delamination on BUC sample

The microscopic crack may be initiated either by thermal stress or mechanical fatigue cycle or both. Either of these two conditions cause surface breaking cracks as shown in Figure 6.1 (a). Thermal stress will cause softening of surface material and associated with plastic flow localization [212]. The plastic flow is possible to initiate fracture or crack when the plastic zone reaches a critical size stress [212]. Cracks are observed in highly oxidized explants which is discussed in detail in Chapter 6.3.

Die approbierte gedruckte Originalversion dieser Dissertation ist an der TU Wien Bibliothek verfügbar.
The approved original version of this doctoral thesis is available in print at TU Wien Bibliothek.
TU Bibliothek Your knowledge hub WIEN

Delamination:

Subsurface failure i.e. cracks resulting in removal of large sheet of UHMWPE is defined as delamination as seen in Figure 6.1 (b) and Figure 6.2 (a). Delamination is initiated by subsurface cracks from the cyclic stress at the contact surface of the explant, which can then spread into the articulating surface. In general, in this study delamination was observed in highly oxidized regions of the explants.

Scratches and Grooves:

Scratches and grooves were both observed on the bearing surface of the explants. Representative examples of such are shown in Figure 6.2 (a) and (b). Scratches are multidirectional indentations into the UHMWPE. In Figure 6.2 (a), the scratch starts from the bearing surface area and extends towards the rim-bearing surface interface. The reasons that the scratch ends at the rim-bearing surface interface could be a third-body particle, such as cement, hydroxyapatite (HA), metal, and/or polyethylene.

Grooves are short scratches and it is easier to see them under higher magnification. An example of a groove is shown in Figure 6.2 (b). Scratches and grooves are characteristic of abrasive wear [213]. Scratches and grooves whose severity differ were observed in all explants.

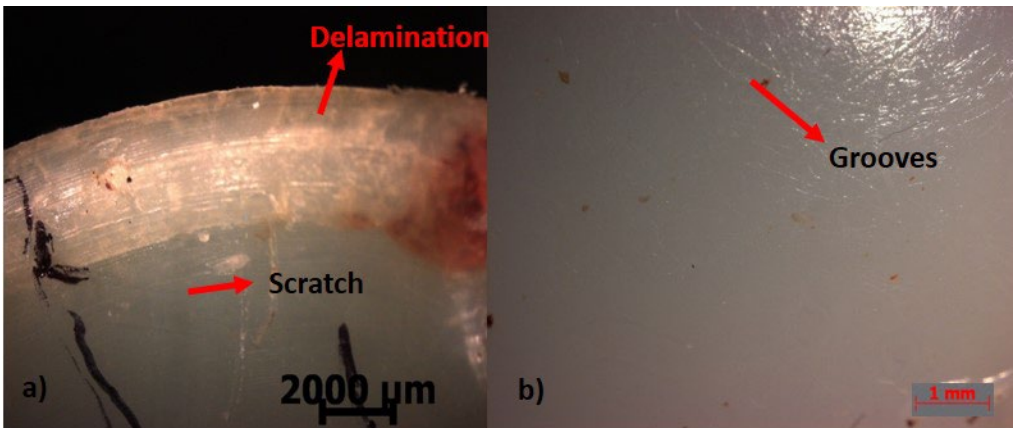

Figure 6. 2 a) Scratch on the AUMA sample, b) Grooves on VOST sample

Die approbierte gedruckte Originalversion dieser Dissertation ist an der TU Wien Bibliothek verfügbar.
The approved original version of this doctoral thesis is available in print at TU Wien Bibliothek.
TU Bibliothek Your knowledge hub WIEN

Color Change:

Figure 6.3 shows LUIN explant which has complete color change at the back surface. The cause of the color change has previously been reported by Schneider et al [214] as in-vivo absorption of proteins from the synovial fluid. Color change was observed for all long in-vivo time explants.

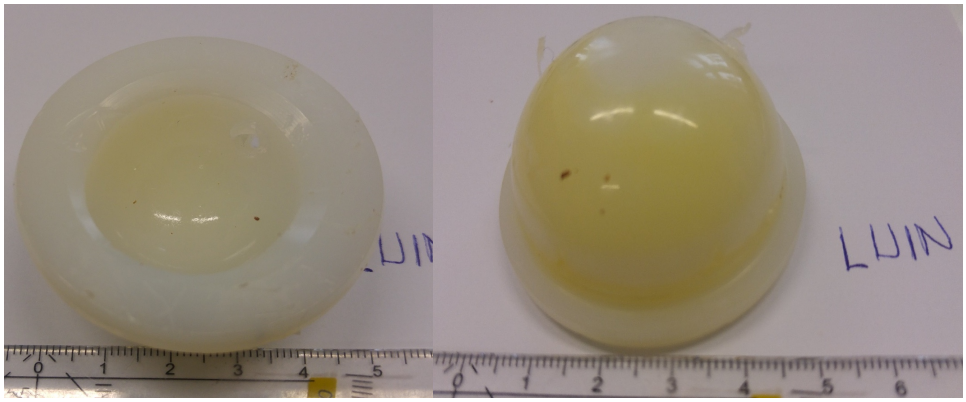

Figure 6. 3 Color change on LUIN sample

Machining Marks:

The presence of machining marks is an indicator of an unworn and undamaged surface and they are commonly observed in short in-vivo time explants. Figure 6.4 (a) shows machining marks on STEL sample.

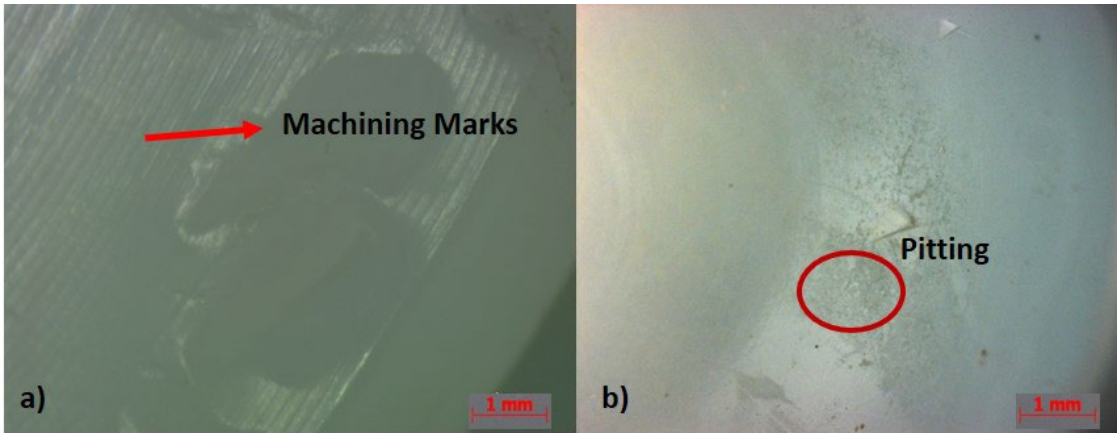

Figure 6. 4 a) Machining marks on STEL, b) Pitting on GOKA sample

Die approbierte gedruckte Originalversion dieser Dissertation ist an der TU Wien Bibliothek verfügbar.
The approved original version of this doctoral thesis is available in print at TU Wien Bibliothek.
TU Bibliothek Your knowledge hub WIEN

Pitting:

Pitting is a group of small round shaped craters observed on the surface. An example of a surface with pitting is shown in Figure 6.4 (b). The high contact stress on the bearing surface causes plastic flow of the UHMWPE and is the main reason of pitting.

Burnishing:

Burnishing is characterized by a shiny and smooth appearance. Burnishing was observed on all long in-vivo time explants at the center of the cup as the bearing surface is a highly worn area. Figure 6.5 shows a burnishing on a cup.

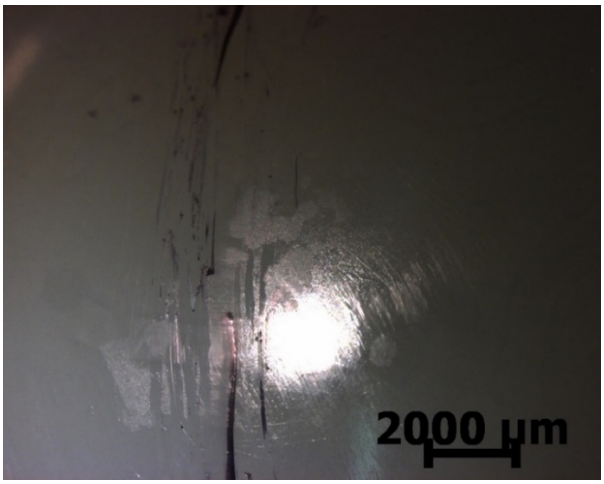

Figure 6. 5 Burnishing on WIRU sample

Other Cases:

The worn region directly at the outside of the inner surface and the bone ingrowth outside of the acetabular cup can be seen in Figure 6.6 (a) and (b), respectively. In Figure 6.6 (a), shows the inter-zonal ridge at the interface between worn and unworn regions of explant. This ridge was present for all highly worn components.

The damage of explant was probably caused by intervention between the acetabular cup and the neck of the femoral component due to debris (UHMWPE or PMMA cement). Third-body wear can result from this debris if it migrates to the bearing surface.

Die approbierte gedruckte Originalversion dieser Dissertation ist an der TU Wien Bibliothek verfügbar.
The approved original version of this doctoral thesis is available in print at TU Wien Bibliothek.
TU Bibliothek Your knowledge hub WIEN

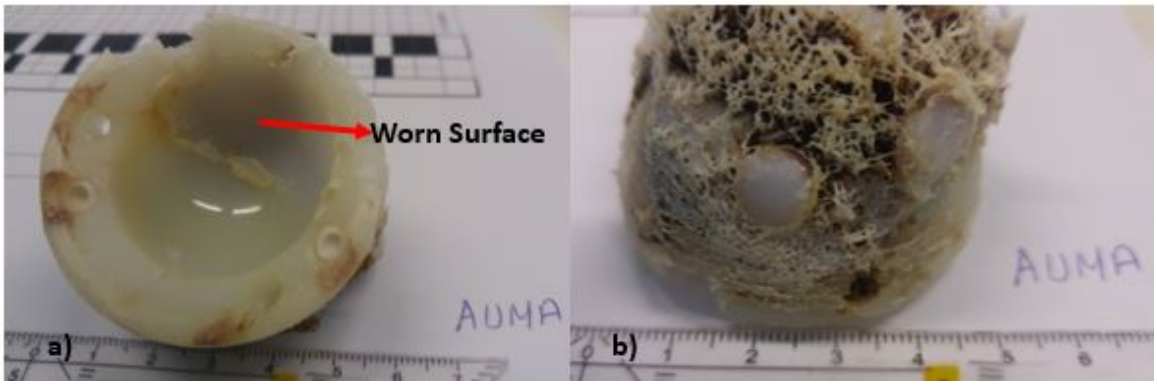

Figure 6. 6 AUMA displaying a) worn surface at articulating part and b) bone ingrowth

Assessment of Damage Scoring Results

Optical damage scoring is given in Table 6.1. Explants were marked to show which type of damage they have. Total damage scoring was calculated as explained in Chapter 5.1. Some cracks for calculation of total damage score were ignored because it might have been during the retrieval process. Scratches and grooves were observed for all explants regardless of their in-vivo time.

Sandwich type of liners was introduced to use in MoM and CoC articulating couples to produce lower contact stress and better stress distribution. The damage score of sandwich type explant samples GIE, BUC and GOKA were low considering their in-vivo time because UHMWPE is used between metal or ceramic inlay and acetabular shell. Hence, synovial fluid and femoral head do not contact with UHMWPE surface. Hence, we neglect their damage score effects on our diagrams and tables.

AUMA has bone ingrowth outside of the acetabular cup, hence it could not be evaluated. Nevertheless, it has the maximum total damage score.

Die approbierte gedruckte Originalversion dieser Dissertation ist an der TU Wien Bibliothek verfügbar.
The approved original version of this doctoral thesis is available in print at TU Wien Bibliothek.
TU Bibliothek Your knowledge hub WIEN

Table 6. 1 Total Damage Scoring

	Damage							
Acronym	**Cracks**	**Scratches**	**Grooves**	**Pitting**	**Burnishing**	**Delamination**	**Color**	**Total**
AUMA	X	X	X	X	X	X	X	57
GOKA	X	X	X	X	X	X	X	43
PLWI		X	X					8
TRCH		X	X		X			31
LAMA1		X	X	X			X	19
LAMA2		X	X				X	17
LOPE		X	X	X			X	16
JEJO		X	X					20
WIRU	X	X	X	X	X			26
STEL		X	X					10
LUIN		X	X	X	X		X	33
KOEV		X	X		X		X	17
MAWO	X	X	X	X	X		X	24
MÜCL	X	X	X	X	X	X		24
VOST	X	X	X	X	X	X	X	44
GIWA		X	X	X	X	X	X	25
GLFR		X	X	X	X		X	37
SCME		X	X	X	X		X	34
FADA		X	X					14
GRMA		X	X	X	X			25

Die approbierte gedruckte Originalversion dieser Dissertation ist an der TU Wien Bibliothek verfügbar.
The approved original version of this doctoral thesis is available in print at TU Wien Bibliothek.
TU Bibliothek Your knowledge hub WIEN

There is a direct proportion (r=0,74) between total damage score and in-vivo time. In the short in-vivo time all explants showed no visible signs of pitting and delamination. On the other hand, pitting, delamination and embrittlement caused by oxidation are observed in long in-vivo time conventional explants. In a cross-section of these explants, it can be seen a so-called white band, which is due to subsurface embrittlement induced by oxidation [165, 215, 216]. The total damage score plotted against in-vivo time (Figure 6.7).

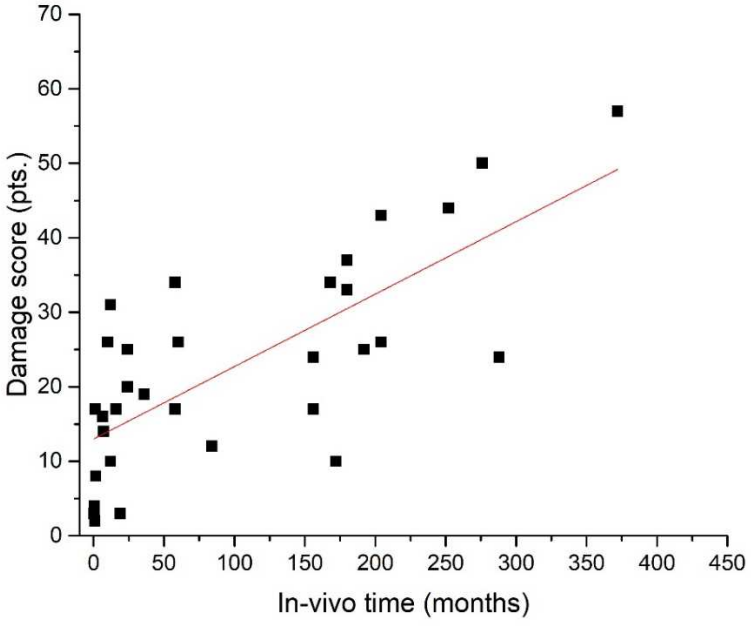

Figure 6. 7 Damage score as a function of in-vivo time (r =0.74)

6.2 Gender Influence on Age, BMI and UCLA Activity

Patient report form sample, which recording the details of the retrieved prothesis can be found in APPENDIX A and correlation of properties are given in APPENDIX A1.

Thirty-eight patients participated in this study of which 23 female and 15 were male. The average ages for female and male patients are 69.4 ± 9.1 years and 68.7 ± 9.0 years, respectively with minimum and maximum ages ranging from 53 to 86. The average in-vivo time of explants is around 8 years. The average age of patients is according to the literature [217] usual for people undergoing

Die approbierte gedruckte Originalversion dieser Dissertation ist an der TU Wien Bibliothek verfügbar.
The approved original version of this doctoral thesis is available in print at TU Wien Bibliothek.
TU Bibliothek Your knowledge hub WIEN

revision hip surgery. Patient weight varied from 41kg to 128kg with a mean value of 78.3 ± 19.2kg and weight of 13 patients is unknown.

Patient BMI versus patient age is shown in Figure 6.8 (a). Patients with the highest BMI values tended to also be the youngest.

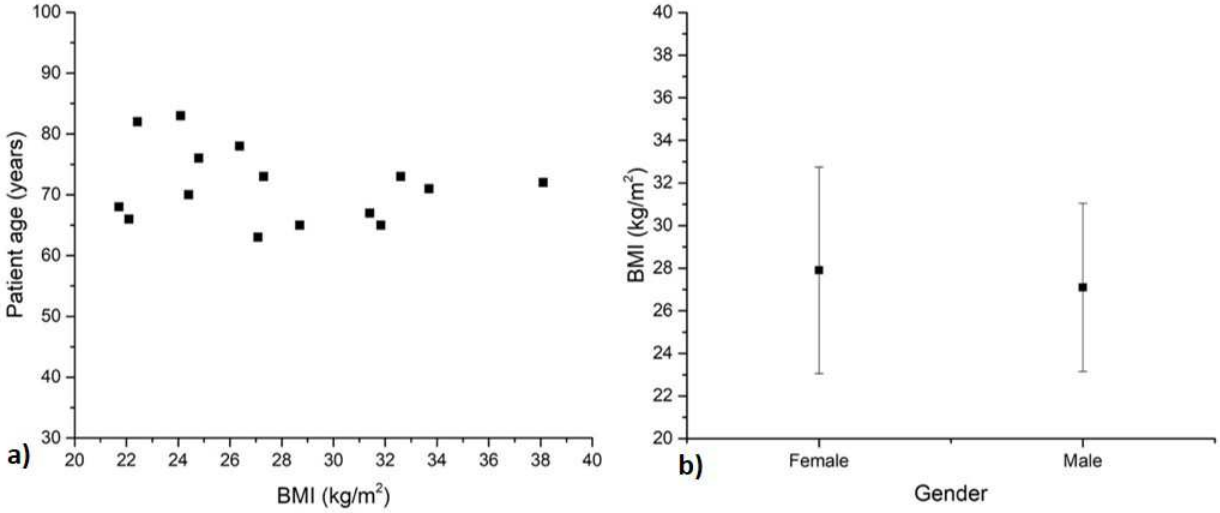

Figure 6. 8 a) BMI versus patient age, b) BMI as a function of gender

Women have slightly higher BMI values then men (Figure 6.8 (b)).

As might be expected, the aged of the patient and their UCLA activity level were negatively correlated indicating a decrease in UCLA activity level with increasing age (Figure 6.9).

Die approbierte gedruckte Originalversion dieser Dissertation ist an der TU Wien Bibliothek verfügbar.
The approved original version of this doctoral thesis is available in print at TU Wien Bibliothek.

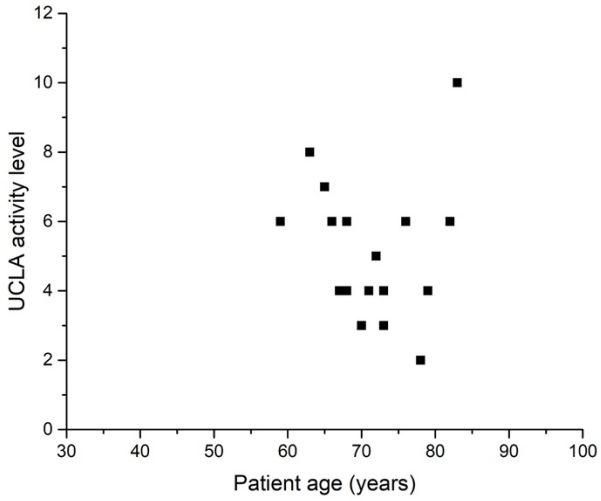

Figure 6. 9 Scatterplot of UCLA activity and patient age

Assessment of Gender Results

There was not a significant correlation between patient weight and in-vivo time of acetabular component. The relation between patient weight and explant in-vivo time was investigated in a study by Surin et al [218]. They found that patients weighing more than 80kg were at significantly greater risk of prosthetic failure requiring revision. In this study, there were known nine patients who greater than 80kg at the time of revision and they had an average in-vivo time of 85.3 ± 94.6 months compared to 77.4 ± 117.4 months for patients who less than 80kg. The reverse result was found correlating with the literature. However, this observation could be derived from the fact that all patient's weight and their body mass index (BMI) data are unknown.

Explants in-vivo time varied greatly from 9 days to 31 years. In this study, there are 10 years in-vivo time of two sandwich type design explants (conventional). Maximum and minimum in-vivo time in conventional explants is 31 and 1.5 years. In cross-linked explants we have maximum 24 years (DePuy) and minimum 9 days (Durasul®) in-vivo time.

The in-vivo time reported in this study were much lower than those reported in the Swedish hip registry of 4,124 patients who had a survival rate at 18 years of 83% [219].

Die approbierte gedruckte Originalversion dieser Dissertation ist an der TU Wien Bibliothek verfügbar.
The approved original version of this doctoral thesis is available in print at TU Wien Bibliothek.
TU Bibliothek Your knowledge hub WIEN

As can be seen in Figure 5.1 infection was the predominant reason given for joint failure and occurred 46.9%. Then aseptic loosening is seen by 15.6% and wear 12.5%. Wear debris has an important role in the process of aseptic loosening and the dominance of this failure mechanism.

The UCLA activity level varied greatly between patients with some being highly active whilst others engaged in only minimal physical activity. All patients engaged in some sort of household physical activity. However, only 50% of patients took part in sporting leisure activities with this figure being equally split between men and women. Kahan et al found the same trend of men participating in more sports leisure activity following their assessment of 406 adults [220]. UCLA activity level was correlated with length of time that components were implanted for, with increased activity leading to reduced component longevity (except one).

The analysis of patient data also showed that female patients had a significantly higher risk of implant failure than men at 1 year in contrary to other studies [221-223]. The reason could be less tolerance to pain and less mobility after the surgery of female patients [224].

Also, in this study it was investigated if there is any relation to the morphological properties with gender's weight, age and in-vivo time. No significant result was found. The cause of this between men and women is due to the interaction of multiple variables such as age, genetics, and physical activity.

Thirty-eight patients took part in this study with male patients constituting 58 % (n= 14) of the study population. Due to a lack of UCLA activity level for all explants, correlate data with BMI cannot be made.

6.3 FTIR Results

FTIR spectra are collected for all samples and OI (-), degree of crystallinity (%), and TVI (-) are calculated from the FTIR data. All OI, crystallinity, TVI and TV results can be found in APPENDIX D.

FTIR imaging was carried out on conventional explants and cross-linked explants that had been implanted for varying amounts of time (short-term and long-term in -vivo time). Sections of rim inner surface (IO) and rim outer surface (AO) and center IO and center AO regions of each explant

Die approbierte gedruckte Originalversion dieser Dissertation ist an der TU Wien Bibliothek verfügbar.
The approved original version of this doctoral thesis is available in print at TU Wien Bibliothek.
TU Bibliothek Your knowledge hub WIEN

were analyzed using the technique in order to evaluate the depth profiles of the oxidation index (OI) and degree of crystallinity obtained by FTIR spectra.

OI results of conventional explants with long in-vivo time:

The oldest explant is AUMA, woman 31 years in in-vivo. The through thickness variations in OI values for the AUMA rim IO and center IO are shown in Figure 6.10.

An increase in OI values was observed at the bearing surface of AUMA. Increased OI values were observed in the sub-surface regions of AUMA ranging from 400 µm to 2000 µm. AUMA rim IO has a maximum value of 4.2 at a depth of 900 µm and AUMA center IO has 3.5 at a depth of 580 µm. An approximate two-fold increase in OI values was observed at the bearing surface in AUMA rim IO. There were no significant variations in bulk OI in individual parts of the explant.

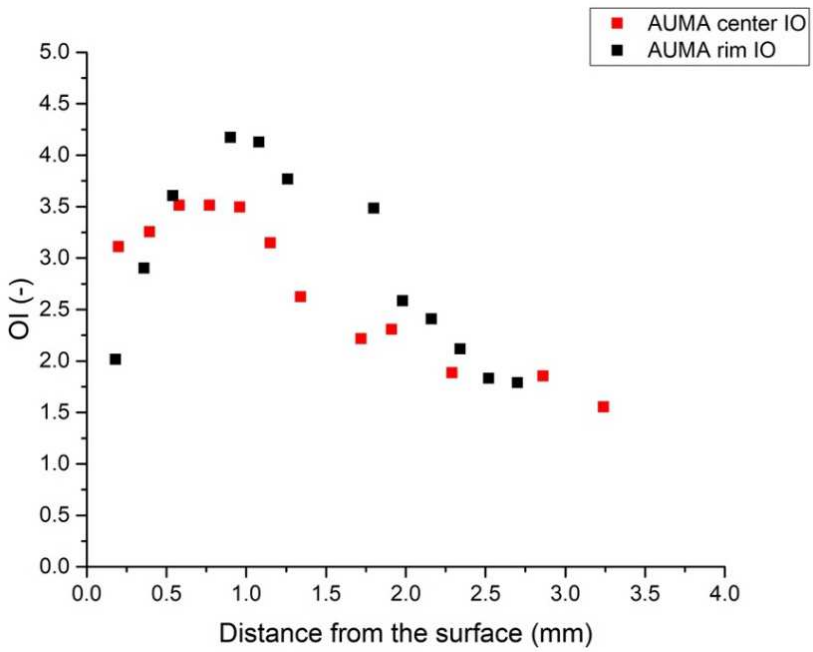

Figure 6. 10 AUMA OI profile as a function of distance

For better correlation, the through thickness variations in OI values for the AUMA rim IO, KOR rim IO and REOP rim IO are shown in Figure 6.11. Increased OI values were observed at the surface of KOR and REOP. There were no significant variations in bulk OI in individual parts of

Die approbierte gedruckte Originalversion dieser Dissertation ist an der TU Wien Bibliothek verfügbar.
The approved original version of this doctoral thesis is available in print at TU Wien Bibliothek.
TU Bibliothek Your knowledge hub WIEN

the explant but KOR and AUMA exhibiting slightly higher OI than the other explant. All explants exhibited approximate three-fold increase in OI when compared with to the bulk values.

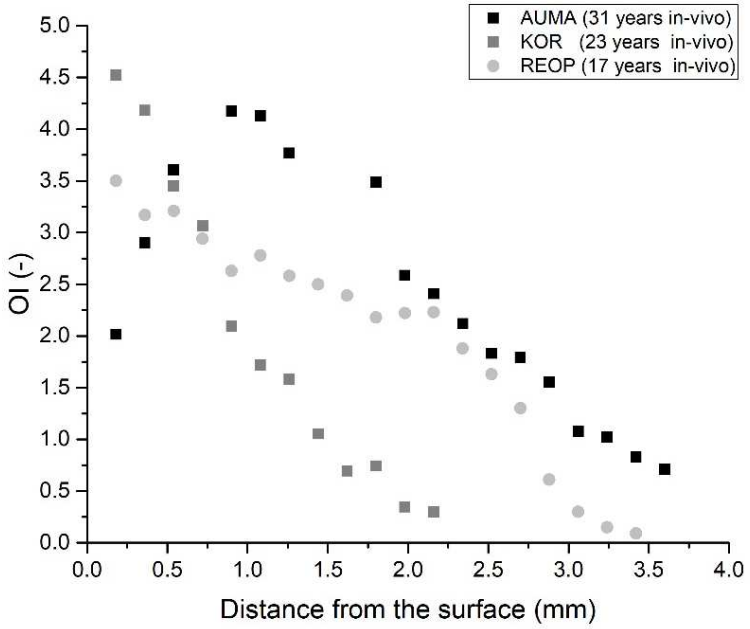

Figure 6. 11 AUMA KOR and REOP rim OI profile as a function of distance

The depth profile of the degree of crystallinity was determined by FTIR in Figure 6.12. The degree of crystallinity on the rim regions and center roughly followed the same pattern as OI. AUMA center IO had a maximum degree of crystallinity of 72.6 % at a depth of 960 µm, AUMA rim IO displayed a peak of 73.8 % at a depth of 1440 µm. On the bulk region degree of crystallinity remains unchanged.

Die approbierte gedruckte Originalversion dieser Dissertation ist an der TU Wien Bibliothek verfügbar.
The approved original version of this doctoral thesis is available in print at TU Wien Bibliothek.
TU Bibliothek Your knowledge hub WIEN

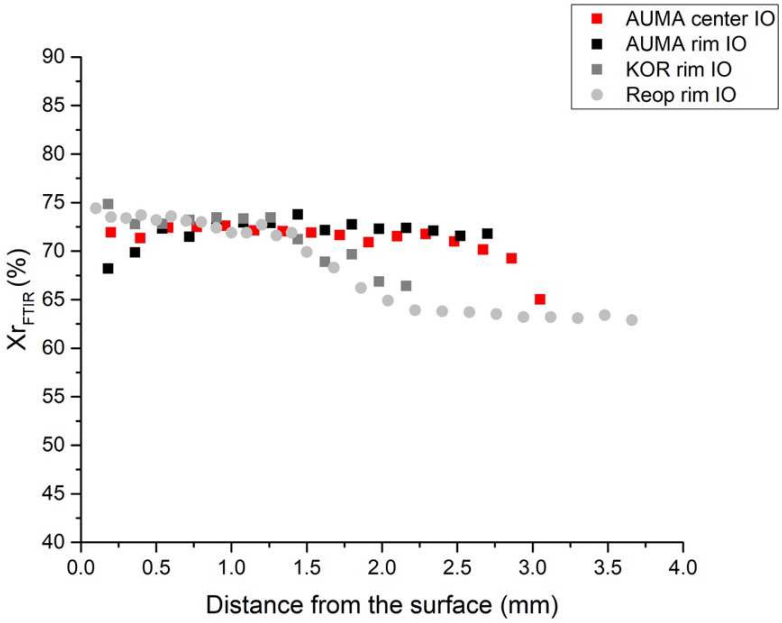

Figure 6. 12 AUMA, KOR and REOP degree of crystallinity profile as a function of distance

Increased OI was observed at the surface for GOKA and BUC and for GIE at the sub-surface region ranging from 400 µm to 2000 µm. GOKA rim IO has a maximum value of 2.2 at a depth of 395 µm and 0.88 at a depth of 1580 µm. There were no significant variations between surface and bulk OI in all explants. Constant OI values were observed at depths greater than approximately 2200 µm (Figure 6.13).

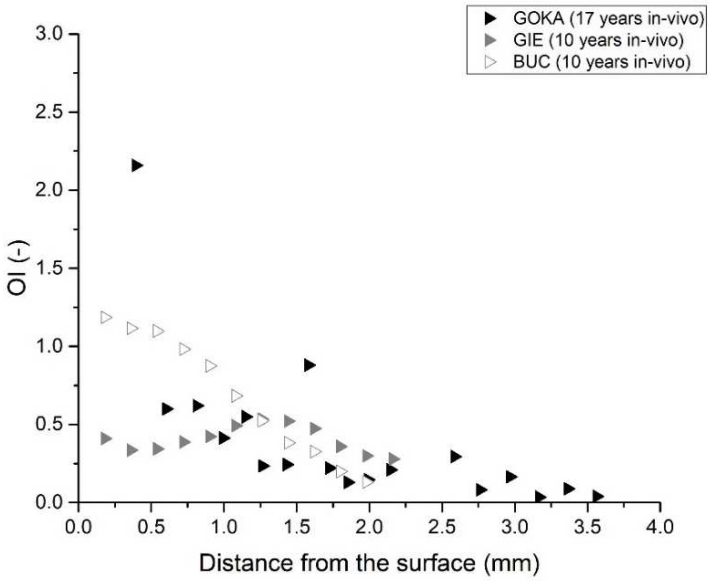

Figure 6. 13 Sandwich types of explant OI profile as a function of distance

Die approbierte gedruckte Originalversion dieser Dissertation ist an der TU Wien Bibliothek verfügbar.
The approved original version of this doctoral thesis is available in print at TU Wien Bibliothek.
TU Bibliothek Your knowledge hub WIEN

All explants show more or less the same degree of crystallinity across the liner thickness at the bearing surface or subsurface region (Figure 6.14).

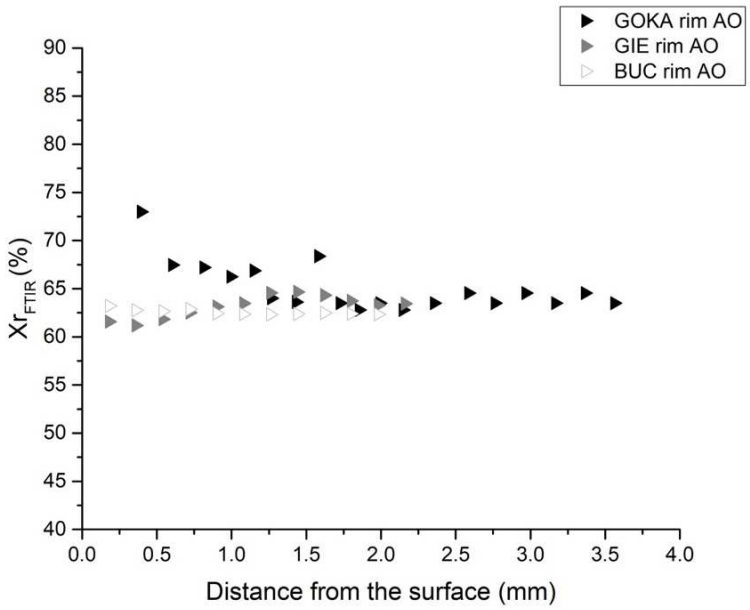

Figure 6. 14 Sandwich type explants degree of crystallinity profile as a function of distance

OI results of cross-linked explants with short and long in-vivo time:

The through thickness variations in OI values for the Durasul® (JEJO and RIE) are shown in Figure 6.16. Increased OI was observed at the surface for all explants. JEJO rim IO exhibited the largest increase on surface OI when compared to the bulk value (approximately 0.6 at the surface and 0.02 in the bulk). Constant OI was found in the bulk material below the depth of 2500 µm.

Die approbierte gedruckte Originalversion dieser Dissertation ist an der TU Wien Bibliothek verfügbar.
The approved original version of this doctoral thesis is available in print at TU Wien Bibliothek.

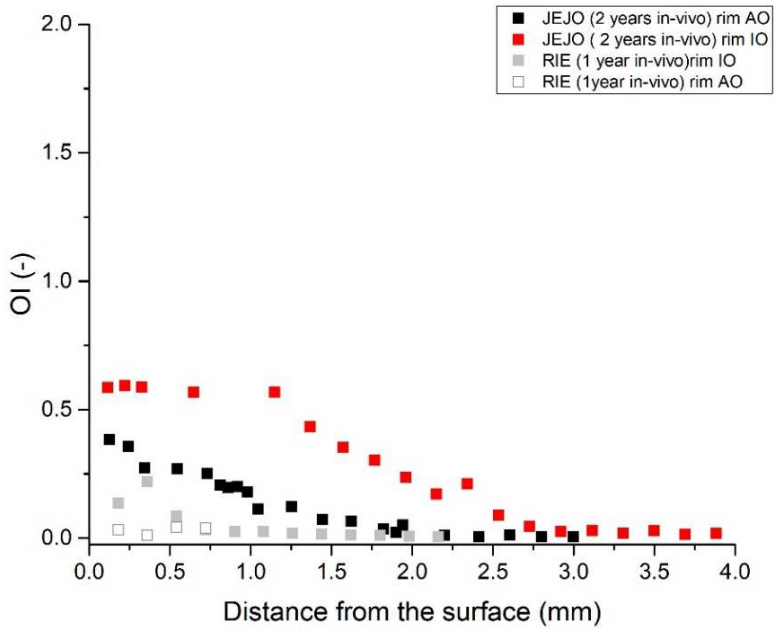

Figure 6. 15 Durasul® OI profile as a function of distance

The degree of crystallinity was plotted as a function of distance in Figure 6.16. No significant variations in degree of crystallinity were observed throughout the distance.

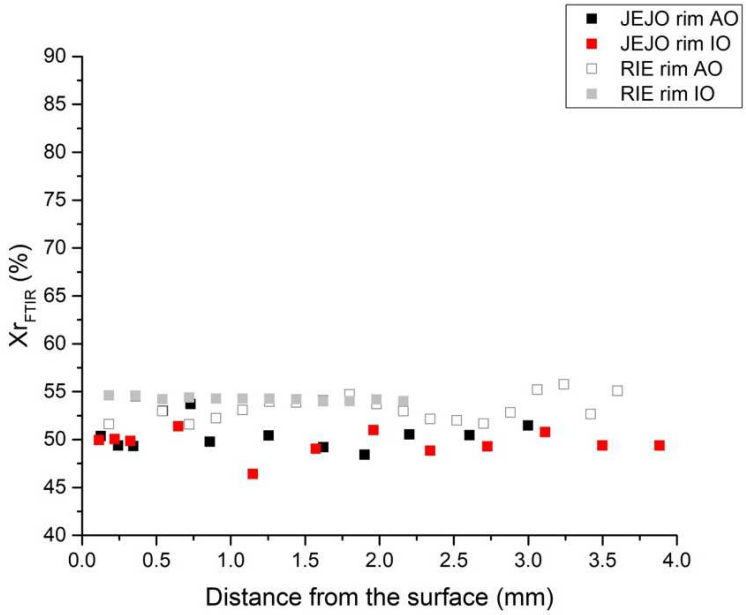

Figure 6. 16 Durasul® degree of crystallinity profile as a function of distance

Die approbierte gedruckte Originalversion dieser Dissertation ist an der TU Wien Bibliothek verfügbar.
The approved original version of this doctoral thesis is available in print at TU Wien Bibliothek.
TU Bibliothek Your knowledge hub WIEN

The through thickness variations in OI values for the X3™ (PLWI, LAMA1, LAMA2 and FIN) are represented in Figure 6.17. Increased OI was observed at the surface and sub-surface for LAMA1 rim IO. LAMA1 rim IO exhibited the largest increase in surface OI when compared to the bulk value (0.7 at the surface and 0.3 in the bulk), then constant OI was found in approximately below the depth of 1000 µm. PLWI, LAMA2 and FIN displayed no significant variations in OI at the surface and the bulk regions.

Figure 6.18 shows the degree of crystallinity of X3™ explants (on the rim regions) as a function of distance, which roughly follows the same pattern as OI. No significant variations in degree of crystallinity can be seen.

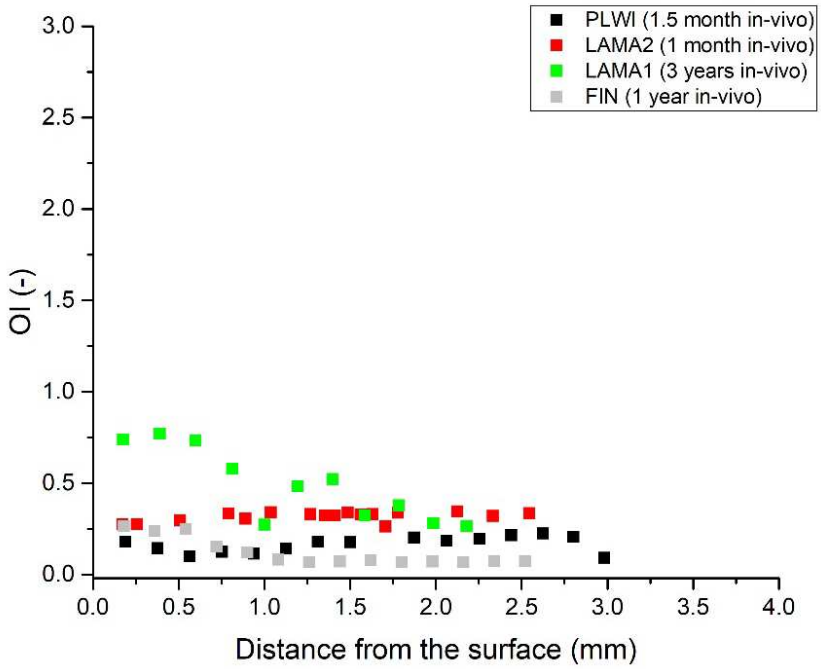

Figure 6. 17 X3™ OI profile as a function of distance

Die approbierte gedruckte Originalversion dieser Dissertation ist an der TU Wien Bibliothek verfügbar.
The approved original version of this doctoral thesis is available in print at TU Wien Bibliothek.

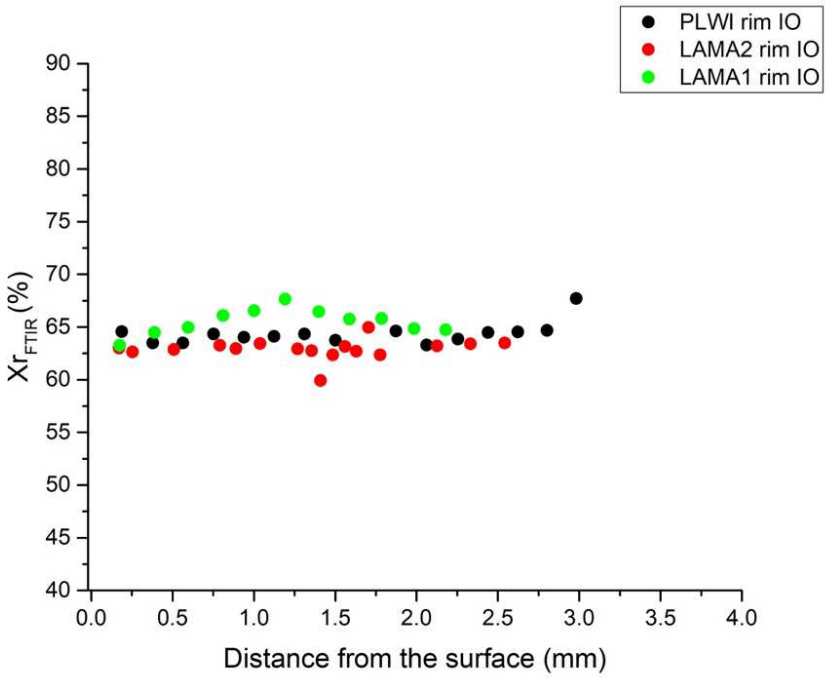

Figure 6. 18 X3™ degree of crystallinity profile as a function of distance

In Figure 6.19, the OI values of DePuy (MAWO) explant are shown as a function of distance. An increase in OI values was observed at the bearing surface of MAWO but also in the sub-surface regions of MAWO ranging from 250 µm to 1850 µm. MAWO rim IO has a maximum value of 1.24 at a depth of 560 µm and MAWO center IO has 1.23 at a depth of 900 µm. In the inner surfaces OI declines to approximately 0.2 at a depth of 2500 µm and stays constant. An approximate six-fold increase in OI values was observed at the bearing surface in MAWO inner surfaces when comparing to outer surfaces. There were no significant OI variations in MAWO outer surfaces and in bulk materials.

Die approbierte gedruckte Originalversion dieser Dissertation ist an der TU Wien Bibliothek verfügbar.
The approved original version of this doctoral thesis is available in print at TU Wien Bibliothek.
TU Bibliothek Your knowledge hub WIEN

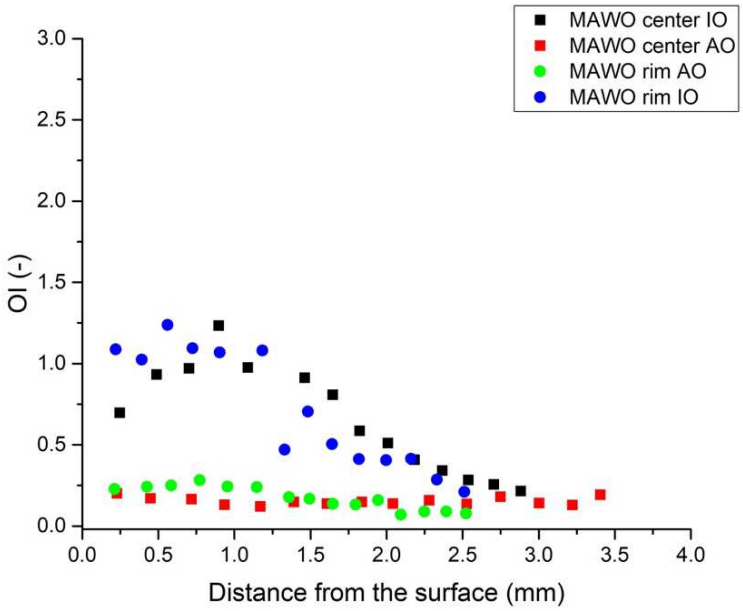

Figure 6. 19 DePuy OI profile as a function of distance

The degree of crystallinity profiles in individual part of the explant more or less followed the same pattern as OI. There was no significant degree of crystallinity variations in outer surfaces and bulk. Inner surfaces of the explant showed slightly higher degree of crystallinity than outer surfaces (Figure 6.20).

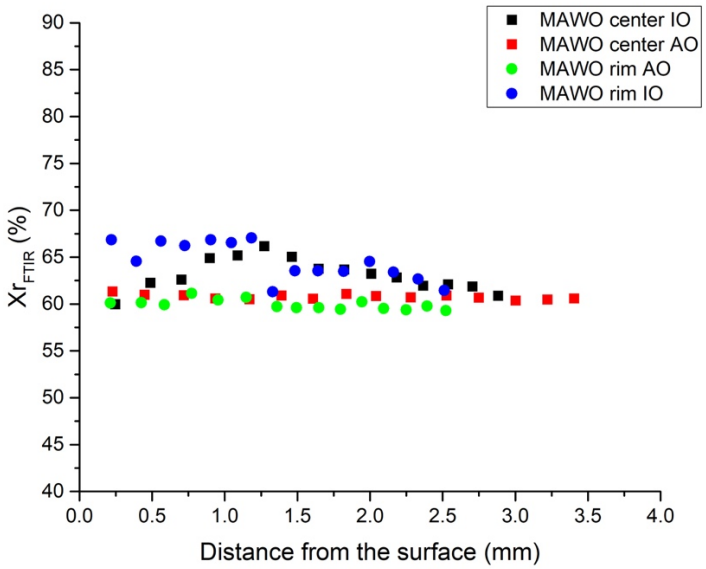

Figure 6. 20 DePuy degree of crystallinity profile as a function of distance

Die approbierte gedruckte Originalversion dieser Dissertation ist an der TU Wien Bibliothek verfügbar.
The approved original version of this doctoral thesis is available in print at TU Wien Bibliothek.
TU Bibliothek Your knowledge hub WIEN

Assessment of OI Results

FTIR imaging is a powerful tool that can accurately map variations in chemical properties across the sample thickness.

In this study, conventional and cross-linked explants were evaluated using FTIR imaging considering their short-term and long-term in-vivo time.

The assessed explants were selected as they represented a range of implant times and followed the same pattern OI and degree of crystallinity in the aforementioned individual groups.

It is difficult to interpret the results of conventional explants without having type of resin, sterilization method and length of shelf time. However, AUMA, GOKA, KOR and REOP might have been gamma irradiated in air due to their implantation time is before the year of 1998 (Gamma irradiation in air was stopped in 1998) [74].

AUMA has bone ingrowth outside of the acetabular cup, hence it could not be evaluated. AUMA rim IO and Centre IO have the same OI distribution. Design of the endoprosthesis can be affect the OI due to contact surface to the synovial fluid. This means both surfaces contact with the synovial fluid in -vivo. Kurtz et al [197] claimed that in-vivo degradation was influenced by a mechanism that uses molecular oxygen dissolved in body fluids as the primary chemical fuel for in-vivo degradation process. They hypothesized that dissolved oxygen diffuses into the UHMWPE component and reacts with residual free radicals from gamma sterilization in a similar manner to shelf aging but at a slower rate.

Increased OI was observed in the subsurface regions of AUMA and at the surface of KOR and REOP. One explanation is that explants are so brittle and while microtoming some samples from the bearing surface might be lost. This brittle subsurface layer commonly referred to as 'white band' [225-227] is essentially governed by the availability of oxygen to free radicals generated during gamma irradiation. At the surface of components, there is an abundance of atmospheric oxygen and high surface area. Free radicals are consumed in this region as they rapidly react with the atmospheric oxygen. As the distance from the bearing surface increases, the availability of oxygen decreases but the presence of free radicals increases enabling oxidation of the material. In the bulk of the material, there are available free radicals, but oxygen levels are not sufficient to promote

Die approbierte gedruckte Originalversion dieser Dissertation ist an der TU Wien Bibliothek verfügbar.
The approved original version of this doctoral thesis is available in print at TU Wien Bibliothek.
TU Bibliothek Your knowledge hub WIEN

oxidation of the material. The presence of 'white band' has been reported in a number of UHMWPE component retrieval studies [227, 228].

In conventional explants, OI increases with increasing in-vivo time. OI value of AUMA is higher than KOR and REOP explants. According to Kurtz, the value of oxidation can be defined as follows: If OI is lower than 1, it means there is low oxidation. If it is between 1 and 3, oxidation is moderate. If it is greater than 3, there is critical oxidation [229]. AUMA, KOR and REOP explants show the same oxidation distribution across the liner thickness and having critical oxidation value in the subsurface (down to 2 mm). The oxidation value decreases moving towards the bulk of the materials. This can be due to trapped free radicals in the crystalline region move to amorphous phase and diffusing oxygen from synovial fluid is very slow in-vivo [85]. Another possible oxidation initiator is cyclic loading and/or body fluids absorption [230]. The studies [231-234] implies that the subsurface degradation depends on chemical and physical changes after more than 5 years.

Increasing the chain scission via oxidation leads to increasing degree of crystallinity. Oxidation mostly starts with gamma radiation sterilization method. This breaks the C-C and C-H bonds and generated free radicals. This leads to shortening of molecular chains. Shortening of molecular chains enhances chain mobility and allows to recrystallization by crystal perfection process [40].

There are no severe OI changes in sandwich type conventional explants because the articulating surface is protected somehow by a metal shell. At the surface GOKA has high scattering OI. This could be by mechanical stress during microtoming [235]. Due to inconvenient explant thickness, it is not easy to avoid this kind of problems. Also, there were no significant changes in degree of crystallinity across the distance of the explant. Therefore, comparing sandwich types of explants results with other explant results is not convenient because UHMWPE is not affected by neither synovial fluid nor femoral head contact.

Low OI profile was found for different types of cross-linked explants with very short in-vivo (min. 1 month) and long in-vivo (max.24 years) time. It is observable that X3™ (annealed) explants have slightly higher OI values than Durasul® (remelted) explants (both have short in-vivo time). It seems that the remelted explants are better stabilized against oxidative degradation, but the degree of crystallinity is lower than annealed explants. These results are in concordance with literature findings [74]. If there is no change in OI profile the degree of crystallinity profile does not change

Die approbierte gedruckte Originalversion dieser Dissertation ist an der TU Wien Bibliothek verfügbar.
The approved original version of this doctoral thesis is available in print at TU Wien Bibliothek.
TU Bibliothek Your knowledge hub WIEN

with the distance. It can be hypothesized that differences in a type of acetabulum, liner design and cross-linking also influence the oxidation results.

6.4 DSC Results

The differential scanning calorimetry (DSC) monitors heat effects as a function of temperature. The heat effects in the materials indicate phase transitions and chemical reactions.

The melting point of UHMWPE crystals (T_m) for the first and second heating run and then cooling to measure the crystallization temperature (T_c), onset crystallization temperature (T_{onset}) and degree of crystallinity (Xr) were calculated from the DSC data. DSC results and calculated lamellar thickness distribution of explants can be found in APPENDIX E.

As the characteristic temperatures and degree of crystallinity do not differ as a function of depth (Ref. section 6.3), DSC samples were chosen from the OI values where the highest differentiation observed with respect to distance from the surface.

6.4.1 Crystallinity Results

The following figures are showing the variation of Xr vs. distance from surface for conventional and cross-linked explants. Fig. 6.21 (AUMA) represents conventional, Fig. 6.23 (PLWI) represents cross-linked short in- vivo time and Fig. 6.24 (MAWO) represents cross-linked long in-vivo time sample groups. All other crystallinity degree results can be found in APPENDIX E for each sample group.

Die approbierte gedruckte Originalversion dieser Dissertation ist an der TU Wien Bibliothek verfügbar.
The approved original version of this doctoral thesis is available in print at TU Wien Bibliothek.
TU Bibliothek Your knowledge hub WIEN

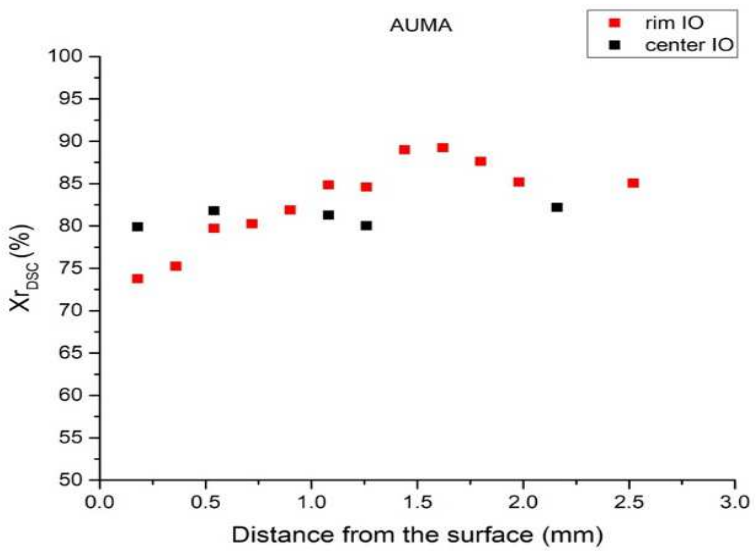

Figure 6. 21 AUMA (31 years in-vivo) degree of crystallinity profile as a function of distance

An increase in Xr values was observed at the bearing surface of AUMA rim IO. Increased Xr values were observed in the sub-surface regions of AUMA rim IO ranging from 400 µm to 2000 µm. There were no significant variations in Xr in AUMA center IO and it has slightly lower Xr than AUMA rim IO. The Xr on the rim region and center roughly followed the same pattern as OI which were obtained from FTIR data. AUMA center IO had a maximum Xr of 82.2 % at a depth of 2000 µm, AUMA rim IO displayed a peak of 89.2 % at a depth of 1620 µm. Higher Xr was found in the highly oxidized regions.

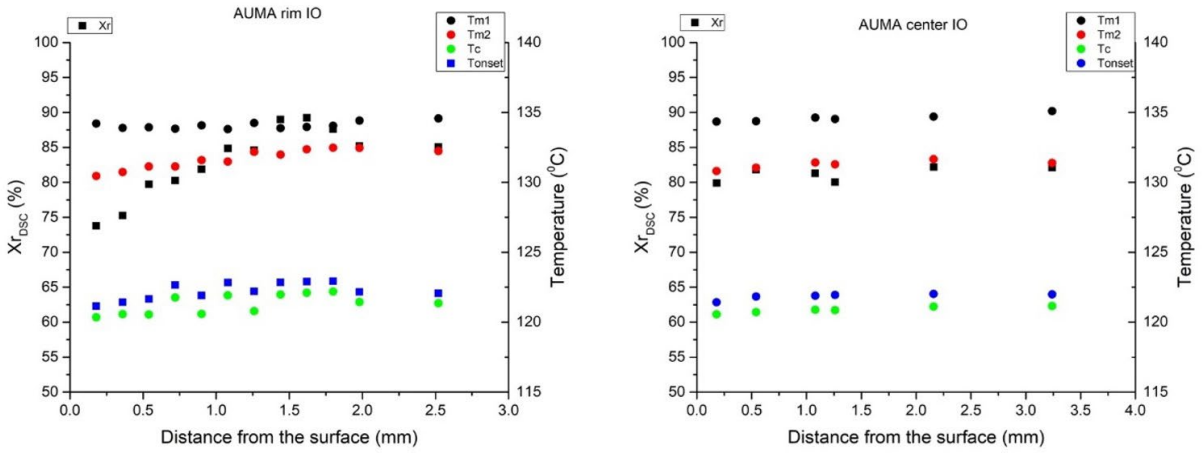

Figure 6. 22 AUMA degree of crystallinity and thermal data profile as a function of distance

Die approbierte gedruckte Originalversion dieser Dissertation ist an der TU Wien Bibliothek verfügbar.
The approved original version of this doctoral thesis is available in print at TU Wien Bibliothek.
TU Bibliothek Your knowledge hub WIEN

There is a slight change in the thermal data of AUMA. The difference in T_{m1} and T_{m2} was approximately 2°C and did not vary much through the distance from the surface.

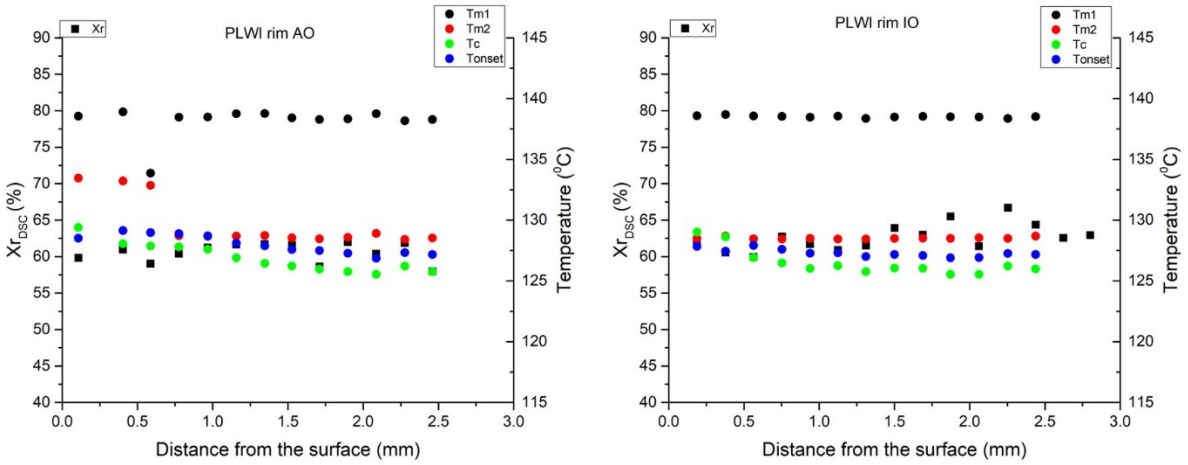

Figure 6. 23 PLWI degree of crystallinity and thermal data profile as a function of distance

There were no significant variations between surface and bulk Xr in PLWI rim IO and rim AO. The difference in T_{m1} and T_{m2} was approximately 10°C and did not vary with a through the distance of a depth.

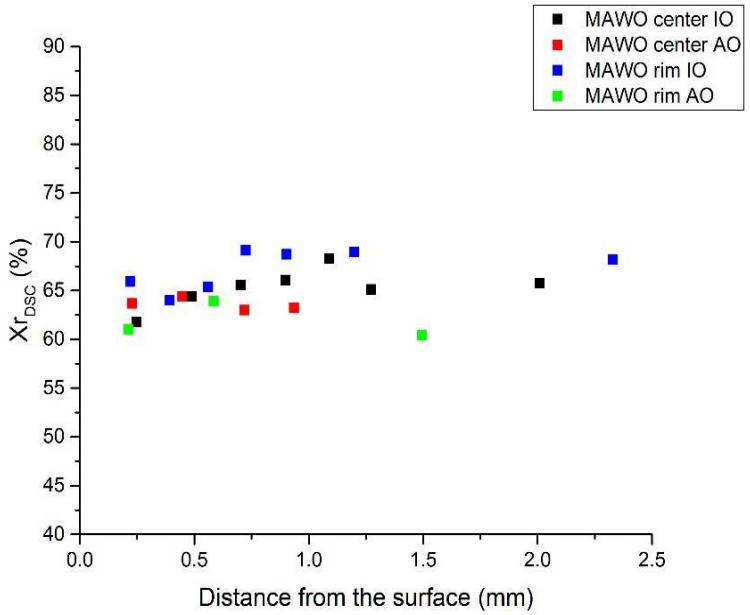

Figure 6. 24 MAWO degree of crystallinity profile as a function of distance

Die approbierte gedruckte Originalversion dieser Dissertation ist an der TU Wien Bibliothek verfügbar.
The approved original version of this doctoral thesis is available in print at TU Wien Bibliothek.
TU Bibliothek Your knowledge hub WIEN

Increased Xr was observed at the surface for all regions. MAWO rim IO exhibited the largest increase on surface Xr when compared to the outer surfaces of explant (approximately 63 % at the outer surfaces and 68 % in rim IO).

An increase in Xr values was observed at the bearing surface, also in the sub-surface regions of MAWO ranging from 250 µm to 1000 µm. MAWO center IO had a maximum degree of crystallinity of 82.2 % at a depth of 2000 µm, MAWO rim IO displayed a peak of 89.2 % at a depth of 1620 µm. On the bulk region Xr remains unchanged. There were no significant Xr variations in MAWO outer surfaces and in bulk materials. Inner surfaces of the explant showed slightly higher Xr than outer surfaces (Figure 6.25).

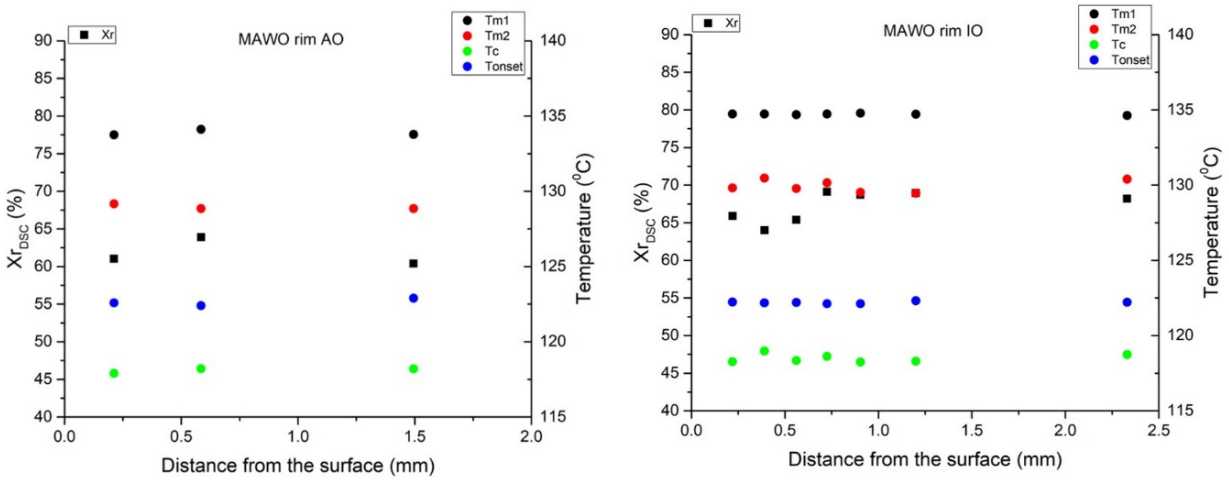

Figure 6. 25 MAWO degree of crystallinity and thermal data profile as a function of distance

There were no significant variations between surface and bulk thermal data of MAWO.

The lamellar thickness distribution (LTD) was calculated from the first and second DSC heating runs. AUMA (conventional) has a more uniform lamellar thickness distribution and the existence of bigger lamella with an average value of 35 nm is not seen. After the first melting in DSC maximum lamellar thickness reduced significantly. For AUMA maximum peak shifted to from 22nm to 18 nm, for KOEV (Link) from 38 nm to16 nm and for TRCH (X3™) from 30 nm to 9 nm. JEJO (Durasul®) has more distinct two peaks; the second peak located around 28 nm and decreased to 24 nm after the first heating run. However, its first peak did not change much. The calculated LTD from the second run is reduced remarkably for KOEV and TRCH explants (Figure 6.26).

Die approbierte gedruckte Originalversion dieser Dissertation ist an der TU Wien Bibliothek verfügbar.
The approved original version of this doctoral thesis is available in print at TU Wien Bibliothek.
TU Bibliothek Your knowledge hub WIEN

Increasing the radiation dose leads to broader lamellar thickness distribution (KOEV and TRCH have 75 kGy, JEJO has 95 kGy irradiation dose). Hence very thick lamellae occur approximately up to 65 nm for JEJO and 75 nm for KOEV and TRCH.

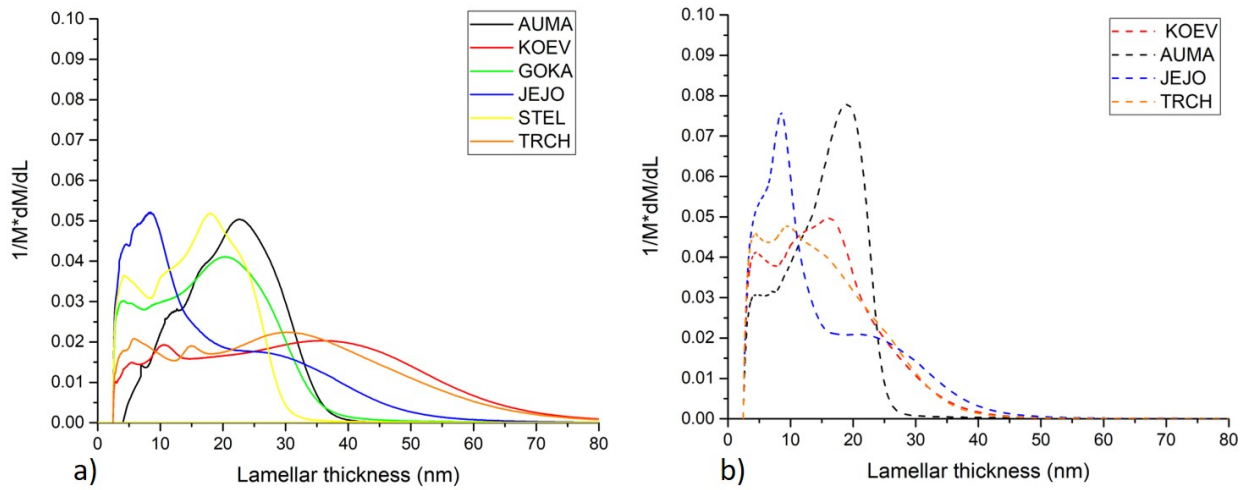

Figure 6. 26 Lamellar thickness distribution (LTD) of explants rim IO as a function of depth; a) LTD calculated from the first heating run, b) LTD calculated from the second heating run

Assessment of DSC Results

It is obvious that after long in-vivo time in conventional explant, the degree of crystallinity has increased significantly, while melting point (T_m) values slightly change. This can be explained by chain scission on implanted UHMWPE samples, which leads to a reduction in the molecular weight of the material. This allows the chains to rearrange to form crystalline regions and Xr increasing.

With increasing in-vivo time, the cross-linked explant shows no change in T_m. On the other hand, the Xr slightly increases. In addition, the second melting temperature shows very similar traces for all individual groups because the thermal history is erased by melting and recrystallizing and no degradation can be found.

The first melting temperature indicates that crosslinking increases the melting temperature of the explant. The second melting temperature is lower than the first melting temperature because the crosslinking and disentanglements have inhibited recrystallization after the first melt. Irradiation leads to thicker crystals that take more energy to melt, hence they have higher melting point than conventional explants. The melt temperature reflects the thickness of the crystals, as well as their

Die approbierte gedruckte Originalversion dieser Dissertation ist an der TU Wien Bibliothek verfügbar.
The approved original version of this doctoral thesis is available in print at TU Wien Bibliothek.
TU Bibliothek Your knowledge hub WIEN

perfection. Thicker and more perfect polyethylene crystals will tend to melt at a higher temperature than smaller crystals [83, 95].

As stated in the Literature [83, 155, 236] GUR 1050 (Durasul®) Xr degree is lower than GUR 1020 (X3™). With higher molar mass the chains are more entangled therefore during crystallization it is difficult for them to incorporate. Thermal remelting reduces the degree of crystallinity [237]. T_{m2} is lower than T_{m1} and there is a big difference between them in crosslinked and remelted explants (PLWI-X3™). The crosslinks produced prevents recrystallization to the same degree and this effect can be observed for all T_{m2}.

The increase in Xr is more dramatic in long in-vivo time conventional explant, however there was slight difference in Tm between the conventional and cross-linked explants. Overall, it can be stated that Xr is increasing with in-vivo time.

The changing the irradiation dose leads to alteration to lamellar thickness distribution. Irradiation causes the scission of the stretched tie molecules. This phenomenon allows the recrystallization of broken chains in the amorph phase, which is probably thickening existing crystals or new formation of thick crystals [173]. It was found that increasing the radiation dose leads to broader lamellar thickness. However, Durasul® has a higher irradiation dose than other explants (shown in Table 5.2). It can be said that after irradiation thermal treatment plays an important role in lamellae morphology. With the annealing effect, polymer chains have enough time to disentanglement and incorporation of growing lamellae due to slow kinetics [238]. Remelting results in forming small lamellae, a shift of the maximum first peak around 8 nm in JEJO explant (Durasul®).

The formation of broadening lamellae of explants due to high-pressure crystallization (KOEV/Link) or sequentially irradiation and annealed (X3™/Stryker) leads to a melting temperature above 140 ^{o}C.

High melting temperature indicates the formation of extended chain lamellae. Thermodynamically, extended chain crystals have lower free energy than folded chains under high pressure and increasing the pressure increases the formation of extended chains [239, 240].

Calculated lamellar thicknesses depend on the heating run and parameters in the Equation 5.6 and 5.7 (In Chapter 5.2.2). In the study [241] reported that the suitable heating run is 10 °C /min for semi-crystalline polymers which is used in this study. Small lamellae formation adversely affects

Die approbierte gedruckte Originalversion dieser Dissertation ist an der TU Wien Bibliothek verfügbar.
The approved original version of this doctoral thesis is available in print at TU Wien Bibliothek.
TU Bibliothek WIEN Your knowledge hub

the mechanical properties such as low values of E-modulus and toughness which is discussed in the next chapters.

6.5 Depth Sensing Indentation Results

There was no change in indentation values for short in-vivo time explants. Therefore, all micro hardness and indentation modulus results can be found in APPENDIX F.

Micro hardness (H_{IT}) and indentation modulus (E_{IT}) depth profiles for AUMA are shown in Figure 6.27. The H_{IT} and E_{IT} depth profiles showed reduced values at the bearing surface between 100 µm and 500 µm. Increased values of H_{IT} and E_{IT} can be observed between 750 µm and 2000 µm. There was a minimal variation at bulk (>2000 µm) E_{IT}-depth profile roughly followed a similar pattern as the H_{IT}-depth profile. There is a good correlation of the mechanical properties with the crystallinity results collected from the DSC (see in Chapter 6.4.1).

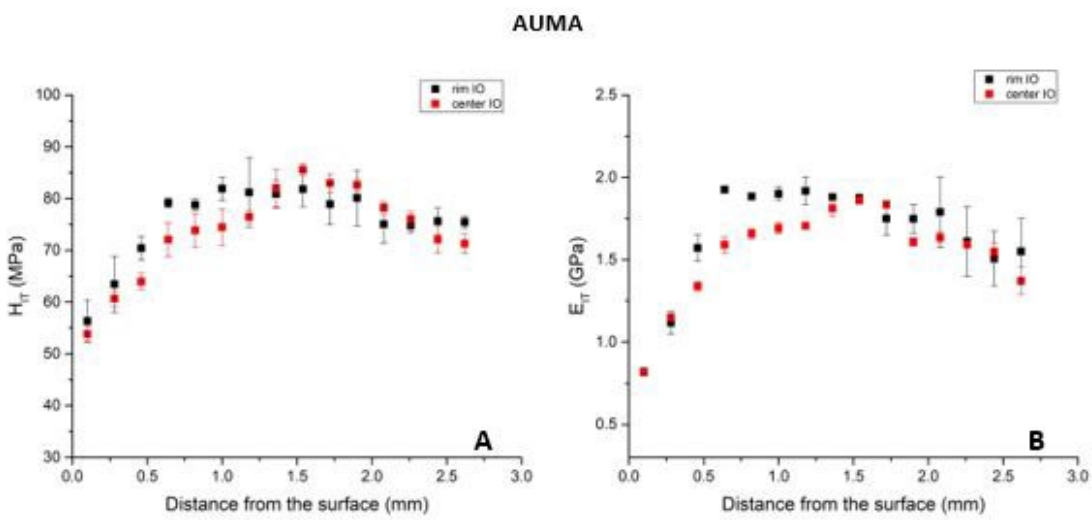

Figure 6. 27 a) Hardness profile as a function of depth b) Indentation modulus profile as a function of depth

Unlike the distribution of data for conventional explant, variation in H_{IT} and E_{IT} profiles was very similar and no significant variations were seen in H_{IT} and E_{IT} at the bearing and sub-surfaces of cross-linked explants (in Figure 6.28).

Die approbierte gedruckte Originalversion dieser Dissertation ist an der TU Wien Bibliothek verfügbar.
The approved original version of this doctoral thesis is available in print at TU Wien Bibliothek.
TU Bibliothek Your knowledge hub WIEN

The E_{IT}-depth profile followed a similar pattern as the H_{IT}-depth profile. No significant variations in E_{IT} values were observed through the distance.

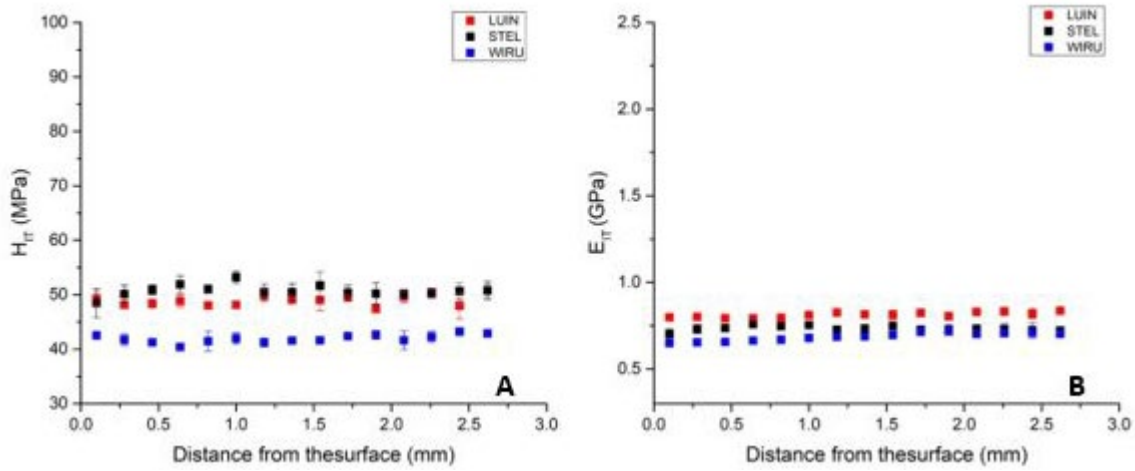

Figure 6. 28 a) H_{IT} profiles as a function of depth for all cross-linked explants b) E_{IT} profiles as a function of depth for all cross-linked explants

Assessment of DSI Results

In DSI, micro hardness and elastic-modulus through the thickness of conventional and cross-linked UHMWPE explants have been investigated. Hardness and elastic modulus are effective on the abrasive and adhesive wear resistance of polymeric bearing surfaces [242]. These mechanical properties play a key role in the longevity of the joint replacement and wear mechanisms.

The results showed significant differences through the thickness of conventional and cross-linked explants. In conventional explants, there was a significant decrease in H_{IT} and E_{IT} of the UHMWPE at the bearing surface whereas such a variation was not statistically significant in cross-linked explants.

For the conventional explants, the variations in mechanical properties in the sub-surface and bulk of UHMWPE were a direct result of time-dependent post irradiation effects. Oxidation process is in good agreement with indentation modulus values. Post irradiation effects and oxidation process were discussed in Section 6.3.

Die approbierte gedruckte Originalversion dieser Dissertation ist an der TU Wien Bibliothek verfügbar.
The approved original version of this doctoral thesis is available in print at TU Wien Bibliothek.
TU Bibliothek Your knowledge hub WIEN

In the sub surface region, the increase in in-vivo oxidation, results in elevated H_{IT} and E_{IT} values whereas in the bulk, there was no change as the oxidation moves in a slower rate in-vivo. The hardness and elastic modulus values in the bulk of explants with individual parts i.e. rim and center were comparable indicating that at depths >2000 µm, the progression of oxidation was uniform. This observation is similar to the results reported in [243-245].

There was an increase in H_{IT} and E_{IT} values in sub-surface regions (750 µm to 2000 µm) for conventional explants. Increase in hardness and elastic modulus are dependent on in-vivo time strongly.

In DePuy cross-linked explants, the H_{IT} and E_{IT} were found to be independent of the in-vivo time i.e no change in mechanical properties with long in-vivo time.

The results also demonstrated the sensitivity of the indentation test method to variations in the structure of UHMWPE. Reduction in H_{IT} of the bearing surface in conventional explants may be associated to the ingress of constituents of synovial fluid into the surface of the material. In contrast to conventional explants, cross-linked explants didn't display a decrease in hardness or elastic modulus at the bearing surface. Secondly, degradation at the bearing surface of conventional explants is thought to be due to the multi-directional re-orientation of surface layers of worn regions [93, 246, 247]. Removal of particles from the surface causes shearing of the polyethylene. This permanent re-orientation results in a reduction of surface hardness [74].

6.6 Small-punch Results

The peak load (N), the ultimate load (N), the ultimate load -displacement (mm), and work to failure (mJ) were calculated from the small punch test (SPT). All tabulated data and SPT curves of materials can be found in APPENDIX G.

The general features in SPT load-displacement curves indicates whether a material has high or low ductility. Low ductility behavior is identified by predominately linear load-displacement curves and a sharp load-drop at failure, whereas high ductility behavior is identified by bending and stretching regions as shown in section 5.3.2 [196].

SPT sample preparation was not so easy and repeatability of the test was affected from the degradation of the UHMWPE, thus SPT was run for three to four sub samples of each UHMWPE

Die approbierte gedruckte Originalversion dieser Dissertation ist an der TU Wien Bibliothek verfügbar.
The approved original version of this doctoral thesis is available in print at TU Wien Bibliothek.
TU Bibliothek Your knowledge hub WIEN

type. As the standard deviation of work to failure was too high among sub samples, only the average curves are used as shown in Figures 6.29 to 6.32.

Figure 6.29 shows that lower molecular weight of the UHMWPE is causing a lower ultimate load with a strain softening effect. Figure 6.29 also shows that GUR 1020 is more ductile than GUR 1050, since the displacement is longer.

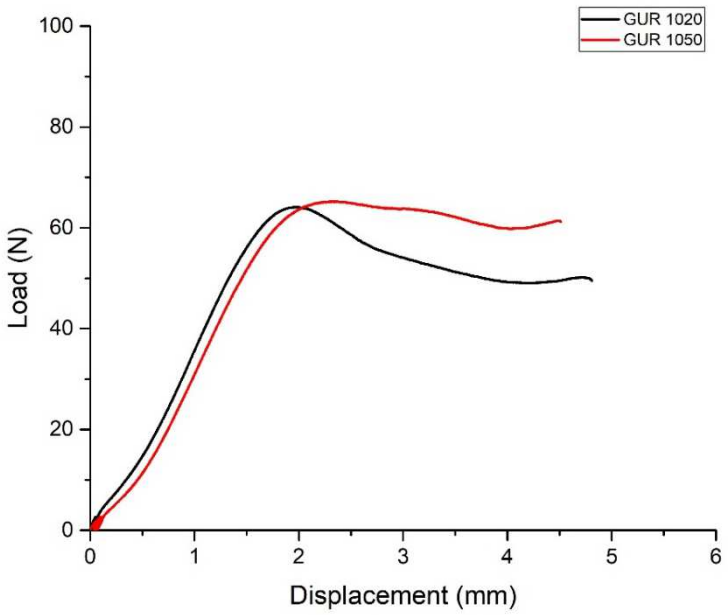

Figure 6. 29 The load-displacement curve of GUR 1020 and GUR 1050

Figures 6.30 A and B show two load-displacement plots of polymer block (GUR 1020, non-cross-linked) vs. two different types of cross-linked UHMWPE, X3™ and KOEV. In cross-linked explants (X3™ and KOEV) the ultimate tensile strength is increasing as ductility and fracture toughness are decreasing. The post-peak load region of the load-displacement curve showed strain-hardening for cross-linked explants.

Die approbierte gedruckte Originalversion dieser Dissertation ist an der TU Wien Bibliothek verfügbar.
The approved original version of this doctoral thesis is available in print at TU Wien Bibliothek.
TU Bibliothek Your knowledge hub WIEN

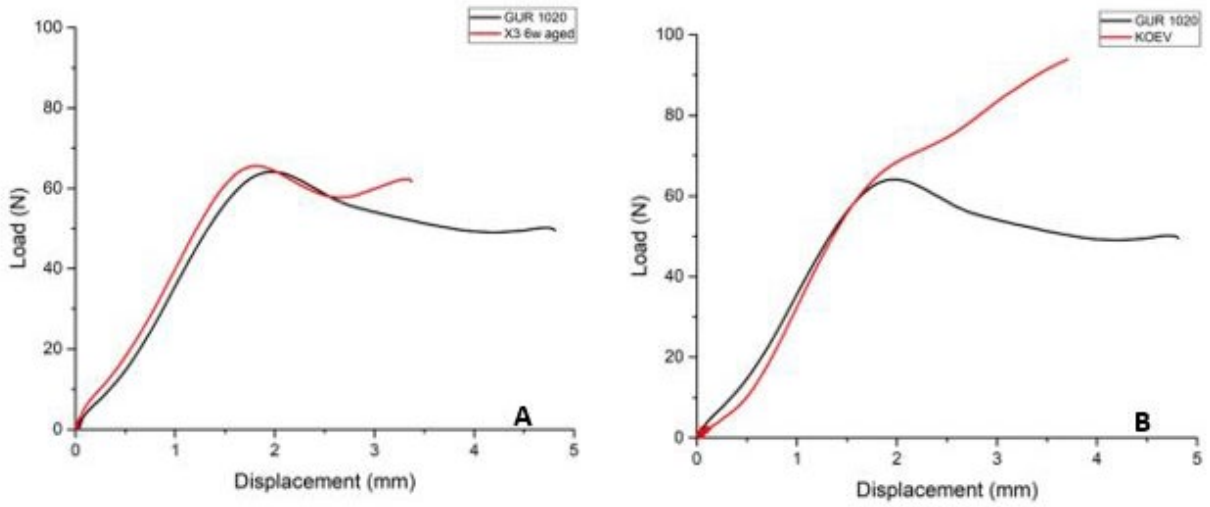

Figure 6. 30 The load displacement curve of A) GUR 1020 and X3™ and B) GUR 1020 and cross-linked explant

Figure 6.31A shows that strain softening is clearly seen for UHMWPE which have long in-vivo time and shelf aging. As the area under the curve and the initial slope of the curve represents toughness and stiffness, respectively, long in-vivo time leads to a dramatic fall in the toughness of the material. In addition, AUMA and REOP had a typical fracture of ductile behavior as they have an elongation trend, whereas KOR had a brittle fracture as it has sudden downward trend at around 2 mm.

In Fig.6.31B, the load-displacement curves are identical for three cross-linked explants (DePuy), which have approximately 15 years in-vivo time. They all displayed strain hardening during the drawing phase. The peak load, the ultimate load and work to failure were significantly greater than conventional explants shown in Figure 6.31A.

Die approbierte gedruckte Originalversion dieser Dissertation ist an der TU Wien Bibliothek verfügbar.
The approved original version of this doctoral thesis is available in print at TU Wien Bibliothek.

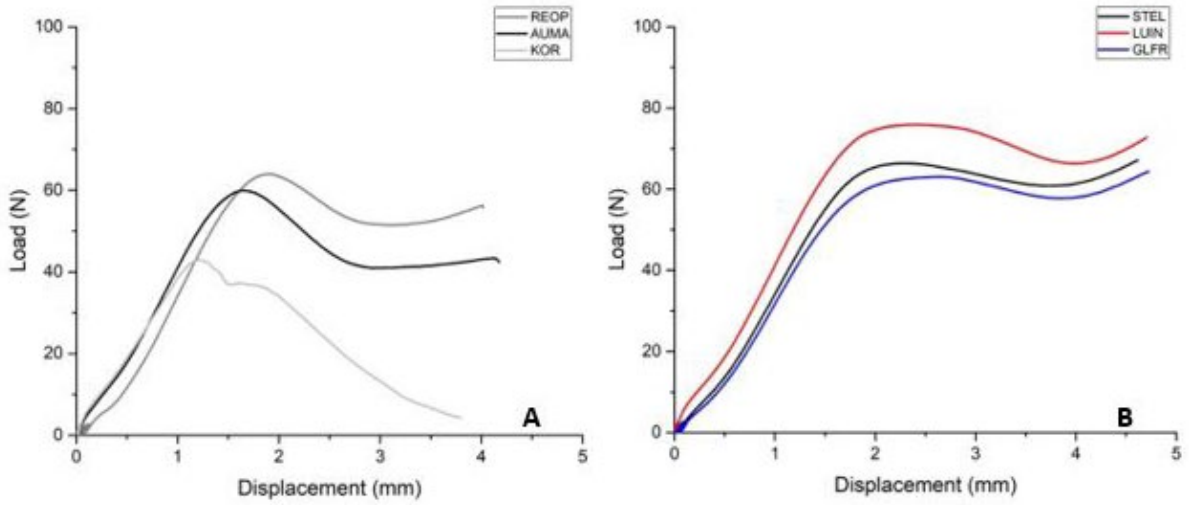

Figure 6. 31 The load displacement curve of A) conventional and B) cross-linked explants

Figure 6.32A shows the load-displacement curve comparison of GUR 1050 and Durasul® (Dsa) cross-linked implants with accelerated aging conditions. The characteristic curve of GUR 1050 and Durasul® is clearly different from each other at the maximum load and in the end part of the curve. The Durasul® first reaches the maximum load and then slightly drops and continues with hardening process, which develops until the rupture of the specimen.

In Figure 6.32 B shows the comparison of Durasul® after 3 and 6weeks aging. The curve of the 3 weeks aged Durasul® is slightly different from the 6 weeks aged Durasul® curve. The ultimate tensile strength increases with aging, however, the work to failure decreases indicating a loss of toughness.

Die approbierte gedruckte Originalversion dieser Dissertation ist an der TU Wien Bibliothek verfügbar.
The approved original version of this doctoral thesis is available in print at TU Wien Bibliothek.

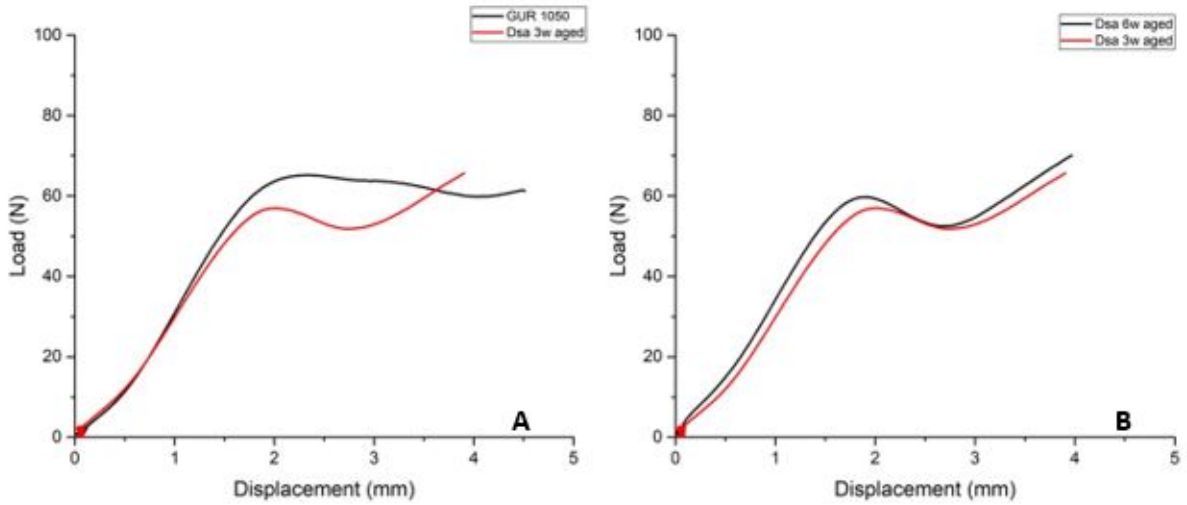

Figure 6. 32 The load displacement curve of A) GUR 1050 and Durasul® (Dsa) 3weeks aged implant and B) Different aging time of Dsa implants

Assessment of SPT Results

The aim of using SPT is to characterize the mechanical performance of UHMWPE especially ductility and toughness. The specimens for SPT were prepared from both bulk material and some of the explants and implants (sample preparation from articulating surface was not possible for each explant and implant as most of the material was consumed for FTIR, DSC and nano indentation for those).

Some explant samples became brittle as a result of oxidation. This situation created some difficulties in cutting the samples. The small variations in the thickness of samples causes great standard deviations in the experimental results due to high sensitivity of the SPT device. Thus, SPT was run for three to four sub samples of each such explant type and average sample result curves are used as shown in Figures 6.29 to 6.32.

Downward trends in the load-displacement curves indicate the degradation of the UHMWPE as well as high oxidation of the material. KOR is the maximum degraded explant (see in chapter 6.3) and has the minimum value of work to failure. Long in-vivo time explants show decrease in peak load and ultimate load displacement. Oxidative degradation reduces the molecular weight and peak load of the polymer [198, 248].

The strain hardening was observed especially for cross-linked explants. Crosslinking is associated with lower work to failure in SPT [248]. Forming bonds between chains decreases chain mobility

Die approbierte gedruckte Originalversion dieser Dissertation ist an der TU Wien Bibliothek verfügbar.
The approved original version of this doctoral thesis is available in print at TU Wien Bibliothek.
TU Bibliothek Your knowledge hub WIEN

(provides ductility and plasticity) hence resulting in decreased mechanical properties [249]. Cross-linked materials have loss of toughness compared to non-crosslinked samples in Figure 6.30 and 6.32A. Cross-linking increases ultimate strength and decreases the ductility. This observation is similar to the results reported in literature [248, 250]. DePuy cross-linked explants in Figure 6.31B displayed neither low ductility nor less toughness. This could be due to irradiation dose, thermal treatment or different sterilization method. Fatigue, wear and oxidation of highly crosslinked and thermally processed materials were examined in study [112]. The moderately crosslinked and remelted UHMWPE showed good oxidation resistance but moderate fatigue crack propagation and wear resistance. The highly crosslinked remelted UHMWPE showed good oxidation resistance and wear resistance but poor fatigue crack propagation resistance. Lastly, the highly cross linked and annealed UHMWPE showed good wear resistance and fatigue crack propagation resistance but poor oxidation resistance.

Thermal treatment after cross-linking affects the mechanical behavior of UHMWPE. Cross-linked and remelted explants in Figure 6.32 showed lower ultimate tensile strength and toughness. KOEV has no thermal treatment after cross-linking (see in Table 5.2) hence has the highest peak and ultimate load.

According to the presented results, SPT is a suitable test method to evaluate the mechanical effects of oxidative degradation on UHMWPE explants. Furthermore, SPT values were compared with nano indentation and wear test to find if there is a correlation between them. A correlation was found and discussed in detail in Chapter 7.

6.7 Tribological results

In this chapter, a rotational ball-on-plate (BOP) wear simulator was used to determine the wear rate of UHMWPE materials. This study aimed at researching the effect of extended (beyond the standard) aging conditions on different types of UHMWPE (different molecular weights and Vit.E added) and cross-linked implants (X3™ and Durasul®). All tabulated wear results and wear tracks images (by using the 3D Profilometer) and materials' morphological and mechanical changes due to aging are given in APPENDIX H.

Die approbierte gedruckte Originalversion dieser Dissertation ist an der TU Wien Bibliothek verfügbar.
The approved original version of this doctoral thesis is available in print at TU Wien Bibliothek.
TU Bibliothek Your knowledge hub WIEN

These tests were specifically performed on a BOP apparatus to separate the effects of the material wear from the effects of lubrication. Working conditions for 30 N has extremely higher contact pressure for hip-joints. The results therefore showed the worst-case scenario.

6.7.1 Wear results

Figure 6.33 shows the average and standard deviation of volumetric wear rate at 85000 cycles for each material. The overall result, Figure 6.33, shows the GUR 1020 virgin is the lowest wear rate, GUR 1020 9 weeks aged has the highest wear rate and the GUR 1020 Vit. E and GUR 1050 till 3 weeks aged lies in between them. Wear rate increases rapidly from 3 weeks aged to 6 weeks aged sample for GUR 1050.

There was no remarkable change in the volumetric wear rate observed between the virgin and extended aged GUR 1020 Vit. E materials.

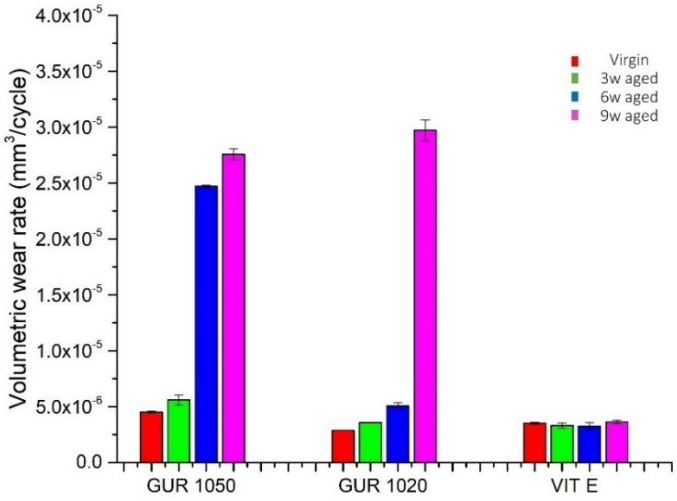

Figure 6. 33 Comparison of the specific volumetric wear rates of three UHMWPE types. Working load: 30 N

In Figure 6.34, the different volumetric wear rates of the GUR 1020 and GUR 1050 (working load 2 N) are shown. GUR 1050 and GUR 1020 virgin and 6 weeks aged samples were chosen for tribology tests due to marked difference was obtained in structural properties. Approximately 99% decrease was seen in volumetric wear rate for each sample comparing the study of 30 N (Figure 6.33).

Die approbierte gedruckte Originalversion dieser Dissertation ist an der TU Wien Bibliothek verfügbar.
The approved original version of this doctoral thesis is available in print at TU Wien Bibliothek.
TU Bibliothek Your knowledge hub WIEN

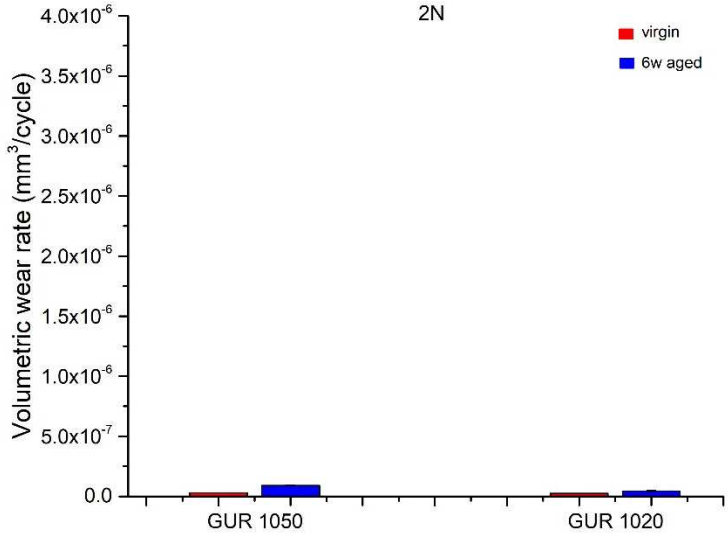

Figure 6. 34 Comparison of the specific volumetric wear rates of two UHMWPE types. Working load: 2N

In Figure 6.35 the volumetric wear rates of cross-linked implants (working load 30 N) are shown. Comparing to conventional materials depicted in Figure 6.33 in X3™ (GUR 1020) there is 60% and 75% decrease in wear rate for virgin and 6 w aged materials respectively. The Durasul®-Dsa (GUR 1050) implant has 69% and 95% decrease in volumetric wear rate for virgin and 6 w aged materials.

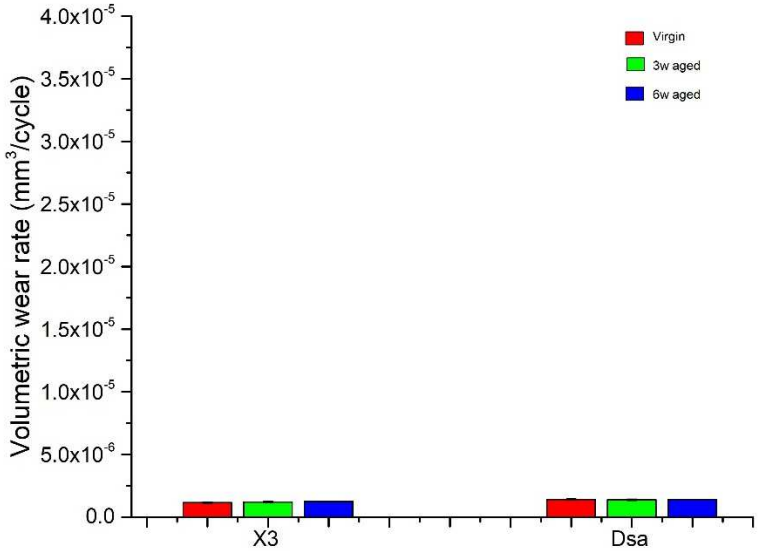

Figure 6. 35 Comparison of the specific volumetric wear rates of cross-linked implants. Working load: 30 N

Die approbierte gedruckte Originalversion dieser Dissertation ist an der TU Wien Bibliothek verfügbar.
The approved original version of this doctoral thesis is available in print at TU Wien Bibliothek.
TU Bibliothek Your knowledge hub WIEN

The surface images indicated that the primary form of wear was abrasive indicted by the grooves running in the direction of the motion along the wear path in Figure 6.36. These grooves were created by the harder steel ball through the softer UHMWPE. The UHMWPE eventually breaks off due to fatigue. With subsurface rupture more damage was seen on the surfaces of the extended aging conditions of GUR 1020 and GUR 1050.

Moderate deformation starts for GUR 1020 in 6 weeks aged samples. Severe plastic deformation is seen both 9 weeks aged GUR 1020 and GUR 1050 samples. On the other hand, for GUR 1020 Vit. E samples, the same wear track was observed with extended aging conditions.

For GUR 1050 and GUR 1020 increase in E-modulus and OI induced by aging correlates with the increase in the wear rate. For the samples GUR 1020 Vit. E, not such changes are measurable.

Figure 6.37 shows wear mechanisms obtained by 2 N load. It is clearly seen that wear tracks are narrower compared to 30 N. Despite this, the main wear mechanism is the same i.e abrasive wear. The PAA samples having high degree of OI and crystallinity showed higher amounts of wear debris during the BOP testing as a result of mechanical degradation and embrittlement [251]. In other words, severe oxidation leads even by low loads to abrasion.

Die approbierte gedruckte Originalversion dieser Dissertation ist an der TU Wien Bibliothek verfügbar.
The approved original version of this doctoral thesis is available in print at TU Wien Bibliothek.
TU Bibliothek Your knowledge hub WIEN

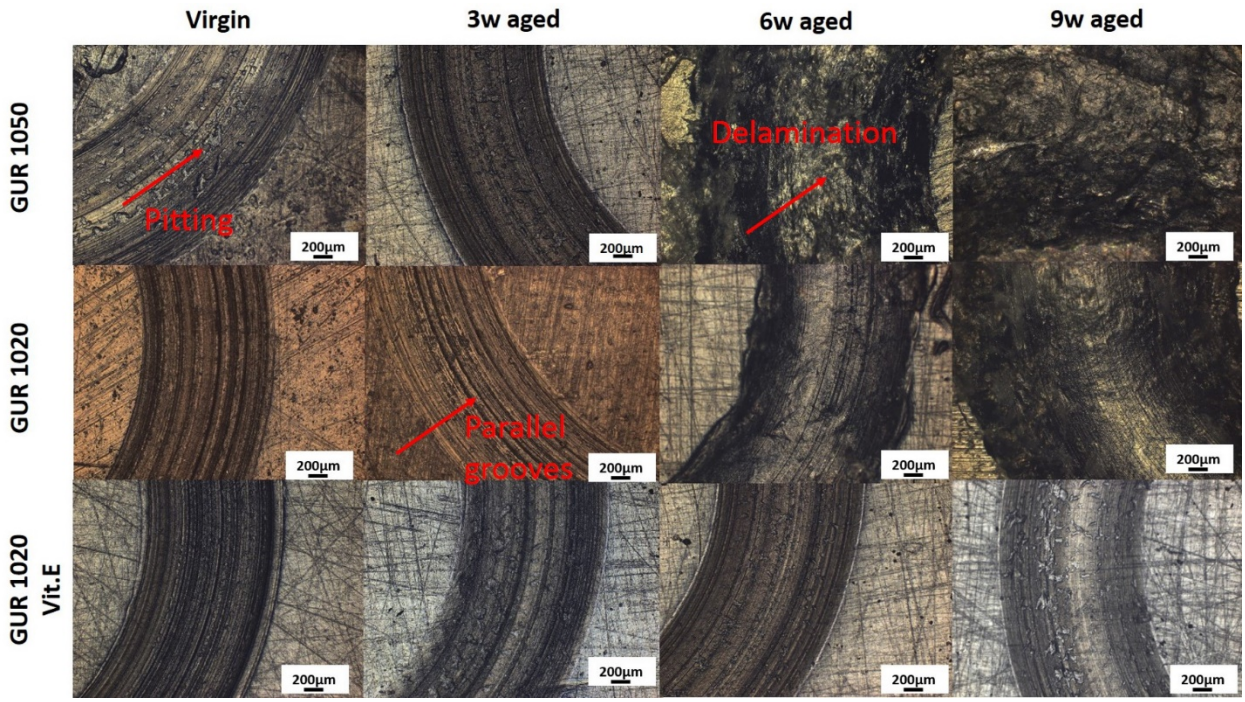

Figure 6. 36 Wear tracks for GUR 1050; GUR 1020 and GUR 1020 Vit. E. Working load: 30 N

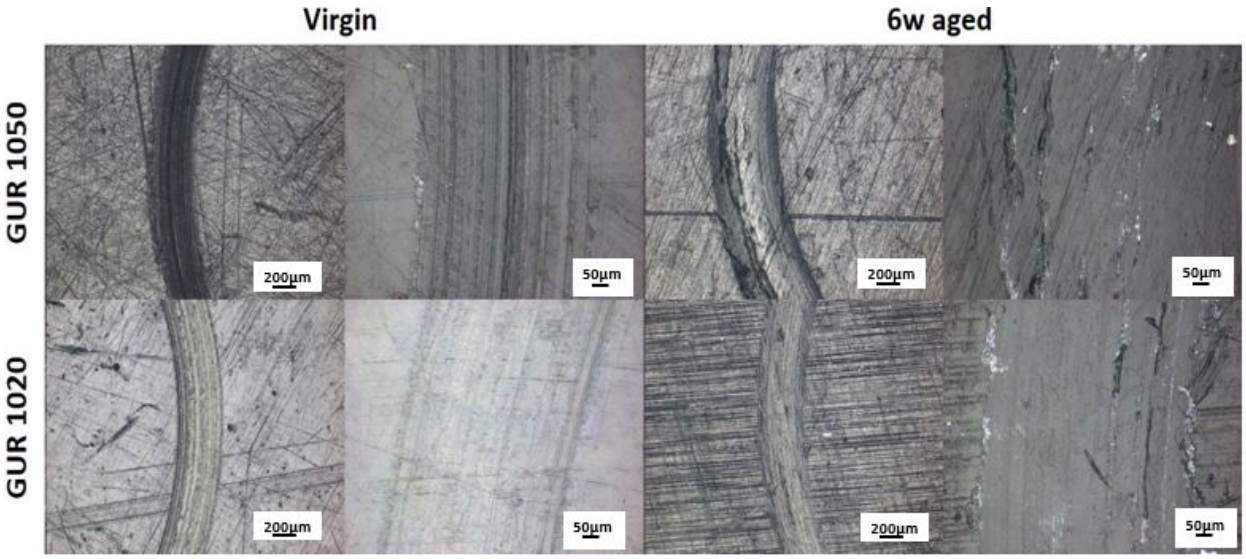

Figure 6. 37 Wear tracks for GUR 1050; GUR 1020. Working load: 2N

Assessment of Tribology Results

The volumetric wear rate of the GUR1020 UHMWPE was slightly lower than the mean wear rate for the GUR1050 UHMWPE material. The main difference between these two materials is the resin used due to different average molecular weights of the materials. The GUR1050 resin has a higher

Die approbierte gedruckte Originalversion dieser Dissertation ist an der TU Wien Bibliothek verfügbar.
The approved original version of this doctoral thesis is available in print at TU Wien Bibliothek.
TU Bibliothek Your knowledge hub WIEN

average molecular weight (7.3 x 10^6 g/mol) compared to the GUR1020 resin (4.4 x 10^6 g/mol). These differences were not expected to generate a significant difference in the wear rate, and a previous study by Tipper et al., showed no significant difference in the wear rates of GUR1050 and GUR1020 UHMWPE when using a hip simulator [97]. However, GUR 1020 shows a more ductile behavior (see in Chapter 6.6) than GUR 1050, and this fact may affect the tribological behaviour. Lower molecular weight GUR 1020 shows the peak load decreased and increasing the elongation to break (see in Figure 6.29). The existence of the Vit. E had a significant effect on the wear rate of UHMWPE against extended aging conditions. In this study, unfortunately no explants doped with Vit. E were tested.

Wear results showed that crosslinked materials had the greatest wear resistance even though working with extremely high load. Crosslinking reduces the amount of orientational hardening and softening, as it slows down chain mobility and provides resistance to the cross-shear forces [252]. Crosslinking also results in more C-C bonds between molecules which makes it harder to split them. The more crosslinking in the material, the more bonds that are present. This means that less orientational hardening and softening is possible, which is why a reduction in wear rate was seen in the cross-linked explants [253]. The crosslinking material is more protected against formation of wear debris, which is shown by its significantly lower wear rate.

Long term durability varied significantly depending on structural and mechanical properties. FTIR and DSC results showed that GUR 1050 and GUR 1020 non-crosslinked materials underwent substantial OI and increasing Xr. The increasing OI let the UHMWPE susceptible to severe wear. Protective effect of Vit E. hindered oxidation so GUR 1020 Vit. E samples' wear rate haven't changed dramatically.

3D profilometer images enables the supplementary information concerning the width and the depth of the wear tracks. During unidirectional motion orientational hardening occurs. This means that the molecules orientate themselves with the direction of sliding resulting in a material which is strong in the direction of motion but weaker perpendicular to it. The frictional force remains in a constant direction, and therefore the direction in which the molecules are aligned remains constant [249, 254].

Material wear behavior is sensitive to loading conditions. Thus, results of wear under a 2N load will not be similar to results under a 30N load. However, working above yield strength (the yield

Die approbierte gedruckte Originalversion dieser Dissertation ist an der TU Wien Bibliothek verfügbar.
The approved original version of this doctoral thesis is available in print at TU Wien Bibliothek.
TU Bibliothek Your knowledge hub WIEN

strength of UHMWPE is 21-28 MPa [151]) leads to plastic deformation and for all materials the dominant wear mechanism is abrasive wear.

As indicated in [255], the elastic deformation is not significant factor for wear mechanisms in total joint replacement. Therefore, a minimum load of 2N is elaborated. In this way a contact pressure which is slightly higher than the yield strength of UHMWPE can be obtained.

Aging causes higher contact pressure. During aging, the increase in E-modulus due to chain rearrangements may lead to an undesired increase in contact pressure as E-modulus goes into calculation in Hertzian contact theory [256]. Moreover, the more aged samples are more oxidized resulting in an increase in wear rate. This could be explained by the decrease of fatigue resistance [8, 91].

Die approbierte gedruckte Originalversion dieser Dissertation ist an der TU Wien Bibliothek verfügbar.
The approved original version of this doctoral thesis is available in print at TU Wien Bibliothek.
TU Bibliothek Your knowledge hub WIEN

Chapter 7: General Discussion

UHMWPE is a successful material in total hip joint replacement. Different processing methods e.g. molding or extrusion temperatures and pressures, sterilization, postproduction treatment or intertwining conditions can potentially affect in-vivo UHMWPE performance. This study investigates the structural, physical, mechanical and tribological performance of conventional and cross-linked explants and commercial engineering polymer blocks by optical evaluation, FTIR, DSC, DSI, SPT and BOP methods. Furthermore, accelerated aging was applied in order to better understand the in-vivo structural, physical, mechanical and tribological properties.

A total of twenty explants (two conventional and eighteen cross-linked) are investigated. Additionally, the data of eighteen more explants which were formerly studied by TU-Wien are also discussed. The average value of the OI of explant samples till 1mm depth is shown in Figure 7.1. Oxidation leads to the degradation of the polymer chains, change the degree of crystallinity and degrades the mechanical properties [257]. In conventional explants, OI increases with increasing in-vivo time and the value of OI is higher than all different types of cross-linked explants. The higher OI values of conventional explants can be explained by gamma irradiation in air ambient atmosphere. The oxygen in air reacts with free radicals and causes oxidative degradation. Free radicals are consumed at the surface as they rapidly react with the atmospheric oxygen hence decreasing the molecular weight and increasing the degradation. Another reason of higher OI values of conventional explants could be the lack of thermal treatment step during the manufacture of conventional implants as thermal treatment eliminates free radicals.

However, there are no severe OI changes in sandwich type conventional explants because the articulating surface made of metal or ceramic shell, the polymer is not in direct contact with the synovial fluid and the femur head. So, obviously in direct contact, the oxygen in the synovial fluid interacts with the free radicals in the explant. Using sandwich type of implants prevent oxidation.

Die approbierte gedruckte Originalversion dieser Dissertation ist an der TU Wien Bibliothek verfügbar.
The approved original version of this doctoral thesis is available in print at TU Wien Bibliothek.
TU Bibliothek Your knowledge hub WIEN

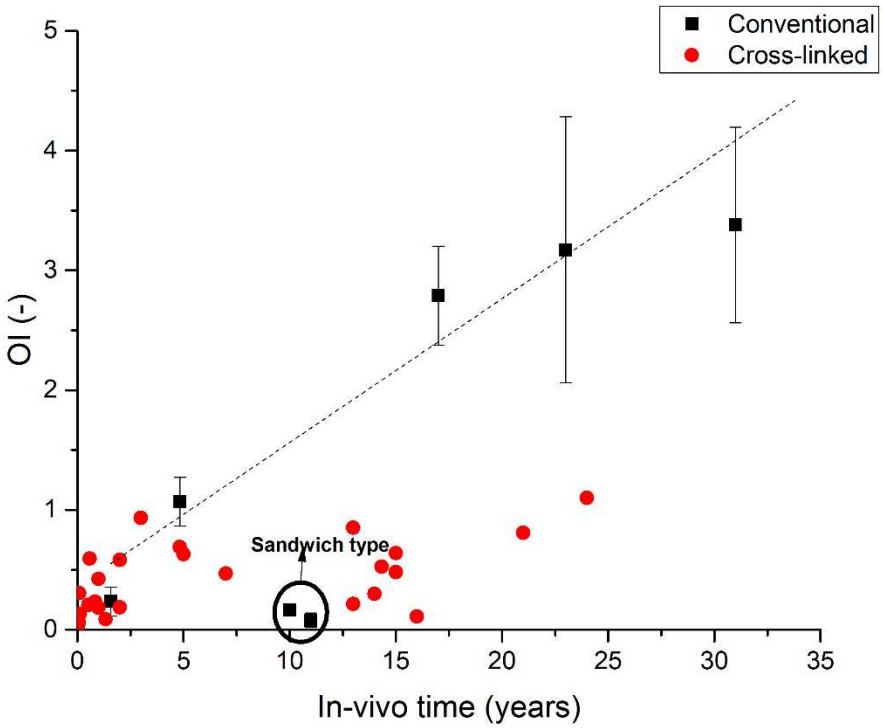

Figure 7. 1 Oxidation index versus in-vivo time.

The mechanical properties of UHMWPE are influenced on both its crystallinity (the degree of crystallinity, crystalline morphology) and amorphous phases (crosslinking or entanglements). The degree of crystallinity vs. oxidation index of conventional and cross-linked explants is shown in Figure 7.2. The degree of crystallinity depends upon a variety factors such as UHMWPE's molecular weight, processing conditions, after irradiation thermal treatment and in-vivo conditions.

In the low OI region, the first-generation cross-linked remelted explants show the lowest degree of crystallinity. This is an expected result as higher remelting temperatures to eliminate free radicals above melting point causes degradation of the crystalline structure.

The second-generation cross-linked explants show higher degree of crystallinity than the first-generation remelted and annealed explants, this result is in accordance to the literature [258]. Concerning the conventional explants (in-vivo time > 15 years), it is shown that the higher the oxidation index (OI > 2) is, the more increases the degree of crystallinity. Increasing the degree of crystallinity in conventional explants can be explained that time-dependent tie chain scission process leads to further crystal perfection [259, 260]. The high degree of crystallinity is a result of oxidative chain scission which decreases the molecular weight of the polymer [259, 260].

Die approbierte gedruckte Originalversion dieser Dissertation ist an der TU Wien Bibliothek verfügbar.
The approved original version of this doctoral thesis is available in print at TU Wien Bibliothek.
TU Bibliothek Your knowledge hub WIEN

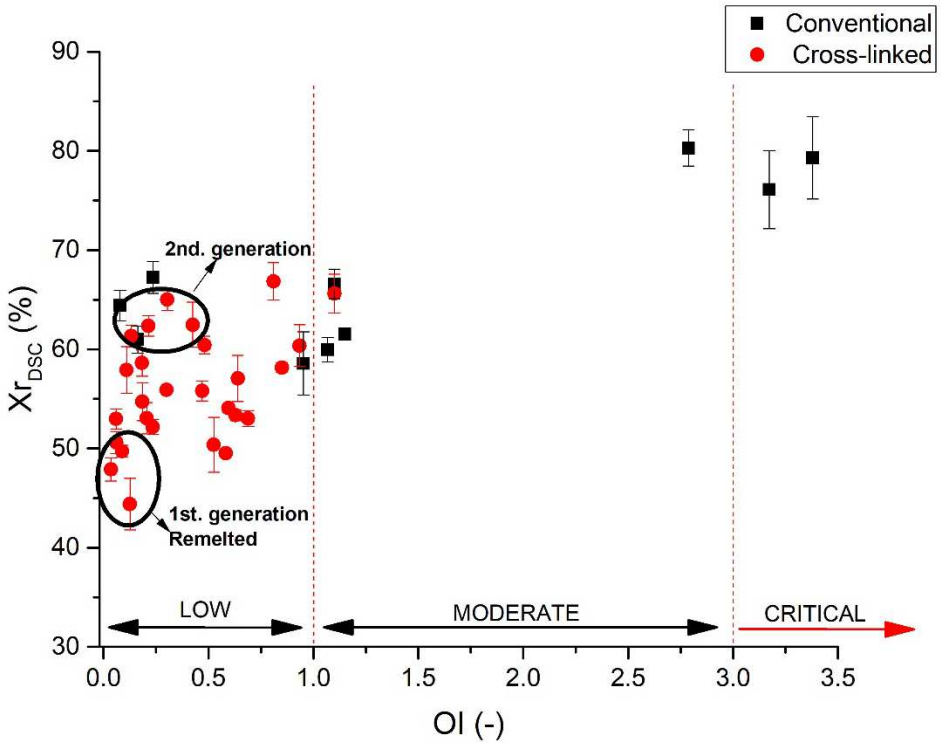

Figure 7. 2 Degree of crystallinity as a function of OI

The correlation between indentation modulus (E-modulus), microhardness and degree of crystallinity is an important relation to understand polymer mechanical properties. The results of the DSI tests of cross-linked explants as a function of degree of crystallinity is shown in Figure 7.3. The first-generation remelted cross-linked explants show lower degree of crystallinity than the first-generation annealed cross-linked explants and second-generation cross-linked explants. This observation is similar to the results reported in literature [261] and can be similarly explained as above by the degradation of the crystalline structure at higher remelting temperatures above melting point. Another explanation of this observation is the totally different manufacturing procedure of the second-generation cross-linked explants which preserves the degree of crystallinity and micromechanical properties, as explained in detail in Chapter 5.

Die approbierte gedruckte Originalversion dieser Dissertation ist an der TU Wien Bibliothek verfügbar.
The approved original version of this doctoral thesis is available in print at TU Wien Bibliothek.
TU Bibliothek Your knowledge hub WIEN

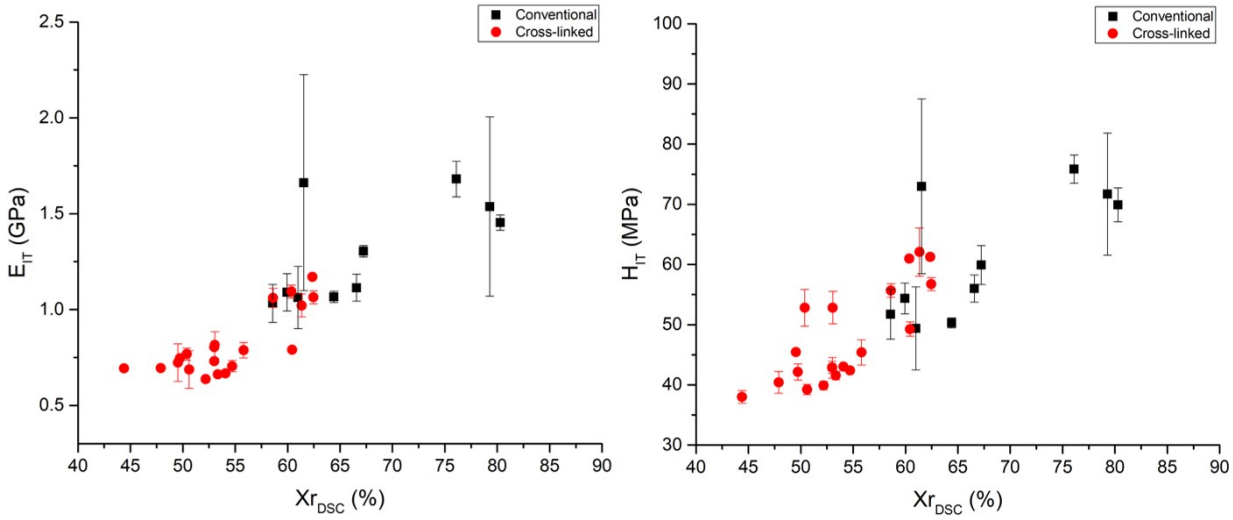

Figure 7. 3 E-modulus and micro hardness as a function of degree of crystallinity

In Figure 7.4, E-modulus of all explants is represented as a function of OI. Here there is the same tendency like in Figure 7.2. Increasing the chain scission via oxidation leads to increasing degree of crystallinity and results in increasing E- Modulus in conventional explants. The big standard deviation was seen in conventional explants due to increased OI which is observed in the subsurface regions (white bands).

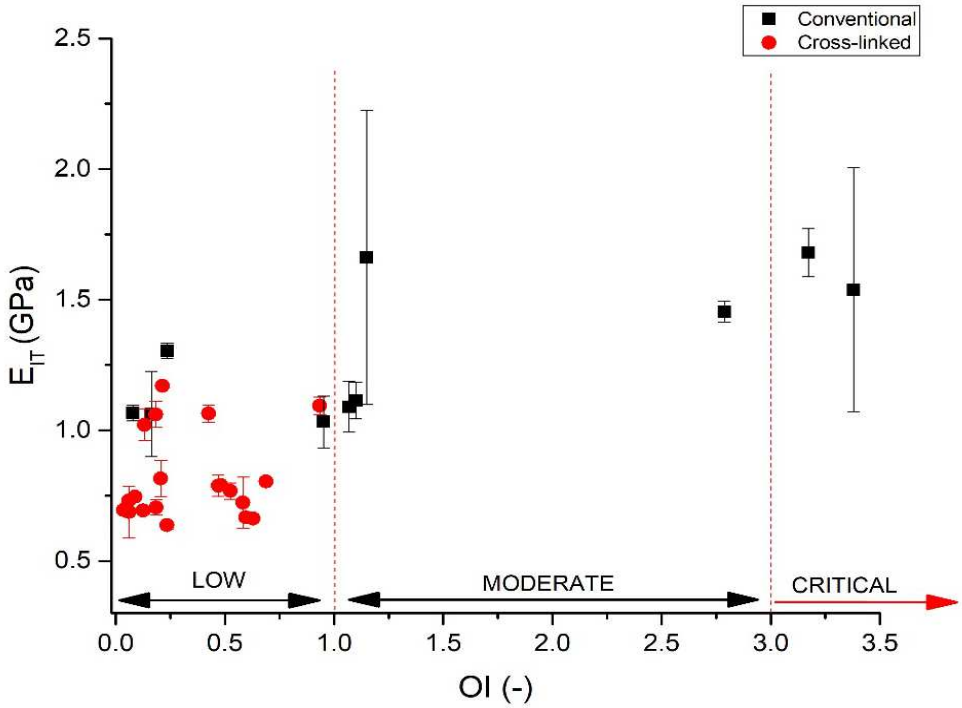

Figure 7. 4 E-modulus as a function of OI.

Die approbierte gedruckte Originalversion dieser Dissertation ist an der TU Wien Bibliothek verfügbar.
The approved original version of this doctoral thesis is available in print at TU Wien Bibliothek.
TU Bibliothek Your knowledge hub WIEN

Figure 7.5 shows the comparison of wear rate of three UHMWPE types and the change in E-modulus and OI with aging time. FTIR and DSI results show that, with aging, the OI and E-modulus substantially increases for GUR 1050 and GUR 1020 type bulk materials and higher OI makes material susceptible to severe wear. As Vit E. hinders oxidation, GUR 1020 Vit. E samples' wear rate does not change dramatically.

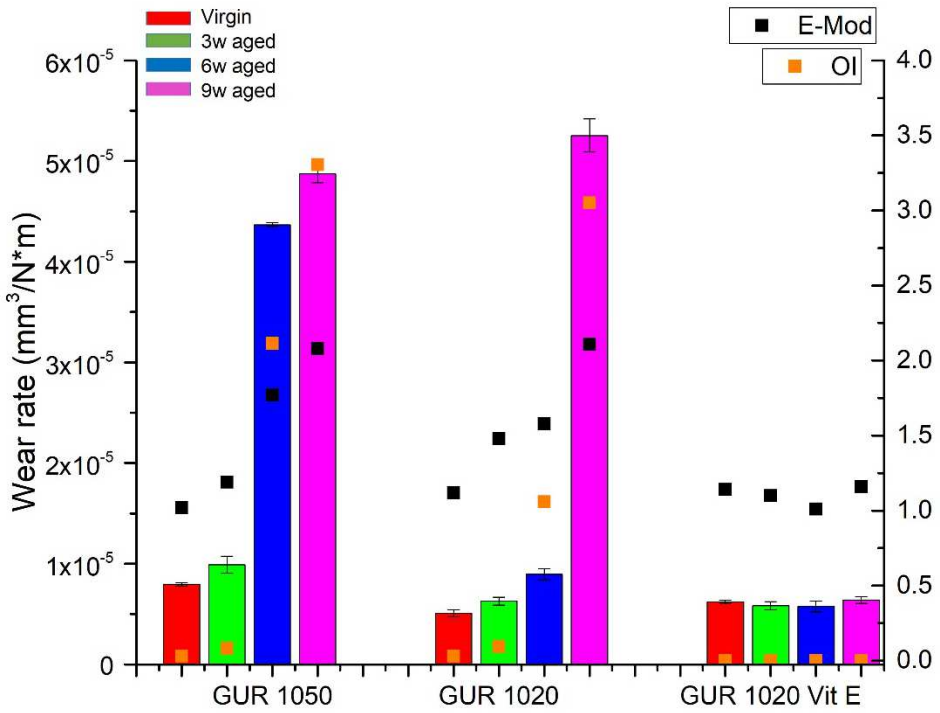

Figure 7. 5 Comparison of the wear rates of three UHMWPE types under 30N and change in E-modulus and OI

In this work an attempt was taken to correlate stiffness values obtained from two different methods. Table 7.1 shows the E-modulus values obtained from DSI and SPT methods. E-modulus values obtained from SPT method are lower than the ones from DSI method and the values are not comparable. The E-modulus obtained from DSI method is in better agreement with the values obtained in other studies [151]. The relatively lower E-modulus values obtained from SPT method can be attributed to the calculation procedure where a fixed coefficient obtained from the finite element method was used as reported by study [262].

Die approbierte gedruckte Originalversion dieser Dissertation ist an der TU Wien Bibliothek verfügbar.
The approved original version of this doctoral thesis is available in print at TU Wien Bibliothek.
TU Bibliothek Your knowledge hub WIEN

In [263], statistically similar values of E-modulus were found between SPT and bulk mechanical test, however, the type of the bulk mechanical test was not specified. Whereas in [151] an average of 0.799 ±0.08 GPa was computed for GUR 1050 acetabular liner which is very similar to the values found in this study.

Table 7. 1 E-modulus values were obtained from DSI and SPT

Name	**E-modulus from DSI (GPa)**	**E-modulus from SPT (GPa)**
GUR 1020 Vit. E	1.14 ±0.06	0.68
GUR 1020	1.12	0.78
GUR 1050	1.02±0.04	0.76
REOP	1.45±0.04	0.78
KOR	1.68±0.093	1.08
AUMA	1.54±0.468	0.77
Durasul® (Dsa) 3 weeks aged	0.73±0.03	0.51
Dsa 6 weeks aged	0.74	0.75
X3™ 6 weeks aged	0.94±0.04	0.96
STEL	0.77±0.03	0.49
LUIN	0.79±0.01	0.96
WIRU	0.66±0.011	0.44
KOEV	1.17±0.01	0.94
GLFR	-	0.43

Figure 7.6 shows the total damage score versus work to failure of the explants. The correlation of the toughness of the material with damage score is clearly seen. Increasing in total damage score results in decreasing in work to failure. The similar relation between damage score and work to failure was found in [262].

Die approbierte gedruckte Originalversion dieser Dissertation ist an der TU Wien Bibliothek verfügbar.
The approved original version of this doctoral thesis is available in print at TU Wien Bibliothek.
TU Bibliothek Your knowledge hub WIEN

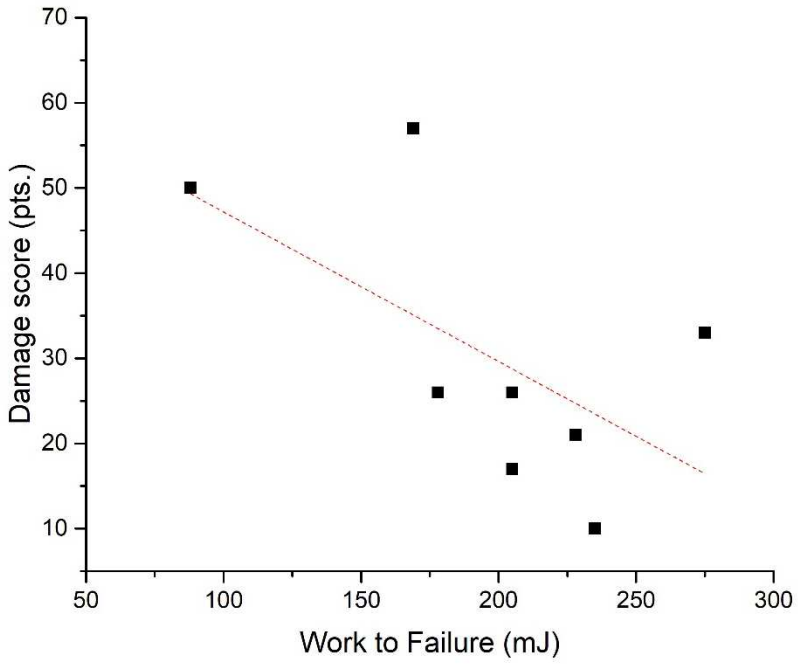

Figure 7. 6 Total damage score versus work to failure of the explants (r =-0.61)

Figure 7.7 shows work to failure of conventional and cross-linked explants and implants. The more oxidized conventional explants are less tough in the surface than in the bulk material. The relatively higher work to failure i.e. toughness values of DePuy (cross-linked, remelted) and second-generation (cross-linked, sequentially annealed or using high pressure to form) explants is a result of the higher irradiation dose and thermal treatment after cross-linking. Moreover, DePuy explants have higher toughness values than other second-generation explants which is believed to be a result of moderate irradiation dose exposure of the explant during cross-linking. This observation is similar to the results reported in literature [250, 264].

One other result that can be seen in Figure 7.7 is that extended aging i.e. beyond six weeks causes cross-linked explants having low and close toughness values with oxidized in-vivo aged conventional explants. It can be argued that beyond six weeks of aging, the implant's structural and physical parameters deteriorate. In a study [248], they found the same trend between wear rate in a hip simulator versus work to failure in SPT.

Die approbierte gedruckte Originalversion dieser Dissertation ist an der TU Wien Bibliothek verfügbar.
The approved original version of this doctoral thesis is available in print at TU Wien Bibliothek.
TU Bibliothek Your knowledge hub WIEN

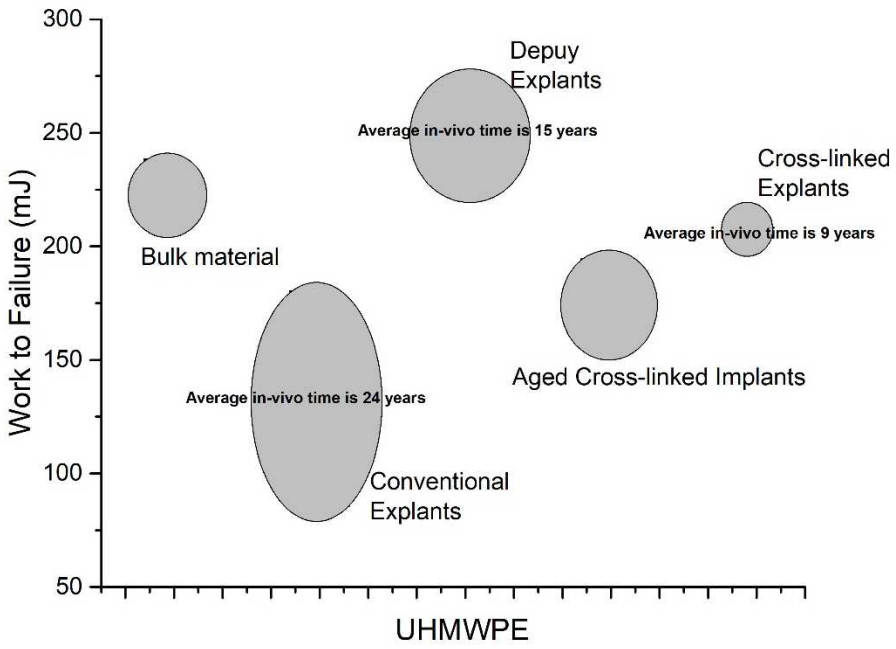

Figure 7. 7 Work to failure of conventional and cross-linked explants and implants (Greyed parts show the areas where data points are more concentrated)

Figure 7.8 shows work to failure versus wear rate (from BOP test) of commercial engineering polymers blocks (GUR 1020 and GUR 1050, respectively) and cross-linked-aged implants up to six weeks. Cross-linked implants are far more wear resistant than bulk material but less tough because cross-linking slows down chain mobility and results in more C-C bonds formation between molecules which makes it harder to split them [74]. Additionally, with aging, toughness decreases. Cross-linked and remelted implant (GUR 1050 in Figure 7.8 (b)) has lower toughness compared to cross-linked and annealed implant (GUR 1020 in Figure 7.8 (a)). Remelting results in lower degree of crystallinity and small lamellae formation which adversely affects its mechanical properties such as low values of E-modulus and toughness, respectively.

Die approbierte gedruckte Originalversion dieser Dissertation ist an der TU Wien Bibliothek verfügbar.
The approved original version of this doctoral thesis is available in print at TU Wien Bibliothek.

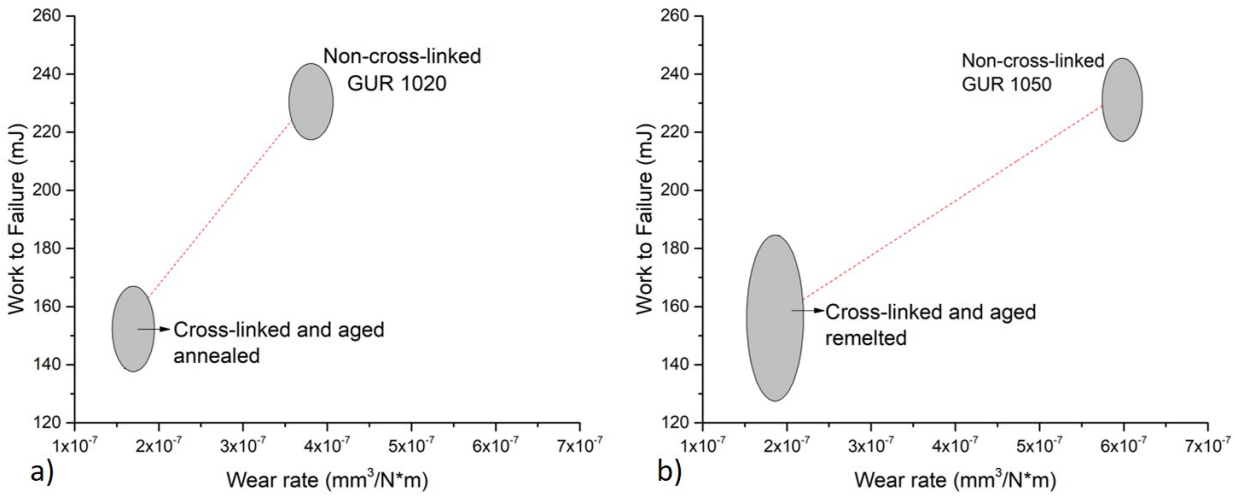

Figure 7. 8 Work to failure versus wear rate of a bulk material and conventional implants a) GUR 1020 (r=0.97) b) GUR 1050 (r =0.92)

SUMMARY OF FINDINGS

Oxidation: OI correlates with in-vivo time. There are no severe OI changes in sandwich type conventional explants even after seventeen years in vivo and no oxidation changes were seen with in-vivo time in DePuy samples. In conventional explants, OI increases with increasing in-vivo time and the value of OI is higher than all different types of cross-linked explants.

Sterilization method: The results of this study confirmed that irradiation sterilized samples show higher oxidation level (however, also due to long in-vivo time), resulting to higher wear rates, higher degree of crystallinity, indentation modulus and hardness. Thus, ethylene oxide and gas plasma method could be used for sterilization as the free radicals generated during irradiation sterilization causes oxidation.

Cross-linking: The advantage of cross-linked UHMWPE is its low wear rate in hard on hard bearings. But it has a negative impact on mechanical properties such as decreasing the ductility and toughness. However, DePuy cross-linked explants displayed neither low ductility nor less toughness. Additionally, increasing the radiation dose leads to broader lamellar thickness.

Thermal treatment method: Post irradiation thermal treatment reduces the tendency to oxidation. However, thermal treatment after cross-linking affects the mechanical behavior of UHMWPE. Remelted explants are better stabilized against oxidative degradation but the degree of crystallinity is lower than annealed explants. This results in reduced mechanical properties such as low values

Die approbierte gedruckte Originalversion dieser Dissertation ist an der TU Wien Bibliothek verfügbar.
The approved original version of this doctoral thesis is available in print at TU Wien Bibliothek.
TU Bibliothek Your knowledge hub WIEN

of E-modulus, ultimate tensile strength and toughness. Concerning the result of this study, it is showed that thermal treatment by annealing is better for preserving mechanical properties.

Stabilization: Vit. E has been added the last years in the crosslinked UHMWPE implants in order to stabilize residual free radicals. In this study Vit. E stabilized UHMWPE was oxidation resistant even after 9 weeks of accelerated aging add the aging conditions. Hence, the existence of the Vit. E had a significant effect on the wear rate of UHMWPE against extended aging conditions. Also due to its plasticizer effect, GUR 1020 doped Vit. E samples were the most ductile materials measured toughness values were higher than GUR 1020 and GUR 1050.

Gender, age etc: This study did not find any correlation between BMI and in-vivo time, patients' weight vs. in-vivo time, UCLA activity level vs. BMI and UCLA activity level and in-vivo time.

It is the limitation factor of this study that 38 samples are not enough to make a general conclusion on gender effect. As it is depicted in several comparisons studies between men and women is due to the interaction of multiple variables such as age, genetics, and physical activity.

Aging: The results revealed that implant material structural and physical parameters deteriorate beyond six weeks of aging. Because:

- Moderate oxidation
- Increasing of the degree of crystallinity and indentation modulus
- High contact stress

Ductility and toughness: SPT is a suitable test method to evaluate ductility and toughness. It is also used to characterize the mechanical effects of oxidative degradation on UHMWPE explants. However, non-comparable E-modulus values were obtained with SPT and DSI methods.

Tribology and Wear: Tribology tests were performed on a specially designed BOP test apparatus. However, the test method did not allow the simulation of the body fluids' lubrication effects on wear measurements as the system lacks a lubricant. Moreover, one can also infer that the use of a multidirectional tribology system instead of a rotational tribology system could better simulate the actual contact conditions of a hip joint. This test revealed that for all samples the dominant wear mechanism was abrasive wear.

Die approbierte gedruckte Originalversion dieser Dissertation ist an der TU Wien Bibliothek verfügbar.
The approved original version of this doctoral thesis is available in print at TU Wien Bibliothek.
TU Bibliothek Your knowledge hub WIEN

The volumetric wear rate of the GUR1020 UHMWPE was slightly lower than the mean wear rate for the GUR1050 UHMWPE material. Different molecular weights were not expected to generate a significant difference in the wear rate. However, more ductile material (GUR 1020) may be affecting the tribology results.

Die approbierte gedruckte Originalversion dieser Dissertation ist an der TU Wien Bibliothek verfügbar.
The approved original version of this doctoral thesis is available in print at TU Wien Bibliothek.
TU WIEN Bibliothek Your knowledge hub

Chapter 8: References

1. Besong A, Tipper J, Ingham E, Stone M, Wroblewski B, Fisher J. Quantitative comparison of wear debris from UHMWPE that has and has not been sterilised by gamma irradiation. The Journal of bone and joint surgery British volume. 1998;80(2):340-4.
2. Kurtz SM, Muratoglu OK, Evans M, Edidin AA. Advances in the processing, sterilization, and crosslinking of ultra-high molecular weight polyethylene for total joint arthroplasty. Biomaterials. 1999;20(18):1659-88.
3. McKellop H, Shen F-w, Lu B, Campbell P, Salovey R. Effect of sterilization method and other modifications on the wear resistance of acetabular cups made of ultra-high molecular weight polyethylene: a hip-simulator study. JBJS. 2000;82(12):1708.
4. del Prever EB, Crova M, Costa L, Dallera A, Camino G, Gallinaro P. Unacceptable biodegradation of polyethylene in vivo. Biomaterials. 1996;17(9):873-8.
5. Wolf C, Krivec T, Blassnig J, Lederer K, Schneider W. Examination of the suitability of α-tocopherol as a stabilizer for ultra-high molecular weight polyethylene used for articulating surfaces in joint endoprostheses. Journal of Materials Science: Materials in Medicine. 2002;13(2):185-9.
6. Al-Malaika S, Ashley H, Issenhuth S. The antioxidant role of α-tocopherol in polymers. I. The nature of transformation products of α-tocopherol formed during melt processing of LDPE. Journal of Polymer Science Part A: Polymer Chemistry. 1994;32(16):3099-113.
7. Al-Malaika S, Goodwin C, Issenhuth S, Burdick D. The antioxidant role of α-tocopherol in polymers II. Melt stabilising effect in polypropylene. Polymer degradation and stability. 1999;64(1):145-56.
8. Oral E, Malhi AS, Wannomae KK, Muratoglu OK. Highly cross-linked ultrahigh molecular weight polyethylene with improved fatigue resistance for total joint arthroplasty: recipient of the 2006 Hap Paul Award. The Journal of arthroplasty. 2008;23(7):1037-44.
9. Neumann L, Freund K, Sorenson KH. Long-term results of Charnley total hip replacement. Review of 92 patients at 15 to 20 years. Bone & Joint Journal. 1994;76(2):245-51.
10. Harris WH. Osteolysis and particle disease in hip replacement: a review. Acta Orthopaedica Scandinavica. 1994;65(1):113-23.
11. Harris W. Aseptic loosening in total hip arthroplasty secondary to osteolysis induced by wear debris from titanium-alloy modular femoral heads. JBJS. 1991;73(3):470-2.
12. Peters JP, Engh G, Dwyer K, Vinh T. Osteolysis after total knee arthroplasty without cement. The Journal of bone and joint surgery American volume. 1992;74(6):864-76.
13. Schmalzried TP, Guttmann D, Grecula M, Amstutz HC. The relationship between the design, position, and articular wear of acetabular components inserted without cement and the development of pelvic osteolysis. JBJS. 1994;76(5):677-88.
14. Willert H-g, Bertram H, Buchhorn GH. Osteolysis in alloarthroplasty of the hip. The role of ultra-high molecular weight polyethylene wear particles. Clinical orthopaedics and related research. 1990(258):95-107.
15. Moore KL, Agur AM, Dalley AF. Essential clinical anatomy: Lippincott Williams & Wilkins Philadelphia; 2002.
16. Blewis M, Nugent-Derfus G, Schmidt T, Schumacher B, Sah R. A model of synovial fluid lubricant composition in normal and injured joints. Eur Cell Mater. 2007;13(1):26-39.

Die approbierte gedruckte Originalversion dieser Dissertation ist an der TU Wien Bibliothek verfügbar.
The approved original version of this doctoral thesis is available in print at TU Wien Bibliothek.
TU Bibliothek Your knowledge hub WIEN

17. Palastanga N, Field D, Soames R. Anatomy and human movement: structure and function: Elsevier Health Sciences; 2006.
18. Gray H. Gray's Anatomy of the Human Body, (Original by Philadelphia: Lea and Febiger, 1918). New York: Bartleby com. 2000.
19. Charlish A. The Complete Arthritis Handbook. London: Carnel Ltd.; 1996.
20. Le Graverand-Gastineau M-PH. OA clinical trials: current targets and trials for OA. Choosing molecular targets: what have we learned and where we are headed? Osteoarthritis and Cartilage. 2009;17(11):1393-401.
21. Northmore-Ball MD. Clinical challenges in orthopaedics:. The Hip. 2002.
22. Rona Z. Osteoarthritis: Alive Books; 2002.
23. Sundfeldt M, V Carlsson L, B Johansson C, Thomsen P, Gretzer C. Aseptic loosening, not only a question of wear: a review of different theories. Acta orthopaedica. 2006;77(2):177-97.
24. Ingham E, Fisher J. The role of macrophages in osteolysis of total joint replacement. Biomaterials. 2005;26(11):1271-86.
25. Maloney WJ, Smith RL. Periprosthetic osteolysis in total hip arthroplasty: the role of particulate wear debris. JBJS. 1995;77(9):1448-61.
26. Kadoya Y, Kobayashi A, Ohashi H. Wear and osteolysis in total joint replacements. Acta Orthopaedica Scandinavica. 1998;69(sup278):i-16.
27. Goldfing S, Clark C, Wright T. The problem in tota1~ joint arthroplasty: Aseptic loosening [Editorial]. J Bone Joint Surg A. 1993;75:799-801.
28. Harris WH. The problem is osteolysis. Clinical orthopaedics and related research. 1995(311):46-53.
29. Maloney WJ, Smith RL, Schmalzried TP, Chiba J, Huene D, Rubash H. Isolation and characterization of wear particles generated in patients who have had failure of a hip arthroplasty without cement. JBJS. 1995;77(9):1301-10.
30. Campbell P, Ma S, Yeom B, McKellop H, Schmalzried T, Amstutz H. Isolation of predominantly submicron-sized UHMWPE wear particles from periprosthetic tissues. Journal of biomedical materials research. 1995;29(1):127-31.
31. Ulrich-Vinther M, Carmody EE, Goater JJ, Søballe K, O'keefe RJ, Schwarz EM. Recombinant adeno-associated virus-mediated osteoprotegerin gene therapy inhibits wear debris-induced osteolysis. JBJS. 2002;84(8):1405-12.
32. Clohisy JC, Calvert G, Tull F, McDonald D, Maloney WJ. Reasons for revision hip surgery: a retrospective review. Clinical Orthopaedics and Related Research®. 2004;429:188-92.
33. WANG J-T, YOSHITADA H, editors. Biological mechanisms involved in the pathogenesis of aseptic loosening after total joint replacement. Seminars in Arthroplasty; 1993.
34. Murray D, Rushton N. Macrophages stimulate bone resorption when they phagocytose particles. The Journal of bone and joint surgery British volume. 1990;72(6):988-92.
35. Huiskes R, editor The Current State and Future of Cemented and Noncemented Total Hip Replacement. 1st European congress of Orthopaedics; 1993.
36. McCormack B, Prendergast P. Microdamage accumulation in the cement layer of hip replacements under flexural loading. Journal of Biomechanics. 1999;32(5):467-75.
37. Jones LC, Hungerford DS. Cement disease. Clinical orthopaedics and related research. 1987(225):192-206.

Die approbierte gedruckte Originalversion dieser Dissertation ist an der TU Wien Bibliothek verfügbar.
The approved original version of this doctoral thesis is available in print at TU Wien Bibliothek.
TU Bibliothek Your knowledge hub WIEN

38. Willert H-g, Bertram H, Buchhorn GH. Osteolysis in alloarthroplasty of the hip. The role of bone cement fragmentation. Clinical orthopaedics and related research. 1990(258):108-21.
39. Hirakawa K, Jacobs JJ, Urban R, Saito T. Mechanisms of failure of total hip replacements: lessons learned from retrieval studies. Clinical Orthopaedics and Related Research®. 2004;420:10-7.
40. Tong J, Zanta, N. P., Wanga, J. Y., Heaton-Adegbilea, P. and Hussella, J. G. . Fatigue in cemented acetabular replacements. International Journal of Fatigue. 2008;30(8):1366-75.
41. Coultrup OJ, Browne M, Hunt C, Taylor M. Accounting for inclusions and voids allows the prediction of tensile fatigue life of bone cement. Journal of biomechanical engineering. 2009;131(5):051007.
42. Gardiner R, Hozack W. Failure of the cement-bone interface. A consequence of strengthening the cement-prosthesis interface? The Journal of bone and joint surgery British volume. 1994;76(1):49-52.
43. Woo RY, Morrey BF. Dislocations after total hip arthroplasty. The Journal of bone and joint surgery American volume. 1982;64(9):1295-306.
44. Scifert CF, Brown TD, Pedersen DR, Callaghan JJ. A finite element analysis of factors influencing total hip dislocation. Clinical Orthopaedics and Related Research (1976-2007). 1998;355:152-62.
45. Bader R, Steinhauser E, Zimmermann S, Mittelmeier W, Scholz R, Busch R. Differences between the wear couples metal-on-polyethylene and ceramic-on-ceramic in the stability against dislocation of total hip replacement. Journal of materials science: materials in medicine. 2004;15(6):711-8.
46. Pedersen D, Callaghan J, Brown T. Activity-dependence of the “safe zone” for impingement versus dislocation avoidance. Medical engineering & physics. 2005;27(4):323-8.
47. Barrack RL. Dislocation after total hip arthroplasty: implant design and orientation. JAAOS-Journal of the American Academy of Orthopaedic Surgeons. 2003;11(2):89-99.
48. Nadzadi ME, Pedersen DR, Yack HJ, Callaghan JJ, Brown TD. Kinematics, kinetics, and finite element analysis of commonplace maneuvers at risk for total hip dislocation. Journal of biomechanics. 2003;36(4):577-91.
49. Kerschbaumer F, Kerschbaumer G, Deghani F. Is a dorsal access associated with an elevated luxation rate following total hip replacement? 2007.
50. Hummel MT, Malkani AL, Yakkanti MR, Baker DL. Decreased dislocation after revision total hip arthroplasty using larger femoral head size and posterior capsular repair. the Journal of Arthroplasty. 2009;24(6):73-6.
51. Konan S, Rhee S-J, Haddad FS. Total hip arthroplasty for displaced fracture of the femoral neck using size 32 mm femoral head and soft tissue repair after a posterior approach. Hip International. 2009;19(1):30-5.
52. Hardidge AJ, Hooper J, McMahon S. Current attitudes to total hip replacement in younger patients: a comparison of two nations. ANZ journal of surgery. 2003;73(5):280-3.
53. Callaghan JJ, Bracha P, Liu SS, Piyaworakhun S, Goetz DD, Johnston RC. Survivorship of a Charnley total hip arthroplasty: a concise follow-up, at a minimum of thirty-five years, of previous reports. JBJS. 2009;91(11):2617-21.

Die approbierte gedruckte Originalversion dieser Dissertation ist an der TU Wien Bibliothek verfügbar.
The approved original version of this doctoral thesis is available in print at TU Wien Bibliothek.
TU Bibliothek Your knowledge hub WIEN

54. Derbyshire B, Fisher J, Dowson D, Hardaker C, Brummitt K. Comparative study of the wear of UHMWPE with zirconia ceramic and stainless steel femoral heads in artificial hip joints. Medical engineering & physics. 1994;16(3):229-36.
55. Galvin A, Jennings L, Tipper J, Ingham E, Fisher J. Wear and creep of highly crosslinked polyethylene against cobalt chrome and ceramic femoral heads. Proceedings of the Institution of Mechanical Engineers, Part H: Journal of Engineering in Medicine. 2010;224(10):1175-83.
56. Barrack RL, Burak C, Skinner HB. Concerns about Ceramics in THA. Clinical Orthopaedics and Related Research (1976-2007). 2004;429:73-9.
57. Nevelos J, Ingham E, Doyle C, Streicher R, Nevelos A, Walter W, et al. Microseparation of the centers of alumina-alumina artificial hip joints during simulator testing produces clinically relevant wear rates and patterns. The Journal of arthroplasty. 2000;15(6):793-5.
58. Surgery RTHR. [Available from: https://physio4fight.wordpress.com/2016/11/23/total-hip-arthroplasty-physiotherapy-protocol-some-guidelines/.
59. Bannister GC. History and basic science in clinical challenges in orthopaedics. The Hip. 2002:59-67.
60. Anon. A. Century in orthopaedics. Orthopaedics today. 2000.
61. Murphy JB. Annals of surgery. Arthroplasty. 1913(5):513.
62. Smith-Petersen MN. Evolution of the mold arthroplasty of the hip joint. Bone Joint Surg. 1948:59-75.
63. Law WA. Results of virallium mold arthroplasty of the hip. Bone Joint Surg. 1962:1497-517
64. Waugh W. The Growth of an Idea 1951–1961. John Charnley: Springer; 1990. p. 99-112.
65. Charnley J. The lubrication of animal joints in relation to surgical reconstruction by arthroplasty. Annals of the rheumatic diseases. 1960;19(1):10.
66. Waugh W. John Charnley: the man and the hip: Springer Science & Business Media; 2012.
67. Charnley J. Low Friction Arthroplasty of the Hip: Theory and Practice. Splinger-Verlag Berlin. 1979;137:182-3,246.
68. Waugh W. The Plan Fulfilled: Wrightington 1959–1969. John Charnley: Springer; 1990. p. 113-38.
69. WHO. Chronic Rheumatic Conditions 2014 [Available from: www.who.int/chp/topics/rheumatic/en/.
70. OECD. Geographic Variations in Health Care: What Do We Know and What Can Be Done to Improve Health System Performance? Paris; 2014.
71. Austria S. 2015.
72. Singh D, Merrill R. Molecular weight distribution of polyethylene produced by Ziegler-Natta catalysts. Macromolecules. 1971;4(5):599-604.
73. Registry NJ. 12th Annual Report. 2014.
74. Kurtz SM. UHMWPE biomaterials handbook: ultra high molecular weight polyethylene in total joint replacement and medical devices: Academic Press; 2009.
75. Eyerer P, et al. Polyethylene, in Concise Encylopaedia of medical and Dental Materials.
76. Peacock A. Handbook of polyethylene: structures: properties, and applications: CRC Press; 2000.
77. Watanabe E, Suzuki M, Nagata K, Kaneeda T, Harada Y, Utsumi M, et al. Oxidation-induced dynamic changes in morphology reflected on freeze-fractured surface of gamma-irradiated ultra-high molecular weight polyethylene components. Journal of Biomedical Materials Research: An

Die approbierte gedruckte Originalversion dieser Dissertation ist an der TU Wien Bibliothek verfügbar.
The approved original version of this doctoral thesis is available in print at TU Wien Bibliothek.
TU Bibliothek Your knowledge hub WIEN

Official Journal of The Society for Biomaterials, The Japanese Society for Biomaterials, and The Australian Society for Biomaterials and the Korean Society for Biomaterials. 2002;62(4):540-9.
78. Wang A, Essner A, Polineni V, Stark C, Dumbleton J. Lubrication and wear of ultra-high molecular weight polyethylene in total joint replacements. Tribology International. 1998;31(1-3):17-33.
79. Han K, Wallace J, Truss R, Geil P. Powder compaction, sintering, and rolling of ultra high molecular weight polyethylene and its composites. Journal of Macromolecular Science, Part B: Physics. 1981;19(3):313-49.
80. Bellare A, Cohen R. Morphology of rod stock and compression-moulded sheets of ultra-high-molecular-weight polyethylene used in orthopaedic implants. Biomaterials. 1996;17(24):2325-33.
81. Kurtz SM. Analysis of contemporary resins and conversion methods.; 2001.
82. Costa L, BRACH DEL PREVER EM. UHMWPE for arthroplasty: Edizione Minerva Medica; 2000.
83. Kurtz SM. The UHMWPE handbook: ultra-high molecular weight polyethylene in total joint replacement: Elsevier; 2004.
84. Campbell P, Shen F-W, McKellop H. Biologic and tribologic considerations of alternative bearing surfaces. Clinical Orthopaedics and Related Research (1976-2007). 2004;418:98-111.
85. Premnath V, Harris W, Jasty M, Merrill E. Gamma sterilization of UHMWPE articular implants: an analysis of the oxidation problem. Biomaterials. 1996;17(18):1741-53.
86. Collier JP, Sperling DK, Currier JH, Sutula LC, Saum KA, Mayor MB. Impact of gamma sterilization on clinical performance of polyethylene in the knee. The Journal of arthroplasty. 1996;11(4):377-89.
87. Costa L, Bracco P, Brach del Prever EM, Kurtz SM, Gallinaro P. Oxidation and oxidation potential in contemporary packaging for polyethylene total joint replacement components. Journal of Biomedical Materials Research Part B: Applied Biomaterials: An Official Journal of The Society for Biomaterials, The Japanese Society for Biomaterials, and The Australian Society for Biomaterials and the Korean Society for Biomaterials. 2006;78(1):20-6.
88. Edidin A, Jewett C, Kalinowski A, Kwarteng K, Kurtz S. Degradation of mechanical behavior in UHMWPE after natural and accelerated aging. Biomaterials. 2000;21(14):1451-60.
89. Currier BH, Currier JH, Mayor MB, Lyford KA, Collier JP, Van Citters DW. Evaluation of oxidation and fatigue damage of retrieved crossfire polyethylene acetabular cups. JBJS. 2007;89(9):2023-9.
90. Puolakka T, Keränen J, Juhola K, Pajamäki K, Halonen P, Nevalainen J, et al. Increased volumetric wear of polyethylene liners with more than 3 years of shelf-life time. International orthopaedics. 2003;27(3):153-9.
91. Pruitt LA. Deformation, yielding, fracture and fatigue behavior of conventional and highly cross-linked ultra high molecular weight polyethylene. Biomaterials. 2005;26(8):905-15.
92. [Available from: https://www.jnjmedicaldevices.com/en-US/companies/DePuy-synthes.
93. Bragdon C, O'connor D, Lowenstein J, Jasty M, Syniuta W. The importance of multidirectional motion on the wear of polyethylene. Proceedings of the Institution of Mechanical Engineers, Part H: Journal of Engineering in Medicine. 1996;210(3):157-65.

Die approbierte gedruckte Originalversion dieser Dissertation ist an der TU Wien Bibliothek verfügbar.
The approved original version of this doctoral thesis is available in print at TU Wien Bibliothek.
TU Bibliothek Your knowledge hub WIEN

94. Muratoglu OK, Bragdon CR, O'Connor DO, Jasty M, Harris WH, Gul R, et al. Unified wear model for highly crosslinked ultra-high molecular weight polyethylenes (UHMWPE). Biomaterials. 1999;20(16):1463-70.
95. McKellop H, Shen Fw, Lu B, Campbell P, Salovey R. Development of an extremely wear-resistant ultra high molecular weight polythylene for total hip replacements. Journal of Orthopaedic Research. 1999;17(2):157-67.
96. Ries MD, Scott ML, Jani S. Relationship between gravimetric wear and particle generation in hip simulators: conventional compared with cross-linked polyethylene. JBJS. 2001;83:116-22.
97. Endo M, Tipper J, Barton D, Stone M, Ingham E, Fisher J. Comparison of wear, wear debris and functional biological activity of moderately crosslinked and non-crosslinked polyethylenes in hip prostheses. Proceedings of the Institution of Mechanical Engineers, Part H: Journal of Engineering in Medicine. 2002;216(2):111-22.
98. Martell JM, Verner JJ, Incavo SJ. Clinical performance of a highly cross-linked polyethylene at two years in total hip arthroplasty: a randomized prospective trial. The Journal of arthroplasty. 2003;18:55-9.
99. Dorr LD, Wan Z, Shahrdar C, Sirianni L, Boutary M, Yun A. Clinical performance of a Durasul highly cross-linked polyethylene acetabular liner for total hip arthroplasty at five years. JBJS. 2005;87(8):1816-21.
100. Calvert GT, Devane PA, Fielden J, Adams K, Horne JG. A double-blind, prospective, randomized controlled trial comparing highly cross-linked and conventional polyethylene in primary total hip arthroplasty. The Journal of arthroplasty. 2009;24(4):505-10.
101. Engh Jr CA, Hopper Jr RH, Huynh C, Ho H, Sritulanondha S, Engh Sr CA. A prospective, randomized study of cross-linked and non–cross-linked polyethylene for total hip arthroplasty at 10-year follow-up. The Journal of arthroplasty. 2012;27(8):2-7. e1.
102. García-Rey E, García-Cimbrelo E, Cruz-Pardos A. New polyethylenes in total hip replacement: A ten-to 12-year follow-up study. The bone & joint journal. 2013;95(3):326-32.
103. Glyn-Jones S, Thomas GE, Garfjeld-Roberts P, Gundle R, Taylor A, McLardy-Smith P, et al. The John Charnley Award: Highly crosslinked polyethylene in total hip arthroplasty decreases long-term wear: a double-blind randomized trial. Clinical Orthopaedics and Related Research®. 2015;473(2):432-8.
104. Galvin A, Tipper J, Jennings L, Stone M, Jin Z, Ingham E, et al. Wear and biological activity of highly crosslinked polyethylene in the hip under low serum protein concentrations. Proceedings of the Institution of Mechanical Engineers, Part H: Journal of Engineering in Medicine. 2007;221(1):1-10.
105. Lu Z, McKellop H. Frictional heating of bearing materials tested in a hip joint wear simulator. Proceedings of the Institution of Mechanical Engineers, Part H: Journal of Engineering in Medicine. 1997;211(1):101-8.
106. Liao YS, Benya PD, McKellop HA. Effect of protein lubrication on the wear properties of materials for prosthetic joints. Journal of biomedical materials research. 1999;48(4):465-73.
107. Babovic N, Trousdale RT. Total hip arthroplasty using highly cross-linked polyethylene in patients younger than 50 years with minimum 10-year follow-up. The Journal of arthroplasty. 2013;28(5):815-7.
108. Baker D, Bellare A, Pruitt L. The effects of degree of crosslinking on the fatigue crack initiation and propagation resistance of orthopedic-grade polyethylene. Journal of Biomedical

Die approbierte gedruckte Originalversion dieser Dissertation ist an der TU Wien Bibliothek verfügbar.
The approved original version of this doctoral thesis is available in print at TU Wien Bibliothek.
TU Bibliothek Your knowledge hub WIEN

Materials Research Part A: An Official Journal of The Society for Biomaterials, The Japanese Society for Biomaterials, and The Australian Society for Biomaterials and the Korean Society for Biomaterials. 2003;66(1):146-54.
109. Bradford L, Baker DA, Graham J, Chawan A, Ries MD, Pruitt LA. Wear and surface cracking in early retrieved highly cross-linked polyethylene acetabular liners. JBJS. 2004;86(6):1271-82.
110. Wannomae KK, Bhattacharyya S, Freiberg A, Estok D, Harris WH, Muratoglu O. In vivo oxidation of retrieved cross-linked ultra–high-molecular-weight polyethylene acetabular components with residual free radicals. The Journal of arthroplasty. 2006;21(7):1005-11.
111. Kurtz SM, Hozack WJ, Purtill JJ, Marcolongo M, Kraay MJ, Goldberg VM, et al. 2006 Otto Aufranc Award Paper: significance of in vivo degradation for polyethylene in total hip arthroplasty. Clinical Orthopaedics and Related Research (1976-2007). 2006;453:47-57.
112. Atwood SA, Van Citters DW, Patten EW, Furmanski J, Ries MD, Pruitt LA. Tradeoffs amongst fatigue, wear, and oxidation resistance of cross-linked ultra-high molecular weight polyethylene. Journal of the Mechanical Behavior of Biomedical Materials. 2011;4(7):1033-45.
113. Dumbleton JH, D'Antonio JA, Manley MT, Capello WN, Wang A. The basis for a second-generation highly cross-linked UHMWPE. Clinical Orthopaedics and Related Research®. 2006;453:265-71.
114. Wang A, Zeng H, Yau S, Essner A, Manely M, Dumbleton J. Wear, oxidation and mechanical properties of a sequentially irradiated and annealed UHMWPE in total joint replacement. Journal of Physics D: Applied Physics. 2006;39(15):3213.
115. Kurtz SM, Mazzucco D, Rimnac CM, Schroeder D. Anisotropy and oxidative resistance of highly crosslinked UHMWPE after deformation processing by solid-state ram extrusion. Biomaterials. 2006;27(1):24-34.
116. Oral E, Wannomae KK, Hawkins N, Harris WH, Muratoglu OK. α-Tocopherol-doped irradiated UHMWPE for high fatigue resistance and low wear. Biomaterials. 2004;25(24):5515-22.
117. Simis KS, Bistolfi A, Bellare A, Pruitt LA. The combined effects of crosslinking and high crystallinity on the microstructural and mechanical properties of ultra high molecular weight polyethylene. Biomaterials. 2006;27(9):1688-94.
118. Oral E, Muratoglu OK. Vitamin E diffused, highly crosslinked UHMWPE: a review. International orthopaedics. 2011;35(2):215-23.
119. Oral E, Neils AL, Doshi BN, Fu J, Muratoglu OK. Effects of simulated oxidation on the in vitro wear and mechanical properties of irradiated and melted highly crosslinked UHMWPE. Journal of Biomedical Materials Research Part B: Applied Biomaterials. 2016;104(2):316-22.
120. Grupp TM, Holderied M, Mulliez MA, Streller R, Jäger M, Blömer W, et al. Biotribology of a vitamin E-stabilized polyethylene for hip arthroplasty–Influence of artificial ageing and third-body particles on wear. Acta biomaterialia. 2014;10(7):3068-78.
121. Kuriyagawa M, Nitta K-h. Structural explanation on natural draw ratio of metallocene-catalyzed high density polyethylene. Polymer. 2011;52(15):3469-77.
122. Humbert S, Lame O, Vigier G. Polyethylene yielding behaviour: What is behind the correlation between yield stress and crystallinity? Polymer. 2009;50(15):3755-61.
123. Hillmansen S, Hobeika S, Haward R, Leevers P. The effect of strain rate, temperature, and molecular mass on the tensile deformation of polyethylene. Polymer Engineering & Science. 2000;40(2):481-9.
124. Ward IM, Sweeney J. Mechanical properties of solid polymers: John Wiley & Sons; 2012.

Die approbierte gedruckte Originalversion dieser Dissertation ist an der TU Wien Bibliothek verfügbar.
The approved original version of this doctoral thesis is available in print at TU Wien Bibliothek.
TU Bibliothek Your knowledge hub WIEN

125. Seguela R, Darras O. Phenomenological aspects of the double yield of polyethylene and related copolymers under tensile loading. Journal of materials science. 1994;29(20):5342-52.
126. Pawlik PS, Reisman H. Elasticity: theory and applications: Wiley; 1980.
127. Fischer-Cripps AC. A simple phenomenological approach to nanoindentation creep. Materials Science and Engineering: A. 2004;385(1-2):74-82.
128. Crist B, Fisher CJ, Howard PR. Mechanical properties of model polyethylenes: tensile elastic modulus and yield stress. Macromolecules. 1989;22(4):1709-18.
129. Kennedy M, Peacock A, Mandelkern L. Tensile properties of crystalline polymers: linear polyethylene. Macromolecules. 1994;27(19):5297-310.
130. Ushui K, Kondo Y, Hatada K, Gima S. Effect of tie molecules on the craze strength of polypropylene. Polymer. 1996;37(24):5375-9.
131. Oleinik E. Series C-Plasticity of Semicrystalline Flexible-Chain Polymers at the Microscopic and Mesoscopic Levels. Vysokomolekuliarnye Soedineniia. 2003;45(12):2137-264.
132. Verker R, Atar N, Quero F, Eichhorn S, Grossman E. Tensile stress effect on the macromolecular orientation and erosion mechanism of an atomic oxygen irradiated polyimide. Polymer degradation and stability. 2013;98(5):997-1005.
133. Zhang S. State-of-the-art of polymer tribology. Tribology International. 1998;31(1-3):49-60.
134. Barbour P, Stone M, Fisher J. A study of the wear resistance of three types of clinically applied UHMWPE for total replacement hip prostheses. Biomaterials. 1999;20(22):2101-6.
135. Rose R, Cimino W, Ellis E, Crugnola A. Exploratory investigations on the structure dependence of the wear resistance of polyethylene. Wear. 1982;77(1):89-104.
136. Walker PS, Blunn GW, Lilley PA. Wear testing of materials and surfaces for total knee replacement. Journal of Biomedical Materials Research: An Official Journal of The Society for Biomaterials and The Japanese Society for Biomaterials. 1996;33(3):159-75.
137. Turell M, Wang A, Bellare A. Quantification of the effect of cross-path motion on the wear rate of ultra-high molecular weight polyethylene. Wear. 2003;255(7-12):1034-9.
138. Korduba L, Wang A. The effect of cross-shear on the wear of virgin and highly-crosslinked polyethylene. Wear. 2011;271(9-10):1220-3.
139. McKellop HA, Campbell P, Park S-H, Schmalzried TP, Grigoris P, Amstutz HC, et al. The origin of submicron polyethylene wear debris in total hip arthroplasty. Clinical orthopaedics and related research. 1995(311):3-20.
140. International A. Friction, Lubrication, and Wear Technology. Wear, Ludema K.C1992.
141. Stachowiak G, Batchelor AW. Engineering tribology: Butterworth-Heinemann; 2013.
142. Hunt TM. Handbook of wear debris analysis and particle detection in liquids: Springer Science & Business Media; 1993.
143. Roylance B, Williams J, Dwyer-Joyce R. Wear debris and associated wear phenomena—fundamental research and practice. Proceedings of the Institution of Mechanical Engineers, Part J: Journal of Engineering Tribology. 2000;214(1):79-105.
144. Myshkin N, Petrokovets M, Kovalev A. Tribology of polymers: adhesion, friction, wear, and mass-transfer. Tribology International. 2005;38(11-12):910-21.
145. Kennedy F, Currier B, Van Citters D, Currier J, Collier J, Mayor M. Oxidation of ultra-high molecular weight polyethylene and its influence on contact fatigue and pitting of knee bearings. Tribology transactions. 2003;46(1):111-8.

Die approbierte gedruckte Originalversion dieser Dissertation ist an der TU Wien Bibliothek verfügbar.
The approved original version of this doctoral thesis is available in print at TU Wien Bibliothek.
TU Bibliothek Your knowledge hub WIEN

146. Patten E, Atwood S, Van Citters D, Jewett B, Pruitt L, Ries M. Delamination of a highly cross-linked polyethylene liner associated with titanium deposits on the cobalt-chromium modular femoral head following dislocation. The Journal of bone and joint surgery British volume. 2010;92(9):1306-11.
147. Mattei L, Di Puccio F, Piccigallo B, Ciulli E. Lubrication and wear modelling of artificial hip joints: A review. Tribology International. 2011;44(5):532-49.
148. Scholes S, Unsworth A. Comparison of friction and lubrication of different hip prostheses. Proceedings of the Institution of Mechanical Engineers, Part H: Journal of Engineering in Medicine. 2000;214(1):49-57.
149. Genda E, Iwasaki N, Li G, MacWilliams BA, Barrance PJ, Chao EY. Normal hip joint contact pressure distribution in single-leg standing—effect of gender and anatomic parameters. Journal of Biomechanics. 2001;34(7):895-905.
150. Bartel DL, Bicknell V, Wright T. The effect of conformity, thickness, and material on stresses in ultra-high molecular weight components for total joint replacement. The Journal of bone and joint surgery American volume. 1986;68(7):1041-51.
151. Edidin AA, Kurtz SM. Influence of mechanical behavior on the wear of 4 clinically relevant polymeric biomaterials in a hip simulator. The Journal of arthroplasty. 2000;15(3):321-31.
152. Galvin AL, Kang L, Udofia I, Jennings LM, McEwen HM, Jin Z, et al. Effect of conformity and contact stress on wear in fixed-bearing total knee prostheses. Journal of biomechanics. 2009;42(12):1898-902.
153. Jin Z, Fisher J. Tribology of Hip Joint Replacement. European Surgical Orthopaedics and Traumatology: The EFORT Textbook. 2014:2365-77.
154. Hertz H. On the contact of rigid elastic solids and on hardness, chapter 6: Assorted papers by H. Hertz. MacMillan, New York; 1882.
155. Laska A, Archodoulaki V-M, Duscher B. Failure analysis of retrieved PE-UHMW acetabular liners. Journal of the mechanical behavior of biomedical materials. 2016;61:70-8.
156. Went P, Krismer M, Frischhut B. Recurrence of infection after revision of infected hip arthroplasties. The Journal of bone and joint surgery British volume. 1995;77(2):307-9.
157. Antti-Poika I, Josefsson G, Konttinen Y, Lidgren L, Santavirta S, Sanzen L. Hip arthroplasty infection: current concepts. Acta Orthopaedica Scandinavica. 1990;61(2):163-9.
158. Bohl JR, Bohl WR, Postak PD, Greenwald AS. The Coventry Award. The effects of shelf life on clinical outcome for gamma sterilized polyethylene tibial components. Clinical orthopaedics and related research. 1999(367):28-38.
159. Hood RW, Wright TM, Burstein AH. Retrieval analysis of total knee prostheses: a method and its application to 48 total condylar prostheses. Journal of biomedical materials research. 1983;17(5):829-42.
160. Costa L, Luda M, Trossarelli L, Del Prever EB, Crova M, Gallinaro P. Oxidation in orthopaedic UHMWPE sterilized by gamma-radiation and ethylene oxide. Biomaterials. 1998;19(7-9):659-68.
161. Affatato S, Bordini B, Fagnano C, Taddei P, Tinti A, Toni A. Effects of the sterilisation method on the wear of UHMWPE acetabular cups tested in a hip joint simulator. Biomaterials. 2002;23(6):1439-46.
162. Goldman M, Lee M, Gronsky R, Pruitt L. Oxidation of ultrahigh molecular weight polyethylene characterized by Fourier Transform Infrared Spectrometry. Journal of Biomedical

Die approbierte gedruckte Originalversion dieser Dissertation ist an der TU Wien Bibliothek verfügbar.
The approved original version of this doctoral thesis is available in print at TU Wien Bibliothek.
TU Bibliothek Your knowledge hub WIEN

Materials Research: An Official Journal of The Society for Biomaterials and The Japanese Society for Biomaterials. 1997;37(1):43-50.
163. Bell C, Blunn G, Walker P, Bosman H, Bartlett G, Scott R. Oxidation and wear resistance of directly moulded UHMWPE. Trans ORS. 1999.
164. Spiegelberg S. Analytical Techniques for Assessing the Effects of Radiation on UHMWPE. Cambridge Polymer Group. Inc, Application Note. 2001;8.
165. Costa L, Jacobson K, Bracco P, Del Prever EB. Oxidation of orthopaedic UHMWPE. Biomaterials. 2002;23(7):1613-24.
166. Buchanan F, White J, Sim B, Downes S. The influence of gamma irradiation and aging on degradation mechanisms of ultra-high molecular weight polyethylene. Journal of Materials Science: Materials in Medicine. 2001;12(1):29-37.
167. Standard A. F2102-06, 2006. Standard guide for evaluating the extent of oxidation in ultra-high-molecular-weight polyethylene fabricated forms intended for surgical implants West Conshohocken (Pa): ASTM International. 2008.
168. Dalborg M, Jacobson K, Jonsson S. Methods for determining the spatial distribution of oxidation in ultra-high molecular-weight polyethylene prostheses. Polymer degradation and stability. 2007;92(3):437-47.
169. van der Plaats G, Benzler B, Meier L. The use of differential scanning calorimetry in chemical education: Part 1, a general description. Thermochimica acta. 1991;187:235-8.
170. 07 AF. “Standard Test Method for Measurement of Enthalpy of Fusion, Percent Crystallinity, and Melting Point of Ultra-High-Molecular Weight Polyethylene by Means of Differential Scanning Calorimetry”.
171. Ho S, Riester L, Drews M, Boland T, LaBerge M. Nanoindentation properties of compression-moulded ultra-high molecular weight polyethylene. Proceedings of the Institution of Mechanical Engineers, Part H: Journal of Engineering in Medicine. 2003;217(5):357-66.
172. Stephens C, Benson R, Martinez-Pardo ME, Barker E, Walker J, Stephens T. The effect of dose rate on the crystalline lamellar thickness distribution in gamma-radiation of UHMWPE. Nuclear Instruments and Methods in Physics Research Section B: Beam Interactions with Materials and Atoms. 2005;236(1-4):540-5.
173. Shen FW, McKellop H, Salovey l. Morphology of chemically crosslinked ultrahigh molecular weight polyethylene. Journal of Biomedical Materials Research: An Official Journal of The Society for Biomaterials, The Japanese Society for Biomaterials, and the Australian Society for Biomaterials. 1998;41(1):71-8.
174. Spiegelberg S. Analytical techniques for assessing the effects of radiation on UHMWPE. Cambridge Polymer Group, Application Note. 2001;8.
175. Flory P, Shih H. Thermodynamics of solutions of poly (dimethylsiloxane) in benzene, cyclohexane, and chlorobenzene. Macromolecules. 1972;5(6):761-6.
176. ASTM D. 2765-01. Standard Test Methods for Determination of Gel Content and Swell Ratio of Crosslinked Ethylene Plastics: ASTM International.
177. Shokrieh M, Hosseinkhani M, Naimi-Jamal M, Tourani H. Nanoindentation and nanoscratch investigations on graphene-based nanocomposites. Polymer Testing. 2013;32(1):45-51.
178. Aldousiri B, Dhakal H, Onuh S, Zhang Z, Bennett N. Nanoindentation behaviour of layered silicate filled spent polyamide-12 nanocomposites. Polymer Testing. 2011;30(6):688-92.

Die approbierte gedruckte Originalversion dieser Dissertation ist an der TU Wien Bibliothek verfügbar.
The approved original version of this doctoral thesis is available in print at TU Wien Bibliothek.
TU Bibliothek Your knowledge hub WIEN

179. Olesiak SE, Oyen ML, Ferguson VL. Viscous-elastic-plastic behavior of bone using Berkovich nanoindentation. Mechanics of Time-Dependent Materials. 2010;14(2):111-24.
180. Yusoh K, Jin J, Song M. Subsurface mechanical properties of polyurethane/organoclay nanocomposite thin films studied by nanoindentation. Progress in Organic Coatings. 2010;67(2):220-4.
181. Oliver WC, Pharr GM. An improved technique for determining hardness and elastic modulus using load and displacement sensing indentation experiments. Journal of materials research. 1992;7(6):1564-83.
182. Fischer-Cripps AC. Critical review of analysis and interpretation of nanoindentation test data. Surface and coatings technology. 2006;200(14-15):4153-65.
183. Menčík J, He LH, Němeček J. Characterization of viscoelastic-plastic properties of solid polymers by instrumented indentation. Polymer Testing. 2011;30(1):101-9.
184. Oliver WC, Pharr GM. Measurement of hardness and elastic modulus by instrumented indentation: Advances in understanding and refinements to methodology. Journal of materials research. 2004;19(1):3-20.
185. Altaf K, Ashcroft IA, Hague R. Modelling the effect of moisture on the depth sensing indentation response of a stereolithography polymer. Computational Materials Science. 2012;52(1):112-7.
186. Briscoe B, Fiori L, Pelillo E. Nano-indentation of polymeric surfaces. Journal of Physics D: Applied Physics. 1998;31(19):2395.
187. Lu Y, Tandon G, Jones D, Schoeppner G. Elastic and viscoelastic characterization of thermally-oxidized polymer resin using nanoindentation. Mechanics of Time-Dependent Materials. 2009;13(3):245-60.
188. Yang S, Zhang Y-W, Zeng K. Analysis of nanoindentation creep for polymeric materials. Journal of Applied Physics. 2004;95(7):3655-66.
189. Chudoba T, Richter F. Investigation of creep behaviour under load during indentation experiments and its influence on hardness and modulus results. Surface and Coatings Technology. 2001;148(2-3):191-8.
190. Park K, Mishra S, Lewis G, Losby J, Fan Z, Park JB. Quasi-static and dynamic nanoindentation studies on highly crosslinked ultra-high-molecular-weight polyethylene. Biomaterials. 2004;25(12):2427-36.
191. ASTM F2183-02. Small punch testing of ultra high molecular weight polyethylene used in surgical implants. 2002. p. 1-4.
192. Edidin A, Muth J, Spiegelberg S, Schaffner S. Sterilization of UHMWPE in nitrogen prevents oxidative degradation for more than ten years.
193. Edidin A, Villarraga M, Herr M, Muth J, Yau S, Kurtz S. Accelerated aging studies of UHMWPE. II. Virgin UHMWPE is not immune to oxidative degradation. Journal of Biomedical Materials Research: An Official Journal of The Society for Biomaterials, The Japanese Society for Biomaterials, and The Australian Society for Biomaterials and the Korean Society for Biomaterials. 2002;61(2):323-9.
194. Edidin A, Herr M, Villarraga M, Muth J, Yau S, Kurtz S. Accelerated aging studies of UHMWPE. I. Effect of resin, processing, and radiation environment on resistance to mechanical degradation. Journal of Biomedical Materials Research: An Official Journal of The Society for

Die approbierte gedruckte Originalversion dieser Dissertation ist an der TU Wien Bibliothek verfügbar.
The approved original version of this doctoral thesis is available in print at TU Wien Bibliothek.
TU Bibliothek Your knowledge hub WIEN

Biomaterials, The Japanese Society for Biomaterials, and The Australian Society for Biomaterials and the Korean Society for Biomaterials. 2002;61(2):312-22.
195. Kurtz SM, Pruitt LA, Jewett CW, Foulds JR, Edidin AA. Radiation and chemical crosslinking promote strain hardening behavior and molecular alignment in ultra high molecular weight polyethylene during multi-axial loading conditions. Biomaterials. 1999;20(16):1449-62.
196. Edidin A, Rimnac C, Goldberg V, Kurtz S. Mechanical behavior, wear surface morphology, and clinical performance of UHMWPE acetabular components after 10 years of implantation. Wear. 2001;250(1-12):152-8.
197. Kurtz SM, Hozack W, Marcolongo M, Turner J, Rimnac C, Edidin A. Degradation of mechanical properties of UHMWPE acetabular liners following long-term implantation. The Journal of arthroplasty. 2003;18:68-78.
198. Edidin AA. Development and application of the small punch test to UHMWPE. UHMWPE Biomaterials Handbook: Elsevier; 2016. p. 739-52.
199. Kurtz S, Jewett C, Foulds J, Edidin A. A miniature specimen mechanical testing technique scaled to articulating surface of polyethylene components for total joint arthroplasty. Journal of Biomedical Materials Research: An Official Journal of The Society for Biomaterials, The Japanese Society for Biomaterials, and The Australian Society for Biomaterials. 1999;48(1):75-81.
200. ASTM G. 99–95a Standard Test Method for Wear Testing with a Pin-on-Disk Apparatus. ASTM International. 2000.
201. Geringer J, Tatkiewicz W, Rouchouse G. Wear behavior of PAEK, poly (aryl-ether-ketone), under physiological conditions, outlooks for performing these materials in the field of hip prosthesis. Wear. 2011;271(11-12):2793-803.
202. Haider H, Baykal D. Wear assessment of UHMWPE with pin-on-disc testing. UHMWPE Biomaterials Handbook: Elsevier; 2016. p. 553-78.
203. Ghaednia H, Wang X, Saha S, Xu Y, Sharma A, Jackson RL. A review of elastic–plastic contact mechanics. Applied Mechanics Reviews. 2017;69(6).
204. Jackson RL, Green I, editors. A finite element study of elasto-plastic hemispherical contact. STLE/ASME 2003 international joint tribology conference; 2003: American Society of Mechanical Engineers Digital Collection.
205. Coote CF, Hamilton JV, McGimpsey WG, Thompson RW. Oxidation of gamma-irradiated ultrahigh molecular weight polyethylene. Journal of applied polymer science. 2000;77(11):2525-42.
206. Collier JP, Sutula LC, Currier BH, Currier JH, Wooding RE, Williams IR, et al. Overview of polyethylene as a bearing material: comparison of sterilization methods. Clinical orthopaedics and related research. 1996(333):76-86.
207. Sun D. A simple accelerated aging method for simulations of long-term oxidative effects in UHMWPE implants. Trans 42 th Orthop Res Soc. 1996;21:493.
208. Sun D, Stark C, Dumbleton J, editors. Development of an accelerated aging method for evaluation of long-term irradiation effects on UHMWPE implants. 208th ACS national meeting; 1994.
209. Sanford W, Saum K. Accelerated oxidative aging testing of UHMWPE. Trans Orthop Res Soc. 1995;20:119.

Die approbierte gedruckte Originalversion dieser Dissertation ist an der TU Wien Bibliothek verfügbar.
The approved original version of this doctoral thesis is available in print at TU Wien Bibliothek.
TU Bibliothek Your knowledge hub WIEN

210. McKellop H, Yeom B, Sun D, Sanford W, editors. Accelerated ageing of irradiated UHMWPE for wear evaluations. Proceedings of the 42nd Annual Meeting, Orthopaedic Research Society; 1996.
211. F2003-00 A. Standard guide for accelerated aging of ultra-highmolecular weight polyethylene. American Society for Testingand Materials. 2000.
212. Hall R. MJK bankes, G. Blunn, Biotribology for joint human joints. Curr Orthop. 2001;15:281-90.
213. Trezona R, Allsopp D, Hutchings I. Transitions between two-body and three-body abrasive wear: influence of test conditions in the microscale abrasive wear test. Wear. 1999;225:205-14.
214. Schneider W, Abt N, Köttig P, editors. O1222 ANALYSIS OF EARLY RETRIEVED ACETABULAR CUPS OF HIGHLY CROSSLINKED UHMWPE. Orthopaedic Proceedings; 2004: The British Editorial Society of Bone & Joint Surgery.
215. Gilbert JL, Cumber J, Butterfield A. Surface micromechanics of ultrahigh molecular weight polyethylene: Microindentation testing, crosslinking, and material behavior. Journal of Biomedical Materials Research Part A. 2002;61(2):270-81.
216. Blanchet TA, Burroughs BR. Numerical oxidation model for gamma radiation-sterilized UHMWPE: Consideration of dose-depth profile. Journal of Biomedical Materials Research Part A. 2001;58(6):684-93.
217. Leitner L, Türk S, Heidinger M, Stöckl B, Posch F, Maurer-Ertl W, et al. Trends and economic impact of hip and knee arthroplasty in Central Europe: findings from the Austrian National Database. Scientific reports. 2018;8(1):1-5.
218. Surin VV, Sundholm K. Survival of patients and prostheses after total hip arthroplasty. Clinical orthopaedics and related research. 1983(177):148-53.
219. Herberts P, Malchau H. Long-term registration has improved the quality of hip replacement: a review of the Swedish THR Register comparing 160,000 cases. Acta Orthopaedica Scandinavica. 2000;71(2):111-21.
220. Kahan E, Fogelman Y, Bloch B. Correlations of work, leisure, and sports physical activities and health status with socioeconomic factors: a national study in Israel. Postgraduate medical journal. 2005;81(954):262-5.
221. Schurman DJ, Bloch DA, Segal MR, Tanner CM. Conventional cemented total hip arthroplasty. Assessment of clinical factors associated with revision for mechanical failure. Clinical orthopaedics and related research. 1989(240):173-80.
222. Fumes O, Lie S, Espehaug B, Vollset S, Engesaeter L, Havelin L. Hip disease and the prognosis of total hip replacements: A review of 53 698 primary total hip replacements reported to the Norwegian arthroplasty register 1987-99. Journal of bone and joint surgery British volume. 2001;83(4):579-86.
223. Roush SE. Patient-perceived functional outcomes associated with elective hip and knee arthroplasties. Physical therapy. 1985;65(10):1496-500.
224. Holtzman J, Saleh K, Kane R. Gender differences in functional status and pain in a Medicare population undergoing elective total hip arthroplasty. Medical care. 2002:461-70.
225. Medel F, Garcia-Alvarez F, Gómez-Barrena E, Puertolas J. Microstructure changes of extruded ultra high molecular weight polyethylene after gamma irradiation and shelf-aging. Polymer degradation and stability. 2005;88(3):435-43.

Die approbierte gedruckte Originalversion dieser Dissertation ist an der TU Wien Bibliothek verfügbar.
The approved original version of this doctoral thesis is available in print at TU Wien Bibliothek.
TU Bibliothek Your knowledge hub WIEN

226. Yeom B, Yu YJ, McKellop H, Salovey R. Profile of oxidation in irradiated polyethylene. Journal of Polymer Science Part A: Polymer Chemistry. 1998;36(2):329-39.
227. Willie B, Gingell D, Bloebaum R, Hofmann A. Possible explanation for the white band artifact seen in clinically retrieved polyethylene tibial components. Journal of Biomedical Materials Research: An Official Journal of The Society for Biomaterials, The Japanese Society for Biomaterials, and The Australian Society for Biomaterials and the Korean Society for Biomaterials. 2000;52(3):558-66.
228. Wernlé JD, Gilbert JL. Micromechanics of shelf-aged and retrieved UHMWPE tibial inserts: Indentation testing, oxidative profiling, and thickness effects. Journal of Biomedical Materials Research Part B: Applied Biomaterials: An Official Journal of The Society for Biomaterials, The Japanese Society for Biomaterials, and The Australian Society for Biomaterials and the Korean Society for Biomaterials. 2005;75(1):113-21.
229. Standard guide for evaluating the extend of oxidation in UHMWPE fabricated forms intended for surgical implants. F2102-01, A: Annual Book of ASTM Standards; 2001. p. 1170-3.
230. Oral E, Ghali BW, Neils A, Muratoglu OK. A new mechanism of oxidation in ultrahigh molecular weight polyethylene caused by squalene absorption. Journal of Biomedical Materials Research Part B: Applied Biomaterials. 2012;100(3):742-51.
231. Blanchet TA, Burroughs BR. Numerical oxidation model for gamma radiation-sterilized UHMWPE: Consideration of dose-depth profile. Journal of Biomedical Materials Research: An Official Journal of The Society for Biomaterials, The Japanese Society for Biomaterials, and The Australian Society for Biomaterials and the Korean Society for Biomaterials. 2001;58(6):684-93.
232. Kurtz SM, Pruitt LA, Crane DJ, Edidin AA. Evolution of morphology in UHMWPE following accelerated aging: the effect of heating rates. Journal of Biomedical Materials Research: An Official Journal of The Society for Biomaterials, The Japanese Society for Biomaterials, and The Australian Society for Biomaterials. 1999;46(1):112-20.
233. Shen FW, McKellop HA. Interaction of oxidation and crosslinking in gamma-irradiated ultrahigh molecular-weight polyethylene. Journal of Biomedical Materials Research: An Official Journal of The Society for Biomaterials, The Japanese Society for Biomaterials, and The Australian Society for Biomaterials and the Korean Society for Biomaterials. 2002;61(3):430-9.
234. Daly BM, Yin J. Subsurface oxidation of polyethylene. Journal of Biomedical Materials Research: An Official Journal of The Society for Biomaterials, The Japanese Society for Biomaterials, and the Australian Society for Biomaterials. 1998;42(4):523-9.
235. Costa L, Jacobson K, Brunella V, Bracco P. Effects of microtomy on the material properties of ultra high molecular weight polyethylene. Polymer testing. 2001;20(6):649-59.
236. Muratoglu OK, Bragdon CR, O'Connor DO, Jasty M, Harris WH. A novel method of cross-linking ultra-high-molecular-weight polyethylene to improve wear, reduce oxidation, and retain mechanical properties: recipient of the 1999 HAP Paul Award. The Journal of arthroplasty. 2001;16(2):149-60.
237. Martínez-Morlanes M, Castell P, Martínez-Nogués V, Martinez M, Alonso PJ, Puértolas J. Effects of gamma-irradiation on UHMWPE/MWNT nanocomposites. Composites Science and Technology. 2011;71(3):282-8.
238. Turell MB, Bellare A. A study of the nanostructure and tensile properties of ultra-high molecular weight polyethylene. Biomaterials. 2004;25(17):3389-98.

Die approbierte gedruckte Originalversion dieser Dissertation ist an der TU Wien Bibliothek verfügbar.
The approved original version of this doctoral thesis is available in print at TU Wien Bibliothek.
TU Bibliothek Your knowledge hub WIEN

239. Reggiani M, Tinti A, Taddei P, Visentin M, Stea S, De Clerico M, et al. Phase transformation in explanted highly crystalline UHMWPE acetabular cups and debris after in vivo wear. Journal of Molecular Structure. 2006;785(1-3):98-105.
240. M.Yaseniwa CN, T. Takemura. Polymer Journal. 1973;4:526.
241. Krumme A, Lehtinen A, Viikna A. Crystallisation behaviour of high density polyethylene blends with bimodal molar mass distribution 1. Basic characteristics and isothermal crystallisation. European polymer journal. 2004;40(2):359-69.
242. Buchanan F, Shipway P. Microabrasion—a simple method to assess surface degradation of UHMWPE following sterilisation and ageing. Biomaterials. 2002;23(1):93-100.
243. Bruni P, Conti C, Corvi A, Rocchi M, Tosi G. Damaged polyethylene acetabular cups microscopy FT-IR and mechanical determinations. Vibrational spectroscopy. 2002;29(1-2):103-7.
244. Flores A, Jordan N, Baltà-Calleja F, Bassett D, Olley R, Smith N. Mechanical changes linked to embrittlement at the wear surface of polyethylene implants in hip joints. Polymer. 2000;41(21):7635-9.
245. Gilbert JL, Merkhan I. Rate effects on the microindentation-based mechanical properties of oxidized, crosslinked, and highly crystalline ultrahigh-molecular-weight polyethylene. Journal of Biomedical Materials Research Part A: An Official Journal of The Society for Biomaterials, The Japanese Society for Biomaterials, and The Australian Society for Biomaterials and the Korean Society for Biomaterials. 2004;71(3):549-58.
246. Wang A, Stark C, Dumbleton J. Mechanistic and morphological origins of ultra-high molecular weight polyethylene wear debris in total joint replacement prostheses. Proceedings of the Institution of Mechanical Engineers, Part H: Journal of Engineering in Medicine. 1996;210(3):141-55.
247. Saikko V, Ahlroos T. Wear simulation of UHMWPE for total hip replacement with a multidirectional motion pin-on-disk device: Effects of counterface material, contact area, and lubricant. Journal of Biomedical Materials Research: An Official Journal of The Society for Biomaterials and The Japanese Society for Biomaterials. 2000;49(2):147-54.
248. Edidin A, Kurtz S, editors. Development and validation of the small punch test for UHMWPE used in total joint replacements. Key Engineering Materials; 2001: Trans Tech Publ.
249. Oral E, Muratoglu OK. Radiation cross-linking in ultra-high molecular weight polyethylene for orthopaedic applications. Nuclear Instruments and Methods in Physics Research Section B: Beam Interactions with Materials and Atoms. 2007;265(1):18-22.
250. Oral E, Godleski-Beckos C, Ghali BW, Lozynsky AJ, Muratoglu OK. Effect of cross-link density on the high pressure crystallization of UHMWPE. Journal of Biomedical Materials Research Part B: Applied Biomaterials: An Official Journal of The Society for Biomaterials, The Japanese Society for Biomaterials, and The Australian Society for Biomaterials and the Korean Society for Biomaterials. 2009;90(2):720-9.
251. Besong A, Hailey J, Ingham E, Stone M, Wroblewski B, Fisher J. A study of the combined effects of shelf ageing following irradiation in air and counterface roughness on the wear of UHMWPE. Bio-medical materials and engineering. 1997;7(1):59-65.
252. Wang A, Sun D, Yau S-S, Edwards B, Sokol M, Essner A, et al. Orientation softening in the deformation and wear of ultra-high molecular weight polyethylene. Wear. 1997;203:230-41.
253. Wang A. A unified theory of wear for ultra-high molecular weight polyethylene in multi-directional sliding. Wear. 2001;248(1-2):38-47.

Die approbierte gedruckte Originalversion dieser Dissertation ist an der TU Wien Bibliothek verfügbar.
The approved original version of this doctoral thesis is available in print at TU Wien Bibliothek.
TU Bibliothek Your knowledge hub WIEN

254. Galvin A, Kang L, Tipper J, Stone M, Ingham E, Jin Z, et al. Wear of crosslinked polyethylene under different tribological conditions. Journal of Materials Science: Materials in Medicine. 2006;17(3):235-43.
255. Wang A, Sun D, Stark C, Dumbleton J. Wear mechanisms of UHMWPE in total joint replacements. Wear. 1995;181:241-9.
256. Johnson KL, Johnson KL. Contact mechanics: Cambridge university press; 1987.
257. Premnath V, Bellare A, Merrill E, Jasty M, Harris W. Molecular rearrangements in ultra high molecular weight polyethylene after irradiation and long-term storage in air. Polymer. 1999;40(9):2215-29.
258. Markut-Kohl R, Archodoulaki VM, Seidler S, Skrbensky G. PE-UHMW in Hip Implants: Properties of Conventional and Crosslinked Prosthetic Components. Advanced Engineering Materials. 2009;11(10):B148-B54.
259. Birkinshaw C, Buggy M, Daly S, O'Neill M. Mechanism of ageing in irradiated polymers. Polymer degradation and stability. 1988;22(3):285-94.
260. Bhateja S. Changes in the crystalline content of irradiated linear polyethylenes upon ageing. Polymer. 1982;23(5):654-5.
261. Archodoulaki VM, Koch T, Rodriguez A, Seidler S. Influence of different sterilization procedures on the morphological parameters and mechanical properties of ultra-high-molecular-weight polyethylene. Journal of applied polymer science. 2011;120(4):1875-84.
262. Kurtz S, Rimnac C, Pruitt L, Jewett C, Goldberg V, Edidin A. The relationship between the clinical performance and large deformation mechanical behavior of retrieved UHMWPE tibial inserts. Biomaterials. 2000;21(3):283-91.
263. Kurtz SM, Foulds JR, Jewett CW, Srivastav S, Edidin AA. Validation of a small punch testing technique to characterize the mechanical behaviour of ultra-high-molecular-weight polyethylene. Biomaterials. 1997;18(24):1659-63.
264. Bistolfi A, Bellare A. The relative effects of radiation crosslinking and type of counterface on the wear resistance of ultrahigh-molecular-weight polyethylene. Acta biomaterialia. 2011;7(9):3398-403.

Die approbierte gedruckte Originalversion dieser Dissertation ist an der TU Wien Bibliothek verfügbar.
The approved original version of this doctoral thesis is available in print at TU Wien Bibliothek.
TU Bibliothek Your knowledge hub WIEN

APPENDIX

APPENDIX A: Patient Report Form

Prothesenregister Tirol
Befindlichkeit vor der Operation
(präoperativer Zustand)

st[redacted]
Ei
Fa
I-Z

Operation geplant an
[redacted]

Sehr geehrte Patientin, sehr geehrter Patient,

um die Veränderungen durch die Behandlung für Sie und uns darzustellen, möchten wir Sie bitten, die folgenden Fragen zu beantworten. Sie werden gebeten, nach diesem Muster die Stärke Ihrer Schmerzen, Ihrer Steifigkeit oder Behinderung anzugeben. Beurteilen Sie den **derzeitigen Zustand des Gelenks, das in den nächsten Tagen operiert werden soll**.

Bitte beachten Sie: Je mehr rechts Sie ankreuzen, umso mehr Schmerzen, Steifigkeit oder Behinderung haben Sie.

Bitte hier das heutige Datum (Ausfülldatum) eintragen: 30 - 06 - 2014

A Schmerzfragen

Die folgenden Fragen beziehen sich auf die Stärke der Schmerzen des Gelenks, das in den nächsten Tagen operiert werden soll. Bitte geben Sie für jede Frage die Stärke der Schmerzen an, die Sie in den letzten 2 Tagen verspürt haben. (Bitte kreuzen Sie das zutreffende Kästchen an).

	keine Schmerzen									extreme Schmerzen
1. Gehen auf ebenem Boden							X			
2. Treppen hinauf- oder hinuntersteigen									X	
3. Nachts im Bett		X								
4. Sitzen oder liegen		X								
5. Aufrecht stehen			X							

B Fragen zur Steifigkeit

Die folgenden Fragen beziehen sich auf die Steifigkeit (nicht die Schmerzen) des Gelenks, das in den nächsten Tagen operiert werden soll. Steifigkeit ist ein Gefühl von Einschränkung oder Langsamkeit in der Beweglichkeit, wenn Sie Ihre Gelenke bewegen. Bitte geben Sie für jede Frage die Stärke der Steifigkeit an, die Sie in den letzten 2 Tagen verspürt haben.

	keine Steifigkeit									extreme Steifigkeit
1. Wie stark ist die Steifigkeit gerade nach dem Erwachen am Morgen?		X								
2. Wie stark ist Ihre Steifigkeit nach Sitzen, Liegen oder Ausruhen im späteren Verlauf des Tages?		X								

Bitte Rückseite beachten

2367514277 Prothesenregister Tirol - WOMAC präoperativer Fragebogen Version 250703 Seite1

Die approbierte gedruckte Originalversion dieser Dissertation ist an der TU Wien Bibliothek verfügbar.
The approved original version of this doctoral thesis is available in print at TU Wien Bibliothek.
TU Bibliothek Your knowledge hub WIEN

C Fragen zur körperlichen Tätigkeit

Die folgenden Fragen beziehen sich auf Ihre körperliche Tätigkeit. Damit ist Ihre Fähigkeit gemeint, sich im Alltag zu bewegen und sich um sich selbst zu kümmern. Bitte geben Sie für jede der folgenden Aktivitäten den Schwierigkeitsgrad an, den Sie in den letzten 2 Tagen wegen Beschwerden des Gelenks hatten, das in den nächsten Tagen operiert werden soll.

	keine Schwierigkeiten									extreme Schwierigkeiten
1. Treppen hinuntersteigen								X		
2. Treppen hinaufsteigen						X				
3. Aufstehen vom Sitzen								X		
4. Stehen						X				
5. Sich zum Boden bücken						X				
6. Gehen auf ebenem Boden								X		
7. Einsteigen ins Auto/Aussteigen aus dem Auto										X
8. Einkaufen gehen										X
9. Socken/Strümpfe anziehen								X		
10. Aufstehen vom Bett								X		
11. Socken/Strümpfe ausziehen								X		
12. Liegen im Bett						X				
13. Ins Bad/aus dem Bad steigen										X
14. Sitzen										
15. Sich auf die Toilette setzen/Aufstehen von der Toilette								X		
16. Anstrengende Hausarbeiten										X
17. Leichte Hausarbeiten								X		

Bitte geben Sie uns abschließend noch folgende Informationen zu Ihrer Gesundheit:

Ihre Körpergröße in cm	168	cm
Ihr Gewicht in Kilogramm	81	Kilogramm
Hatten Sie bereits einen Schlaganfall?	☐ Ja	☒ Nein
Hatten Sie bereits einen Herzinfarkt?	☐ Ja	☒ Nein
Haben Sie schon eine Knie- oder Hüftprothese?	☒ Ja	☐ Nein

Die approbierte gedruckte Originalversion dieser Dissertation ist an der TU Wien Bibliothek verfügbar.
The approved original version of this doctoral thesis is available in print at TU Wien Bibliothek.
TU Bibliothek Your knowledge hub WIEN

Aktivitätsscore nach UCLA ____

Grad	Definition
1	Vollständig inaktiv; von anderen abhängig; kann das Haus nicht verlassen
2	Meistens inaktiv; sehr eingschränkt auf ein Minimum der Aktivitäten des täglichen Lebens
3	Manchmal leichte Aktivitäten wie z.B. Spazierengehen, leichte Hausarbeit, leichtes Einkaufen *Sitzende berufliche Tätigkeit*
4	Regelmäßige leichte Aktivitäten
5	Manchmal mittelstake Aktivitäten wie Schwimmen Kann Hausarbeit und Einkaufen unbegrenzt durchführen
6	Regelmäßige mittelstarke Tätigkeiten *Leichte berufliche Tätigkeiten*
X	Regelmäßige Teilnahme an aktiven Höhepunkten wie Fahrradfahren *Gartenarbeit, Training im Fitness-Center ein- bis zweimal in der Woche*
8	Regelmäßige Teilnahme an sehr aktiven Höhepunkten wie Bowling, Golf, *Reiten, Jagen, Gartenarbeit bzw. Training im Fitness-Center dreimal oder mehr in der Woche.* *Angemessen schwere berufliche Tätigkeit. Bauer*
9	Manchmal Teilnahme an Impakt-Sportarten wie Jogging, Tennis, Skifahren, Akrobatik, Ballett, schwere Arbeit, Rucksacktouren, *Fußball, Kampfsportarten*
10	Regelmäßige Teilnahme an Impakt-Sprotarten

Die approbierte gedruckte Originalversion dieser Dissertation ist an der TU Wien Bibliothek verfügbar.
The approved original version of this doctoral thesis is available in print at TU Wien Bibliothek.
TU Bibliothek Your knowledge hub WIEN

Patienteninformation und Einverständniserklärung (Version 3)

Einladung zur Teilnahme an der Studie *„Analyse von geschlechtsspezifischen in vivo Einflüssen auf die Werkstoffeigenschaften von Hüftgelenksinlays aus Ultrahochmolekularem Polyethylen – eine prospektive Studie"*.

Sehr geehrte Patientin/sehr geehrter Patient!

Bei Ihnen wird im Zeitraum zwischen 1.5.2014 bis 1.5.2015 eine Revisionsoperation Ihres künstlichen Hüftgelenks mit Polyethylen-Metall/Keramik-Gleitpaarung durchgeführt. Durch unterschiedlichste Umgebungseinflüsse im Körper werden Implantatwerkstoffe belastet. Wir wollen durch werkstoffkundliche Methoden an der künstlichen Hüftgelenkspfanne, die Ihnen im Rahmen der Revisionsoperation entnommenen wurde, zeigen, wie sich der Werkstoff im menschlichen Körper verändert. Es soll untersucht werden, ob Faktoren wie Geschlecht (unter Berücksichtigung von Alter, Gewicht und Aktivitätslevel) die verwendeten ultrahochmolekularen Polyethylentypen (linear und hochvernetzt) unterschiedlich beeinflussen.

Wir dürfen Sie dazu einladen, an dieser Studie mitzuarbeiten.

Ablauf der Studie:

Ihnen wurde in der Vergangenheit ein künstliches Hüftgelenk mit Polyethylen-Metall/Keramik-Gleitpaarung eingesetzt. Sie werden im Zeitraum von 1.5.2014 bis 1.5.2015 einer Revisionsoperation unterzogen um dieses künstliche Hüftgelenk auszutauschen.

Anhand der Ihnen entfernten alten, künstlichen Hüftgelenkpfanne werden in einem dafür ausgerichteten Prüflabor werkstoffkundliche Untersuchungen durchgeführt. Mittels dieser Untersuchungen können eventuelle strukturelle Veränderung und Änderungen in den mechanischen Eigenschaften des eingesetzten Werkstoffes untersucht werden.

Es werden keine zusätzlichen klinischen Untersuchungen durchgeführt. Die Studie nimmt auf Ihren Therapieverlauf keinen Einfluss.

Im Rahmen der Studie werden Ihr Geschlecht, Ihr Alter, Ihr Gewicht erhoben und e es werden Fragebögen ausgeteilt, in dem Sie über Ihr Aktivitätslevel befragt werden.

Erhebung, Verwendung u./o. Verarbeitung der Daten:

Im Rahmen Ihrer Behandlung wird Ihr behandelnder Arzt personenbezogene Gesundheitsdaten sammeln, verarbeiten u./o. benutzen. Ihre persönlichen Daten werden erhoben unter Beachtung der EU Direktive 95/46/EC über den Schutz von Individuen hinsichtlich der Verarbeitung und Austausch personenbezogener Daten in Übereinstimmung mit den entsprechenden Durchführungsbestimmungen der Mitgliedsländer. Personenbezogene Daten dürfen im Rahmen der klinischen Prüfung nur mit ausdrücklicher Zustimmung des Betroffenen verwendet werden.

Im Regelfall haben nur der Prüfer und dessen Mitarbeiter, Zugang zu diesen personenbezogenen Daten. Alle Personen, die aufgrund ihrer beruflichen Tätigkeit Zugang zu diesen Daten haben, sind – unbeschadet anderer gesetzlicher Verschwiegenheitspflichten – gemäß § 15 DSG 2000 an das Datengeheimnis gebunden.

Die Übermittlung der Daten im Inland erfolgt ausschließlich zu statistischen Zwecken und in anonymisierter Form. Allfällige Veröffentlichungen der Daten dieser klinischen Prüfung erfolgen ebenfalls in anonymisierter Form.

Auch wenn Sie ohne Zwang und in Kenntnis der Sachlage für den konkreten Fall der Verwendung Ihrer personenbezogenen Daten im Rahmen der klinischen Prüfung der Studie „Analyse von *in vivo*

Die approbierte gedruckte Originalversion dieser Dissertation ist an der TU Wien Bibliothek verfügbar.
The approved original version of this doctoral thesis is available in print at TU Wien Bibliothek.
TU Bibliothek Your knowledge hub WIEN

Einflüssen auf die Werkstoffeigenschaften von Hüftgelenksinlays aus Ultrahochmolekularem Polyethylen – eine prospektive Studie“ zugestimmt haben, steht Ihnen die Möglichkeit offen, diese Zustimmung jederzeit ohne Angabe von Gründen und ohne nachteilige Folgen für Ihre medizinische Betreuung zu widerrufen. Dieser Widerruf bewirkt die Unzulässigkeit der weiteren Verwendung Ihrer personenbezogenen Daten. Der Widerruf wird im Regelfall mit Ihrem Ausscheiden aus der Studie verbunden sein.

Freiwilligkeit:

Die Teilnahme an der Studie ist freiwillig. Es steht Ihnen frei, Ihre Einwilligung zur Teilnahme jederzeit und ohne Abgabe von Gründen zu widerrufen, ohne dass Ihnen dadurch Nachteile für die weitere Behandlung entstehen.

Untersuchungsergebnisse und personenbezogene Daten werden selbstverständlich vertraulich behandelt. Ihre Teilnahme an dieser Prüfung erfolgt freiwillig. Sie können jederzeit ohne Angabe von Gründen aus der Studie ausscheiden. Die Ablehnung der Teilnahme oder ein vorzeitiges Ausscheiden aus dieser Studie hat keine nachteiligen Folgen für Ihre weitere medizinische Betreuung.

Sollten Sie nicht an der Studie teilnehmen, wird die übliche operative und postoperative Behandlung durchgeführt.

Um Sie vor möglichen durch den Studienablauf bedingten Schäden zu bewahren, wurde eine Patientenversicherung für diese Studie abgeschlossen, sodass Sie im Schadensfalle Anspruch auf Vergütung haben.

Risiken:

Im Rahmen der Studie *„Analyse von geschlechtsspezifischen in vivo Einflüssen auf die Werkstoffeigenschaften von Hüftgelenksinlays aus Ultrahochmolekularem Polyethylen – eine prospektive Studie“* wird nicht in Ihre operative oder postoperative Behandlung eingegriffen.

Kontakt

Die approbierte gedruckte Originalversion dieser Dissertation ist an der TU Wien Bibliothek verfügbar.
The approved original version of this doctoral thesis is available in print at TU Wien Bibliothek.
TU Bibliothek Your knowledge hub WIEN

Einwilligungsteil:

Ich wurde für die oben genannte Studie vollständig über Wesen, Bedeutung und Tragweite der Studie aufgeklärt.
Ich habe das Informationsschreiben gelesen und verstanden.
Ich hatte die Möglichkeit, Fragen zu stellen. Ich habe die Antworten verstanden und akzeptiere sie.
Ich bin über die mit der Teilnahme an der Studie verbundenen Risiken und auch über den möglichen Nutzen informiert.
Ich hatte ausreichend Zeit, mich zur Teilnahme an der Studie zu entscheiden und weiß, dass die Teilnahme freiwillig ist.
Ich wurde darüber informiert, dass ich jederzeit und ohne Angabe von Gründen diese Zustimmung widerrufen kann, ohne dass dadurch Nachteile für mich entstehen.
Mir ist bekannt, dass meine Daten anonym gespeichert und ausschließlich für wissenschaftliche Zwecke verwendet werden.
Ich habe eine Kopie des Informationsschreibens und dieser Einverständniserklärung erhalten. Ich erkläre hiermit meine freiwillige Teilnahme an dieser Studie.
Nach der datenschutzrechtlichen Aufklärung erteile ich meine ausdrückliche Zustimmung, dass meine personenbezogenen Daten im Rahmen der Studie *„Analyse von geschlechtsspezifischen in vivo Einflüssen auf die Werkstoffeigenschaften von Hüftgelenksinlays aus Ultrahochmolekularem Polyethylen – eine prospektive Studie"* zu dem eingangs angeführten Studienzweck von Dr. Schuhfried Gerlinde und deren MitarbeiterInnen verarbeitet und, soweit erforderlich, an inländische Gesundheitsbehörden weitergegeben werden.
Zurzeit habe ich keine weiteren Fragen mehr. Sollten sich während der Studie weitere Fragen ergeben, kann ich mich jederzeit an den Stud[redacted]
von der Univ. Klinik für Orthopädie, wenden.
Ich erkläre mich hiermit mit der freiwilligen Teilnahme an der Studie einverstanden. Eine Kopie dieser Einverständniserklärung wurde mir ausgehändigt.

Die approbierte gedruckte Originalversion dieser Dissertation ist an der TU Wien Bibliothek verfügbar.
The approved original version of this doctoral thesis is available in print at TU Wien Bibliothek.
TU Bibliothek Your knowledge hub WIEN

Prüfbogen

Analyse von geschlechtsspezifischen *in vivo* Einflüssen auf die Werkstoffeigenschaften von Hü

Patientennummer	
Alter 65 Jahre	
Geschlecht weiblich	
BMI	
Gewicht 81	
Pfannentyp	auswärts operiert
Pfannengröße	
Schafttyp	
Schaftgröße	
Kopftyp	
Kopfgröße	
Inlaytyp	
Inlaygröße	
UCLA activity level	
Harrison hip score:	
WOMAC score:	
Verweildauer	Einbau am 28.11.2013
Grund des Ausbaus	Infektion durch Propionibakterien

Version 1.3

Datum: 1.5.2014

TU WIEN Bibliothek Your knowledge hub
Die approbierte gedruckte Originalversion dieser Dissertation ist an der TU Wien Bibliothek verfügbar.
The approved original version of this doctoral thesis is available in print at TU Wien Bibliothek.

APPENDIX A1: Gender Correlations of Properties

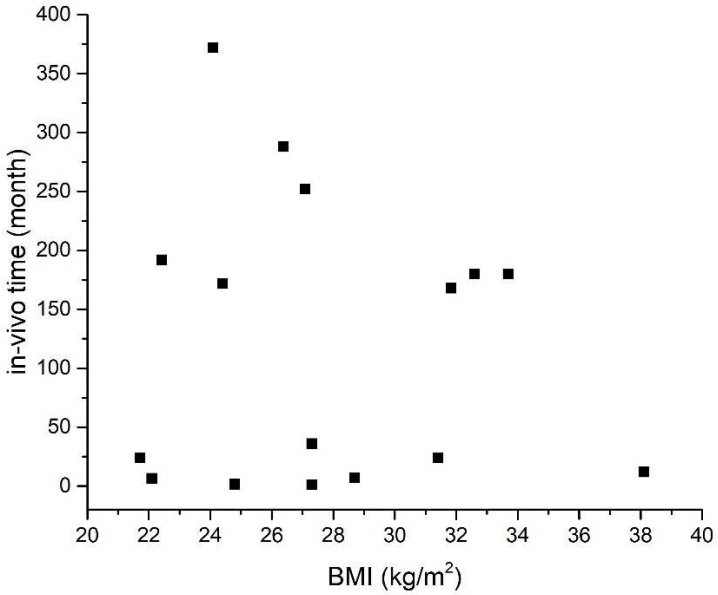

Figure A1.1. BMI (Body mass index) versus in-vivo time

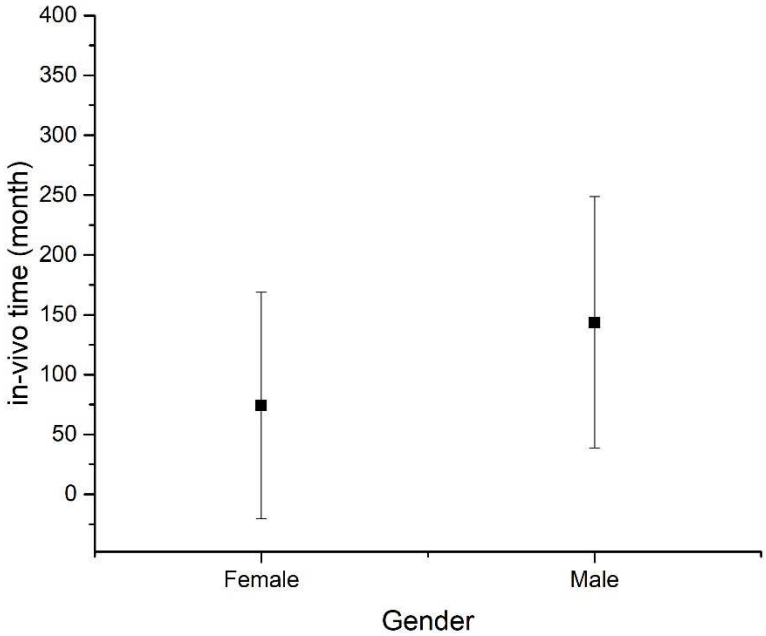

Figure A1.2. In-vivo time as a function of gender

Die approbierte gedruckte Originalversion dieser Dissertation ist an der TU Wien Bibliothek verfügbar.
The approved original version of this doctoral thesis is available in print at TU Wien Bibliothek.

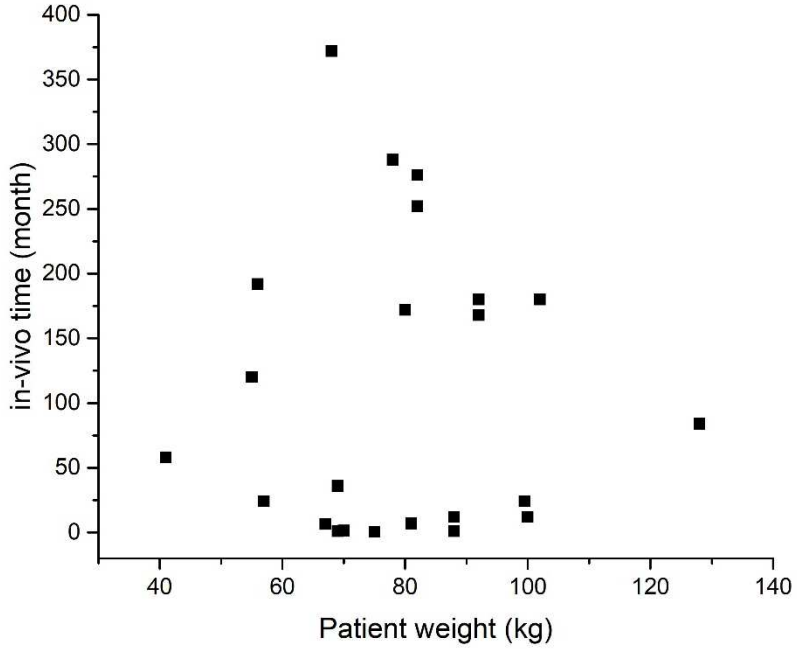

Figure A1.3. Scatterplot of patient weight and in-vivo time

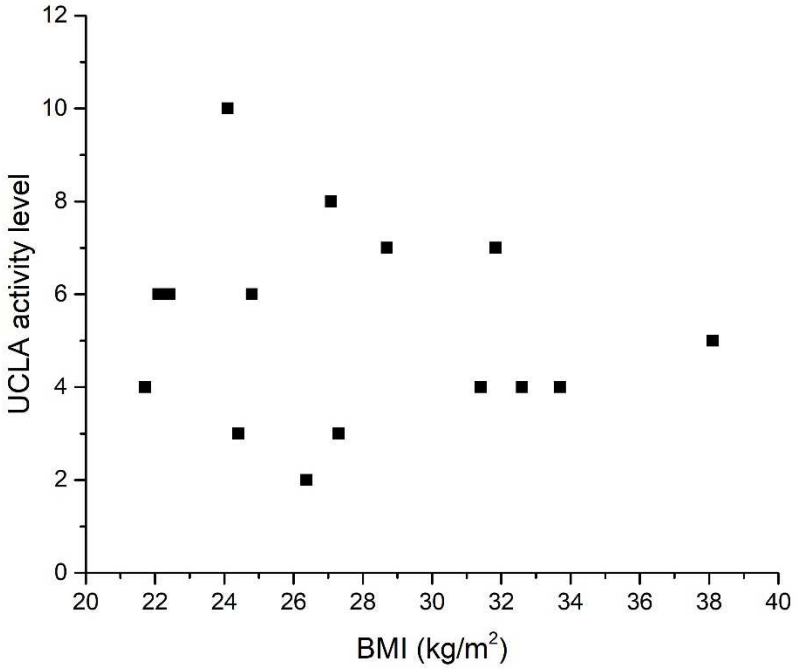

Figure A1.4. Scatterplot of UCLA activity and BMI (Body mass index)

Die approbierte gedruckte Originalversion dieser Dissertation ist an der TU Wien Bibliothek verfügbar.
The approved original version of this doctoral thesis is available in print at TU Wien Bibliothek.

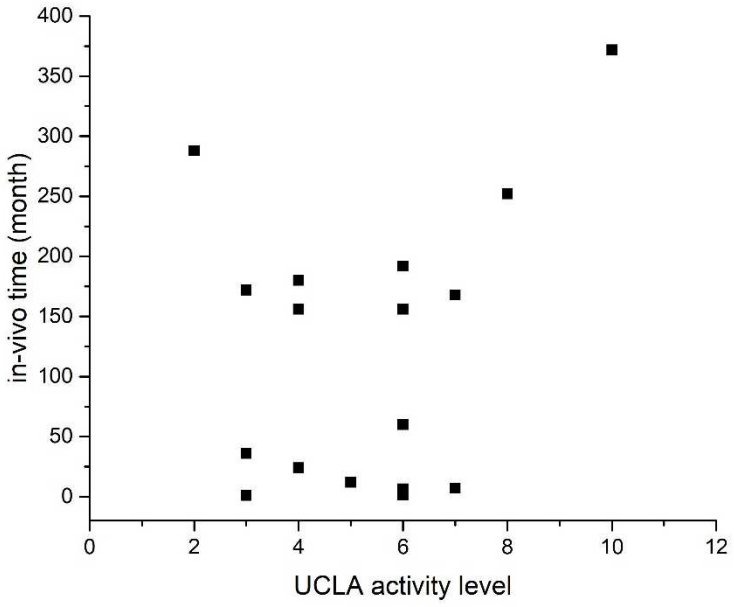

Figure A1.5. Scatterplot of UCLA activity and in-vivo time

Die approbierte gedruckte Originalversion dieser Dissertation ist an der TU Wien Bibliothek verfügbar.
The approved original version of this doctoral thesis is available in print at TU Wien Bibliothek.

APPENDIX B: Damage Scoring Data Sheet

1 Data sheet - Optical damage scoring

Semi-quantification - Optical damage scoring

Sample name: mücl (w-13y) Date:

Operator:

Dimensions (determined by means of a caliper rule):

	(mm)	notes
Inner diameter min.	28,55	
Inner diameter max.	30,11	
Ratio of Inner diameter max/min		
Outer diameter	46,58	
height	23,13	
Minimum PE thickness (after cutting)		
Maximum PE thickness (after cutting)		

Semi-Quantification:

damage:	articulating area												backside											
	V1			V2			V3			V4			H1			H2			H3			H4		
	AS		SS	AS		SS	AS		SS	AS		SS	AS		SS	AS		SS	AS		SS	AS		SS
	1.	2.		1.	2.		1.	2.		1.	2.		1.	2.		1.	2.		1.	2.		1.	2.	
Cracks	0		0	1		1				1		1												
Scratches	0			1			0									1			1					
Grooves	1		1	1		2	1		2	1		1												
Pitting	1	2	1				1		1	1		1	1		1				1		1	1		1
Burnishing	1		2				3		2															
Machining marks																								
De-lamination	1		1				1		1	1		1							1		1	1		1
Color Change																								
Summe: Kat. bis 07-2014, nach [1]																								
Plastic def.																								
Roughness																								
∑ AS x SS: nach[2]																								

1. R. W. Hood et al. (1983)
2. J.-M. Brant et al. (2012)

GESAMTSUMMEN: 4/3/6/4 $\Sigma_V = 17$ 1/1/3/2 $\Sigma_H = 7$

Front V:.....

Back H:.....

Die approbierte gedruckte Originalversion dieser Dissertation ist an der TU Wien Bibliothek verfügbar.
The approved original version of this doctoral thesis is available in print at TU Wien Bibliothek.
TU Bibliothek Your knowledge hub WIEN

APPENDIX C:

Table C1: Swell Ratio and Cross-linked Density Data

Name of the Sample	q (Swell Ratio)	Cross-linked Density (mol/dm3)
LUIN	1.71 ± 0.225	15.34 ± 2.42
LAMA 2	1.67 ± 0.228	15.80 ± 2.63
FADA	1.73 ± 0.214	15.06 ± 2.21
GRMA	1.70 ± 0.218	15.47 ± 2.39

Die approbierte gedruckte Originalversion dieser Dissertation ist an der TU Wien Bibliothek verfügbar.
The approved original version of this doctoral thesis is available in print at TU Wien Bibliothek.
TU Bibliothek Your knowledge hub WIEN

APPENDIX D: FTIR Results

Table D1. FTIR results for all explants; OI: oxidation index (-); TVI: trans vinylene index (-); Xr_{FTIR}: degree of crystallinity (%)

Acronym	OI (-)		TVI (-)		Xr FTIR (%)	
	Mean	St.dev	Mean	St.dev	Mean	St.dev
AUMAcenter IO	2.707	0.690	0.019	0.003	71.320	1.647
AUMA rim IO	0.018	0.004	0.018	0.004	71.956	1.312
GOKA rim IO	0.395	0.484	0.008	0.003	59.387	1.002
GOKA rim AO	0.239	0.959	0.009	0.003	64.663	1.703
LUIN center IO	0.585	0.033	0.003	0.002	58.278	0.408
LUIN center AO	0.466	0.086	0.004	0.001	58.092	0.257
LUIN rim IO	0.405	0.092	0.003	0.001	57.007	0.518
LUIN rim AO	0.214	0.062	0.002	0.001	56.479	0.265
MAWO center IO	0.686	0.301	0.012	0.002	63.242	1.603
MAWO center AO	0.153	0.023	0.010	0.001	60.758	0.251
MAWO rim IO	0.715	0.351	0.014	0.002	64.584	1.941
MAWO rim AO	0.172	0.069	0.012	0.003	59.937	0.511
MUCL center IO	1.208	0.147	0.003	0.001	56.264	0.842
MUCL center AO	0.608	0.107	0.004	0.002	57.687	0.687
MUCL rim IO	0.982	0.224	0.002	0.001	57.007	0.488
MUCL rim AO	0.466	0.128	0.004	0.002	56.244	0.293
JEJO center IO	0.234	0.236	0.049	0.002	54.294	1.022
JEJO center AO	0.100	0.096	0.050	0.003	54.852	0.379
JEJO rim IO	0.257	0.227	0.047	0.003	54.663	1.235
JEJO rim AO	0.135	0.119	0.050	0.002	53.605	0.891
VOST center IO	0.402	0.257	0.013	0.002	59.786	0.938
VOST center AO	0.809	0.125	0.013	0.002	63.597	0.884
VOST rim IO	0.393	0.321	0.013	0.003	61.676	1.330
VOST rim AO	0.199	0.075	0.013	0.003	61.109	0.744

Die approbierte gedruckte Originalversion dieser Dissertation ist an der TU Wien Bibliothek verfügbar.
The approved original version of this doctoral thesis is available in print at TU Wien Bibliothek.
TU Bibliothek Your knowledge hub WIEN

Table D1. FTIR results for all explants; OI: oxidation index (-); TVI: trans vinylene index (-); Xr_{FTIR}: degree of crystallinity (%). Cont.

Acronym	OI (-)		TVI (-)		Xr_{FTIR} (%)	
	Mean	St.dev	Mean	St.dev	Mean	St.dev
WIRU center IO	0.488	0.181	0.041	0.003	54.738	0.611
WIRU center AO	0.149	0.158	0.040	0.002	54.014	0.415
WIRU rim AO	0.132	0.108	0.040	0.002	53.652	0.307
GIWA center IO	0.065	0.008	0.001	0.001	57.727	0.331
GIWA center AO	0.052	0.004	0.001	0.001	57.844	0.146
GIWA rim IO	0.077	0.057	0.001	0.001	57.201	0.269
GIWA rim AO	0.129	0.118	0.001	0.001	57.314	0.501
GLFR center IO	0.458	0.230	0.003	0.001	57.908	0.568
GLFR center AO	0.342	0.162	0.003	0.001	58.819	1.584
GLFR rim IO	0.451	0.238	0.002	0.003	57.914	0.787
GLFR rim AO	0.369	0.109	0.002	0.001	57.899	0.556
STEL center IO	0.756	0.161	0.004	0.002	56.321	0.388
STEL center AO	0.737	0.253	0.005	0.010	56.365	0.949
STEL rim IO	0.458	0.100	0.001	0.001	55.602	0.621
STEL rim AO	0.125	0.040	0.003	0.002	55.521	0.210
FADA center IO	0.137	0.181	0.009	0.001	56.213	0.539
FADA center AO	0.088	0.067	0.008	0.003	55.310	0.383
FADA rim IO	0.311	0.247	0.012	0.003	55.718	0.400
FADA rim AO	0.059	0.024	0.012	0.003	55.115	0.344
GRMA center IO	0.207	0.131	0.004	0.003	57.694	0.390
GRMA center AO	0.049	0.074	0.001	0.001	56.943	0.767
GRMA rim IO	0.074	0.090	0.001	0.002	57.320	0.440
GRMA rim AO	0.041	0.016	0.001	0.002	57.390	0.342

Die approbierte gedruckte Originalversion dieser Dissertation ist an der TU Wien Bibliothek verfügbar.
The approved original version of this doctoral thesis is available in print at TU Wien Bibliothek.
TU Bibliothek Your knowledge hub WIEN

Table D1. FTIR results for all explants; OI: oxidation index (-); TVI: trans vinylene index (-); Xr_{FTIR}: degree of crystallinity (%). Cont.

Acronym	OI (-)		TVI (-)		Xr FTIR (%)	
	Mean	St.dev	Mean	St.dev	Mean	St.dev
KOEV center AO	0.163	0.166	0.013	0.002	64.337	4.900
KOEV rim IO	0.087	0.121	0.013	0.003	63.761	0.745
KOEV rim AO	0.413	0.290	0.013	0.003	65.622	1.937
LOPE center IO	0.028	0.021	0.005	0.002	56.529	0.227
LOPE center AO	0.033	0.009	0.007	0.001	56.691	0.523
LOPE rim IO	0.141	0.129	0.009	0.001	57.244	0.517
LOPE rim AO	0.155	0.115	0.009	0.007	56.527	1.714
TRCH center IO	0.218	0.149	0.029	0.003	61.599	0.832
TRCH center AO	0.214	0.103	0.030	0.003	61.978	0.652
TRCH rim IO	0.198	0.158	0.032	0.003	61.838	0.758
TRCH rim AO	0.149	0.159	0.031	0.005	60.903	0.567
PLWI rim IO	0.146	0.065	0.089	0.258	56.782	20.738
PLWI rim AO	0.143	0.061	0.085	0.222	59.219	16.432
LAMA1 center IO	0.392	0.267	0.030	0.010	64.063	0.747
LAMA1 center AO	0.332	0.227	0.033	0.004	62.672	0.588
LAMA1 rim IO	0.720	0.404	0.031	0.002	65.506	1.147
LAMA1 rim AO	0.302	0.169	0.036	0.011	63.947	3.032
LAMA2 center IO	0.322	0.007	0.035	0.002	63.311	0.223
LAMA2 center AO	0.258	0.105	0.034	0.002	63.140	0.632
LAMA2 rim IO	0.318	0.025	0.039	0.021	62.901	0.942
LAMA2 rim AO	0.292	0.057	0.034	0.003	63.042	0.403
JEJO center IO	0.234	0.236	0.049	0.002	54.294	1.022
JEJO center AO	0.100	0.096	0.050	0.003	54.852	0.379
JEJO rim IO	0.257	0.227	0.047	0.003	54.663	1.235
JEJO rim AO	0.135	0.119	0.050	0.002	53.605	0.891

Die approbierte gedruckte Originalversion dieser Dissertation ist an der TU Wien Bibliothek verfügbar.
The approved original version of this doctoral thesis is available in print at TU Wien Bibliothek.
TU Bibliothek Your knowledge hub WIEN

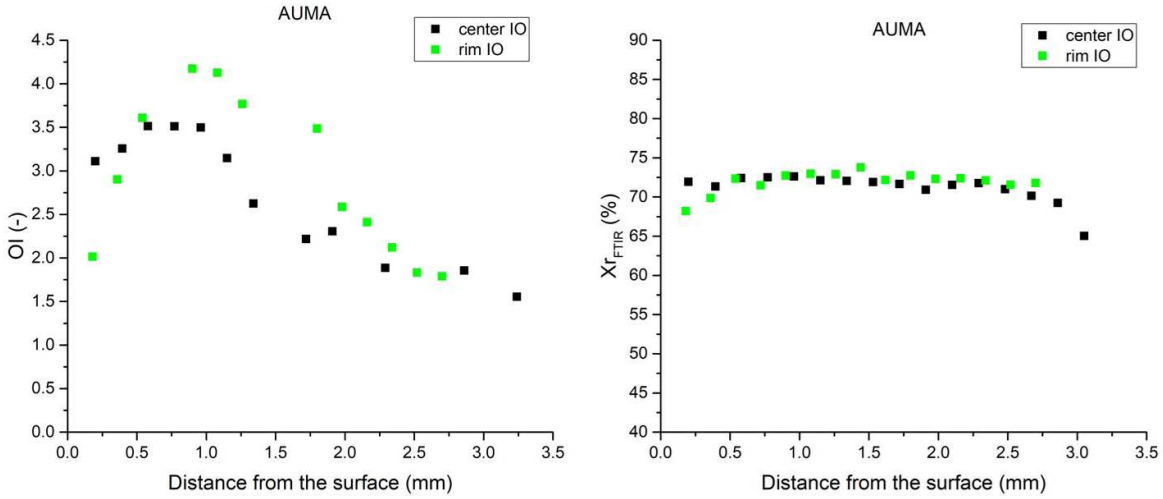

Figure D1. AUMA OI and degree of crystallinity profiles as a function of distance

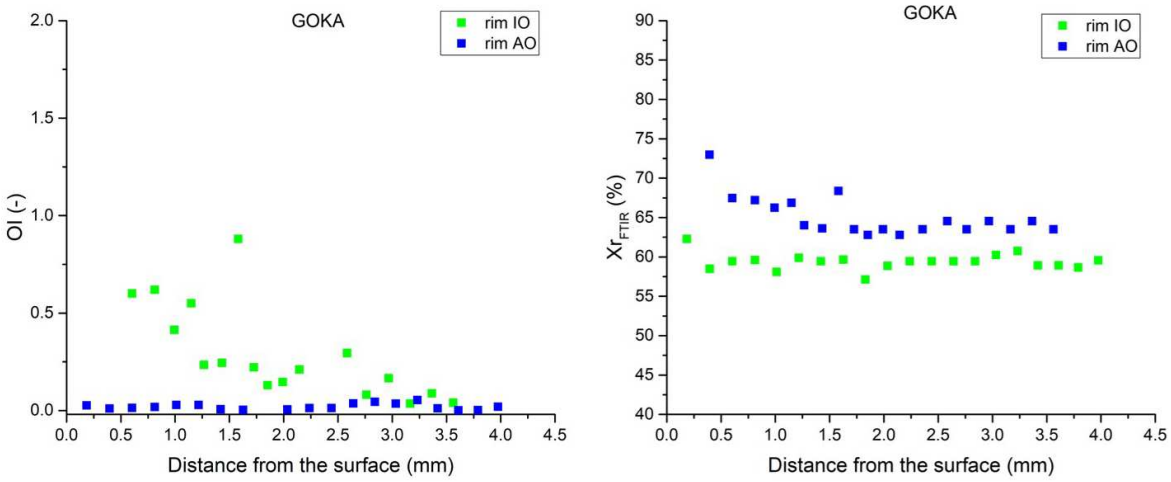

Figure D2. GOKA OI and degree of crystallinity profiles as a function of distance

Die approbierte gedruckte Originalversion dieser Dissertation ist an der TU Wien Bibliothek verfügbar.
The approved original version of this doctoral thesis is available in print at TU Wien Bibliothek.

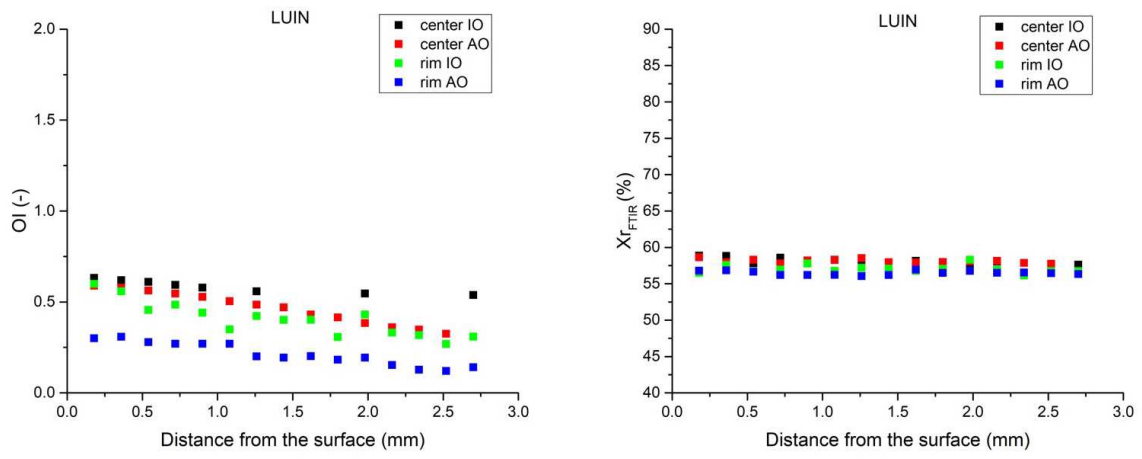

Figure D3. LUIN OI and degree of crystallinity profiles as a function of distance

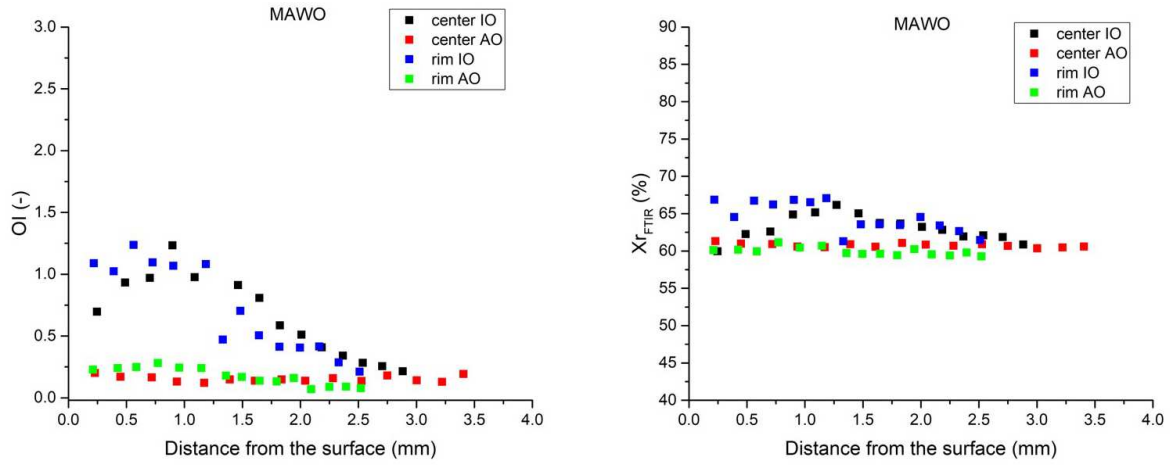

Figure D4. MAWO OI and degree of crystallinity profiles as a function of distance

Die approbierte gedruckte Originalversion dieser Dissertation ist an der TU Wien Bibliothek verfügbar.
The approved original version of this doctoral thesis is available in print at TU Wien Bibliothek.

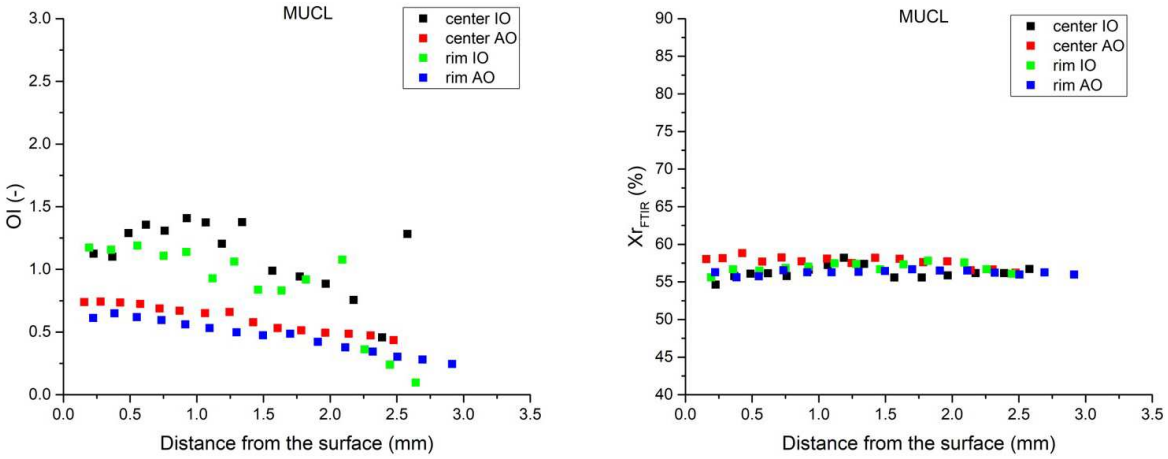

Figure D5. MUCL OI and degree of crystallinity profiles as a function of distance

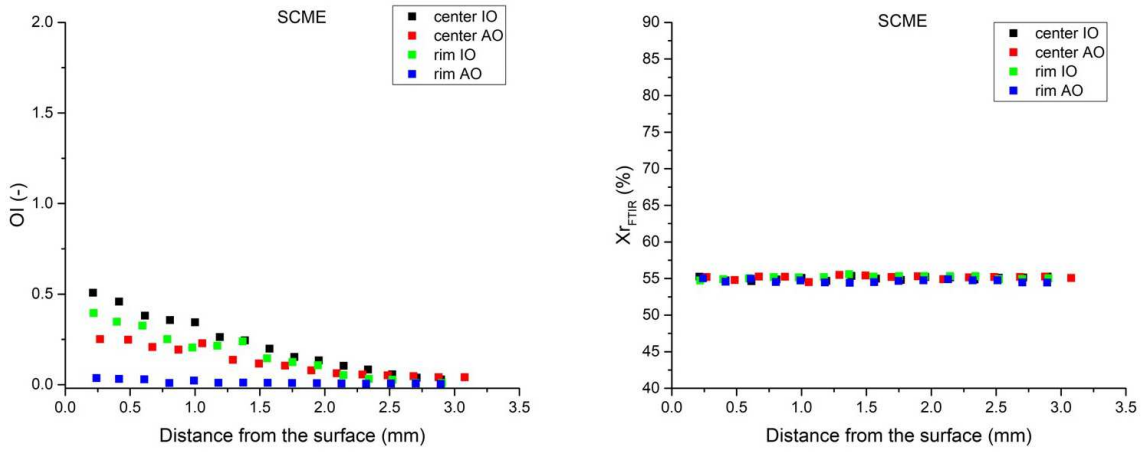

Figure D6. SCME OI and degree of crystallinity profiles as a function of distance

Die approbierte gedruckte Originalversion dieser Dissertation ist an der TU Wien Bibliothek verfügbar.
The approved original version of this doctoral thesis is available in print at TU Wien Bibliothek.

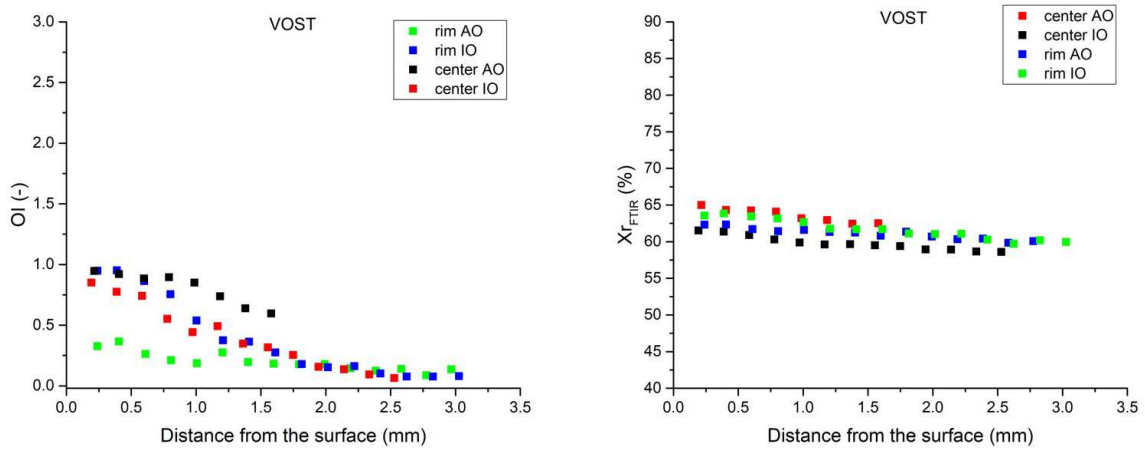

Figure D7. VOST OI and degree of crystallinity profiles as a function of distance

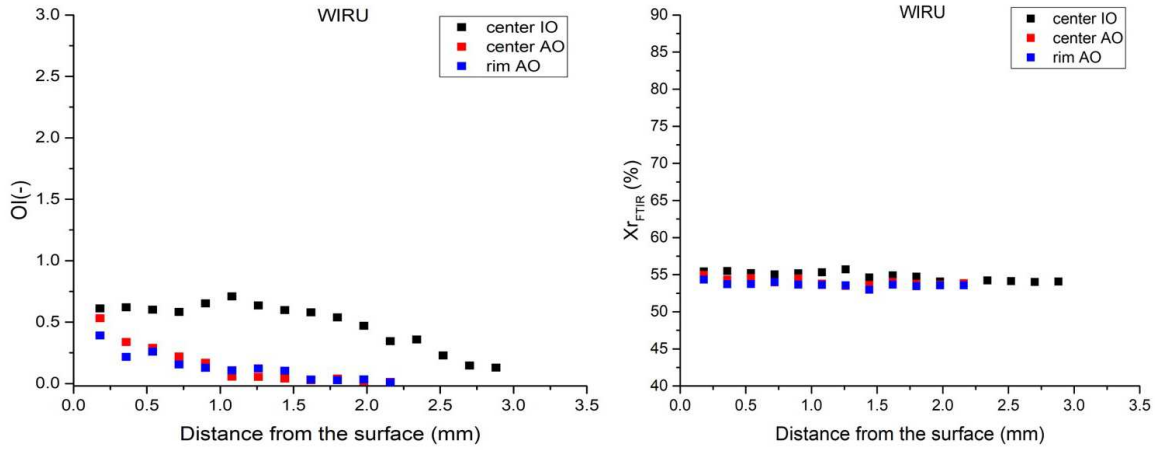

Figure D8. WIRU OI and degree of crystallinity profiles as a function of distance

Die approbierte gedruckte Originalversion dieser Dissertation ist an der TU Wien Bibliothek verfügbar.
The approved original version of this doctoral thesis is available in print at TU Wien Bibliothek.

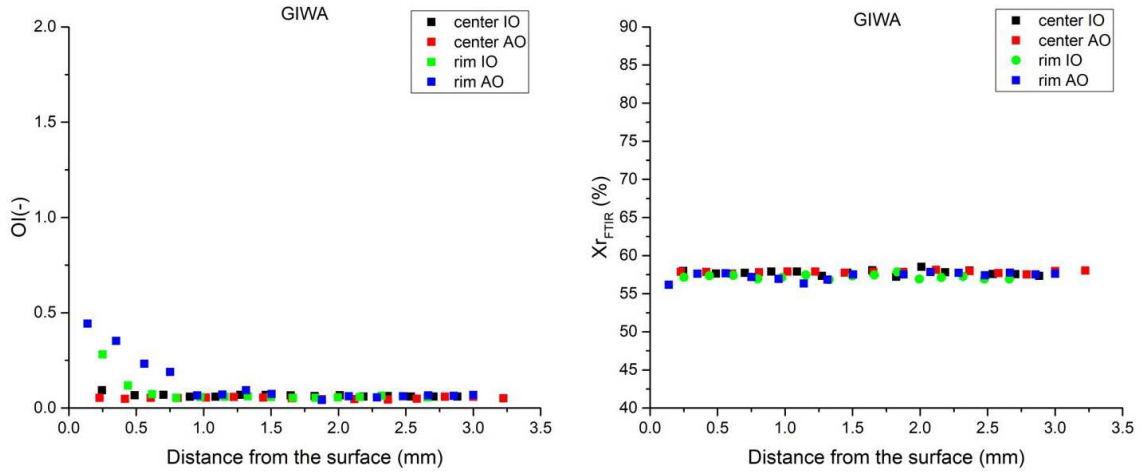

Figure D9. GIWA OI and degree of crystallinity profiles as a function of distance

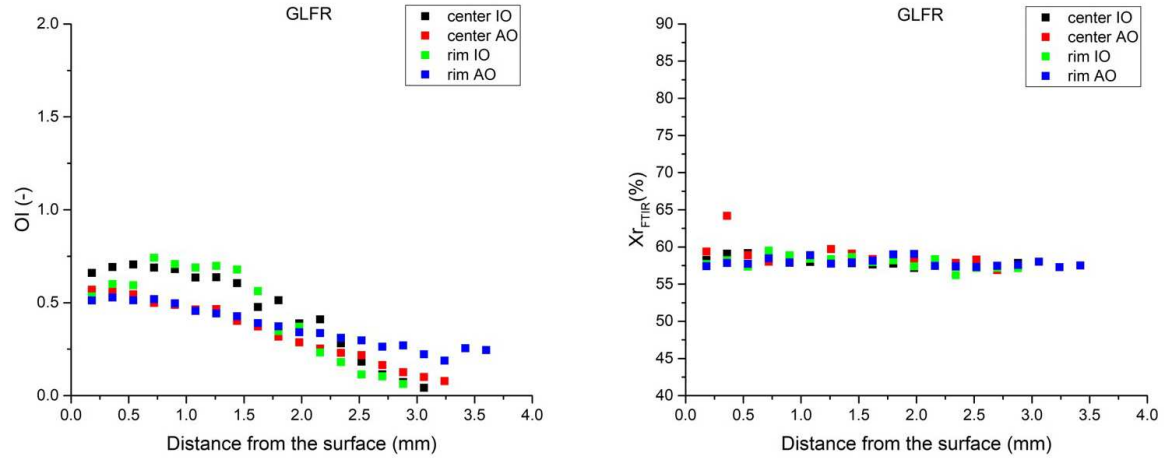

Figure D10. GLFR OI and degree of crystallinity profiles as a function of distance

Die approbierte gedruckte Originalversion dieser Dissertation ist an der TU Wien Bibliothek verfügbar.
The approved original version of this doctoral thesis is available in print at TU Wien Bibliothek.

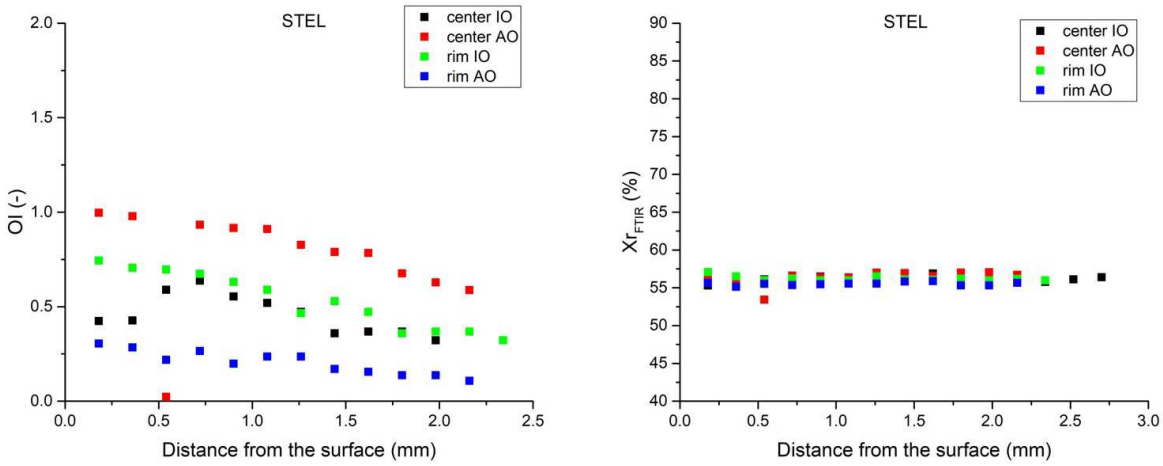

Figure D11. STEL OI and degree of crystallinity profiles as a function of distance

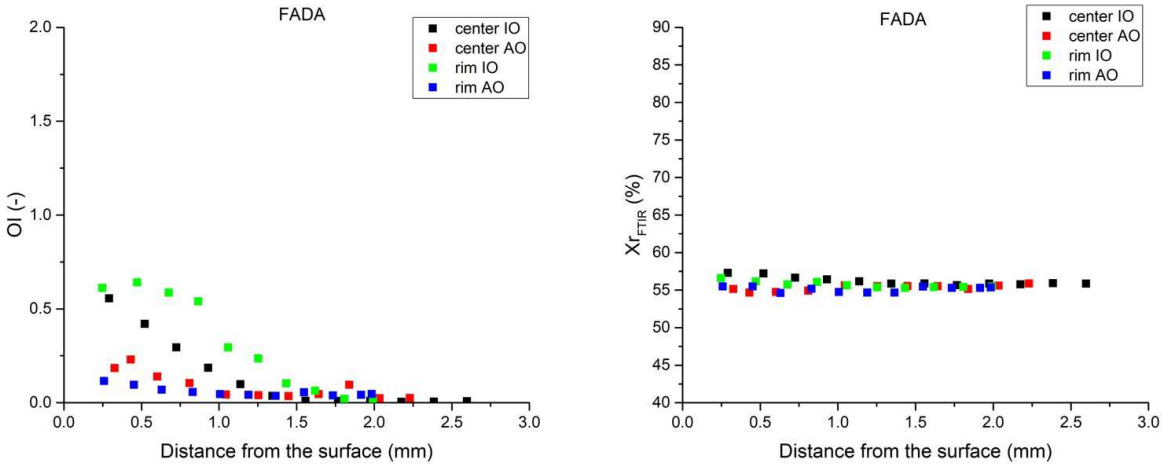

Figure D12. FADA OI and degree of crystallinity profiles as a function of distance

Die approbierte gedruckte Originalversion dieser Dissertation ist an der TU Wien Bibliothek verfügbar.
The approved original version of this doctoral thesis is available in print at TU Wien Bibliothek.

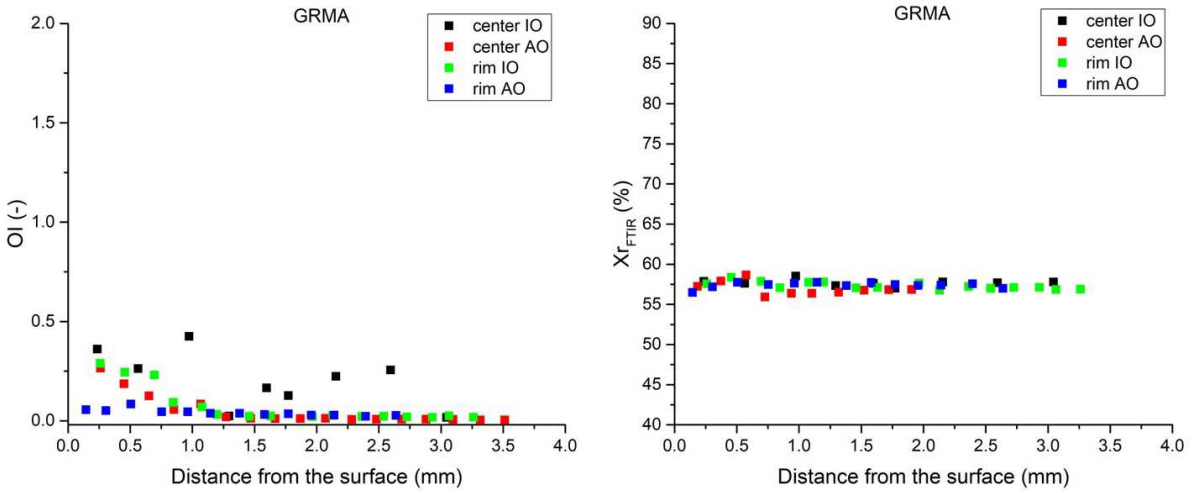

Figure D13. GRMA OI and degree of crystallinity profiles as a function of distance

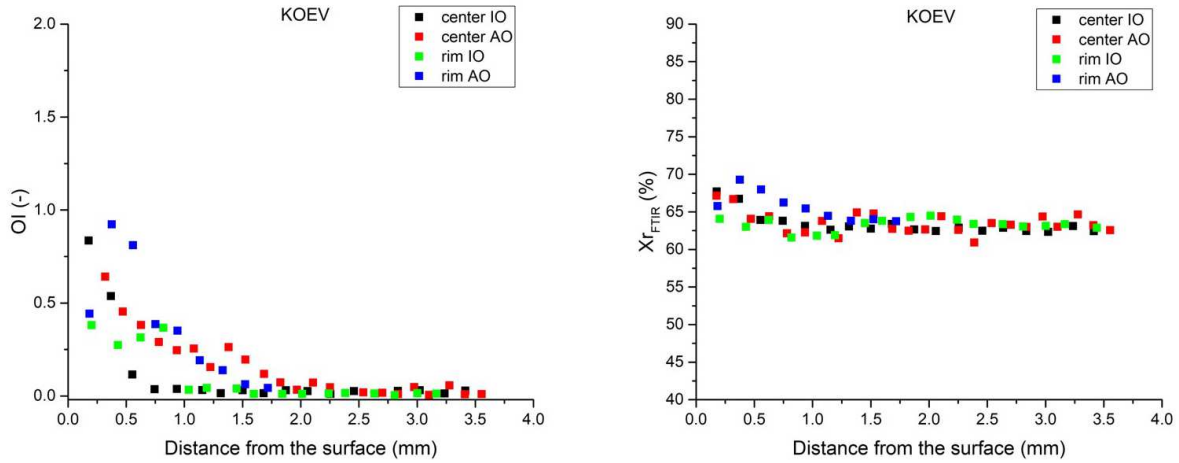

Figure D14. KOEV OI and degree of crystallinity profiles as a function of distance

Die approbierte gedruckte Originalversion dieser Dissertation ist an der TU Wien Bibliothek verfügbar.
The approved original version of this doctoral thesis is available in print at TU Wien Bibliothek.

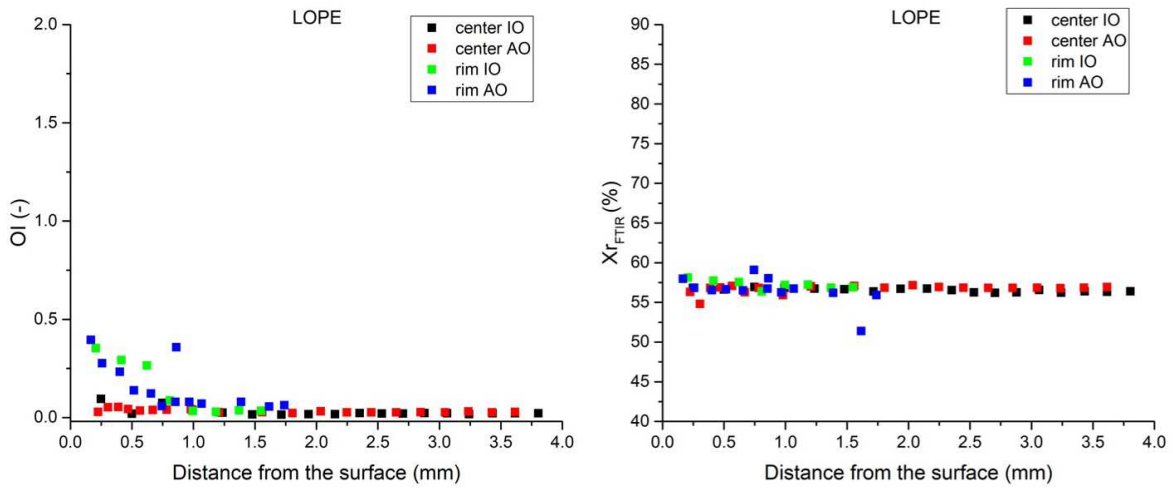

Figure D15. LOPE OI and degree of crystallinity profiles as a function of distance

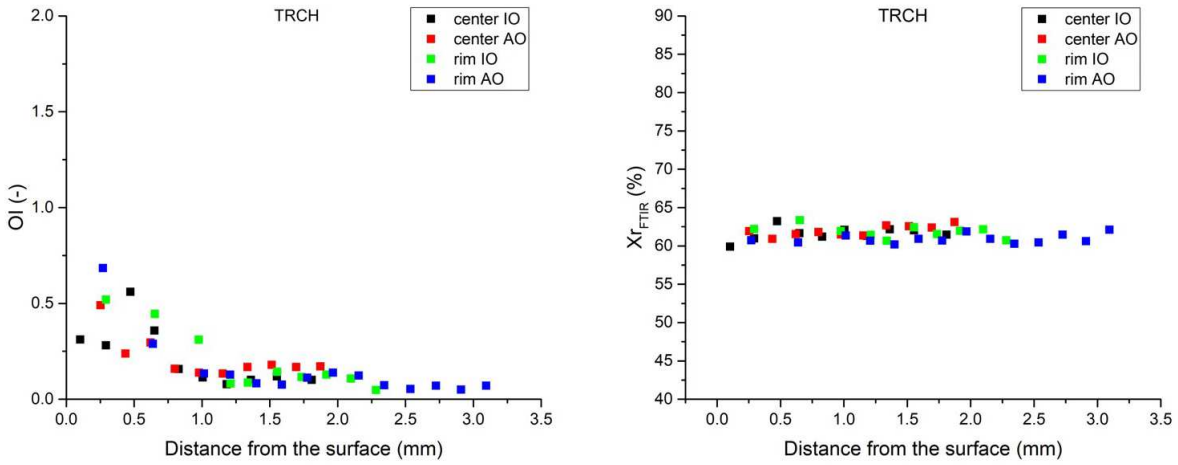

Figure D16. TRCH OI and degree of crystallinity profiles as a function of distance

Die approbierte gedruckte Originalversion dieser Dissertation ist an der TU Wien Bibliothek verfügbar.
The approved original version of this doctoral thesis is available in print at TU Wien Bibliothek.

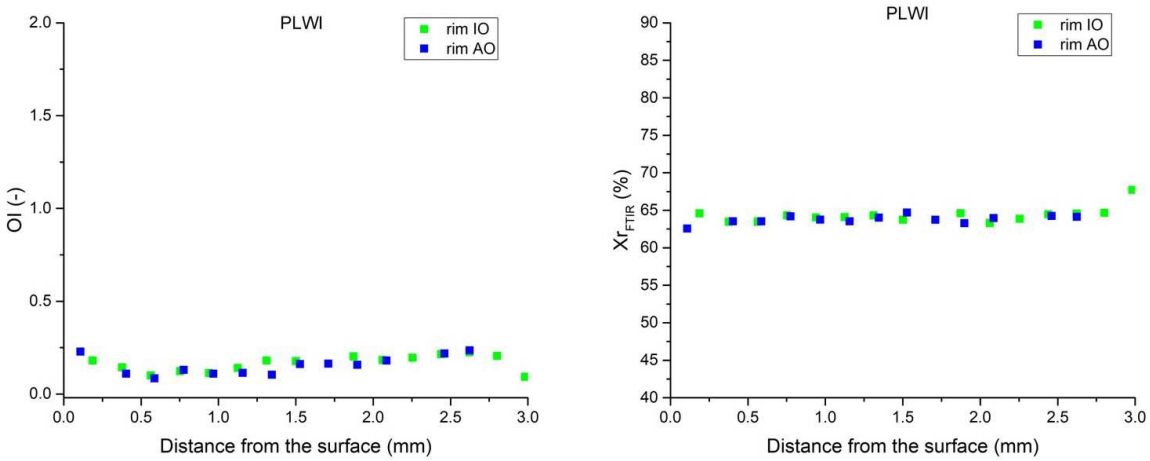

Figure D17. PLWI OI and degree of crystallinity profiles as a function of distance

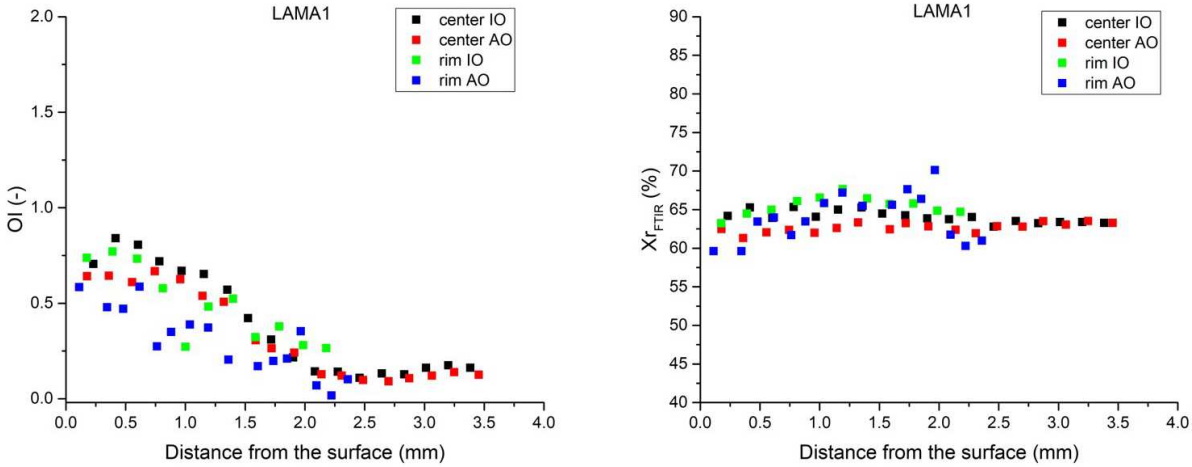

Figure D18. LAMA1 OI and degree of crystallinity profiles as a function of distance

Die approbierte gedruckte Originalversion dieser Dissertation ist an der TU Wien Bibliothek verfügbar.
The approved original version of this doctoral thesis is available in print at TU Wien Bibliothek.

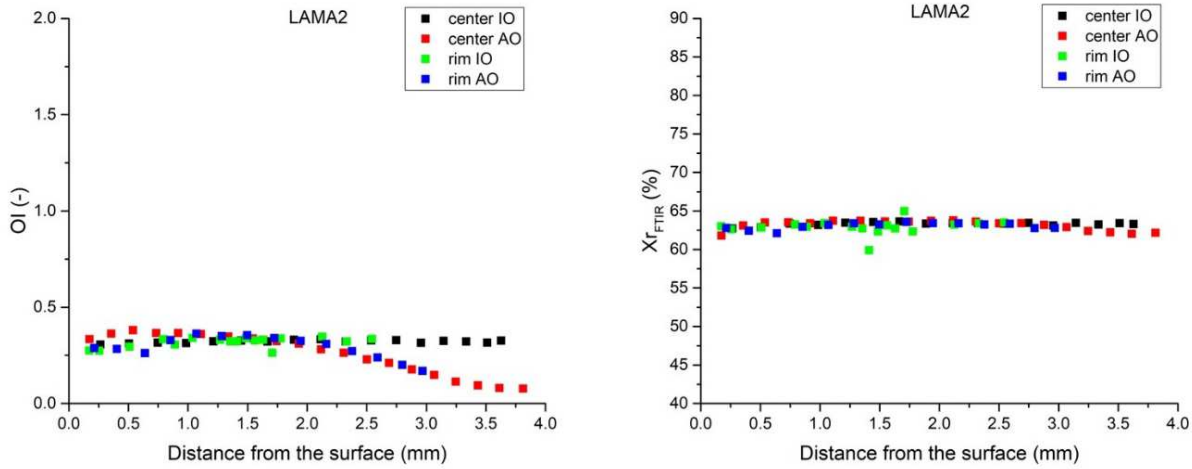

Figure D19. LAMA2 OI and degree of crystallinity profiles as a function of distance

Die approbierte gedruckte Originalversion dieser Dissertation ist an der TU Wien Bibliothek verfügbar.
The approved original version of this doctoral thesis is available in print at TU Wien Bibliothek.

Die approbierte gedruckte Originalversion dieser Dissertation ist an der TU Wien Bibliothek verfügbar.
The approved original version of this doctoral thesis is available in print at TU Wien Bibliothek.

APPENDIX E: DSC Results

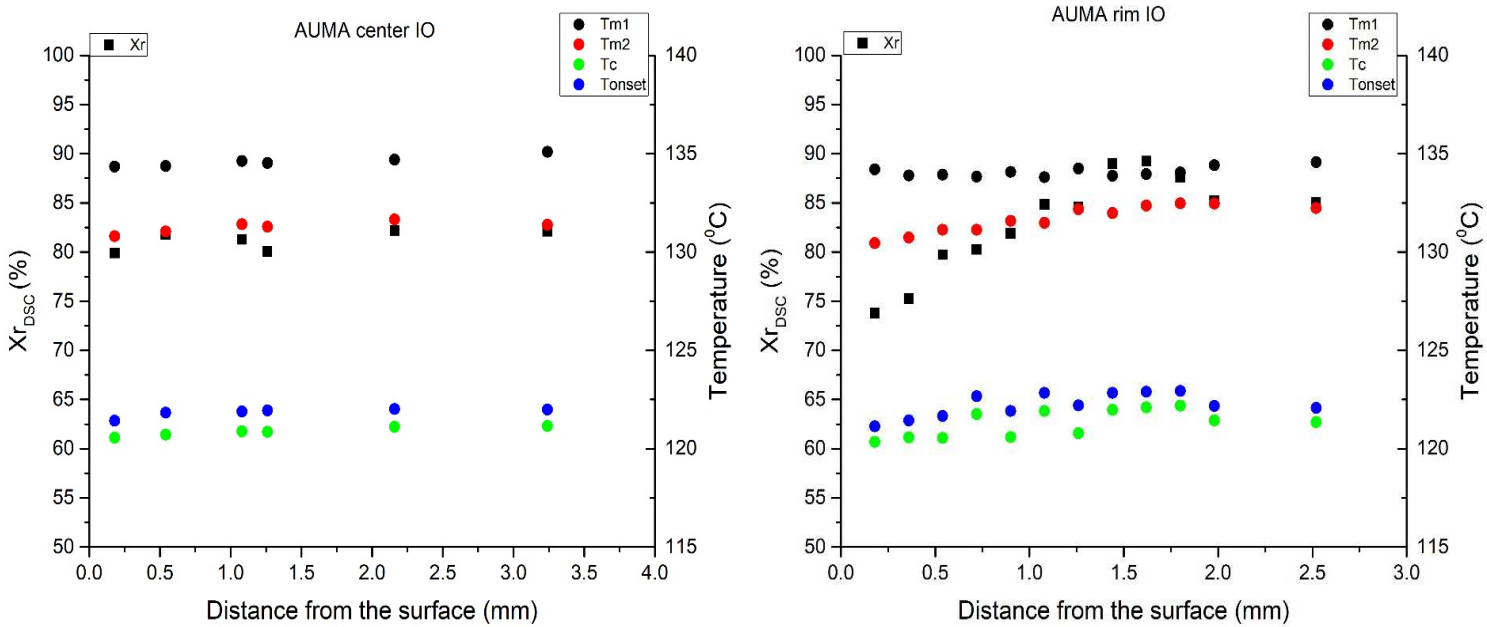

Figure E1. AUMA degree of crystallinity and thermal data profile as a function of distance. T_{m1}: melting point in the first heating run (ºC); T_{m2}: melting point for the second heating run (ºC); T_c: crystallization temperature (ºC); T_{onset}: onset crystallization temperature (ºC)

Die approbierte gedruckte Originalversion dieser Dissertation ist an der TU Wien Bibliothek verfügbar.
The approved original version of this doctoral thesis is available in print at TU Wien Bibliothek.

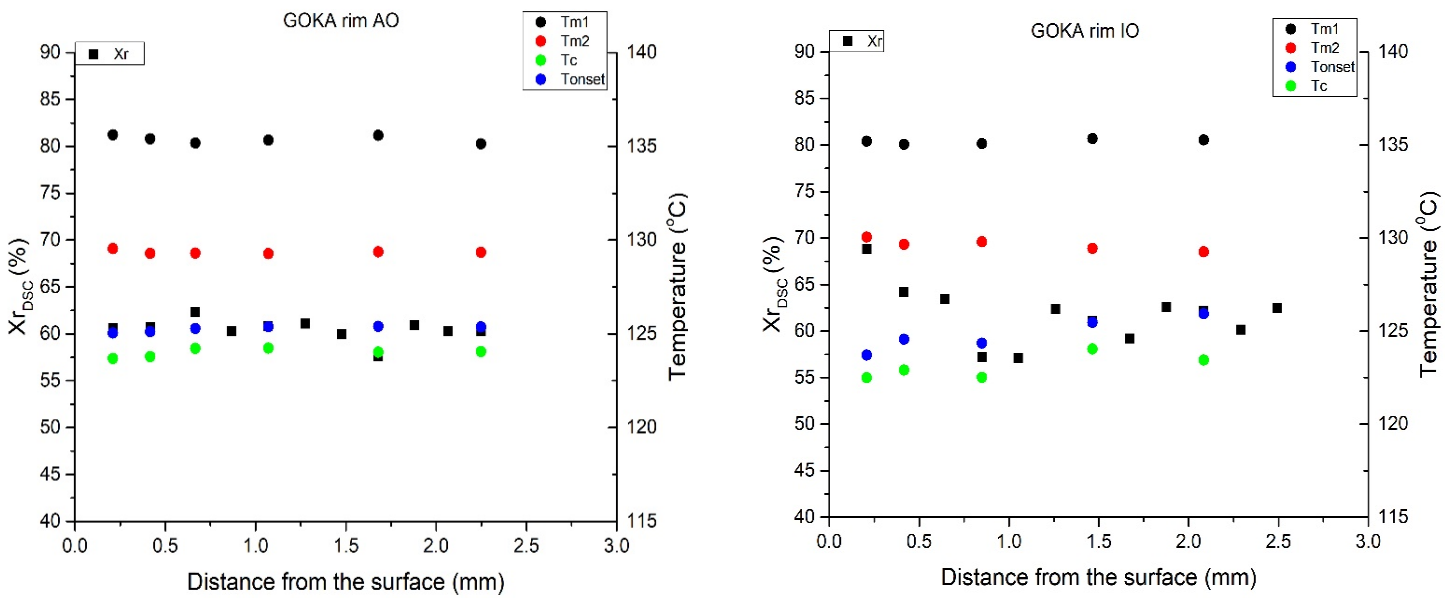

Figure E2. GOKA degree of crystallinity and thermal data profile as a function of distance. $T_{m1:}$ melting point in the first heating run (°C); $T_{m2:}$ melting point for the second heating run (°C); T_c: crystallization temperature (°C); T_{onset}: onset crystallization temperature (°C)

Die approbierte gedruckte Originalversion dieser Dissertation ist an der TU Wien Bibliothek verfügbar.
The approved original version of this doctoral thesis is available in print at TU Wien Bibliothek.

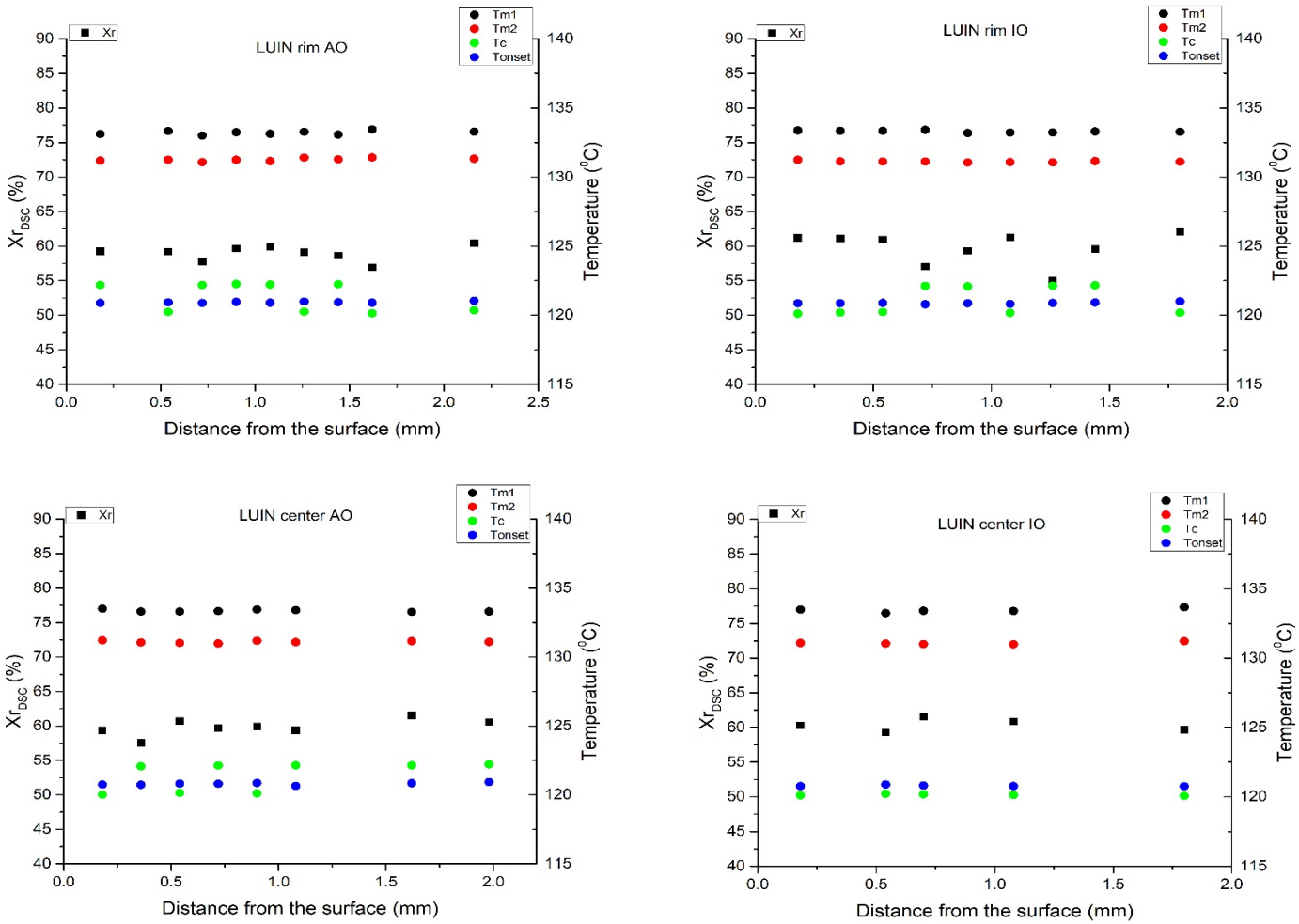

Figure E3. LUIN degree of crystallinity and thermal data profile as a function of distance. $T_{m1:}$ melting point in the first heating run (ºC); $T_{m2:}$ melting point for the second heating run (ºC); T_c: crystallization temperature (ºC); T_{onset}: onset crystallization temperature (ºC)

Die approbierte gedruckte Originalversion dieser Dissertation ist an der TU Wien Bibliothek verfügbar.
The approved original version of this doctoral thesis is available in print at TU Wien Bibliothek.

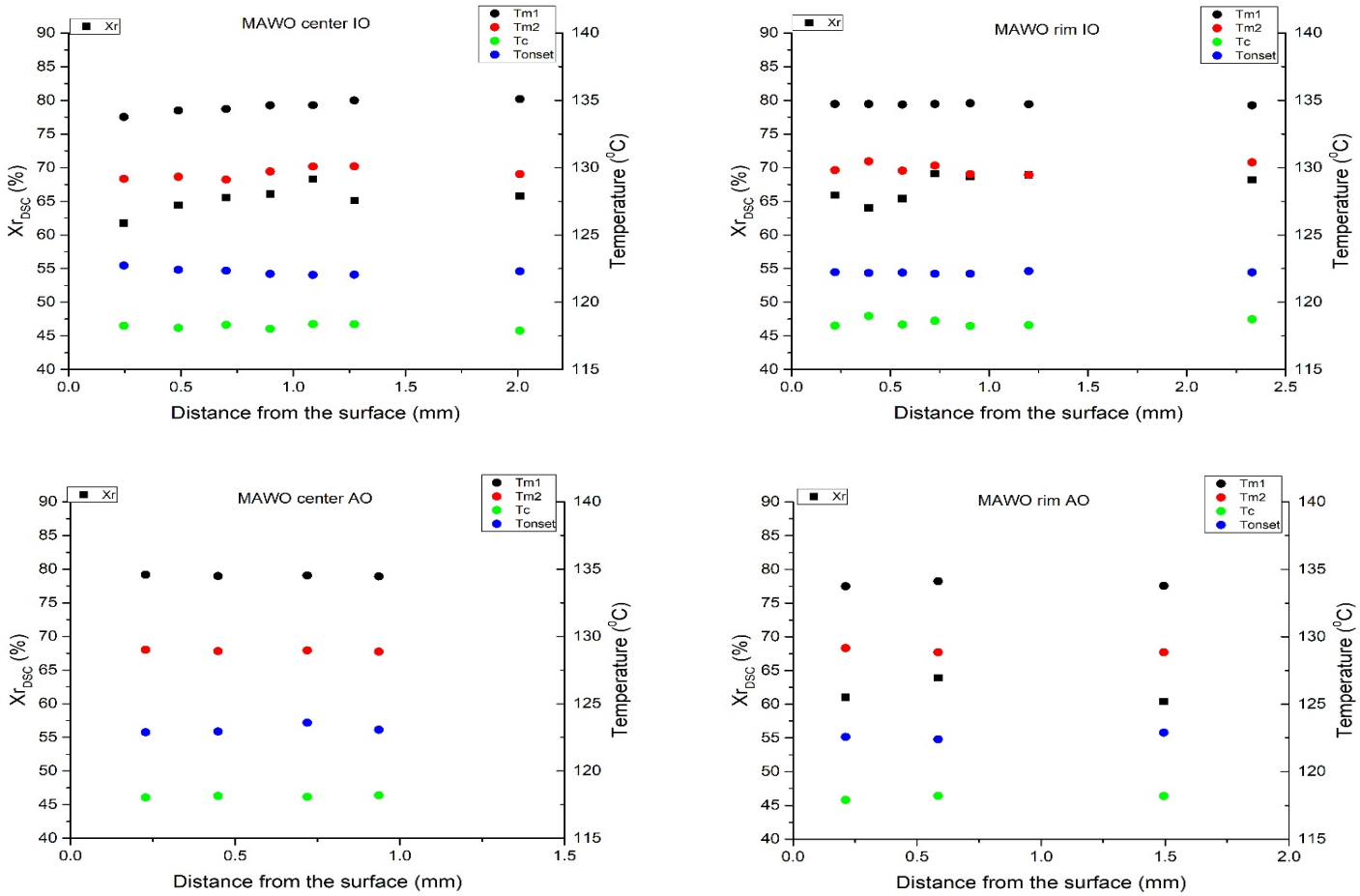

Figure E4. MAWO degree of crystallinity and thermal data profile as a function of distance. $T_{m1:}$ melting point in the first heating run (ºC); $T_{m2:}$ melting point for the second heating run (ºC); T_c: crystallization temperature (ºC); T_{onset}: onset crystallization temperature (ºC)

Die approbierte gedruckte Originalversion dieser Dissertation ist an der TU Wien Bibliothek verfügbar.
The approved original version of this doctoral thesis is available in print at TU Wien Bibliothek.

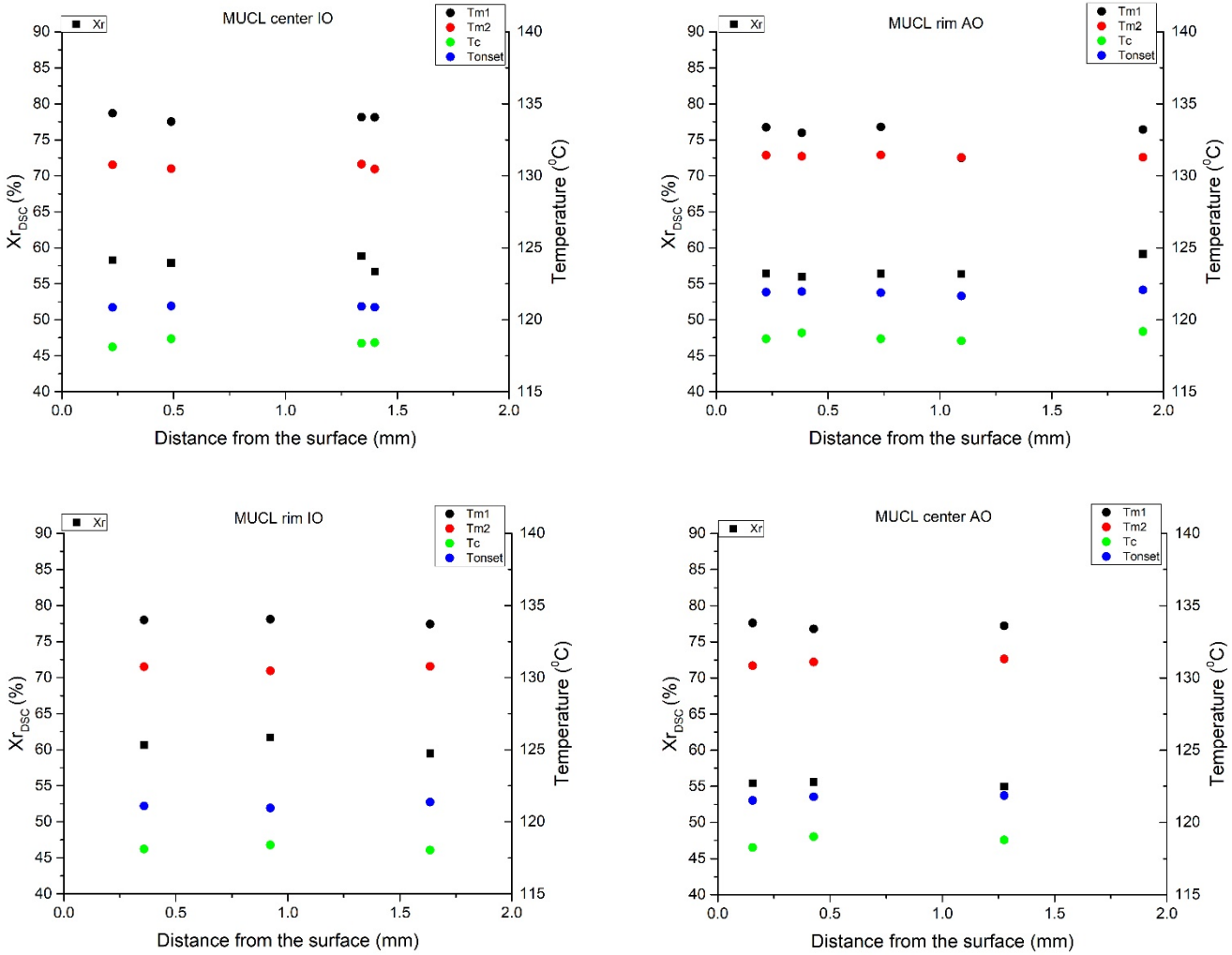

Figure E5. MUCL degree of crystallinity and thermal data profile as a function of distance. T_{m1}: melting point in the first heating run (ºC); T_{m2}: melting point for the second heating run (ºC); T_c: crystallization temperature (ºC); T_{onset}: onset crystallization temperature (ºC)

Die approbierte gedruckte Originalversion dieser Dissertation ist an der TU Wien Bibliothek verfügbar.
The approved original version of this doctoral thesis is available in print at TU Wien Bibliothek.

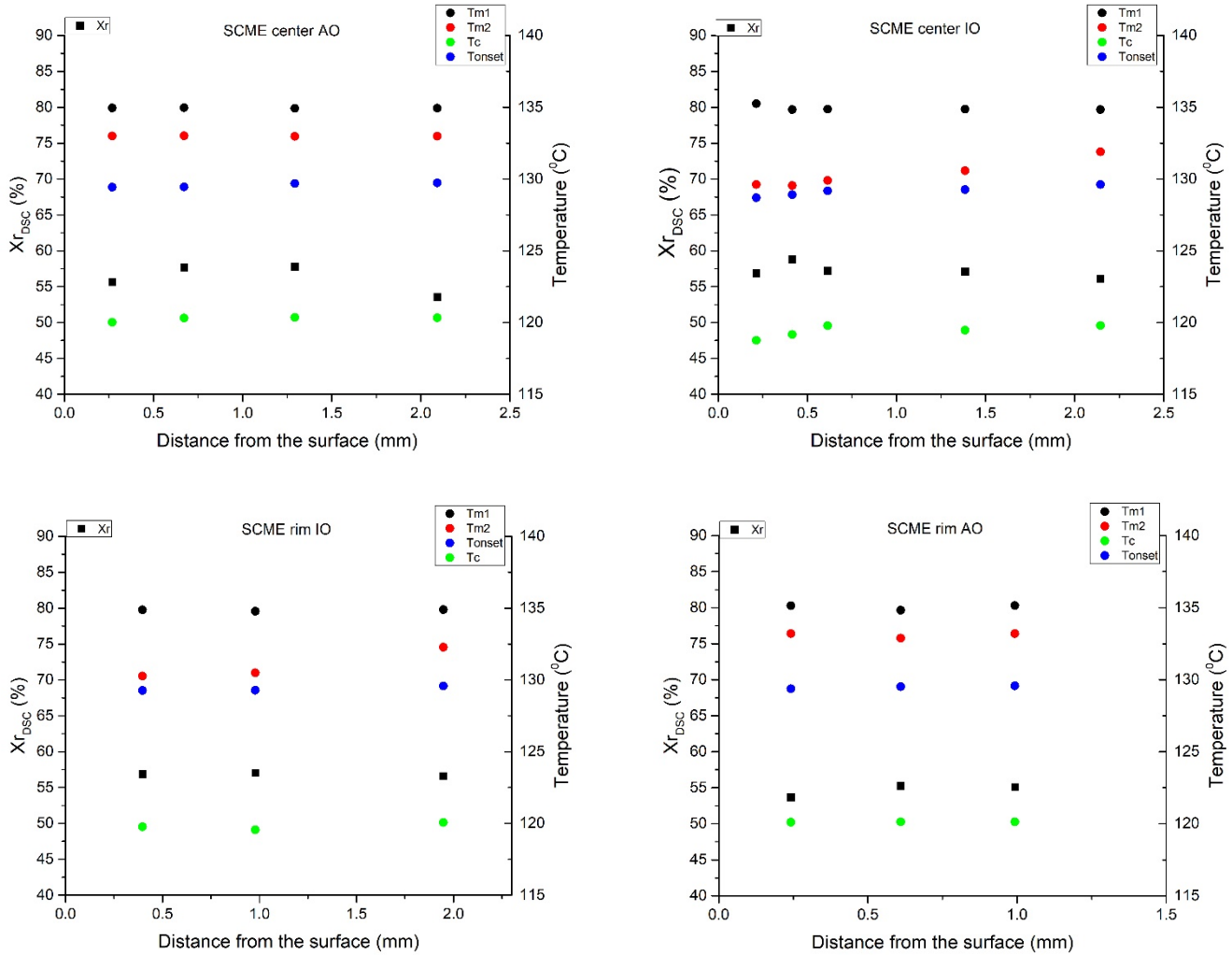

Figure E6. SCME degree of crystallinity and thermal data profile as a function of distance. $T_{m1:}$ melting point in the first heating run (°C); $T_{m2:}$ melting point for the second heating run (°C); T_c: crystallization temperature (°C); T_{onset}: onset crystallization temperature (°C)

Die approbierte gedruckte Originalversion dieser Dissertation ist an der TU Wien Bibliothek verfügbar.
The approved original version of this doctoral thesis is available in print at TU Wien Bibliothek.

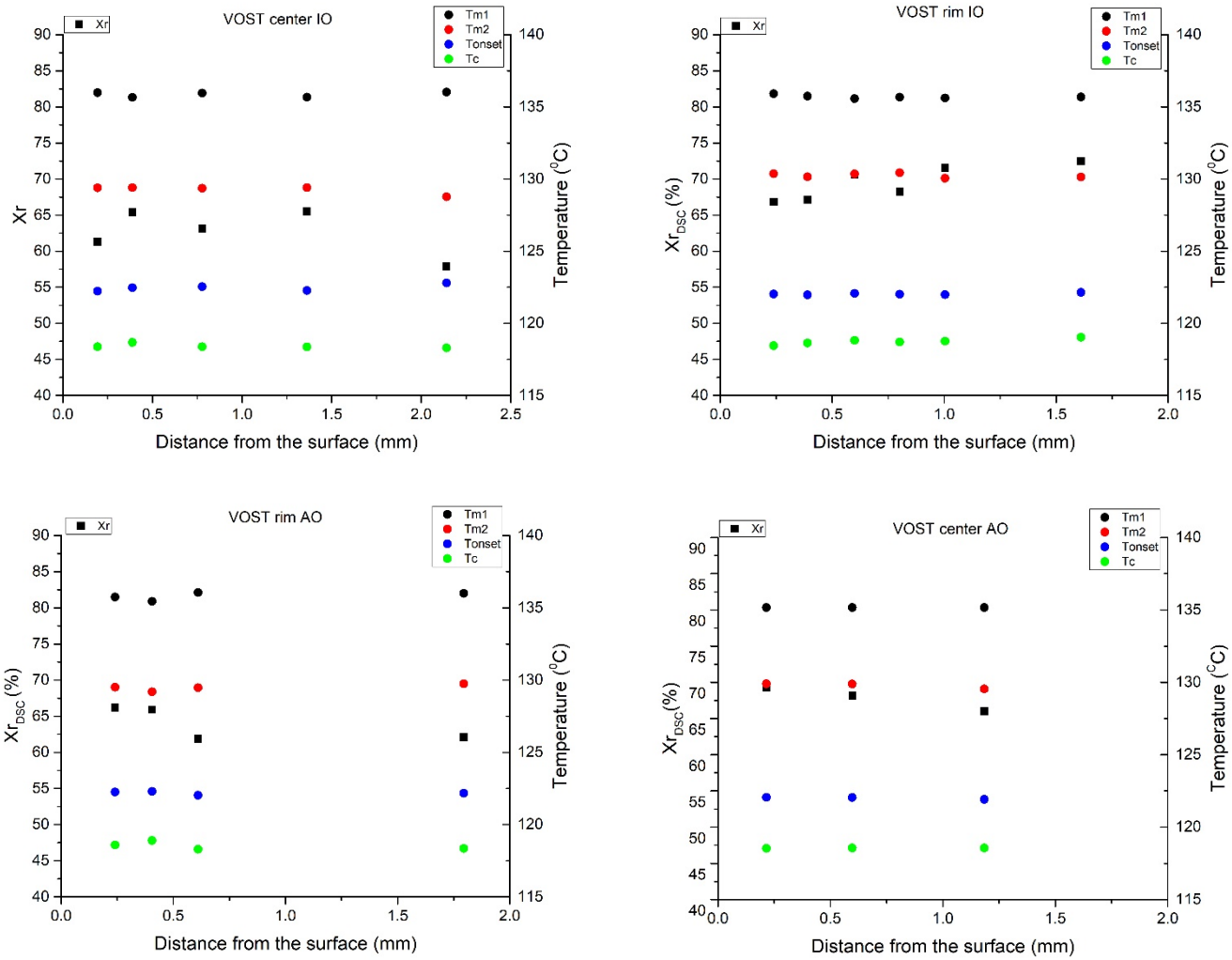

Figure E7. VOST degree of crystallinity and thermal data profile as a function of distance. T_{m1}: melting point in the first heating run (°C); T_{m2}: melting point for the second heating run (°C); T_c: crystallization temperature (°C); T_{onset}: onset crystallization temperature (°C)

Die approbierte gedruckte Originalversion dieser Dissertation ist an der TU Wien Bibliothek verfügbar.
The approved original version of this doctoral thesis is available in print at TU Wien Bibliothek.

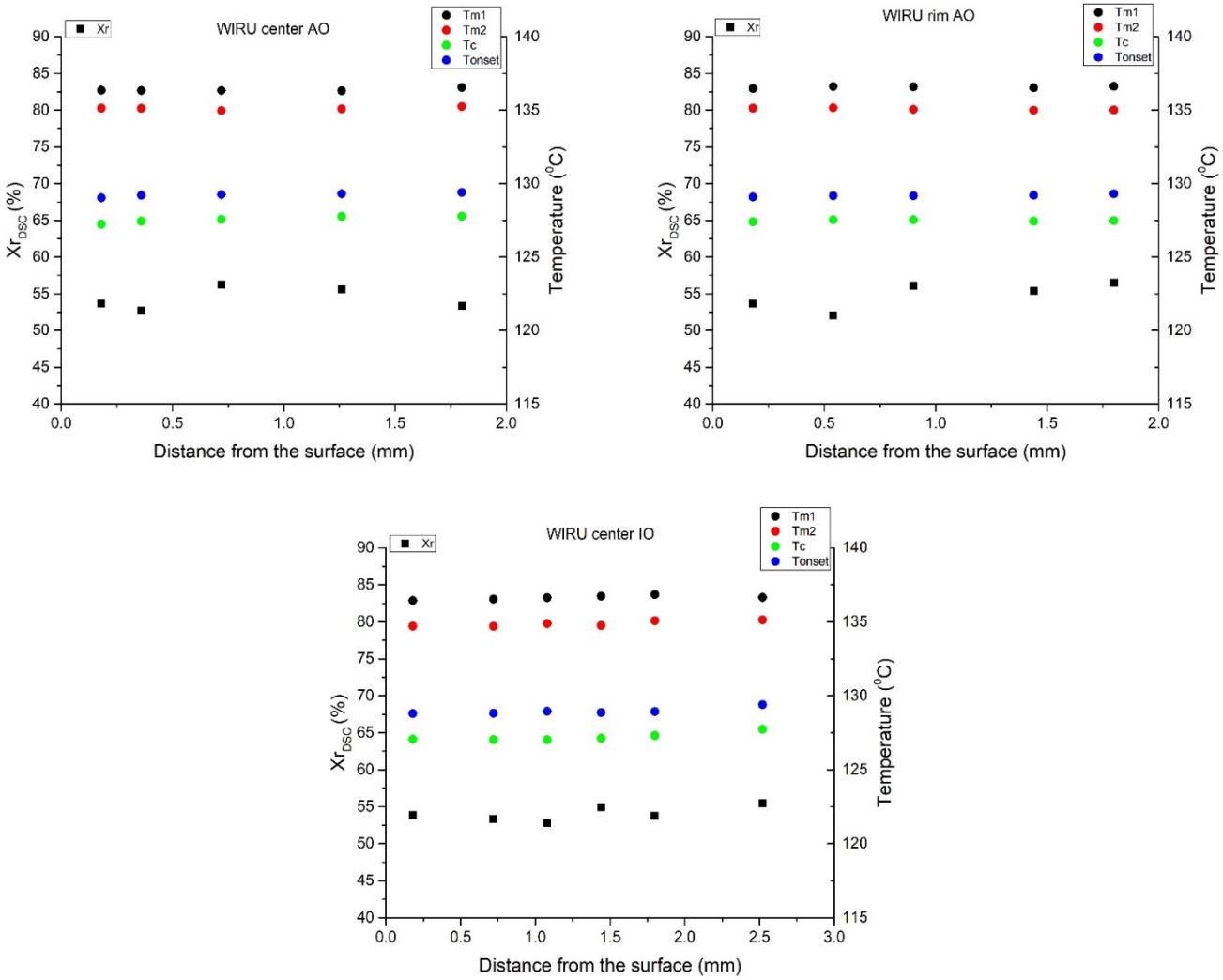

Figure E8. WIRU degree of crystallinity and thermal data profile as a function of distance. T_{m1}: melting point in the first heating run (°C); T_{m2}: melting point for the second heating run (°C); T_c: crystallization temperature (°C); T_{onset}: onset crystallization temperature (°C)

Die approbierte gedruckte Originalversion dieser Dissertation ist an der TU Wien Bibliothek verfügbar.
The approved original version of this doctoral thesis is available in print at TU Wien Bibliothek.

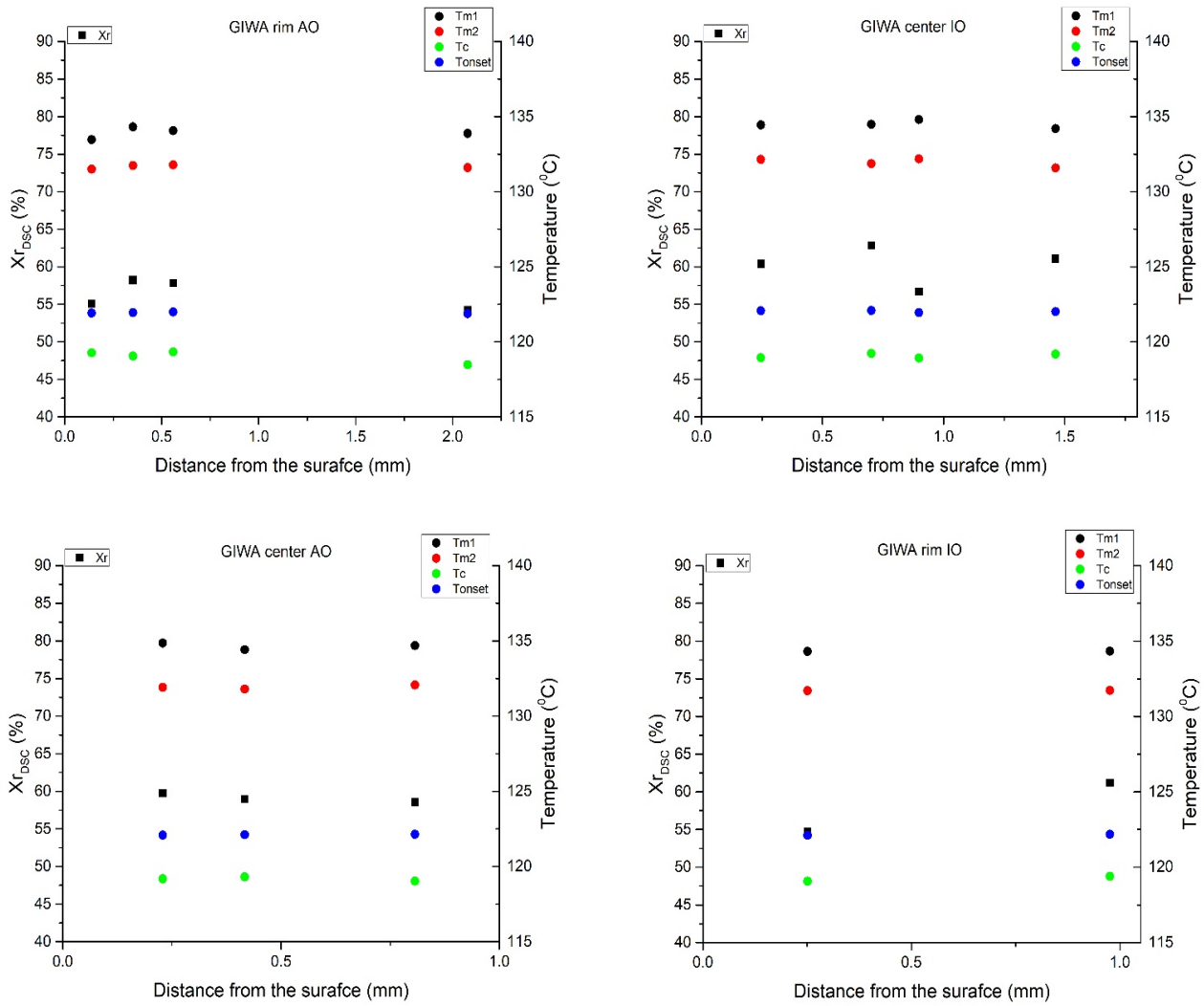

Figure E9. GIWA degree of crystallinity and thermal data profile as a function of distance. T_{m1}: melting point in the first heating run (°C); T_{m2}: melting point for the second heating run (°C); T_c: crystallization temperature (°C); T_{onset}: onset crystallization temperature (°C)

Die approbierte gedruckte Originalversion dieser Dissertation ist an der TU Wien Bibliothek verfügbar.
The approved original version of this doctoral thesis is available in print at TU Wien Bibliothek.

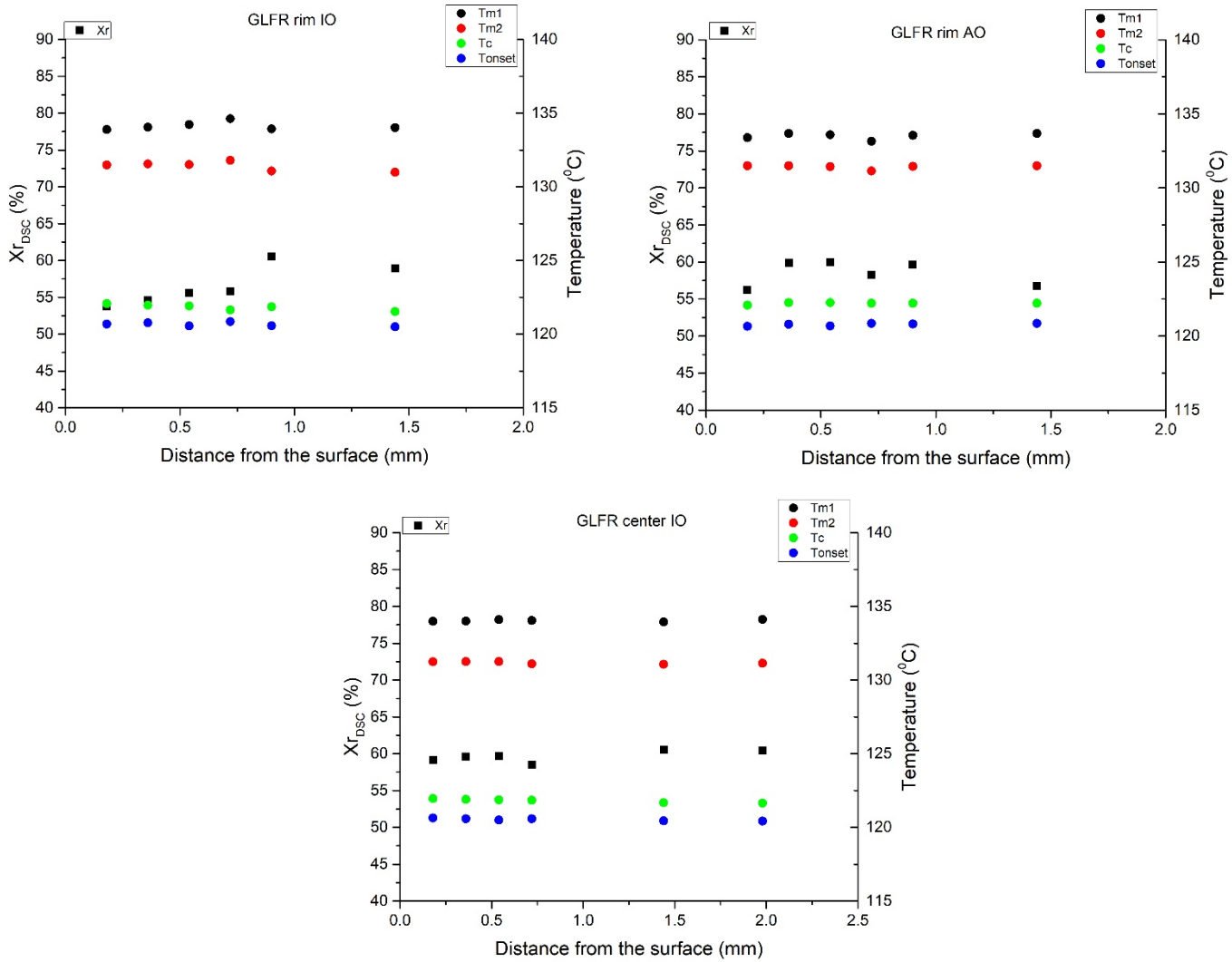

Figure E10. GLFR degree of crystallinity and thermal data profile as a function of distance. $T_{m1:}$ melting point in the first heating run (°C); $T_{m2:}$ melting point for the second heating run (°C); T_c: crystallization temperature (°C); T_{onset}: onset crystallization temperature (°C)

Die approbierte gedruckte Originalversion dieser Dissertation ist an der TU Wien Bibliothek verfügbar.
The approved original version of this doctoral thesis is available in print at TU Wien Bibliothek.

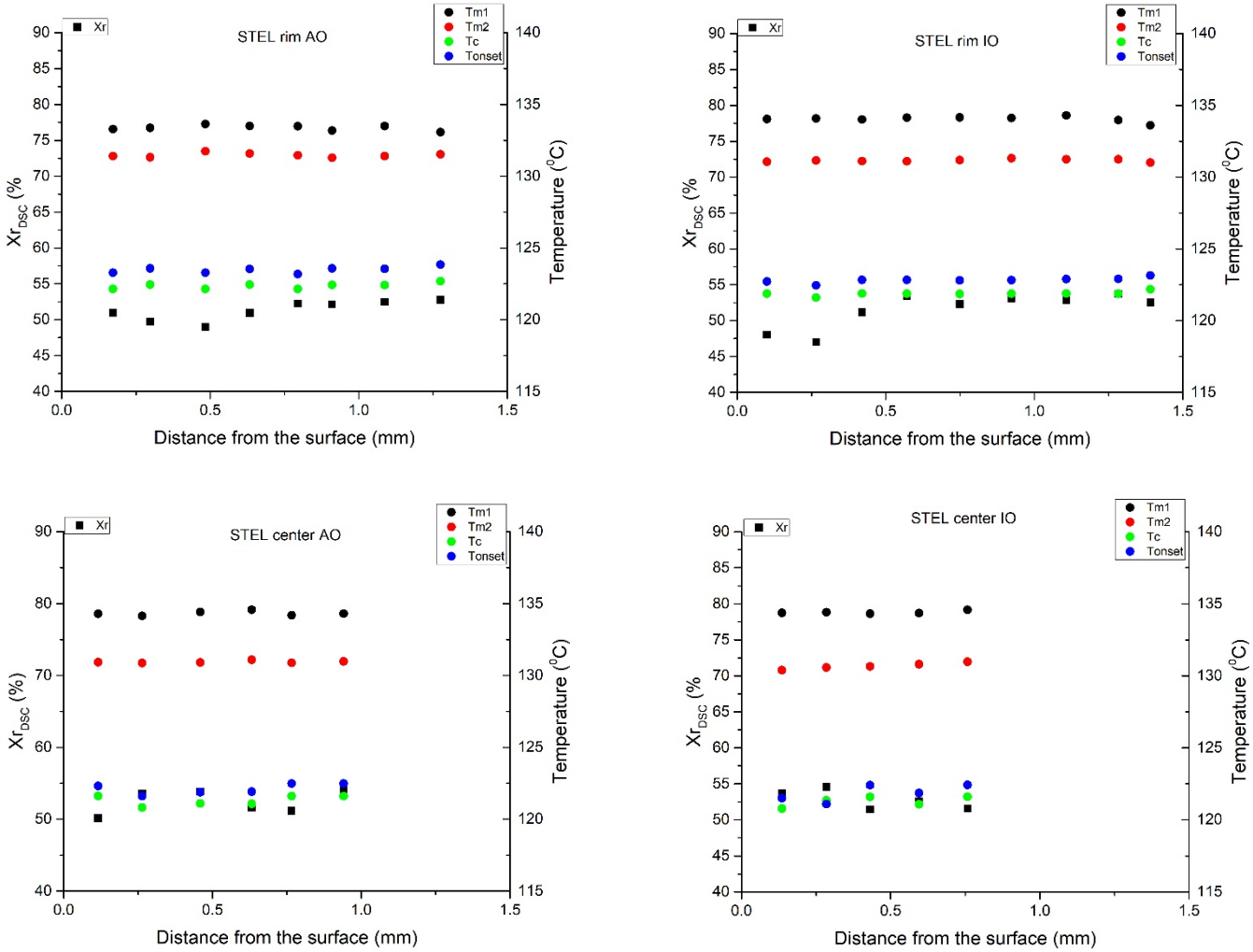

Figure E11. STEL degree of crystallinity and thermal data profile as a function of distance. T_{m1}: melting point in the first heating run (°C); T_{m2}: melting point for the second heating run (°C); T_c: crystallization temperature (°C); T_{onset}: onset crystallization temperature (°C)

Die approbierte gedruckte Originalversion dieser Dissertation ist an der TU Wien Bibliothek verfügbar.
The approved original version of this doctoral thesis is available in print at TU Wien Bibliothek.

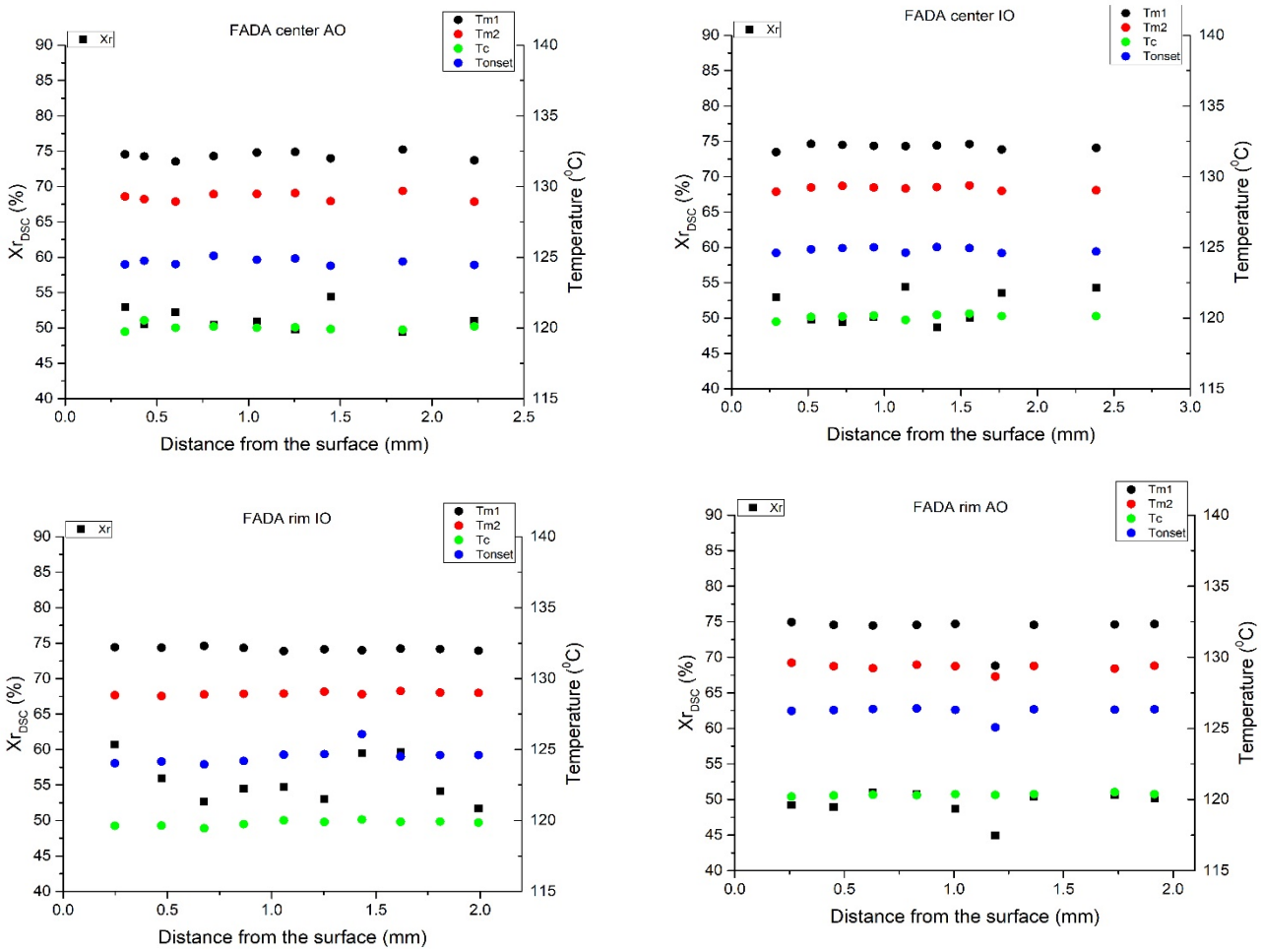

Figure E12. FADA degree of crystallinity and thermal data profile as a function of distance. $T_{m1:}$ melting point in the first heating run (ºC); $T_{m2:}$ melting point for the second heating run (ºC); T_c: crystallization temperature (ºC); T_{onset}: onset crystallization temperature (ºC)

Die approbierte gedruckte Originalversion dieser Dissertation ist an der TU Wien Bibliothek verfügbar.
The approved original version of this doctoral thesis is available in print at TU Wien Bibliothek.

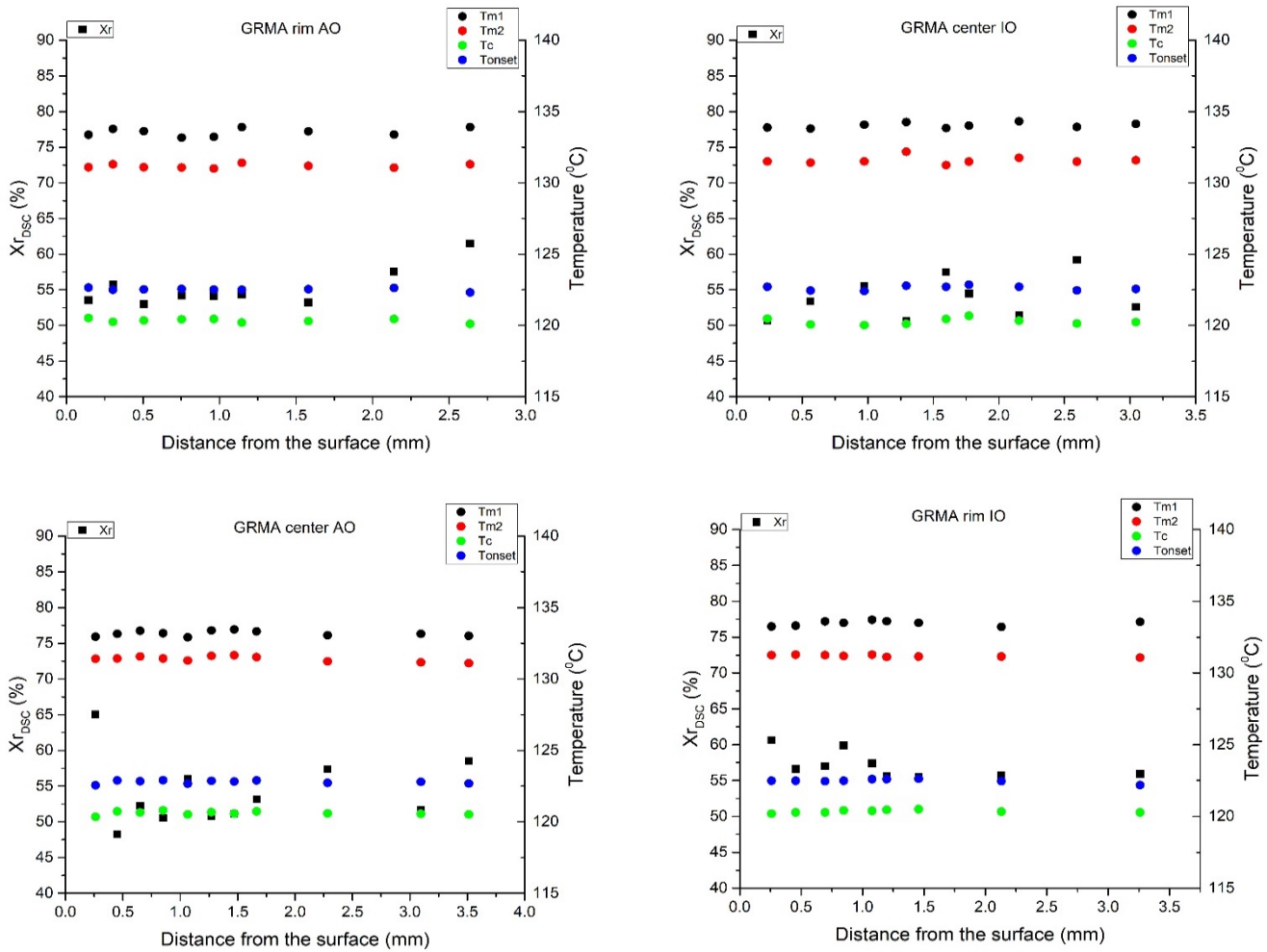

Figure E13. GRMA degree of crystallinity and thermal data profile as a function of distance. $T_{m1:}$ melting point in the first heating run (°C); $T_{m2:}$ melting point for the second heating run (°C); T_c: crystallization temperature (°C); T_{onset}: onset crystallization temperature (°C)

Die approbierte gedruckte Originalversion dieser Dissertation ist an der TU Wien Bibliothek verfügbar.
The approved original version of this doctoral thesis is available in print at TU Wien Bibliothek.

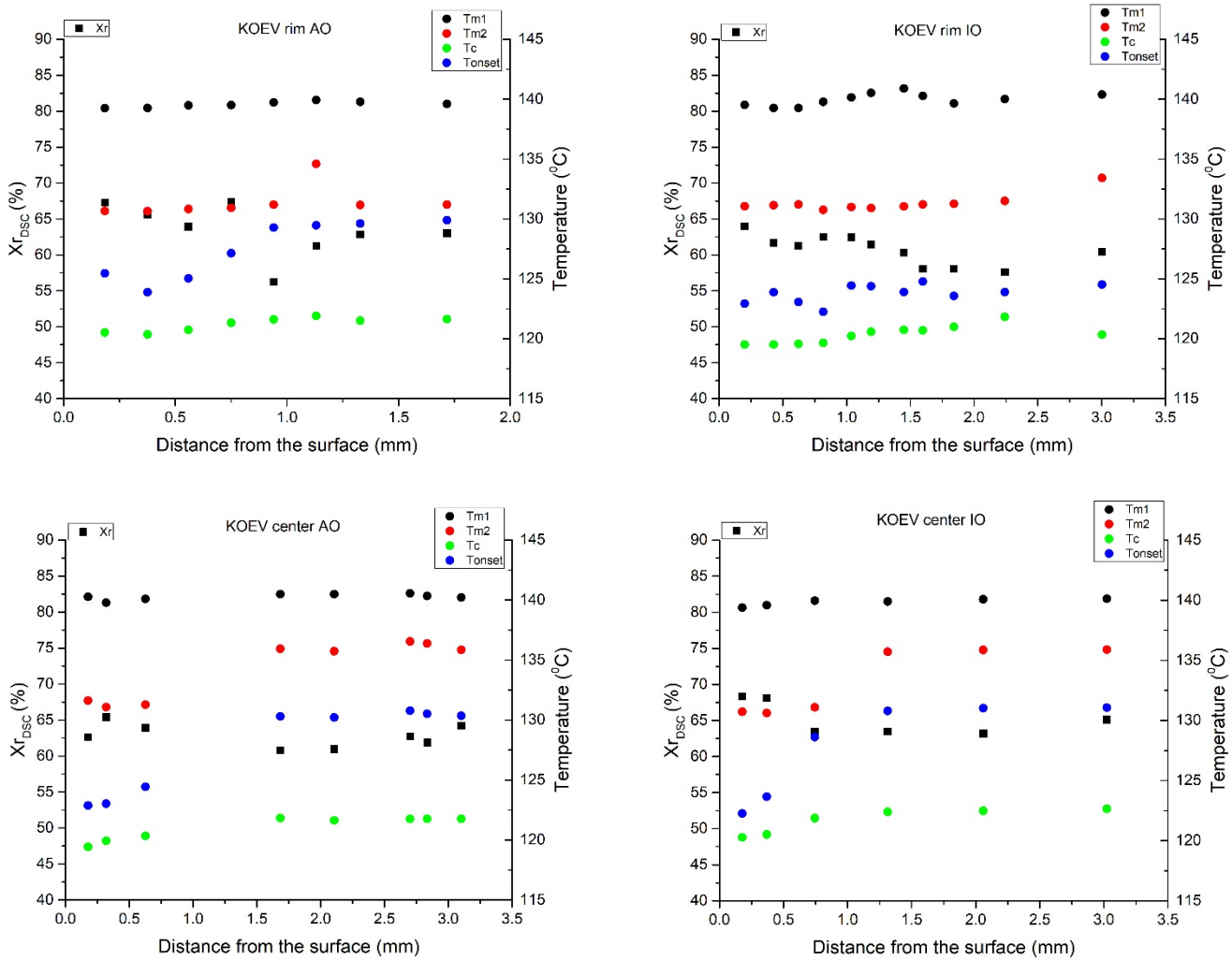

Figure E14. KOEV degree of crystallinity and thermal data profile as a function of distance. $T_{m1:}$ melting point in the first heating run (°C); $T_{m2:}$ melting point for the second heating run (°C); T_c: crystallization temperature (°C); T_{onset}: onset crystallization temperature (°C)

Die approbierte gedruckte Originalversion dieser Dissertation ist an der TU Wien Bibliothek verfügbar.
The approved original version of this doctoral thesis is available in print at TU Wien Bibliothek.

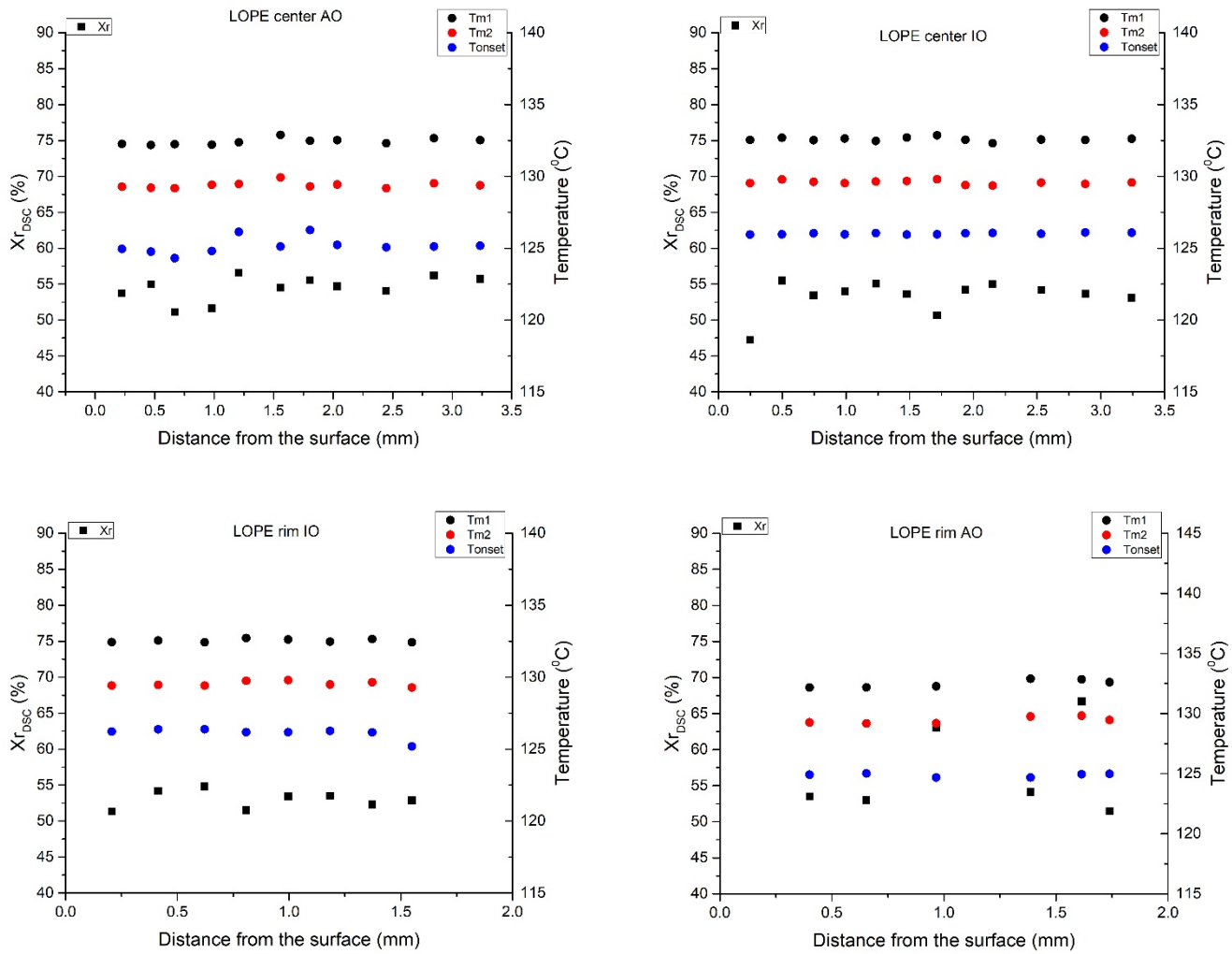

Figure E15. LOPE degree of crystallinity and thermal data profile as a function of distance. T_{m1}: melting point in the first heating run (°C); T_{m2}: melting point for the second heating run (°C); T_c: crystallization temperature (°C); T_{onset}: onset crystallization temperature (°C)

Die approbierte gedruckte Originalversion dieser Dissertation ist an der TU Wien Bibliothek verfügbar.
The approved original version of this doctoral thesis is available in print at TU Wien Bibliothek.

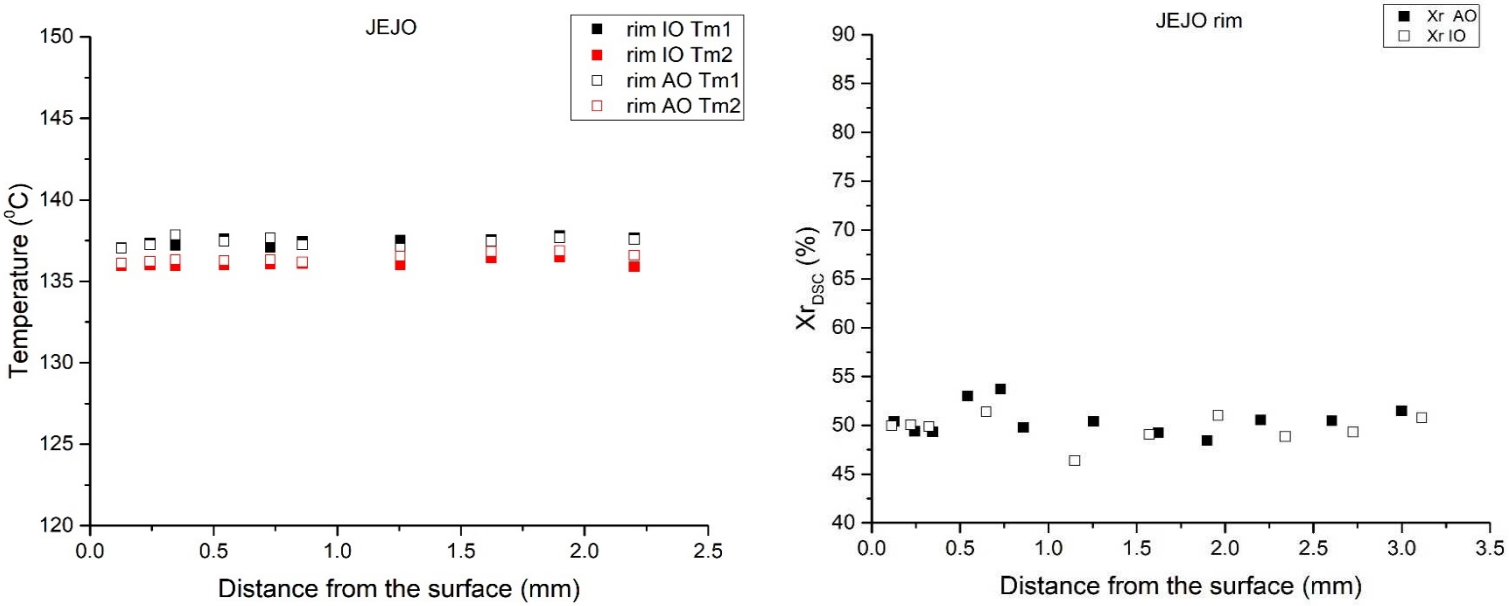

Figure E16. JEJO degree of crystallinity and thermal data profile as a function of distance. $T_{m1:}$ melting point in the first heating run (ºC); $T_{m2:}$ melting point for the second heating run (ºC);

Die approbierte gedruckte Originalversion dieser Dissertation ist an der TU Wien Bibliothek verfügbar.
The approved original version of this doctoral thesis is available in print at TU Wien Bibliothek.

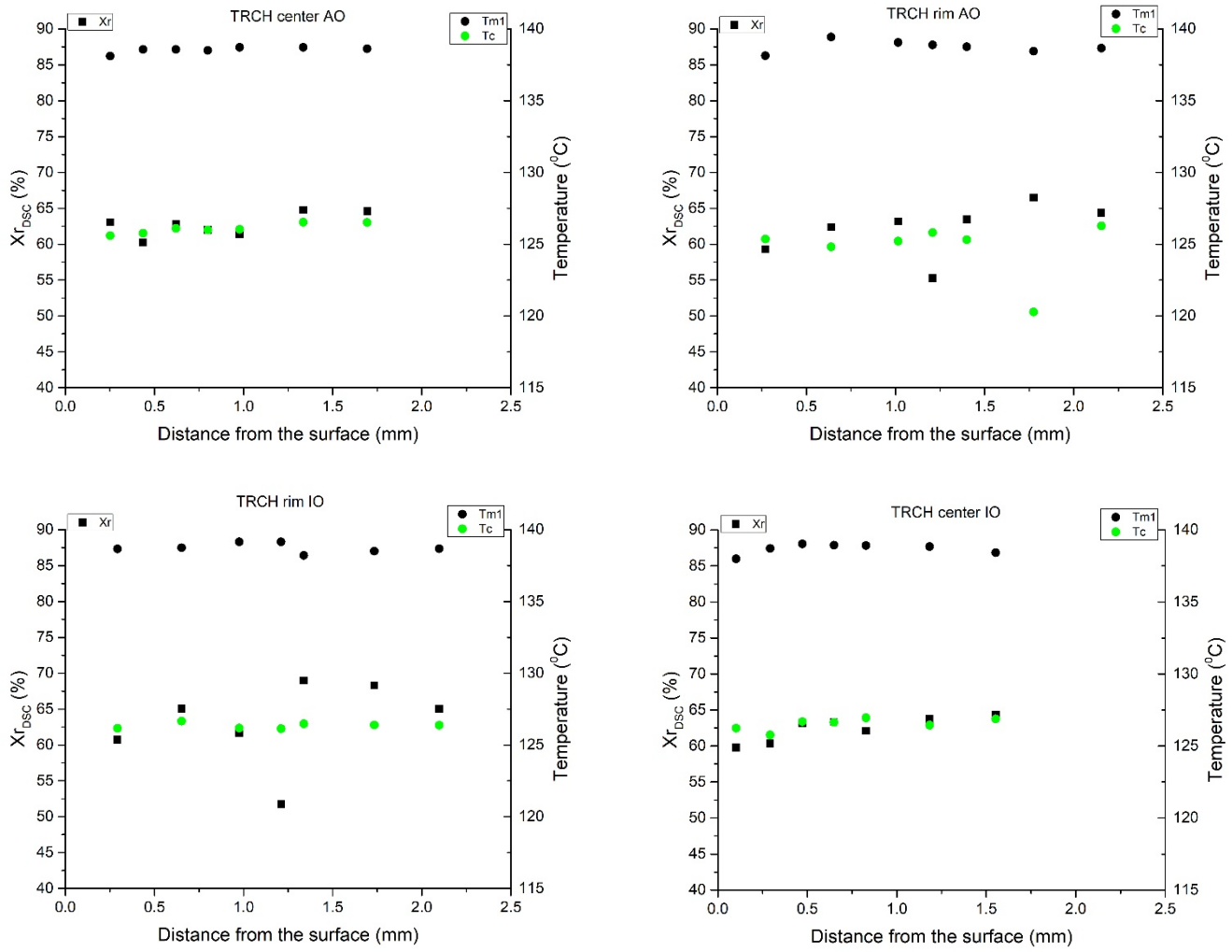

Figure E17. TRCH degree of crystallinity and thermal data profile as a function of distance. $T_{m1:}$ melting point in the first heating run (°C); $T_{m2:}$ melting point for the second heating run (°C); T_c: crystallization temperature (°C); T_{onset}: onset crystallization temperature (°C)

Die approbierte gedruckte Originalversion dieser Dissertation ist an der TU Wien Bibliothek verfügbar.
The approved original version of this doctoral thesis is available in print at TU Wien Bibliothek.

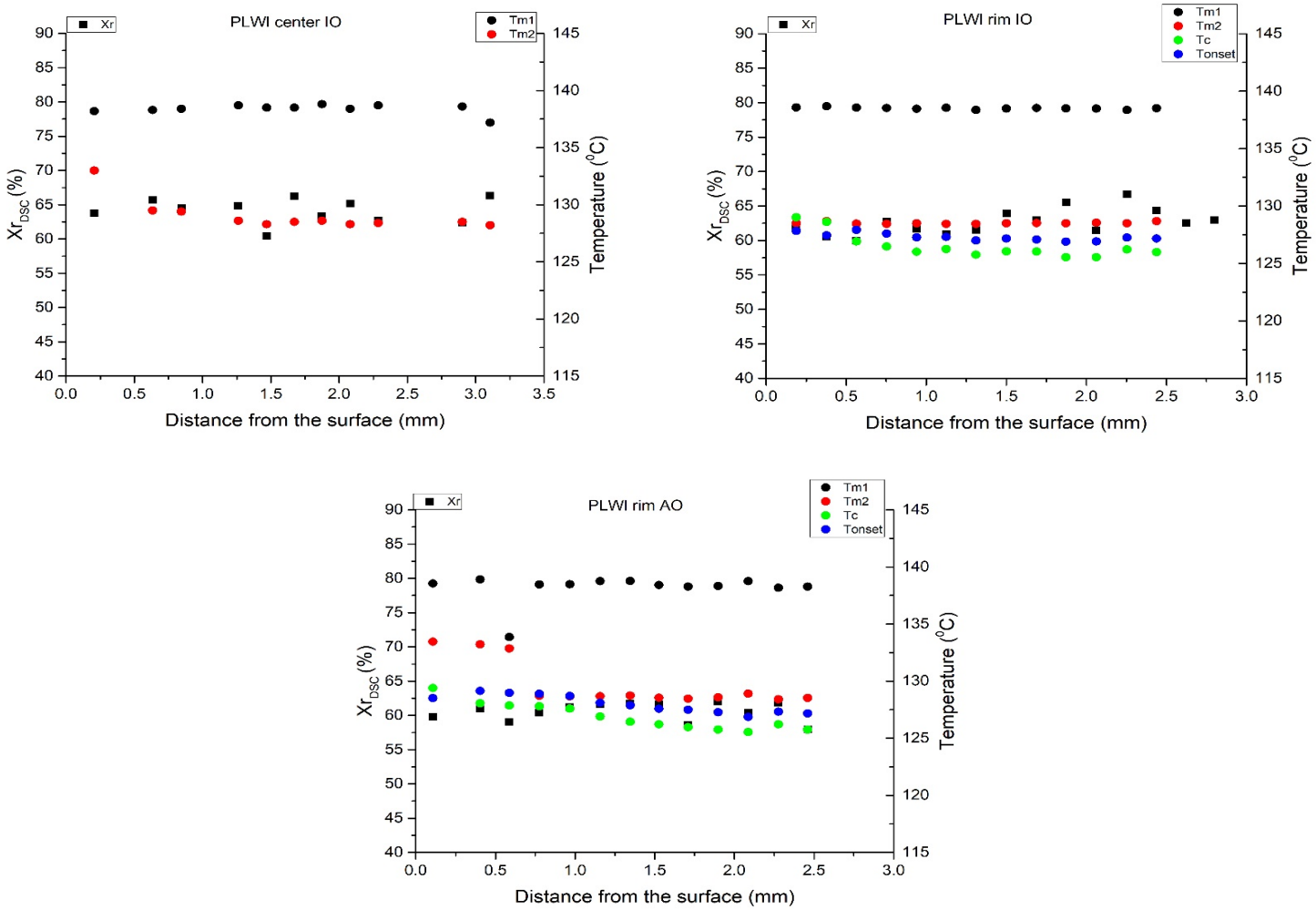

Figure E18. PLWI degree of crystallinity and thermal data profile as a function of distance. T_{m1}: melting point in the first heating run (°C); T_{m2}: melting point for the second heating run (°C); T_c: crystallization temperature (°C); T_{onset}: onset crystallization temperature (°C)

Die approbierte gedruckte Originalversion dieser Dissertation ist an der TU Wien Bibliothek verfügbar.
The approved original version of this doctoral thesis is available in print at TU Wien Bibliothek.

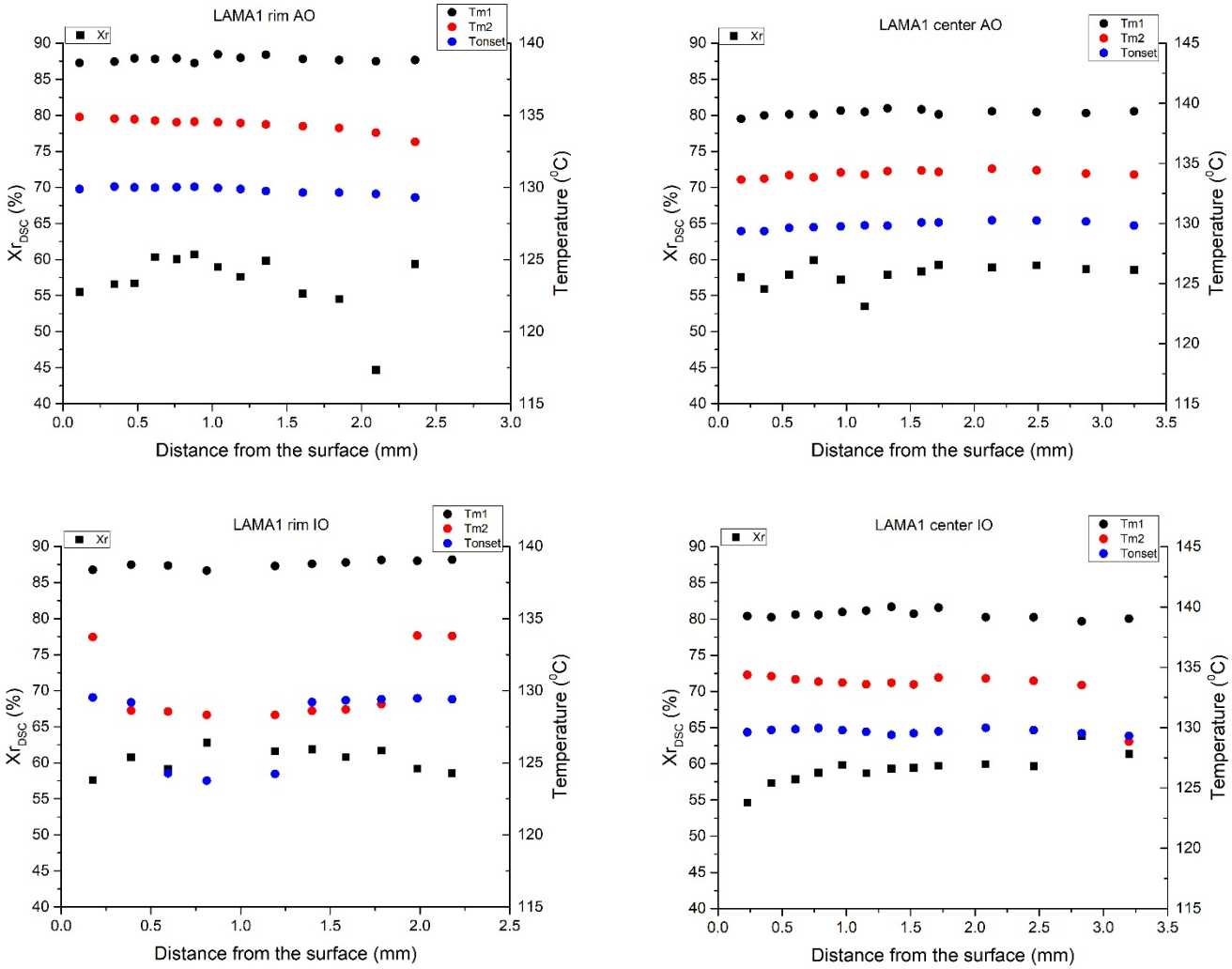

Figure E19. LAMA1 degree of crystallinity and thermal data profile as a function of distance. $T_{m1:}$ melting point in the first heating run (ºC); $T_{m2:}$ melting point for the second heating run (ºC); T_c: crystallization temperature (ºC); T_{onset}: onset crystallization temperature (ºC)

Die approbierte gedruckte Originalversion dieser Dissertation ist an der TU Wien Bibliothek verfügbar.
The approved original version of this doctoral thesis is available in print at TU Wien Bibliothek.

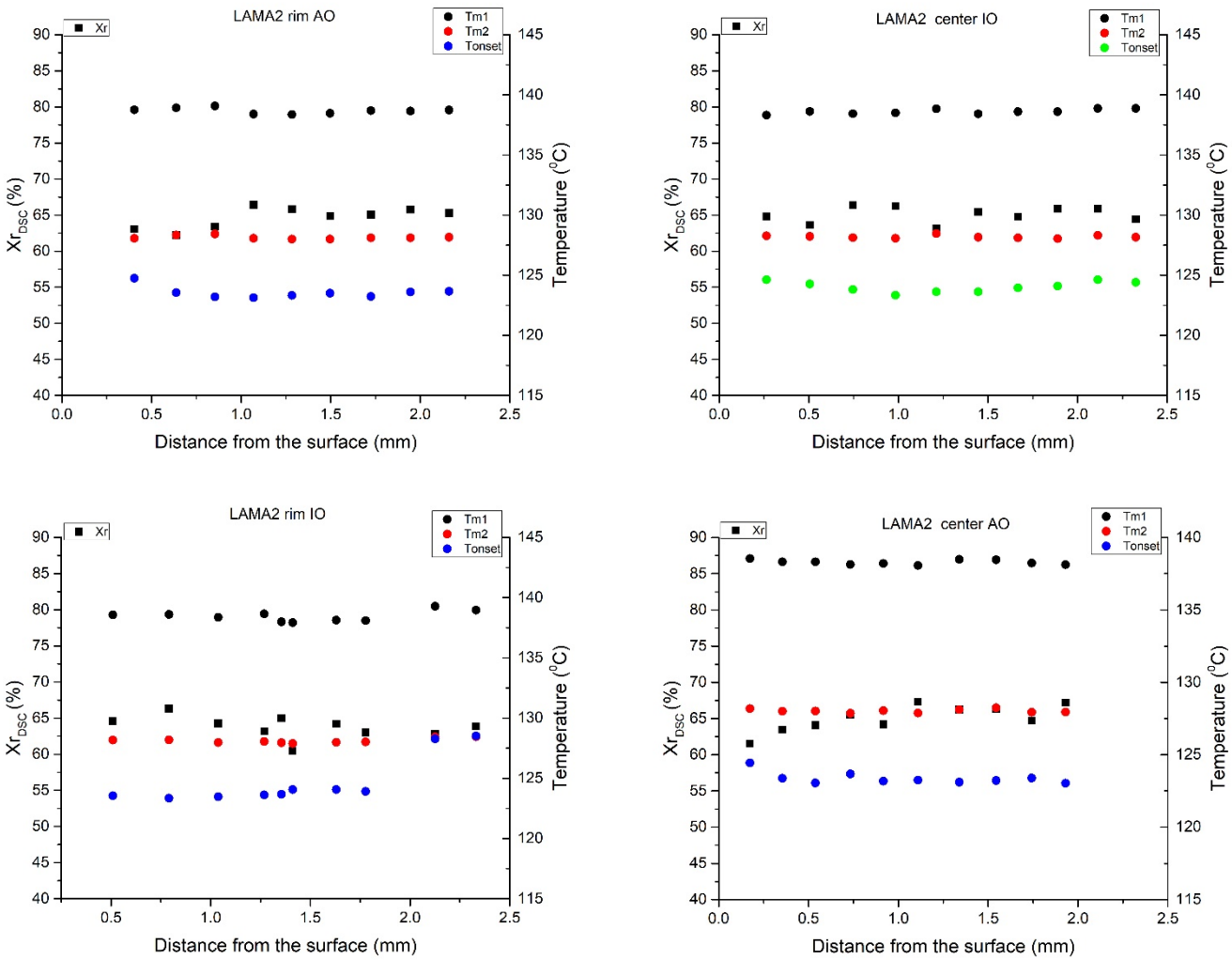

Figure E20. LAMA2 degree of crystallinity and thermal data profile as a function of distance. T_{m1}: melting point in the first heating run (°C); T_{m2}: melting point for the second heating run (°C); T_c: crystallization temperature (°C); T_{onset}: onset crystallization temperature (°C)

Die approbierte gedruckte Originalversion dieser Dissertation ist an der TU Wien Bibliothek verfügbar.
The approved original version of this doctoral thesis is available in print at TU Wien Bibliothek.

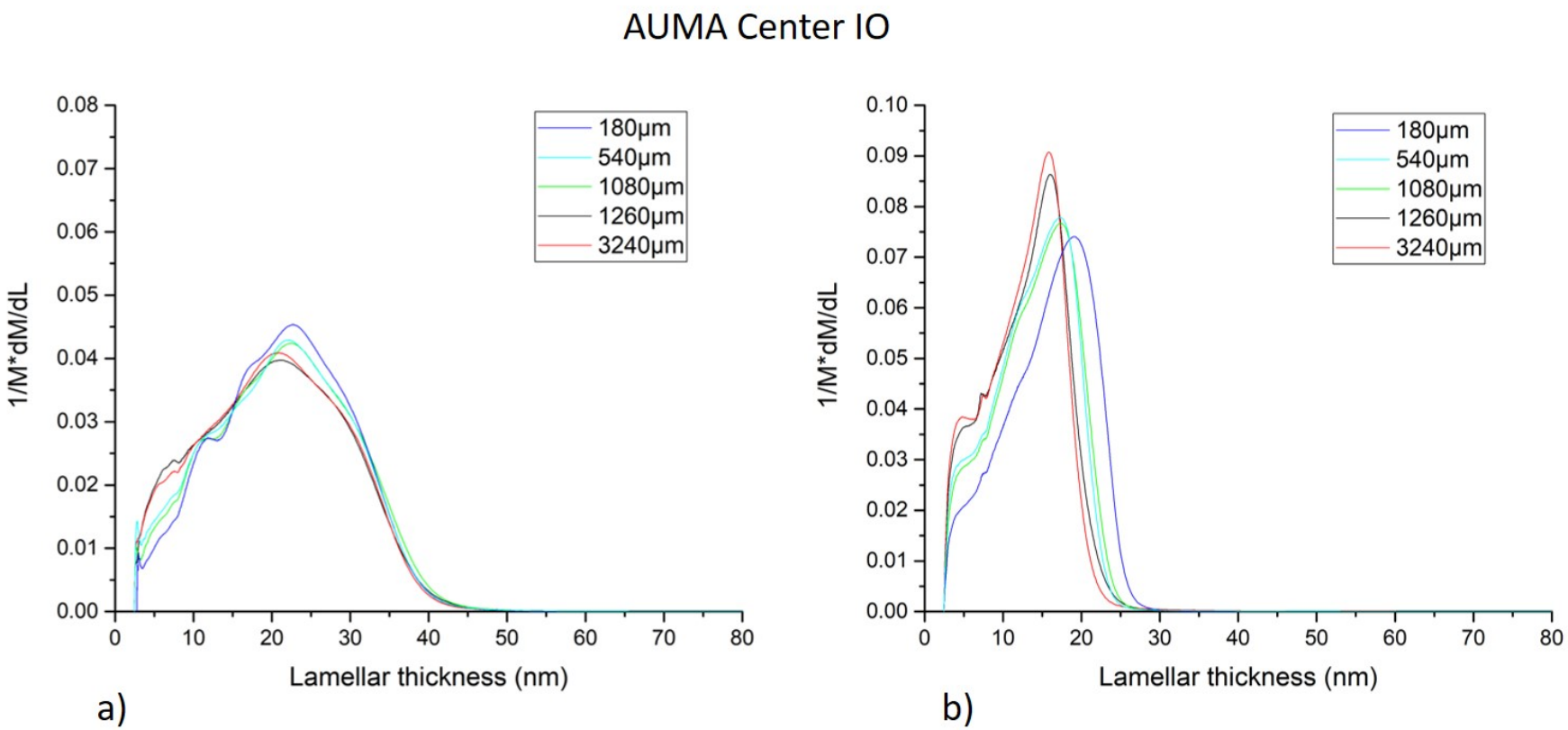

Figure E21. Lamellar thickness distribution (LTD) for AUMA center IO as a function of depth; a) LTD calculated from the first heating run. b) LTD calculated from the second heating run

Die approbierte gedruckte Originalversion dieser Dissertation ist an der TU Wien Bibliothek verfügbar.
The approved original version of this doctoral thesis is available in print at TU Wien Bibliothek.

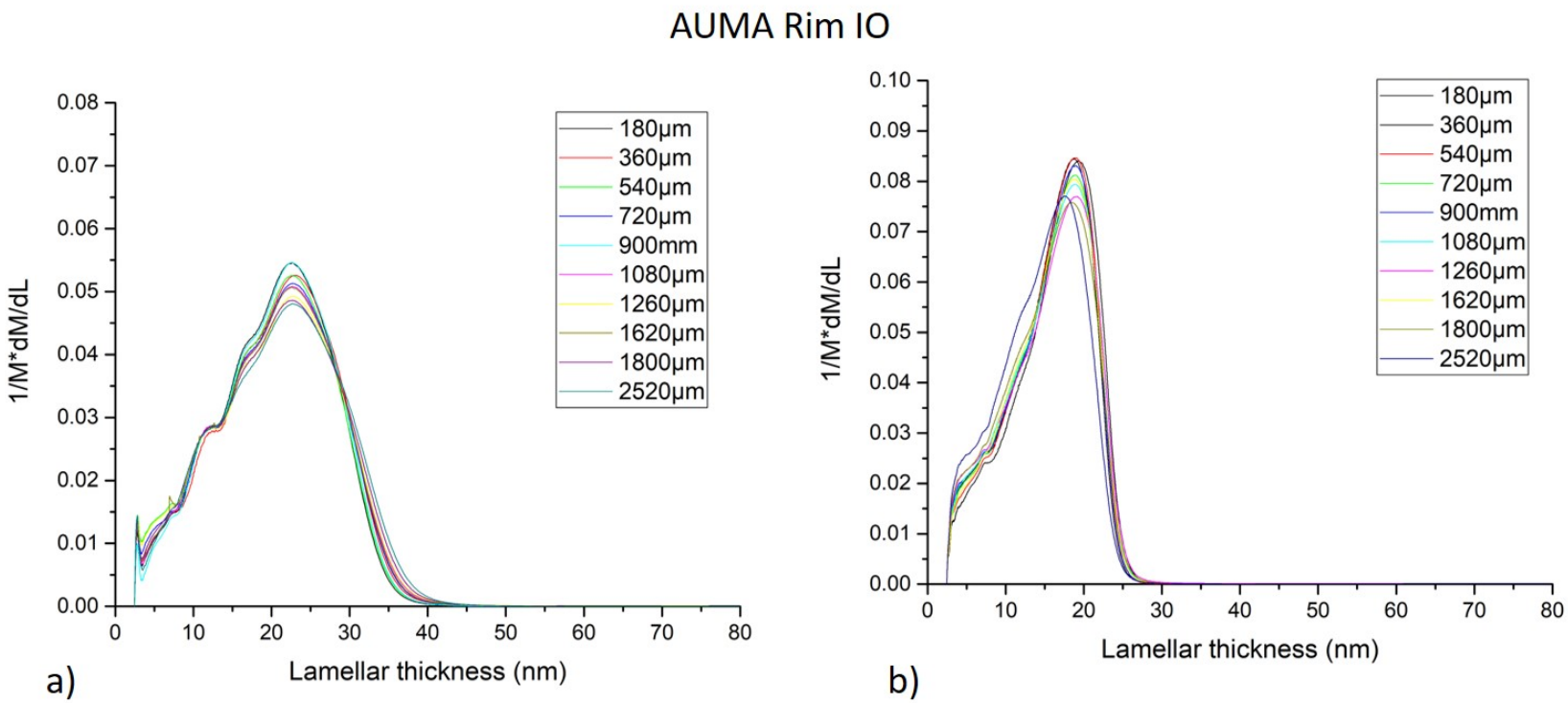

Figure E22. Lamellar thickness distribution (LTD) for AUMA rim IO as a function of depth; a) LTD calculated from the first heating run. b) LTD calculated from the second heating run

Die approbierte gedruckte Originalversion dieser Dissertation ist an der TU Wien Bibliothek verfügbar.
The approved original version of this doctoral thesis is available in print at TU Wien Bibliothek.

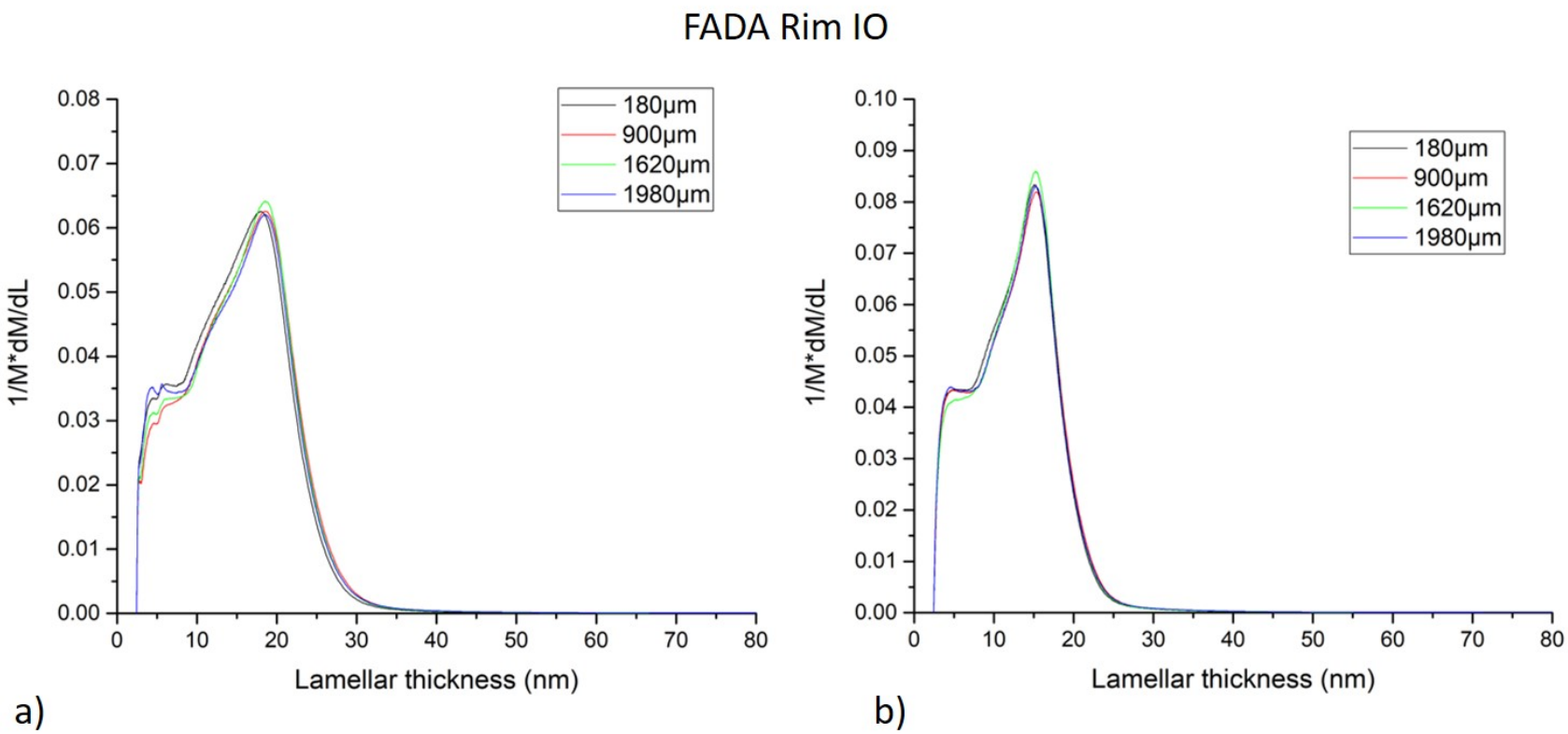

Figure E23. Lamellar thickness distribution (LTD) for FADA rim IO as a function of depth; a) LTD calculated from the first heating run. b) LTD calculated from the second heating run

Die approbierte gedruckte Originalversion dieser Dissertation ist an der TU Wien Bibliothek verfügbar.
The approved original version of this doctoral thesis is available in print at TU Wien Bibliothek.

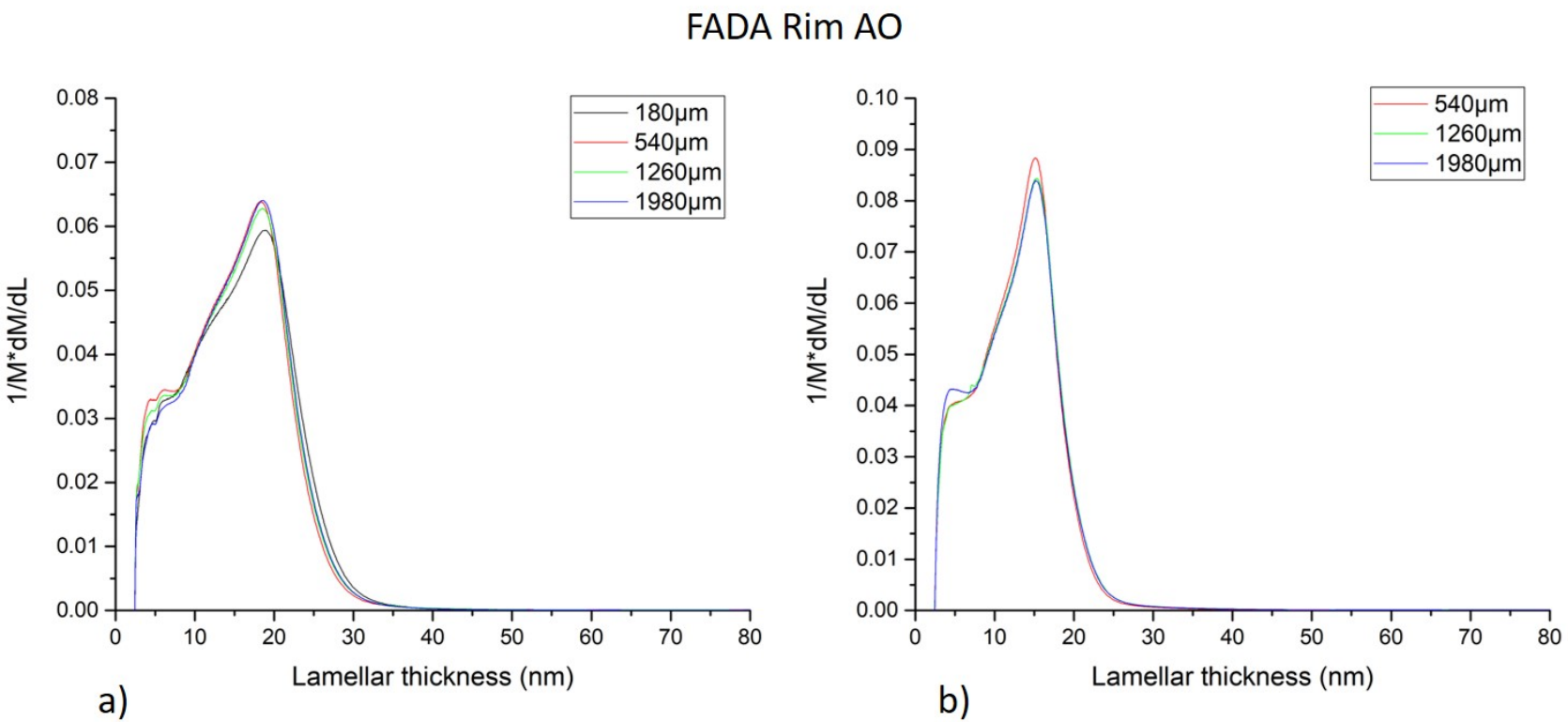

Figure E24. Lamellar thickness distribution (LTD) for FADA rim AO as a function of depth; a) LTD calculated from the first heating ru00n. b) LTD calculated from the second heating run

Die approbierte gedruckte Originalversion dieser Dissertation ist an der TU Wien Bibliothek verfügbar.
The approved original version of this doctoral thesis is available in print at TU Wien Bibliothek.

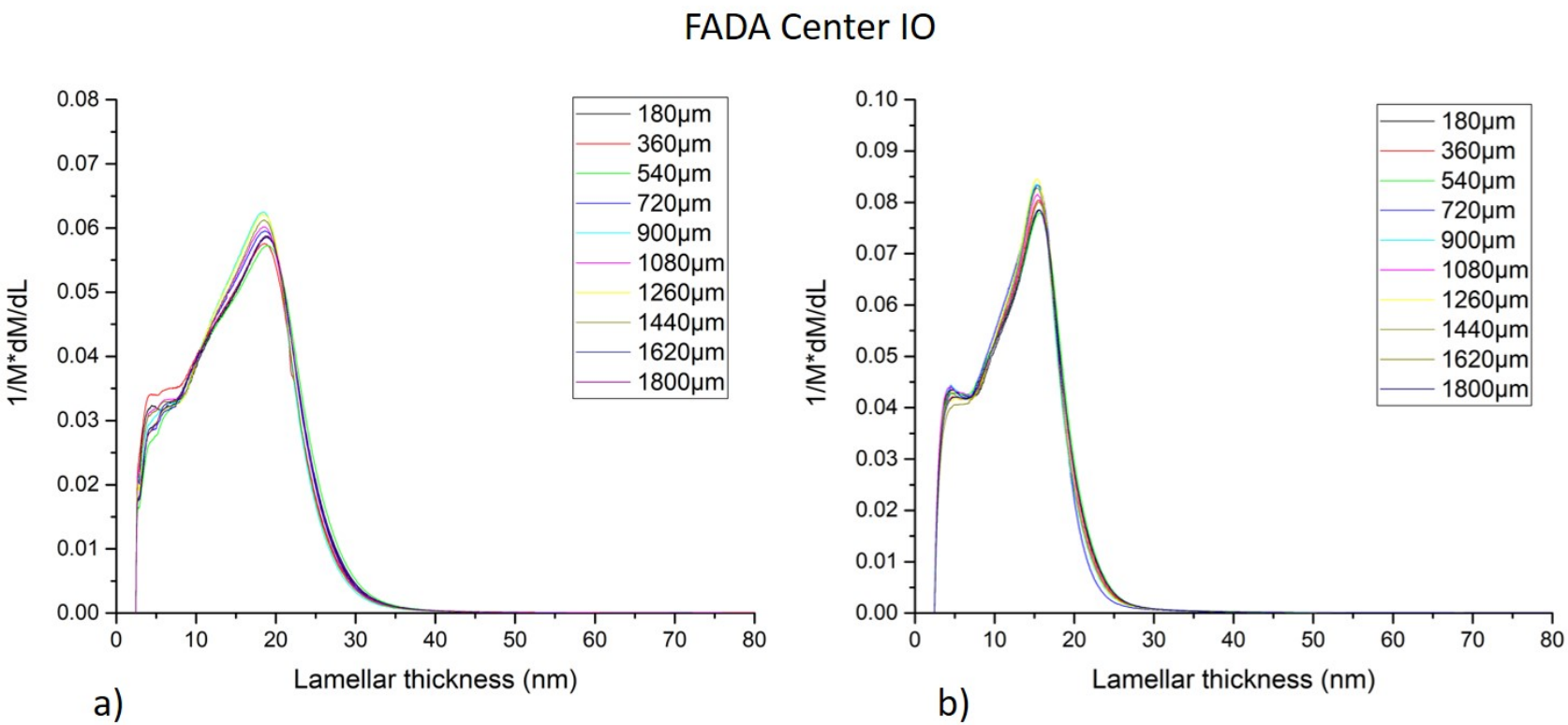

Figure E25. Lamellar thickness distribution (LTD) for FADA center IO as a function of depth; a) LTD calculated from the first heating run. b) LTD calculated from the second heating run

Die approbierte gedruckte Originalversion dieser Dissertation ist an der TU Wien Bibliothek verfügbar.
The approved original version of this doctoral thesis is available in print at TU Wien Bibliothek.

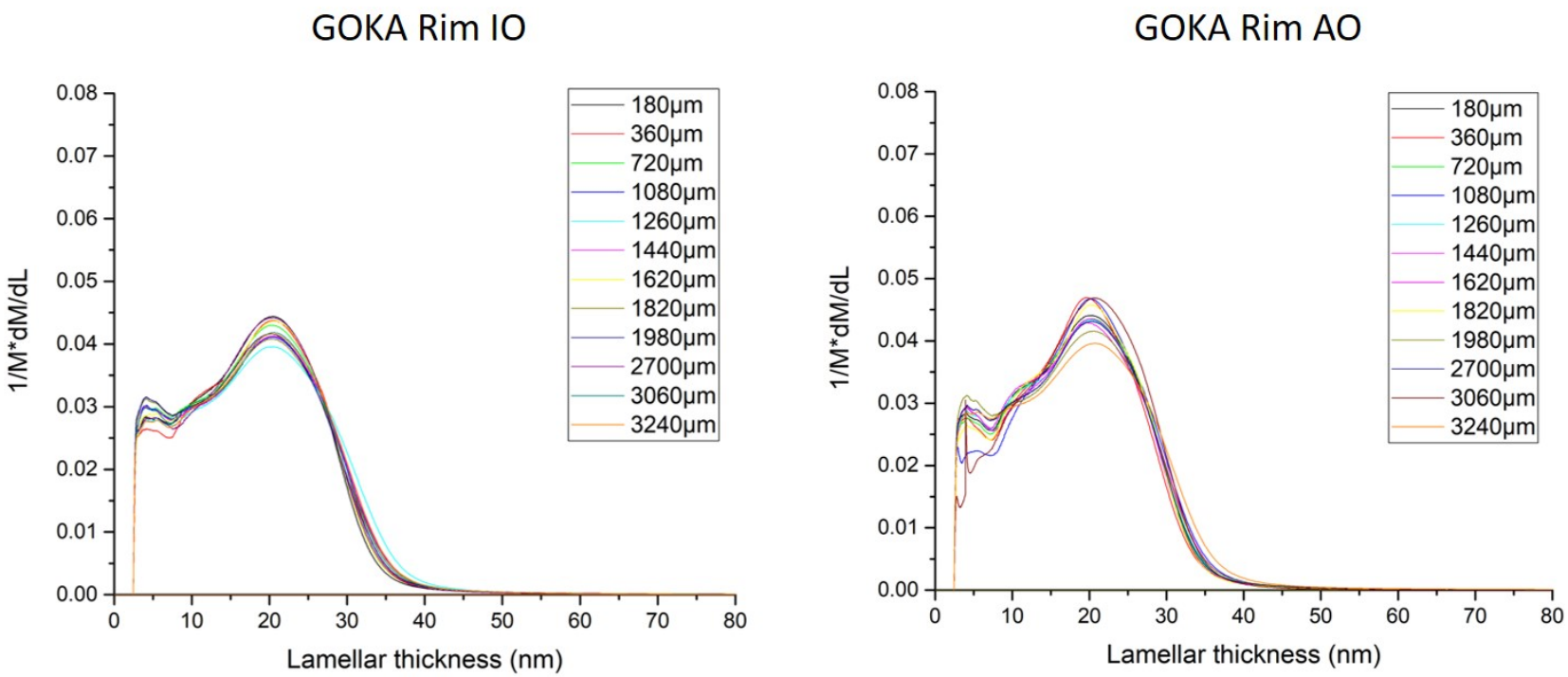

Figure E26. Lamellar thickness distribution (LTD) for GOKA rim IO and rim AO as a function of depth (LTD calculated from the first heating run)

Die approbierte gedruckte Originalversion dieser Dissertation ist an der TU Wien Bibliothek verfügbar.
The approved original version of this doctoral thesis is available in print at TU Wien Bibliothek.

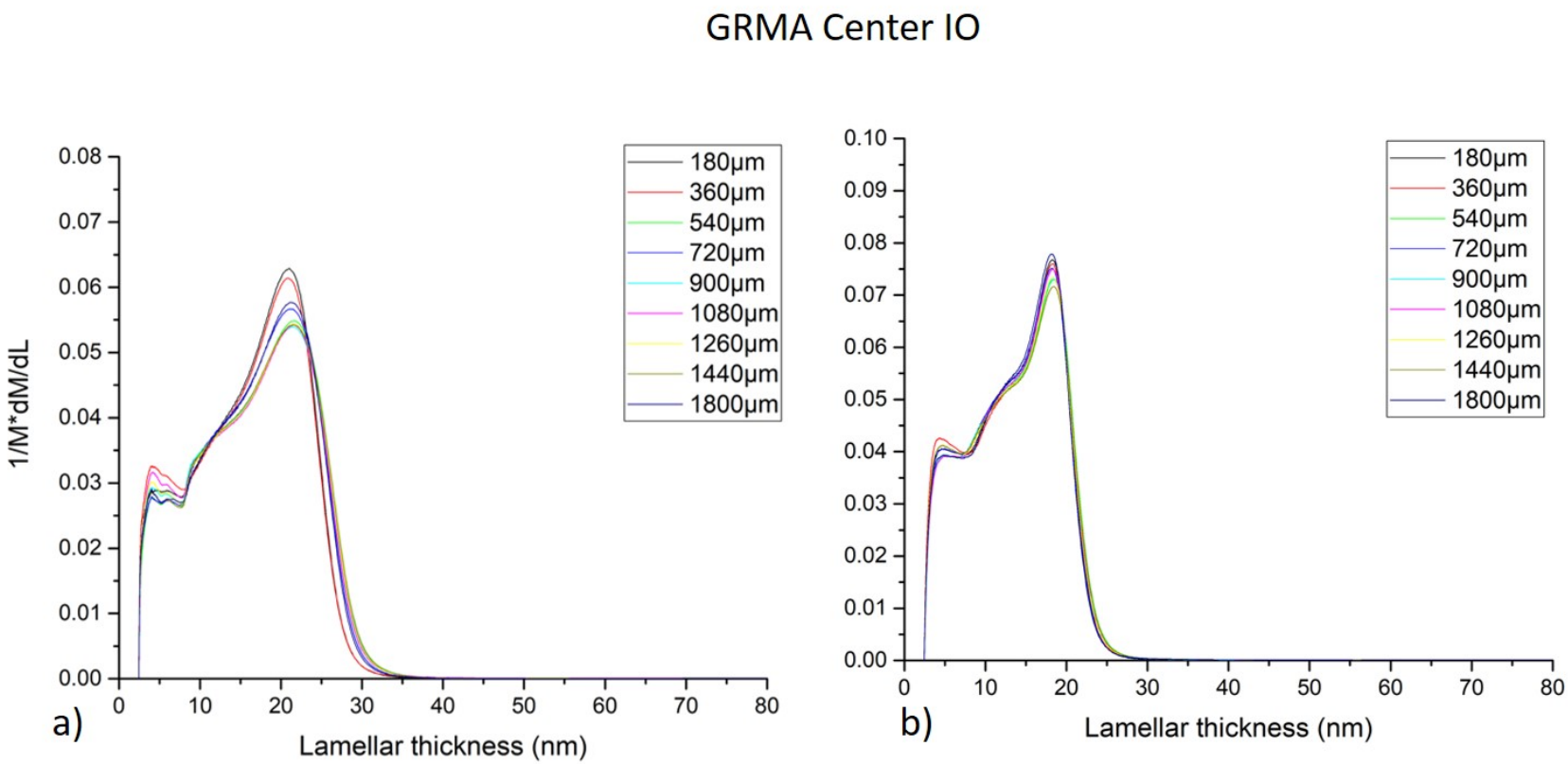

Figure E27. Lamellar thickness distribution (LTD) for GRMA center IO as a function of depth; a) LTD calculated from the first heating run. b) LTD calculated from the second heating run

Die approbierte gedruckte Originalversion dieser Dissertation ist an der TU Wien Bibliothek verfügbar.
The approved original version of this doctoral thesis is available in print at TU Wien Bibliothek.

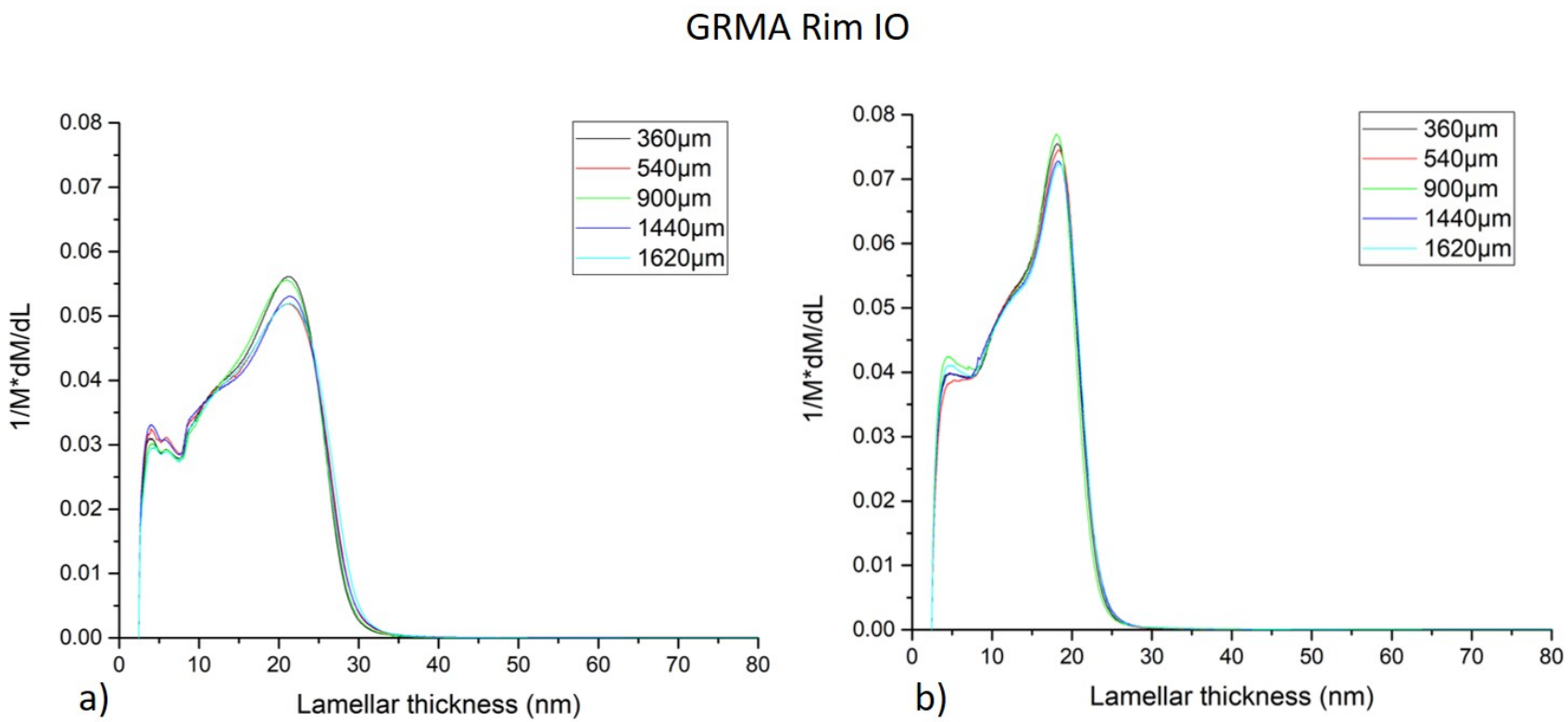

Figure E28. Lamellar thickness distribution (LTD) for GRMA rim IO as a function of depth; a) LTD calculated from the first heating run. b) LTD calculated from the second heating run

Die approbierte gedruckte Originalversion dieser Dissertation ist an der TU Wien Bibliothek verfügbar.
The approved original version of this doctoral thesis is available in print at TU Wien Bibliothek.

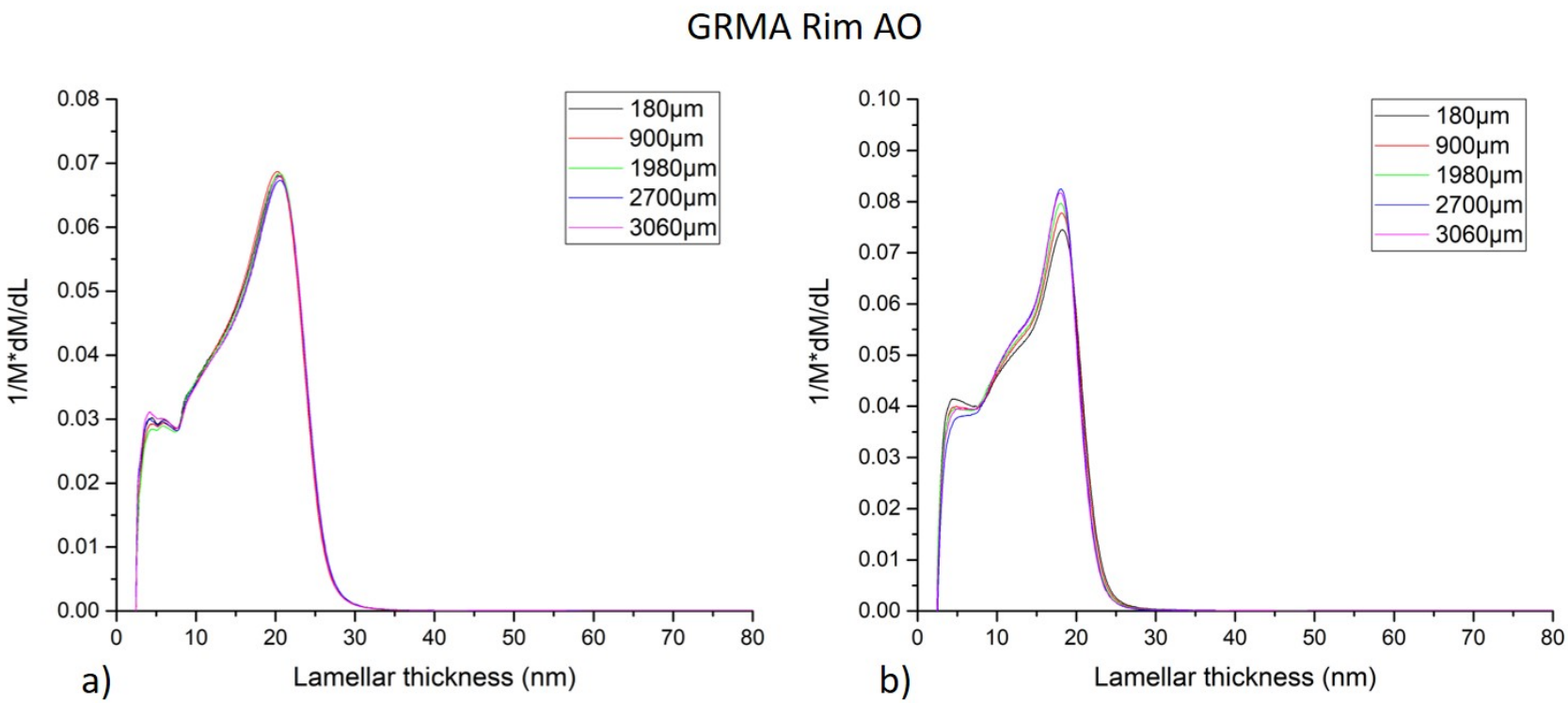

Figure E29. Lamellar thickness distribution (LTD) for GRMA rim AO as a function of depth; a) LTD calculated from the first heating run. b) LTD calculated from the second heating run

Die approbierte gedruckte Originalversion dieser Dissertation ist an der TU Wien Bibliothek verfügbar.
The approved original version of this doctoral thesis is available in print at TU Wien Bibliothek.

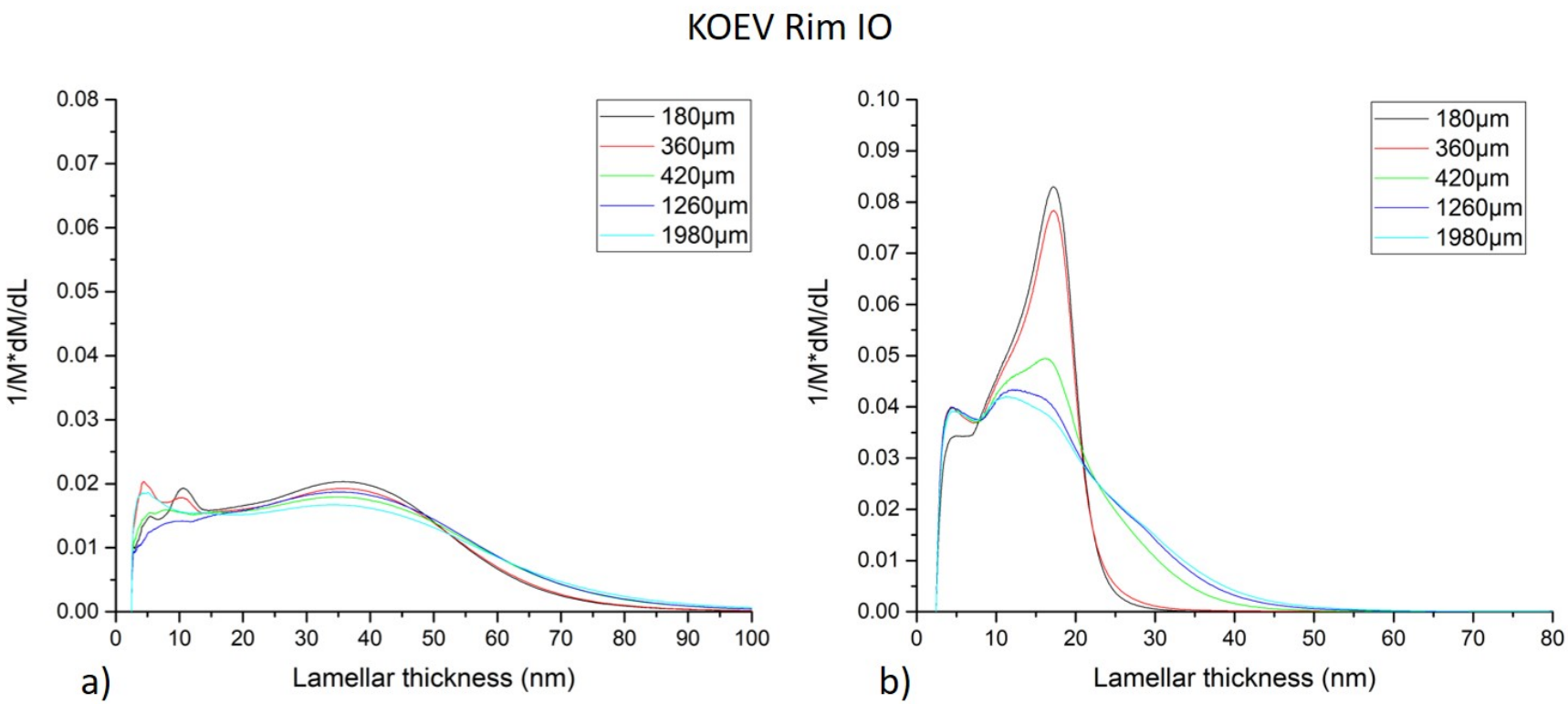

Figure E30. Lamellar thickness distribution (LTD) for KOEV rim IO as a function of depth; a) LTD calculated from the first heating run. b) LTD calculated from the second heating run

Die approbierte gedruckte Originalversion dieser Dissertation ist an der TU Wien Bibliothek verfügbar.
The approved original version of this doctoral thesis is available in print at TU Wien Bibliothek.

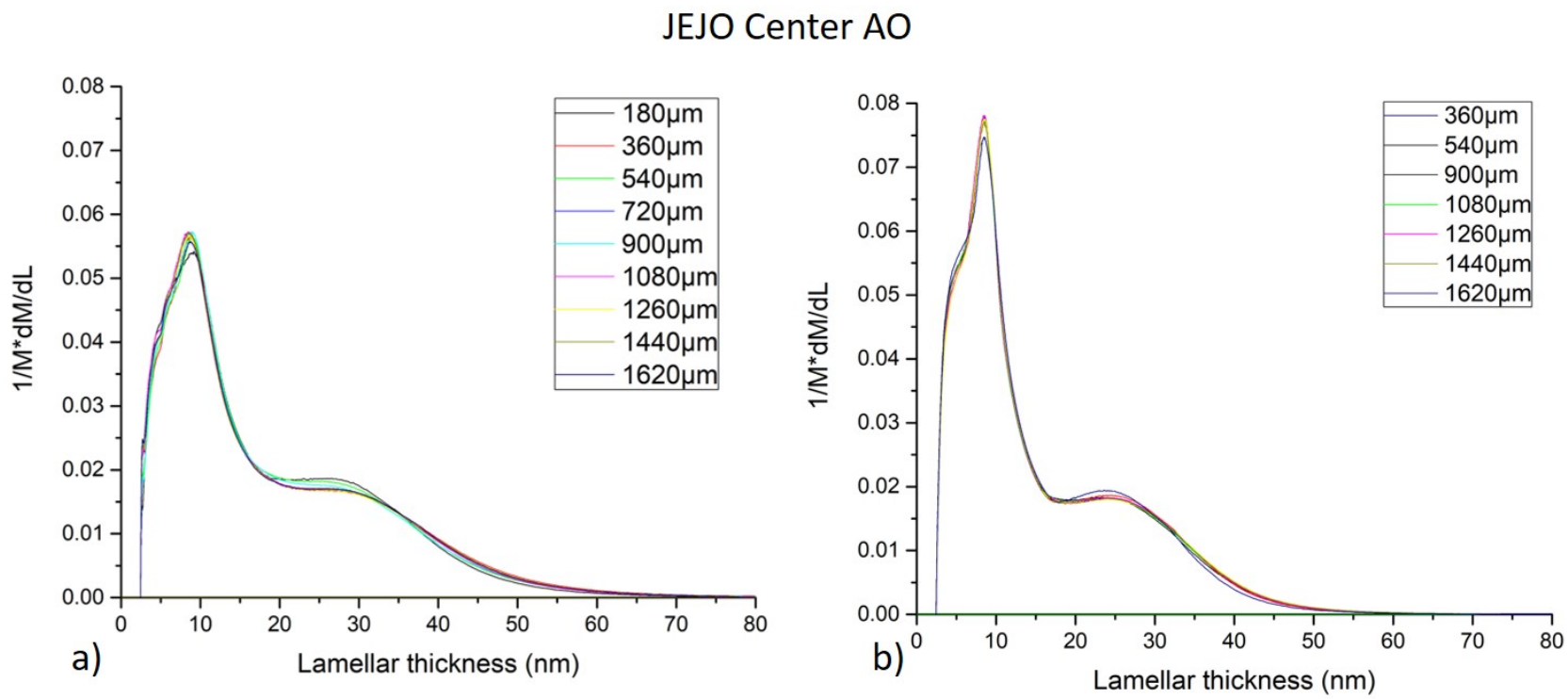

Figure E31. Lamellar thickness distribution (LTD) for JEJO center AO as a function of depth; a) LTD calculated from the first heating run. b) LTD calculated from the second heating run

Die approbierte gedruckte Originalversion dieser Dissertation ist an der TU Wien Bibliothek verfügbar.
The approved original version of this doctoral thesis is available in print at TU Wien Bibliothek.

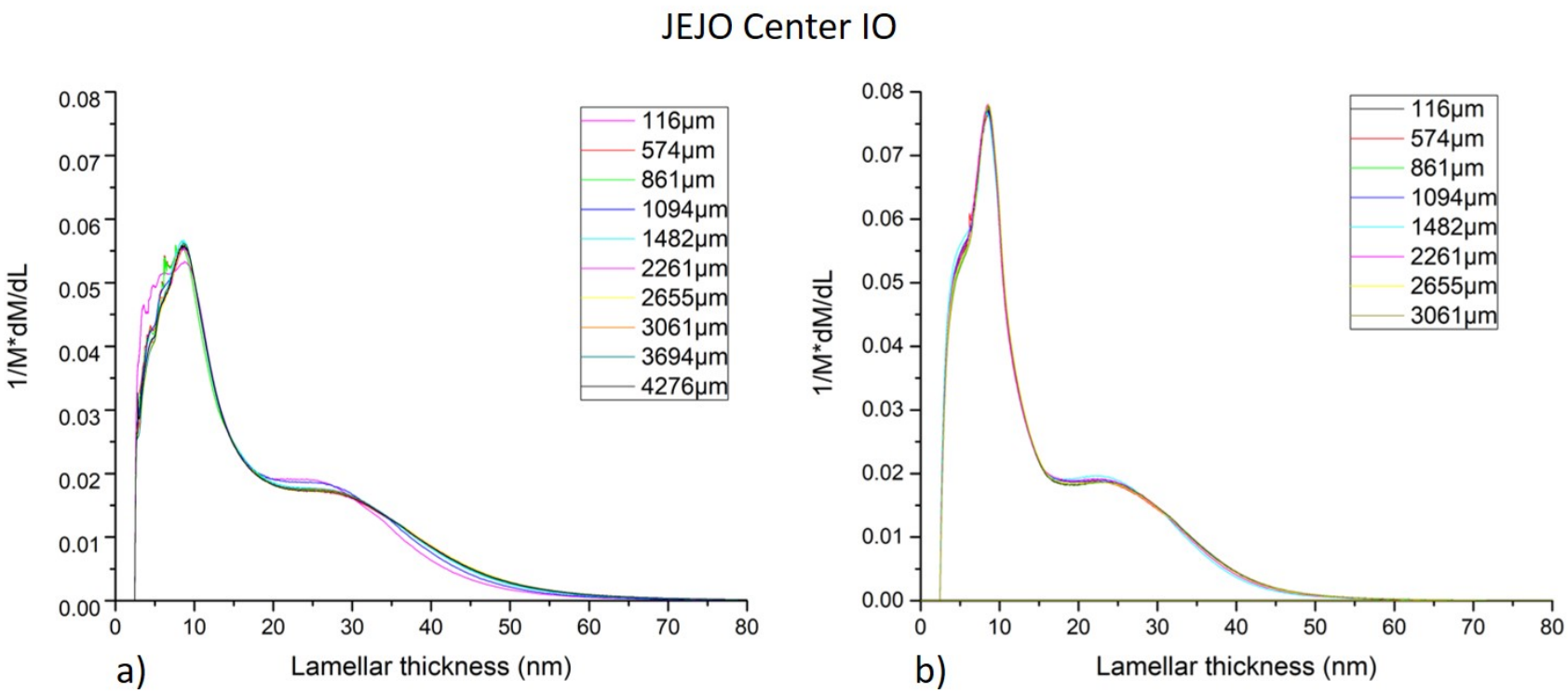

Figure E32. Lamellar thickness distribution (LTD) for JEJO center IO as a function of depth; a) LTD calculated from the first heating run. b) LTD calculated from the second heating run

Die approbierte gedruckte Originalversion dieser Dissertation ist an der TU Wien Bibliothek verfügbar.
The approved original version of this doctoral thesis is available in print at TU Wien Bibliothek.

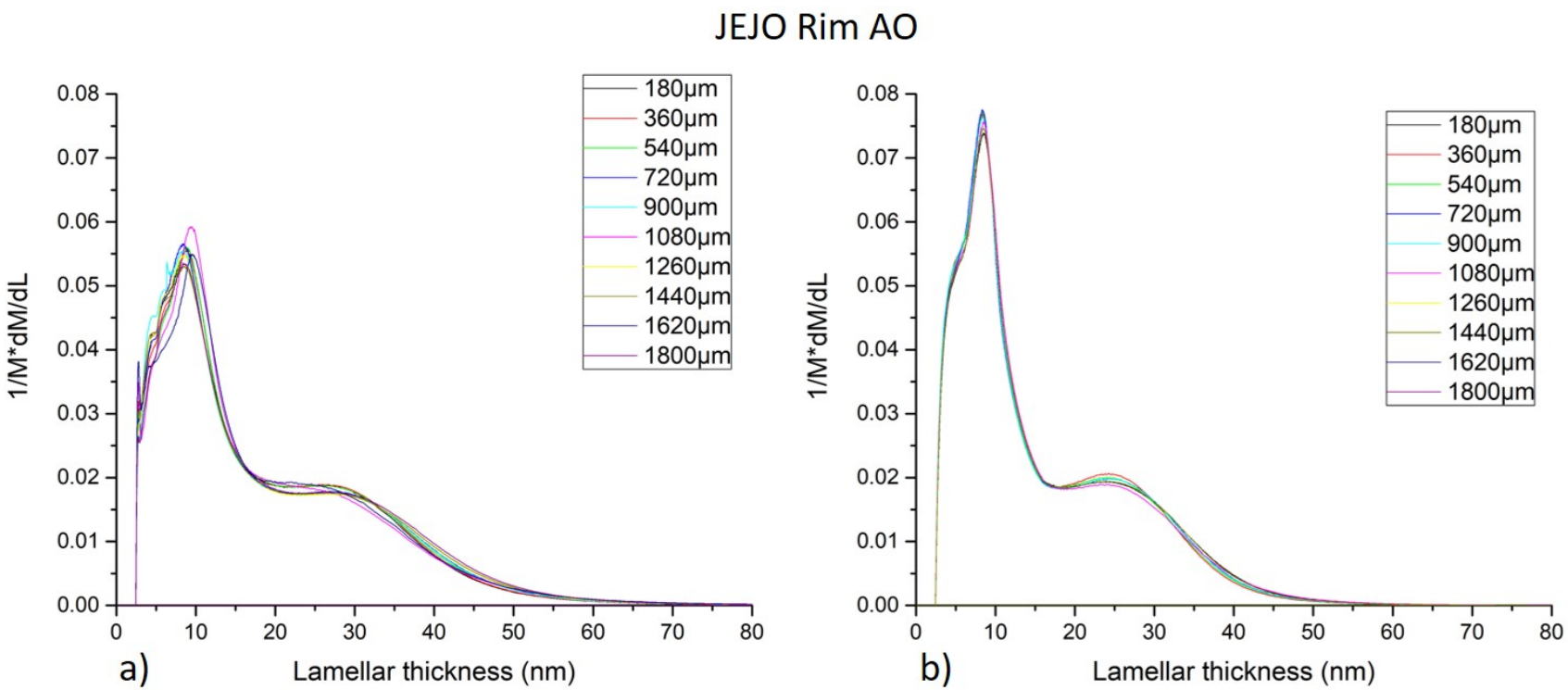

Figure E33. Lamellar thickness distribution (LTD) for JEJO rim AO as a function of depth; a) LTD calculated from the first heating run. b) LTD calculated from the second heating run

Die approbierte gedruckte Originalversion dieser Dissertation ist an der TU Wien Bibliothek verfügbar.
The approved original version of this doctoral thesis is available in print at TU Wien Bibliothek.

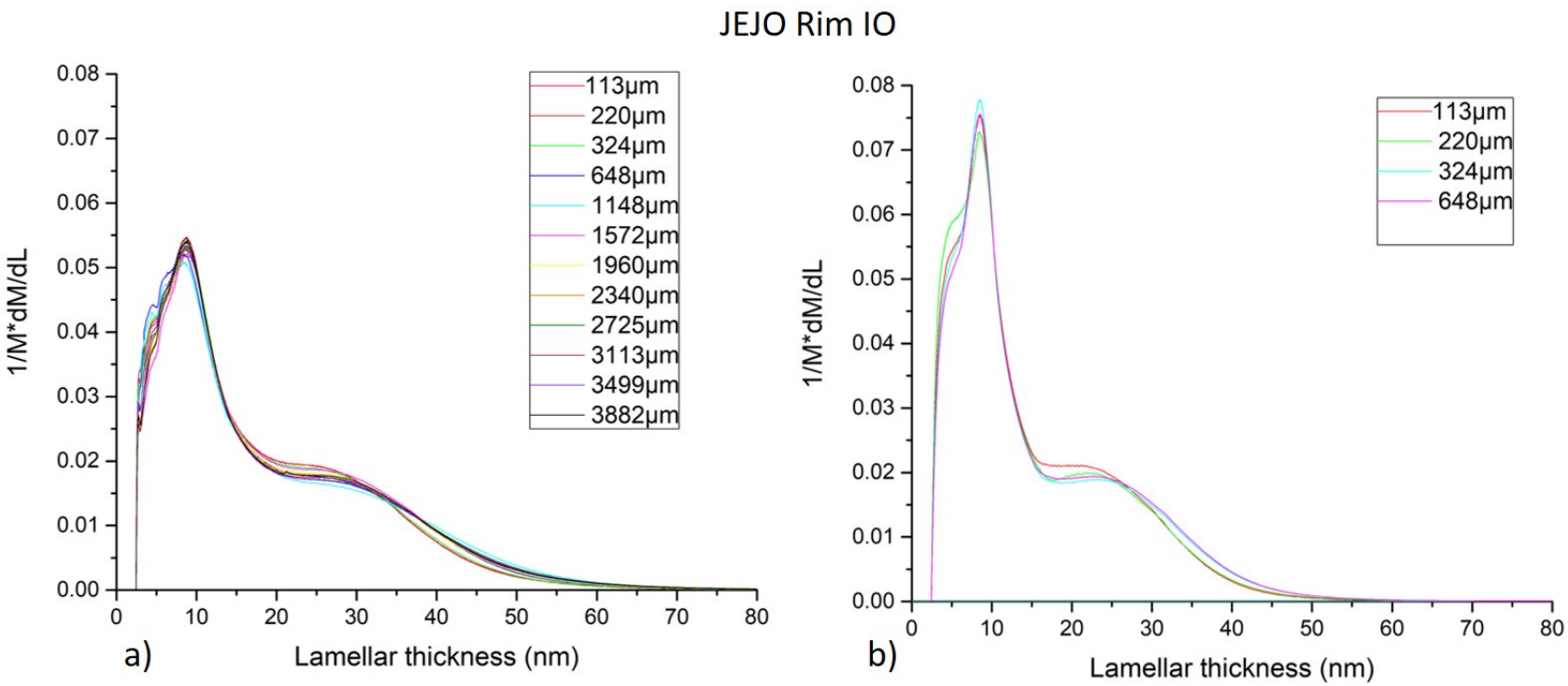

Figure E34. Lamellar thickness distribution (LTD) for JEJO rim IO as a function of depth; a) LTD calculated from the first heating run. b) LTD calculated from the second heating run

Die approbierte gedruckte Originalversion dieser Dissertation ist an der TU Wien Bibliothek verfügbar.
The approved original version of this doctoral thesis is available in print at TU Wien Bibliothek.

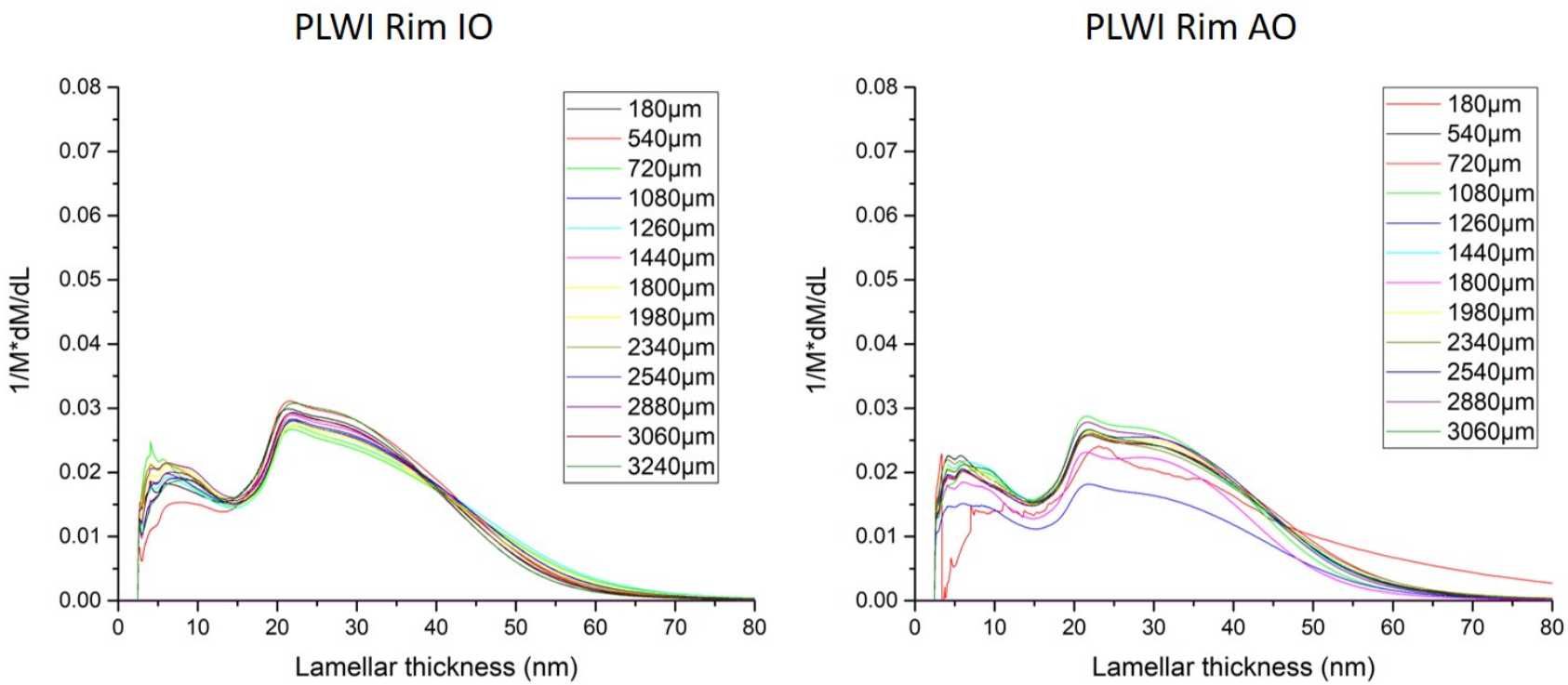

Figure E35. Lamellar thickness distribution (LTD) for PLWI rim IO and rim AO as a function of depth (LTD calculated from the first heating run)

Die approbierte gedruckte Originalversion dieser Dissertation ist an der TU Wien Bibliothek verfügbar.
The approved original version of this doctoral thesis is available in print at TU Wien Bibliothek.

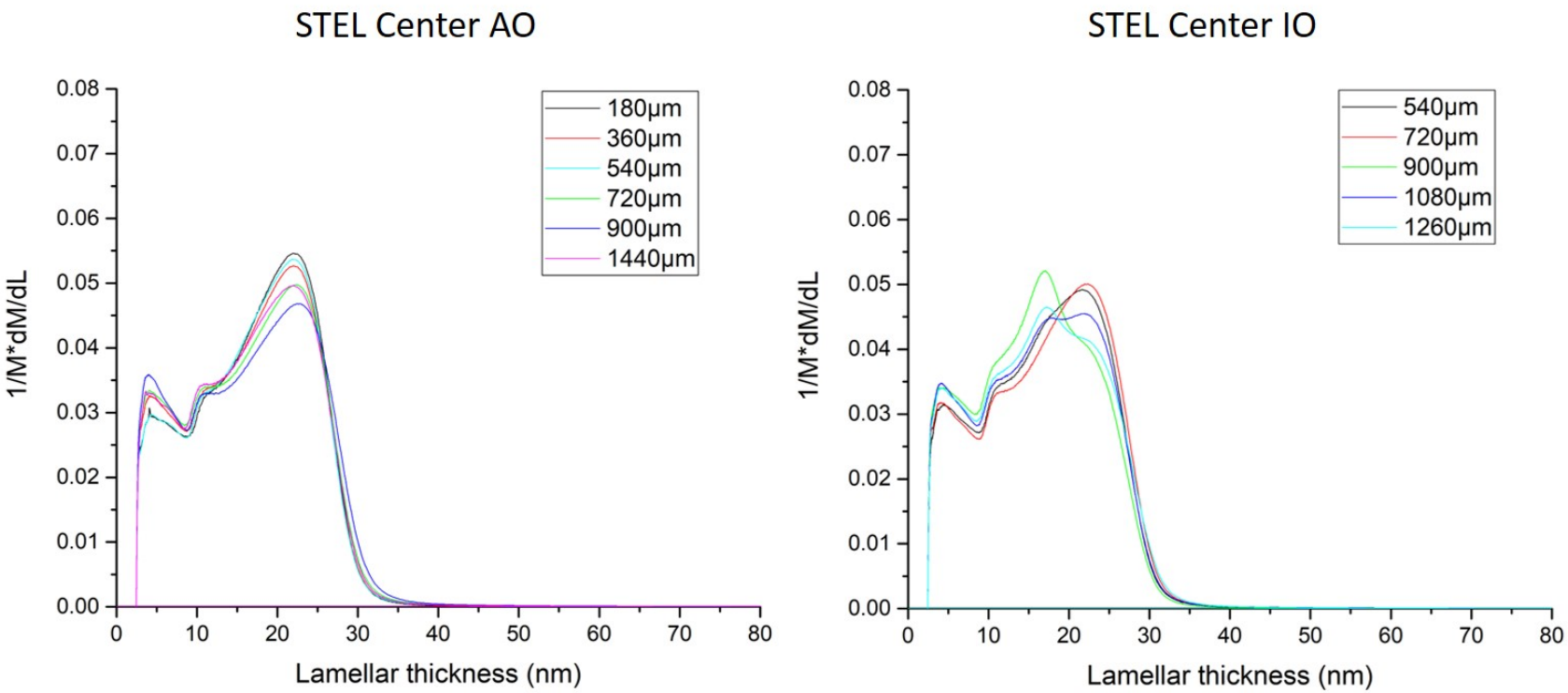

Figure E36. Lamellar thickness distribution (LTD) for STEL center AO and center IO as a function of depth (LTD calculated from the first heating run)

Die approbierte gedruckte Originalversion dieser Dissertation ist an der TU Wien Bibliothek verfügbar.
The approved original version of this doctoral thesis is available in print at TU Wien Bibliothek.

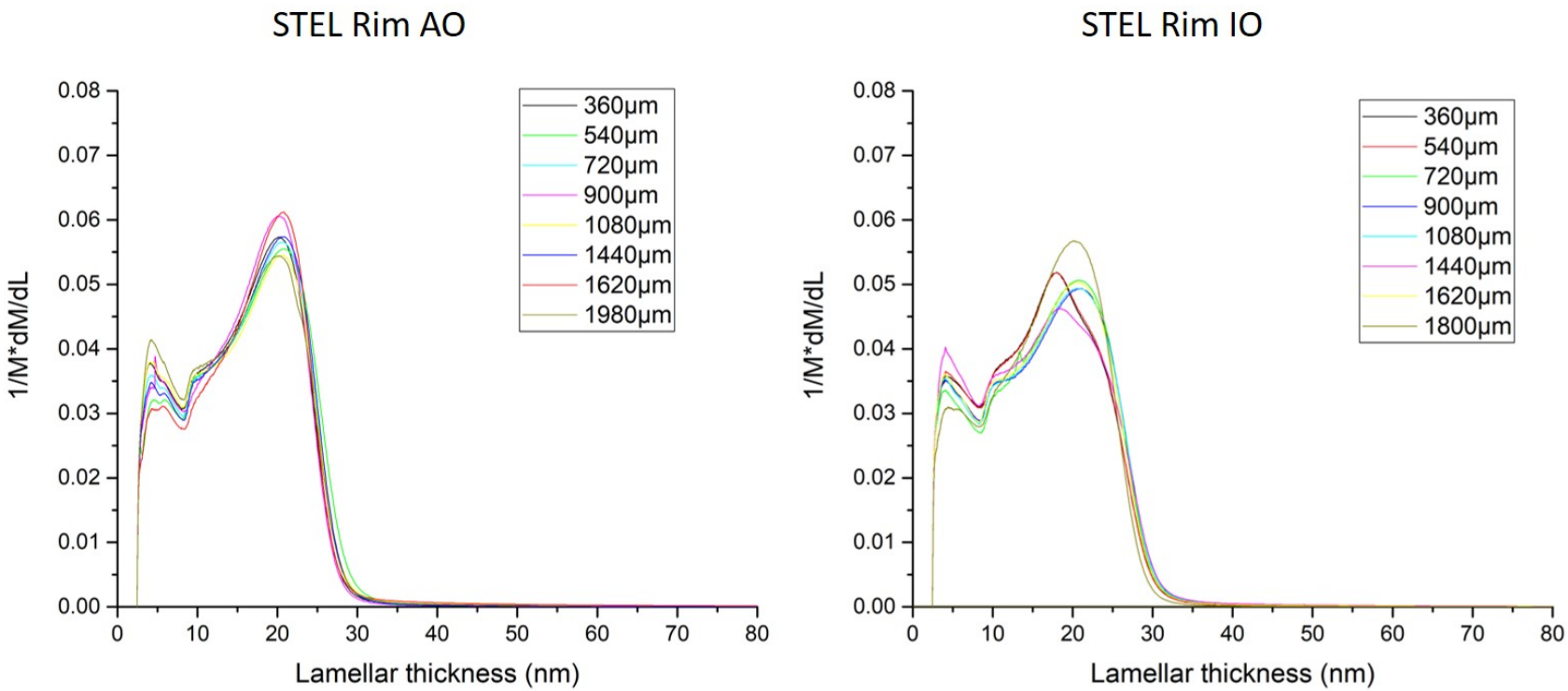

Figure E37. Lamellar thickness distribution (LTD) for STEL rim AO and rim IO as a function of depth (LTD calculated from the first heating run)

Die approbierte gedruckte Originalversion dieser Dissertation ist an der TU Wien Bibliothek verfügbar.
The approved original version of this doctoral thesis is available in print at TU Wien Bibliothek.

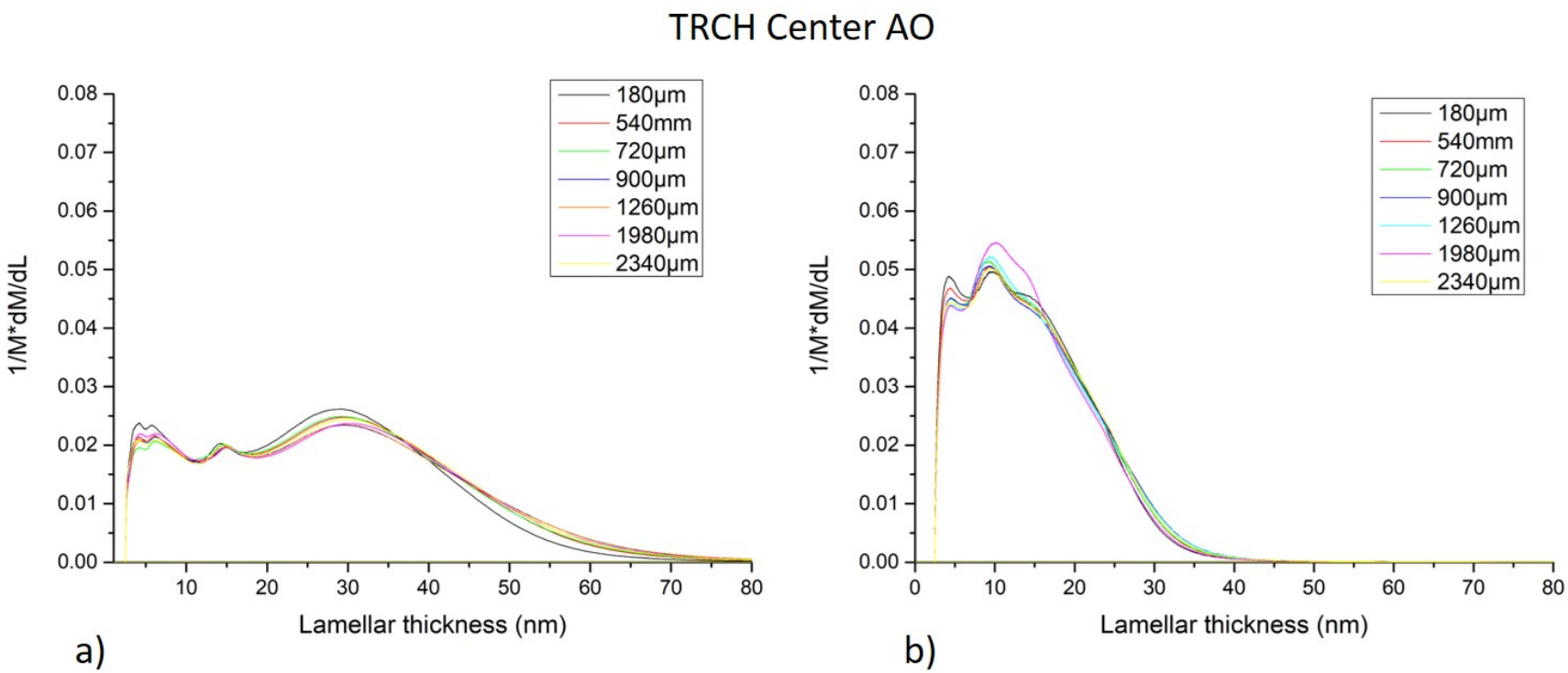

Figure E38. Lamellar thickness distribution (LTD) for TRCH center AO as a function of depth; a) LTD calculated from the first heating run. b) LTD calculated from the second heating run

Die approbierte gedruckte Originalversion dieser Dissertation ist an der TU Wien Bibliothek verfügbar.
The approved original version of this doctoral thesis is available in print at TU Wien Bibliothek.

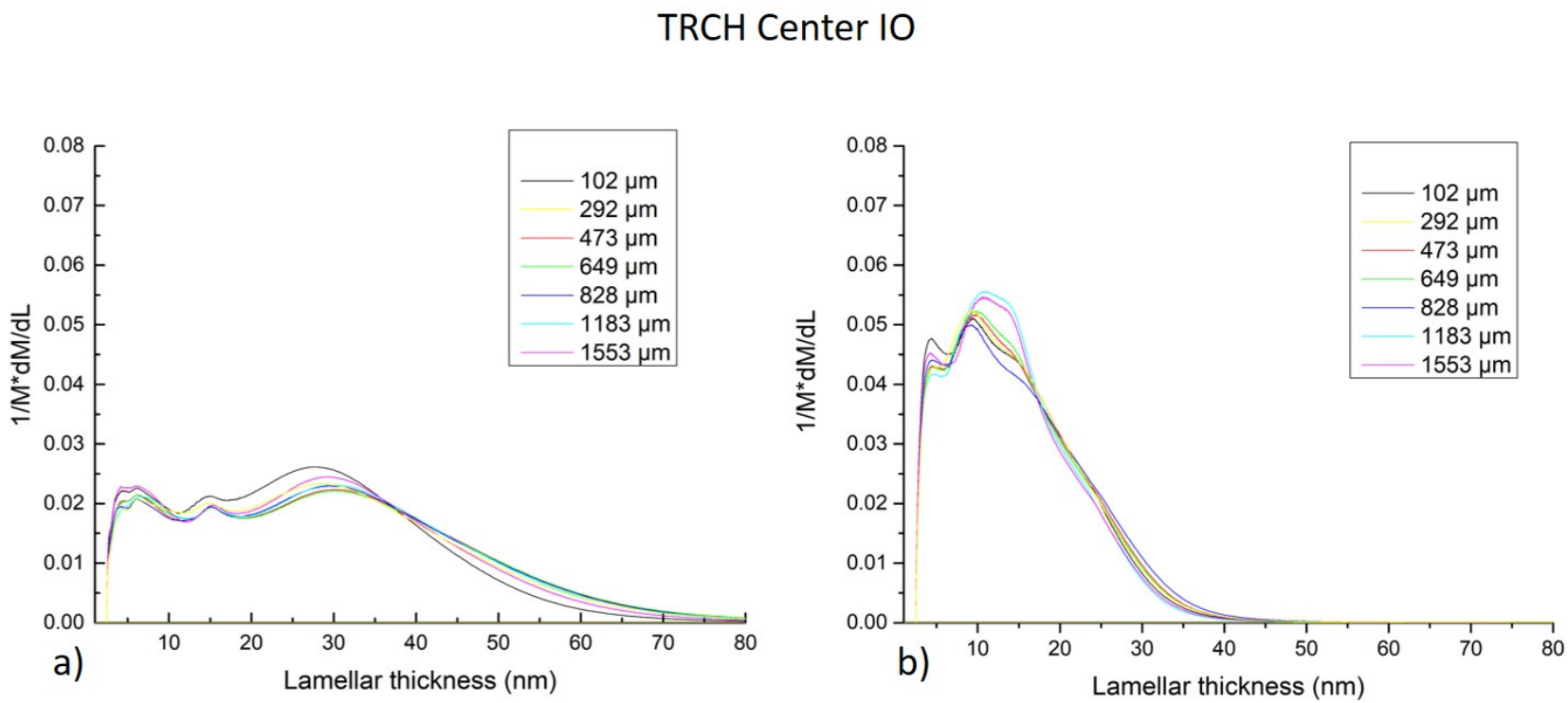

Figure E39. Lamellar thickness distribution (LTD) for TRCH center IO as a function of depth; a) LTD calculated from the first heating run. b) LTD calculated from the second heating run

Die approbierte gedruckte Originalversion dieser Dissertation ist an der TU Wien Bibliothek verfügbar.
The approved original version of this doctoral thesis is available in print at TU Wien Bibliothek.

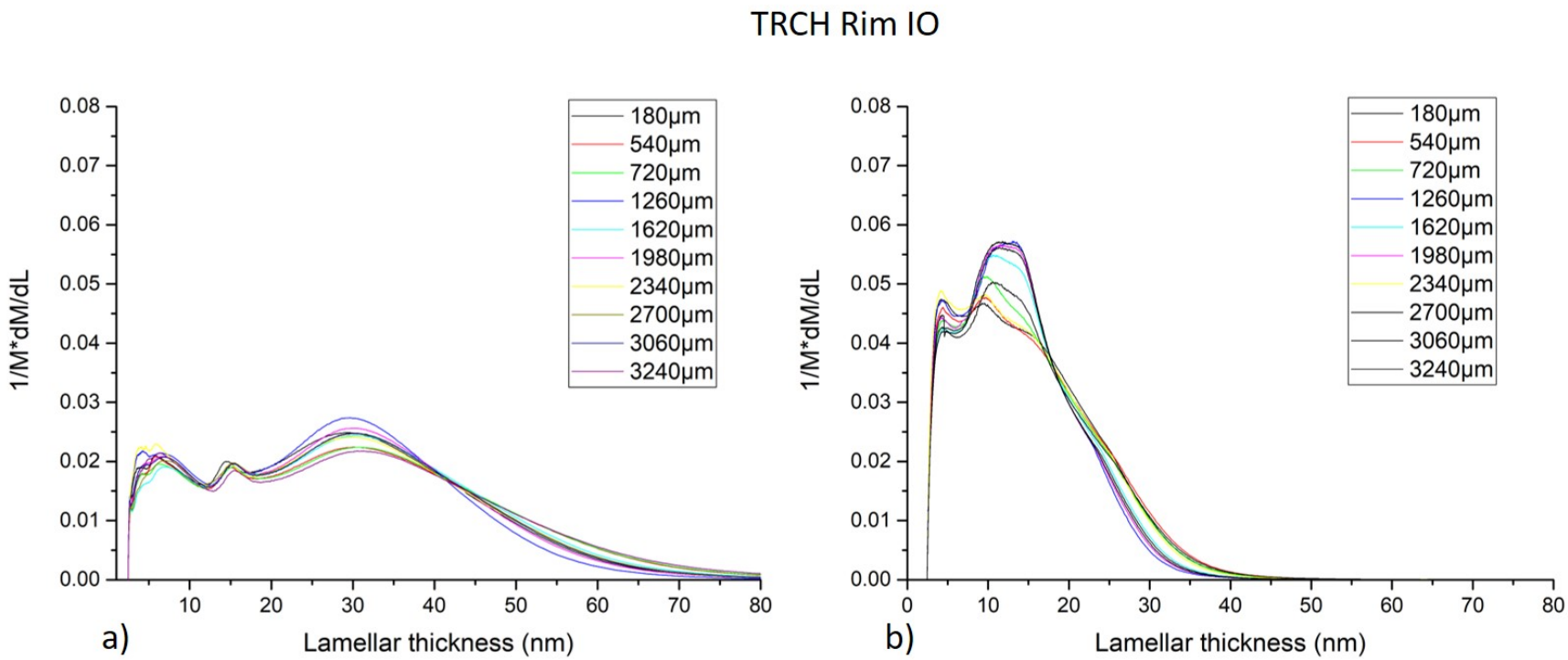

Figure E40. Lamellar thickness distribution (LTD) for TRCH rim IO as a function of depth; a) LTD calculated from the first heating run. b) LTD calculated from the second heating run

Die approbierte gedruckte Originalversion dieser Dissertation ist an der TU Wien Bibliothek verfügbar.
The approved original version of this doctoral thesis is available in print at TU Wien Bibliothek.

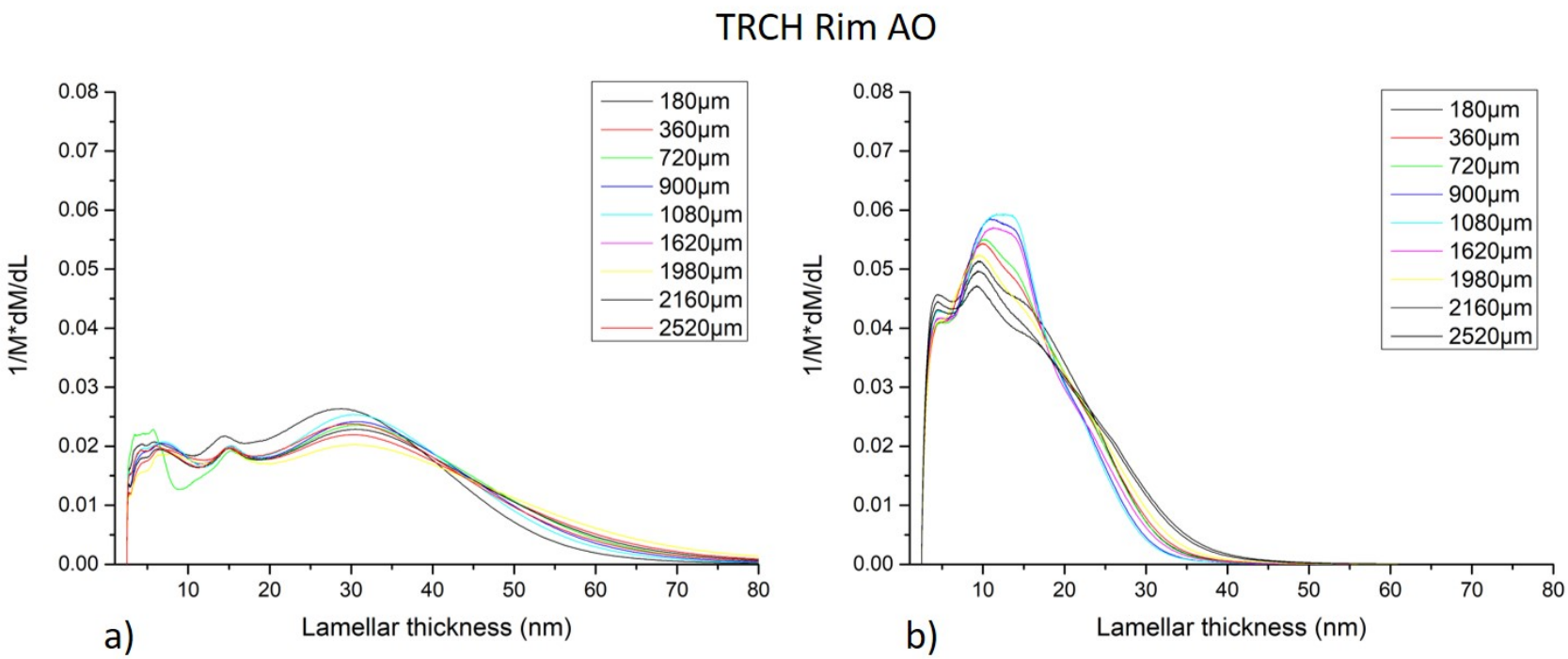

Figure E41. Lamellar thickness distribution (LTD) for TRCH rim AO as a function of depth; a) LTD calculated from the first heating run. b) LTD calculated from the second heating run

APPENDIX F: DSI Results

Table F1. Mechanical properties from the DSI

Acronym	Material	E-Modulus (GPa)	St.dev	Hardness (MPa)	St.dev
AUMA	Conventional	1.54	0.47	71.69	10.15
GOKA	Conventional	0.95	0.04	49.76	2.28
PLWI	XL	1.02	0.06	62.07	4.03
TRCH	XL	1.06	0.03	56.73	1.10
LAMA1	XL	1.09	0.03	60.97	0.50
LAMA2	XL	1.10	0.02	58.56	0.28
LOPE	XL	0.82	0.07	52.83	2.70
JEJO	XL	0.72	0.10	45.46	3.40
WIRU	XL	0.66	0.01	41.55	0.72
STEL	XL	0.77	0.03	52.80	3.04
LUIN	XL	0.79	0.01	49.26	1.18
KOEV	XL	1.17	0.01	61.24	0.49
FADA	XL	0.67	0.01	43.02	0.46
GRMA	XL	0.70	0.03	42.39	0.03
MAWO	XL	-	-	-	-
MÜCL	XL	-	-	-	-
VOST	XL	-	-	-	-
GIWA	XL	-	-	-	-
GLFR	XL	-	-	-	-
SCME	XL	-	-	-	-

Die approbierte gedruckte Originalversion dieser Dissertation ist an der TU Wien Bibliothek verfügbar.
The approved original version of this doctoral thesis is available in print at TU Wien Bibliothek.
TU Bibliothek Your knowledge hub WIEN

APPENDIX G: Small Punch Results

Table G1. Mechanical properties from the SPT

NAME	Peak Load (N)	Utimate Load (N)	Ultimate Load Displacement (mm)	Work to Failure (mJ)	E-Modulus* Gpa
GUR 1020 Vit.E	65.1±5.4	58.1±4.6	4.8±0.12	228.7±24.2	0.68
GUR 1020	65.4±1.6	51.2±1.2	4.7.0.04	232.3±8.2	0.78
GUR 1050	67.2±1.5	63.5±1.9	4.6±0.14	233.3±8.7	0.76
REOP	65.3±3.1	62.9±5.5	4.2±0.2	203±17.9	0.78
AUMA	61.96±1.5	42.3±0.97	4.2±0.04	172.3±5.4	0.77
KOR	24.6±17.3	2.9±1.3	1.7±1.2	43.5±33.9	1.04
DSA 3w aged	56.8±0.1	67.8±2.7	4.1±0.2	178±14	0.51
DSA 6w aged	61.5±3.6	77.5±7.5	4.3±0.4	156±27	0.75
X3 6w aged	65.5±0.5	59.5±2.8	3.3±0.14	150.5±11.5	0.96
STEL	65.5±0.7	64.7±1.7	4.5±0.04	228±7	0.49
WIRU	57.7±0.5	78.1±4.2	4.1±0.3	197±23.4	0.44
LUIN	76.3±1.2	72.9±1.1	4.6±0.05	280.5±5.5	1.02
KOEV	70.3±3.1	100±7	3.9±0.2	243±28	0.94
GLFR	61.2±0.8	65.3±3.4	4.7±0.0	233.3±12:8	0.43

*: Calculated E-Modulus from SPT curve by using finite element method [249]

Die approbierte gedruckte Originalversion dieser Dissertation ist an der TU Wien Bibliothek verfügbar.
The approved original version of this doctoral thesis is available in print at TU Wien Bibliothek.
TU Bibliothek Your knowledge hub WIEN

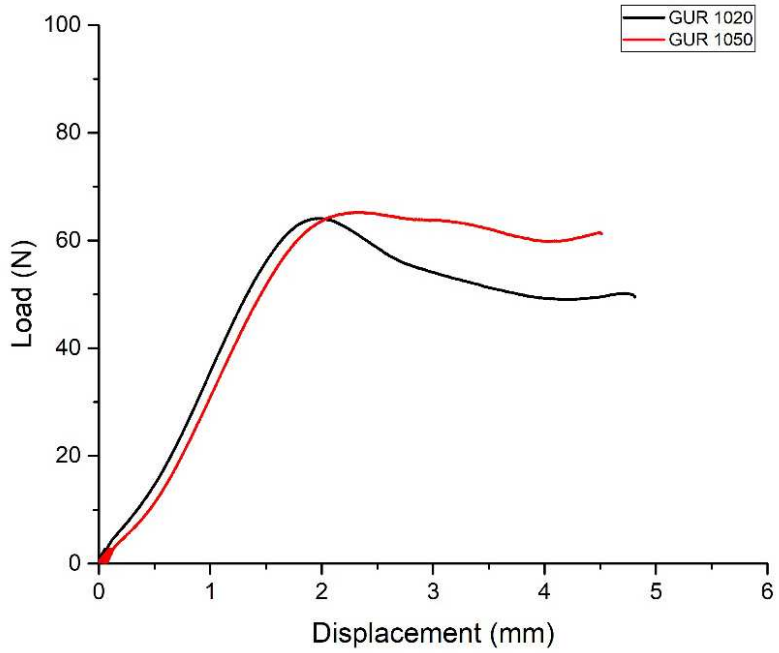

Figure G1. Load displacement curve of GUR 1020 and GUR 1050

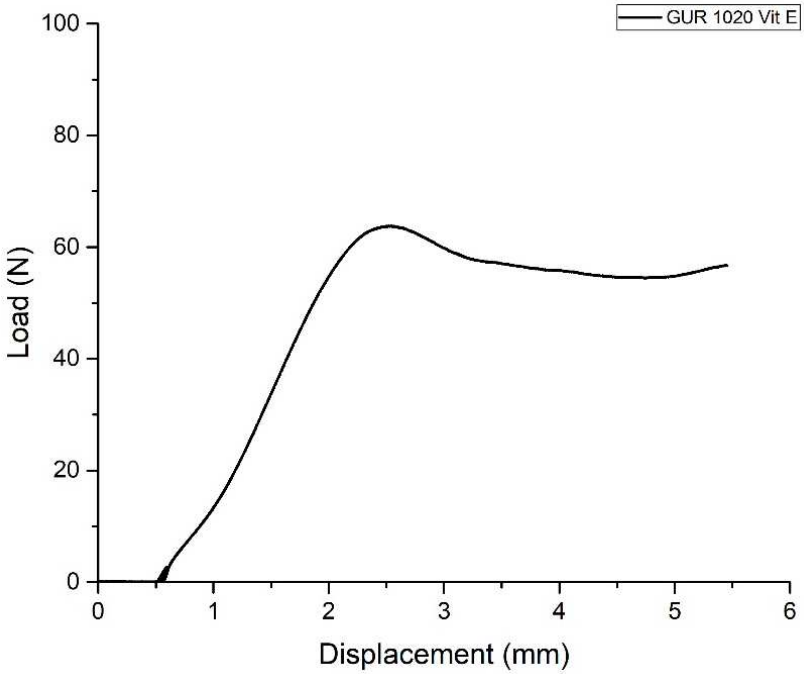

Figure G2. Load displacement curve of GUR 1020 Vit. E

Die approbierte gedruckte Originalversion dieser Dissertation ist an der TU Wien Bibliothek verfügbar.
The approved original version of this doctoral thesis is available in print at TU Wien Bibliothek.

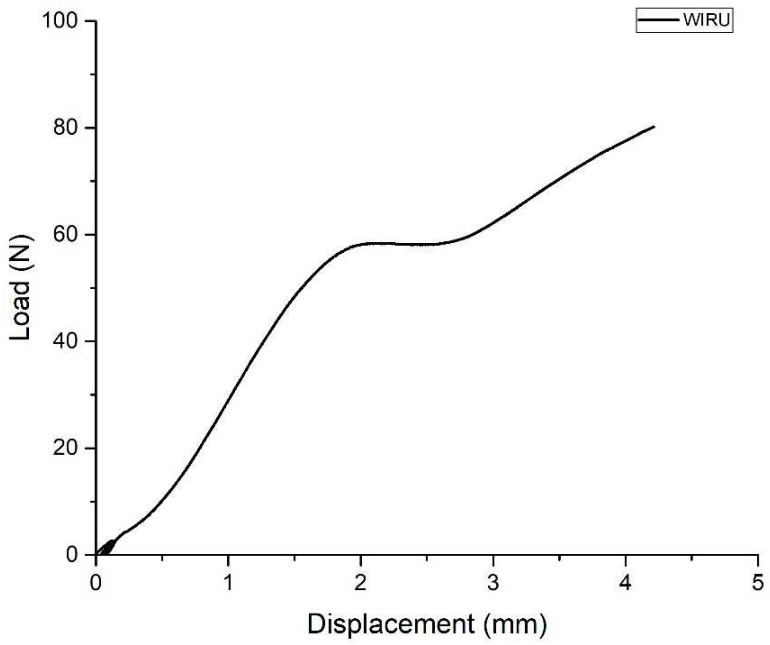

Figure G3. Load displacement curve of WIRU

Die approbierte gedruckte Originalversion dieser Dissertation ist an der TU Wien Bibliothek verfügbar.
The approved original version of this doctoral thesis is available in print at TU Wien Bibliothek.

APPENDIX H: Tribo Results

Table H1. Progressive wear results for virgin and extended accelerated aged of GUR 1050 unirradiated block samples under 30 N

GUR 1050 Virgin

No	Av. Pofile Area (µm2)	St.Dev.	Av. Volume Loss (mm3)	St.Dev.	Av.Wear Rate (mm3/Nm)	St.Dev.	Av. Volumetric Wear (mm3/cycle)	St.Dev
2h-1	11906.07	101.98	0.224	0.002	1.38E-05	1.19E-07	2.61E-06	2.23E-08
2h-2								
2h-3								
4h-1	17005.02	204.14	0.320	0.004	9.89E-06	1.187E-07	3.73E-06	4.47E-08
4h-2								
4h-3								
6h-1	20529.26	428.41	0.387	0.008	7.96E-06	1.661E-07	4.50E-06	9.39E-08
6h-2								
6h-3								

GUR 1050 3 week aged

No	Av. Pofile Area (µm2)	St.Dev.	Av. Volume Loss (mm3)	St.Dev.	Av.Wear Rate (mm3/Nm)	St.Dev.	Av. Volumetric Wear (mm3/cycle)	St.Dev
2h-1	17611.25	391.79	0.332	0.007	2.05E-05	4.56E-07	3.86E-06	8.59E-08
2h-2								
2h-3								
4h-1	21932.47	530.77	0.413	0.010	1.28E-05	3.09E-07	4.81E-06	1.16E-07
4h-2								
4h-3								
6h-1	25564.01	2129.03	0.482	0.040	9.91E-06	8.25E-07	5.60E-06	4.67E-07
6h-2								
6h-3								

GUR 1050 6 week aged

No	Av. Pofile Area (µm2)	St.Dev.	Av. Volume Loss (mm3)	St.Dev.	Av.Wear Rate (mm3/Nm)	St.Dev.	Av. Volumetric Wear (mm3/cycle)	St.Dev
2h-1	77173.92	1784.92	1.454	0.034	8.98E-05	2.08E-06	1.69E-05	3.91E-07
2h-2								
2h-3								
4h-1	84508.34	2298.03	1.592	0.043	4.91E-05	1.34E-06	1.85E-05	5.04E-07
4h-2								
4h-3								
6h-1	112658.39	488.16	2.122	0.009	4.37E-05	1.89E-07	2.47E-05	1.07E-07
6h-2								
6h-3								

Die approbierte gedruckte Originalversion dieser Dissertation ist an der TU Wien Bibliothek verfügbar.
The approved original version of this doctoral thesis is available in print at TU Wien Bibliothek.
TU Bibliothek Your knowledge hub WIEN

GUR 1050 9 week aged

No	Av. Pofile Area (µm2)	St.Dev.	Av. Volume Loss (mm3)	St.Dev.	Av.Wear Rate (mm3/Nm)	St.Dev.	Av. Volumetric Wear (mm3/cycle)	St.Dev
2h-1	90232.61	6052.58	1.700	0.114	1.05E-04	7.04E-06	1.98E-05	1.33E-06
2h-2								
2h-3								
4h-1	116545.91	1042.84	2.196	0.020	6.78E-05	6.06E-07	2.55E-05	2.29E-07
4h-2								
4h-3								
6h-1	125726.27	2307.35	2.369	0.043	4.87E-05	8.94E-07	2.76E-05	5.06E-07
6h-2								
6h-3								

Table H2. Progressive wear results for virgin and extended accelerated aged of GUR 1020 unirradiated block samples under 30 N

GUR 1020 Virgin*

No	Av. Volume Loss (mm3)	St.Dev.	Av.Wear Rate (mm3/Nm)	St.Dev.	Av. Volumetric Wear (mm3/cycle)	St.Dev
2h-1	0.17	0.009	1.05E-05	4.60E-07	1.97E-06	1.05E-07
2h-2						
2h-3						
4h-1	0.229	0.01	7.07E-06	3.44E-07	2.66E-06	1.63E-07
4h-2						
4h-3						
6h-1	0.247	0.02	5.08E-06	3.49E-07	2.87E-06	2.56E-07
6h-2						
6h-3						

GUR 1020 3 week aged*

No	Av. Volume Loss (mm3)	St.Dev.	Av.Wear Rate (mm3/Nm)	St.Dev.	Av. Volumetric Wear (mm3/cycle)	St.Dev
2h-1	0.225	0.012	1.39E-05	5.59E-07	2.62E-06	1.41E-07
2h-2						
2h-3						
4h-1	0.273	0.012	8.43E-06	2.68E-07	3.17E-06	1.35E-07
4h-2						
4h-3						
6h-1	0.306	0.025	6.30E-06	3.85E-07	3.56E-06	2.91E-07
6h-2						
6h-3						

Die approbierte gedruckte Originalversion dieser Dissertation ist an der TU Wien Bibliothek verfügbar.
The approved original version of this doctoral thesis is available in print at TU Wien Bibliothek.
TU Bibliothek Your knowledge hub WIEN

*: **Reference**; Petrica. M. (2016). Study of the wear processes and tribological relevant properties of engineering thermoplastics (PhD/TU Wien)

GUR 1020 6 week aged

No	Av. Pofile Area (µm2)	St.Dev.	Av. Volume Loss (mm3)	St.Dev.	Av.Wear Rate (mm3/Nm)	St.Dev.	Av. Volumetric Wear (mm3/cycle)	St.Dev
2h-1	15006.20	575.07	0.283	0.011	1.75E-05	6.69E-07	3.29E-06	1.26E-07
2h-2								
2h-3								
4h-1	17623.39	581.99	0.332	0.011	1.02E-05	3.38E-07	3.86E-06	1.28E-07
4h-2								
4h-3								
6h-1	23085.72	1383.84	0.435	0.026	8.95E-06	5.36E-07	5.06E-06	3.03E-07
6h-2								
6h-3								

GUR 1020 9 week aged

No	Av. Pofile Area (µm2)	St.Dev.	Av. Volume Loss (mm3)	St.Dev.	Av.Wear Rate (mm3/Nm)	St.Dev.	Av. Volumetric Wear (mm3/cycle)	St.Dev
6h-1	135532.76	4255.48	2.553	0.080	5.25E-05	1.65E-07	2.97E-05	9.33E-07
6h-2								
6h-3								

Die approbierte gedruckte Originalversion dieser Dissertation ist an der TU Wien Bibliothek verfügbar.
The approved original version of this doctoral thesis is available in print at TU Wien Bibliothek.
TU Bibliothek Your knowledge hub WIEN

Table H3. Progressive wear results for virgin and extended accelerated aged of GUR 1020 Vit.E unirradiated block samples under 30 N

GUR 1020 Vit E Virgin

No	Av. Pofile Area (µm2)	St.Dev.	Av. Volume Loss (mm3)	St.Dev.	Av.Wear Rate (mm3/Nm)	St.Dev.	Av. Volumetric Wear (mm3/cycle)	St.Dev
2h-1	10001.42	427.77	0.188	0.008	1.16E-05	4.97E-07	2.19E-06	9.37E-08
2h-2								
2h-3								
4h-1	13259.36	356.37	0.250	0.007	7.71E-06	2.072E-07	2.91E-06	7.81E-08
4h-2								
4h-3								
6h-1	16037.69	358.12	0.302	0.007	6.22E-06	1.388E-07	3.51E-06	7.85E-08
6h-2								
6h-3								

GUR 1020 Vit E 3w aged

No	Av. Pofile Area (µm2)	St.Dev.	Av. Volume Loss (mm3)	St.Dev.	Av.Wear Rate (mm3/Nm)	St.Dev.	Av. Volumetric Wear (mm3/cycle)	St.Dev
2h-1	9892.21	1308.14	0.186	0.025	1.15E-05	1.52E-06	2.17E-06	2.87E-07
2h-2								
2h-3								
4h-1	12914.87	1455.53	0.243	0.027	7.51E-06	8.46E-07	2.83E-06	3.19E-07
4h-2								
4h-3								
6h-1	15039.74	1082.58	0.283	0.020	5.83E-06	4.20E-07	3.30E-06	2.37E-07
6h-2								
6h-3								

GUR 1020 Vit E 6w aged

No	Av. Pofile Area (µm2)	St.Dev.	Av. Volume Loss (mm3)	St.Dev.	Av.Wear Rate (mm3/Nm)	St.Dev.	Av. Volumetric Wear (mm3/cycle)	St.Dev
2h-1	8869.17	875.45	0.167	0.016	1.03E-05	1.02E-06	1.94E-06	1.92E-07
2h-2								
2h-3								
4h-1	12619.64	1215.89	0.238	0.023	7.34E-06	7.07E-07	2.77E-06	2.66E-07
4h-2								
4h-3								
6h-1	14864.52	1388.37	0.280	0.026	5.76E-06	5.38E-07	3.26E-06	3.04E-07
6h-2								
6h-3								

Die approbierte gedruckte Originalversion dieser Dissertation ist an der TU Wien Bibliothek verfügbar.
The approved original version of this doctoral thesis is available in print at TU Wien Bibliothek.
TU Bibliothek Your knowledge hub WIEN

GUR 1020 Vit E 9w aged

No	Av. Pofile Area (µm2)	St.Dev.	Av. Volume Loss (mm3)	St.Dev.	Av.Wear Rate (mm3/Nm)	St.Dev.	Av. Volumetric Wear (mm3/cycle)	St.Dev
2h-1	10358.42	437.19	0.195	0.008	1.20E-05	5.08E-07	2.27E-06	9.58E-08
2h-2								
2h-3								
4h-1	13659.32	2059.70	0.257	0.039	7.94E-06	1.20E-06	2.99E-06	4.51E-07
4h-2								
4h-3								
6h-1	16510.36	895.26	0.311	0.017	6.40E-06	3.47E-07	3.62E-06	1.96E-07
6h-2								
6h-3								

Table H4. Six hours wear results for shelf and extended accelerated aged of DSA/Durasul® explant samples under 30 N

DSA shelf aged

No	Av. Pofile Area (µm2)	St.Dev.	Av. Volume Loss (mm3)	St.Dev.	Av.Wear Rate (mm3/Nm)	St.Dev.	Av. Volumetric Wear (mm3/cycle)	St.Dev
6h-1	6383.97	319.95	0.120	0.006	2.47E-06	1.24E-07	1.40E-06	7.01E-08
6h-2								
6h-3								

DSA 3 week aged

No	Av. Pofile Area (µm2)	St.Dev.	Av. Volume Loss (mm3)	St.Dev.	Av.Wear Rate (mm3/Nm)	St.Dev.	Av. Volumetric Wear (mm3/cycle)	St.Dev
6h-1	6261.54	311.51	0.118	0.006	2.43E-06	1.21E-07	1.37E-06	6.83E-08
6h-2								
6h-3								

DSA 6 week aged

No	Av. Pofile Area (µm2)	St.Dev.	Av. Volume Loss (mm3)	St.Dev.	Av.Wear Rate (mm3/Nm)	St.Dev.	Av. Volumetric Wear (mm3/cycle)	St.Dev
6h-1	6416.42	78.12	0.121	0.001	2.49E-06	3.03E-08	1.41E-06	1.71E-08
6h-2								
6h-3								

Die approbierte gedruckte Originalversion dieser Dissertation ist an der TU Wien Bibliothek verfügbar.
The approved original version of this doctoral thesis is available in print at TU Wien Bibliothek.
TU Bibliothek Your knowledge hub WIEN

Table H5. Six hours wear results for shelf and extended accelerated aged of X3™/Stryker explant samples under 30 N

X3 shelf aged

No	Av. Pofile Area (µm2)	St.Dev.	Av. Volume Loss (mm3)	St.Dev.	Av.Wear Rate (mm3/Nm)	St.Dev.	Av. Volumetric Wear (mm3/cycle)	St.Dev
6h-1	5236.03	311.06	0.099	0.006	2.05E-06	1.21E-07	1.15E-06	6.82E-08
6h-2								
6h-3								

X3 3 week aged

No	Av. Pofile Area (µm2)	St.Dev.	Av. Volume Loss (mm3)	St.Dev.	Av.Wear Rate (mm3/Nm)	St.Dev.	Av. Volumetric Wear (mm3/cycle)	St.Dev
6h-1	5480.68	228.15	0.103	0.004	2.12E-06	8.84E-08	1.20E-06	5.00E-08
6h-2								
6h-3								

X3 6 week aged

No	Av. Pofile Area (µm2)	St.Dev.	Av. Volume Loss (mm3)	St.Dev.	Av.Wear Rate (mm3/Nm)	St.Dev.	Av. Volumetric Wear (mm3/cycle)	St.Dev
6h-1	5657.94	168.40	0.107	0.003	2.19E-06	6.53E-08	1.24E-06	3.69E-08
6h-2								
6h-3								

Table H6. Seventy-two hours wear results for virgin and six weeks aged of GUR 1050 and GUR 1020 unirradiated block samples under 2 N

GUR 1050 Virgin

No	Av. Pofile Area (µm2)	St.Dev.	Av. Volume Loss (mm3)	St.Dev.	Av.Wear Rate (mm3/Nm)	St.Dev.	Av. Volumetric Wear (mm3/cycle)	St.Dev
72h-1	1579.20	131.28	0.030	0.002	5.10E-08	4.24E-09	2.88E-08	2.40E-09
72h-2								
72h-3								

GUR 1050 6w aged

No	Av. Pofile Area (µm2)	St.Dev.	Av. Volume Loss (mm3)	St.Dev.	Av.Wear Rate (mm3/Nm)	St.Dev.	Av. Volumetric Wear (mm3/cycle)	St.Dev
72h-1	4966.86	307.03	0.094	0.006	1.60E-07	9.92E-09	9.07E-08	5.61E-09
72h-2								
72h-3								

Die approbierte gedruckte Originalversion dieser Dissertation ist an der TU Wien Bibliothek verfügbar.
The approved original version of this doctoral thesis is available in print at TU Wien Bibliothek.
TU Bibliothek Your knowledge hub WIEN

GUR 1020 virgin

No	Av. Pofile Area (µm2)	St.Dev.	Av. Volume Loss (mm3)	St.Dev.	Av.Wear Rate (mm3/Nm)	St.Dev.	Av. Volumetric Wear (mm3/cycle)	St.Dev
72h-1	1364.77	54.26	0.026	0.001	4.41E-08	1.75E-09	2.49E-08	9.91E-10
72h-2								
72h-3								

GUR 1020 6w aged

No	Av. Pofile Area (µm2)	St.Dev.	Av. Volume Loss (mm3)	St.Dev.	Av.Wear Rate (mm3/Nm)	St.Dev.	Av. Volumetric Wear (mm3/cycle)	St.Dev
72h-1	2473.76	229.31	0.047	0.004	7.99E-08	7.41E-09	4.52E-08	4.19E-09
72h-2								
72h-3								

Die approbierte gedruckte Originalversion dieser Dissertation ist an der TU Wien Bibliothek verfügbar.
The approved original version of this doctoral thesis is available in print at TU Wien Bibliothek.
TU Bibliothek Your knowledge hub WIEN

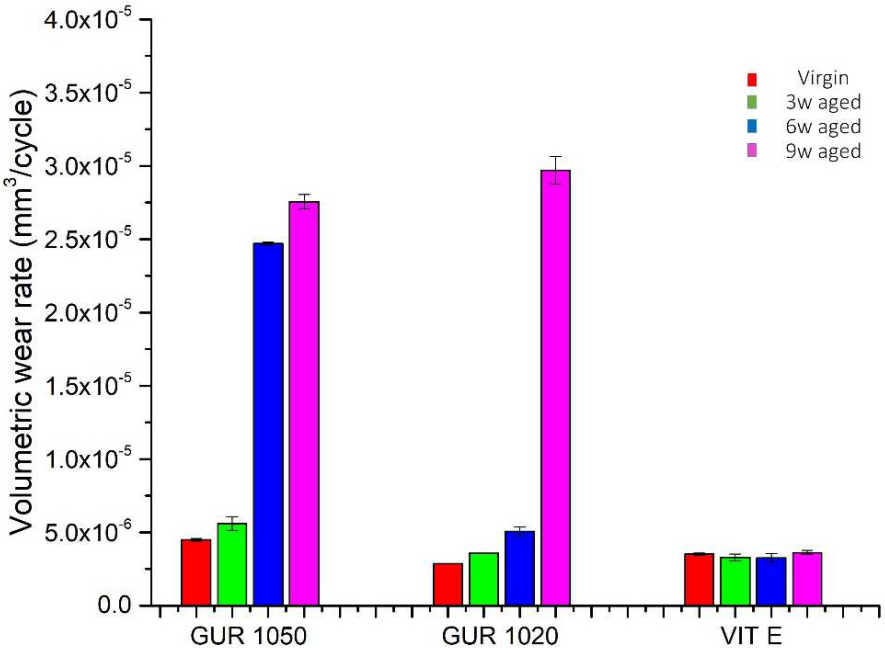

Figure H1. Volumetric wear rate for GUR 1050; GUR 1020 and GUR 1020 Vit. E with 30 N

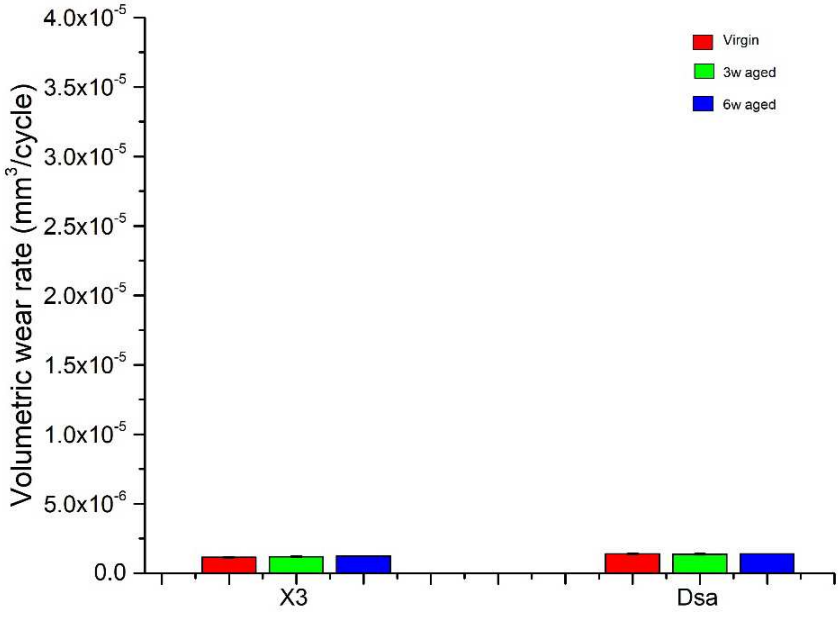

Figure H2. Volumetric wear rate for X3™ and Dsa explants with 30 N

Die approbierte gedruckte Originalversion dieser Dissertation ist an der TU Wien Bibliothek verfügbar.
The approved original version of this doctoral thesis is available in print at TU Wien Bibliothek.
TU Bibliothek Your knowledge hub WIEN

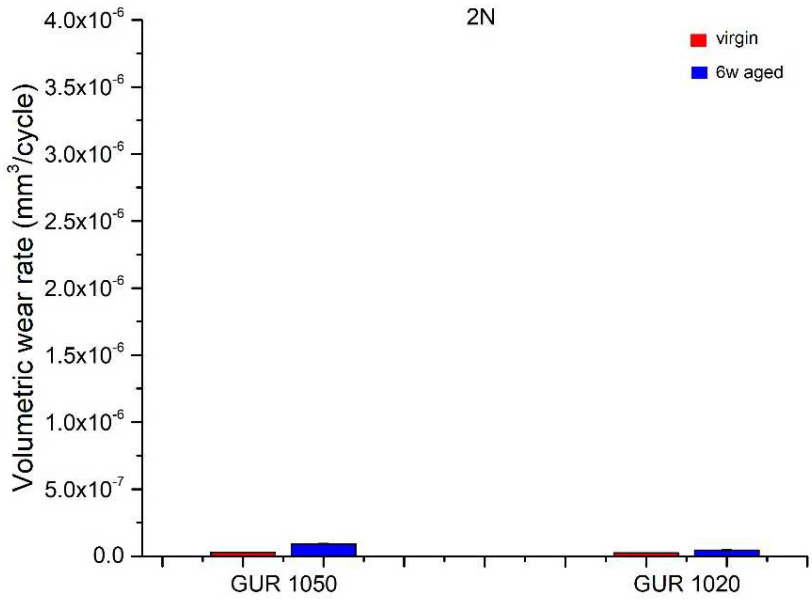

Figure H3. Volumetric wear rate for GUR 1050 and GUR 1020 with 2N

Die approbierte gedruckte Originalversion dieser Dissertation ist an der TU Wien Bibliothek verfügbar.
The approved original version of this doctoral thesis is available in print at TU Wien Bibliothek.

Die approbierte gedruckte Originalversion dieser Dissertation ist an der TU Wien Bibliothek verfügbar.
The approved original version of this doctoral thesis is available in print at TU Wien Bibliothek.

Table H7. Comparison of morphological. mechanical and wear values of GUR1020. GUR 1050 and GUR 1020 Vit. E

	GUR 1020				GUR1050				GUR1020 Vit.E			
w[a]: weeks	**Virgin**	**3w[a] aged**	**6w aged**	**9w aged**	**Virgin**	**3w aged**	**6w aged**	**9w aged**	**Virgin**	**3w aged**	**6w aged**	**9w aged**
OI (-)	0.03± 0.02	0.08± 0.02	0.80± 0.2	2.29± 0.2	0.03± 0.01	0.07± 0.02	1.59±0.3	2.48±0.3	0.01± 0.06	0.01± 0.03	0.01± 0.07	0.01± 0.01
Xr (%)	59±2	62±1	67±2	84±3	53±2	55±1	75±3	81±3	53±2	55±3	56±1	54±1
E-Modulus (GPa)	1.12± 0.03	1.48± 0.05	1.58±0.1	2.11±0.1	1.02± 0.04	1.19± 0.07	1.77± 0.05	2.08± 0.06	1.14± 0.06	1.10± 0.03	1.01±0.07	1.16± 0.01
Hardness (MPa)	60±1	77±1	83±2	85±2	54±2	58±1	65	86±1	62±2	62±3	63±1	61±1
Wear Rate[b] (mm^3/cycle) X10^{-6}	2.9±0.3	3.6±0.3	5.1±0.3	29.7± 0.9	4.5± 0.09	5.6±0.5	24.7± 0.1	27.6± 0.5	3.5± 0.08	3.3± 0.2	3.3± 0.3	3.6± 0.2
Wear Rate[c] (mm^3/cycle) X10^{-8}	2.5±0.9	-	4.5±0.4	-	2.9±0.2	-	9.1±0.6	-	-	-	-	-

b: Six hours wear results for unirradiated block samples under 30 N
c: Seventy-two hours wear results for unirradiated block samples under 2 N

Die approbierte gedruckte Originalversion dieser Dissertation ist an der TU Wien Bibliothek verfügbar.
The approved original version of this doctoral thesis is available in print at TU Wien Bibliothek.

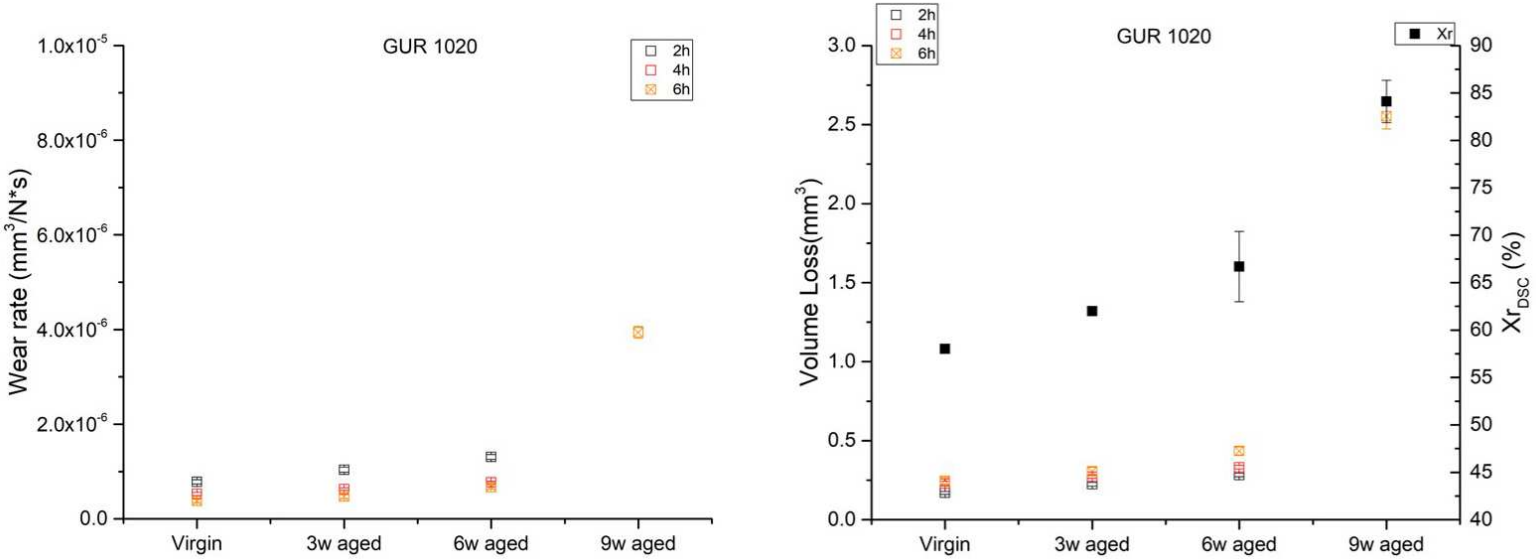

Figure H4. Progressive wear rate and volume loss for virgin and extended accelerated aged of GUR 1020 unirradiated block samples under 30 N

Die approbierte gedruckte Originalversion dieser Dissertation ist an der TU Wien Bibliothek verfügbar.
The approved original version of this doctoral thesis is available in print at TU Wien Bibliothek.

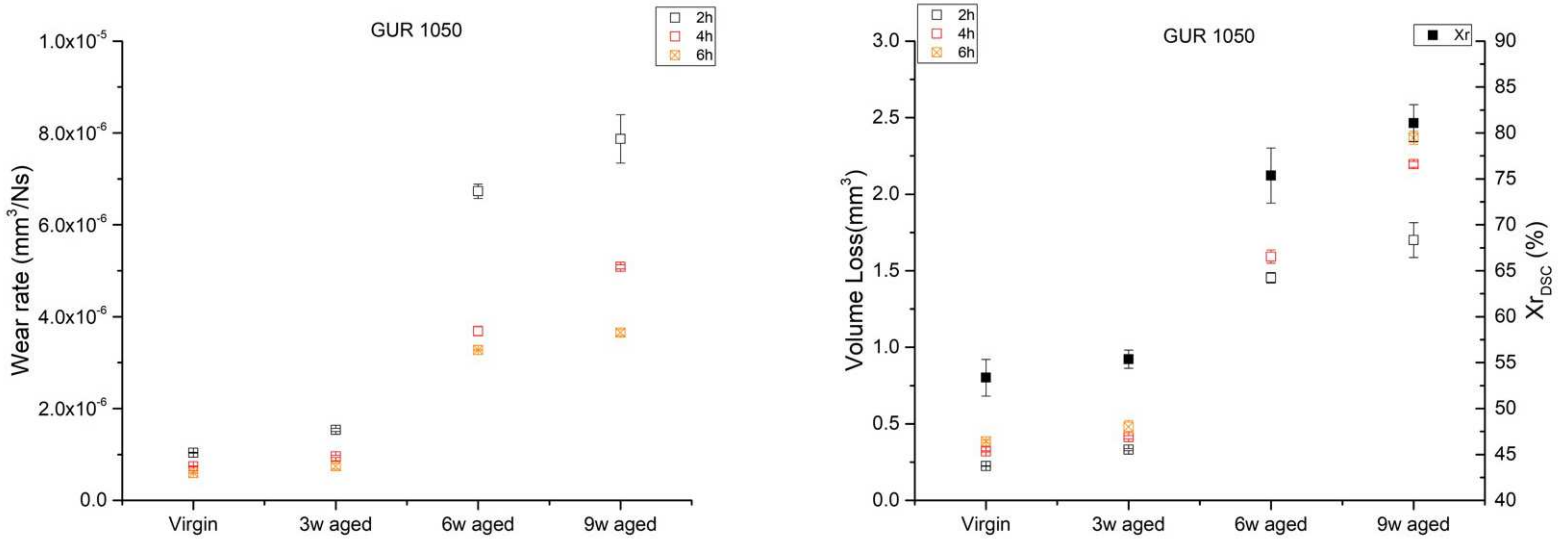

Figure H5. Progressive wear rate and volume loss for virgin and extended accelerated aged of GUR 1050 unirradiated block samples under 30 N

Die approbierte gedruckte Originalversion dieser Dissertation ist an der TU Wien Bibliothek verfügbar.
The approved original version of this doctoral thesis is available in print at TU Wien Bibliothek.

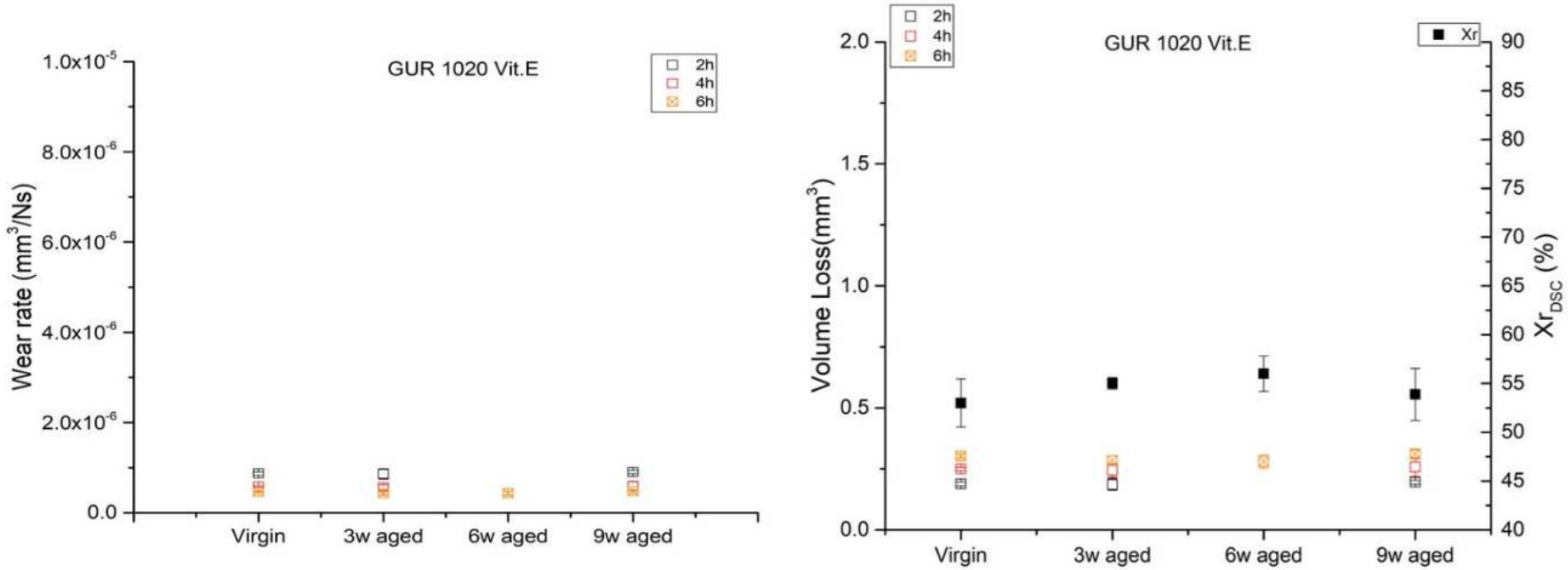

Figure H6. Progressive wear rate and volume loss for virgin and extended accelerated aged of GUR 1020 Vit.E unirradiated block samples under 30 N

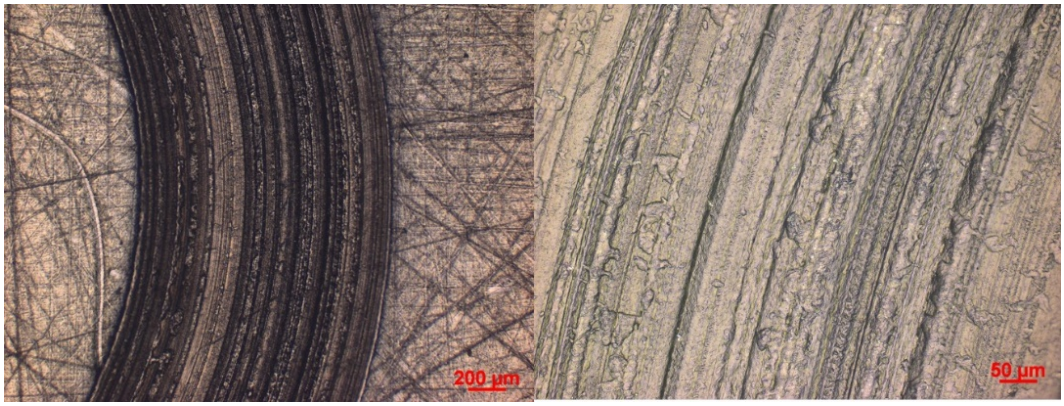

Figure H7. Wear tracks (from 6 hours measurements) for virgin GUR 1020 Vit. E with using 30N

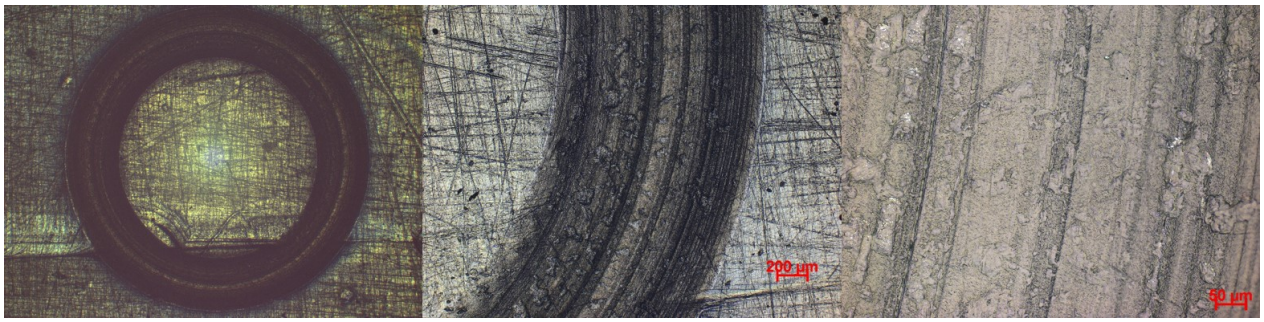

Figure H8. Wear tracks (from 6 hours measurements) for 3 weeks aged GUR 1020 Vit. E unirradiated block samples with using 30 N

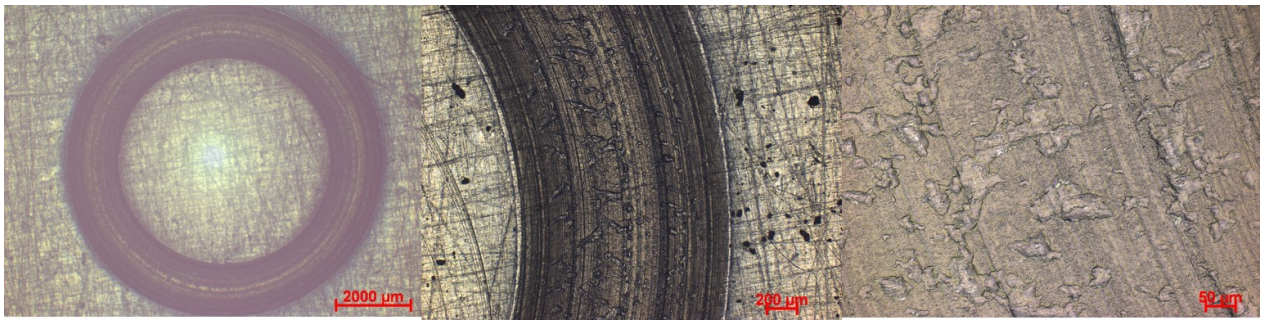

Figure H9. Wear tracks (from 6 hours measurements) for 6 weeks aged GUR 1020 Vit. E unirradiated block samples with using 30 N

Die approbierte gedruckte Originalversion dieser Dissertation ist an der TU Wien Bibliothek verfügbar.
The approved original version of this doctoral thesis is available in print at TU Wien Bibliothek.
TU Bibliothek Your knowledge hub WIEN

Figure H10. Wear tracks (from 6 hours measurements) for 9 weeks aged GUR 1020 Vit. E unirradiated block samples with using 30 N

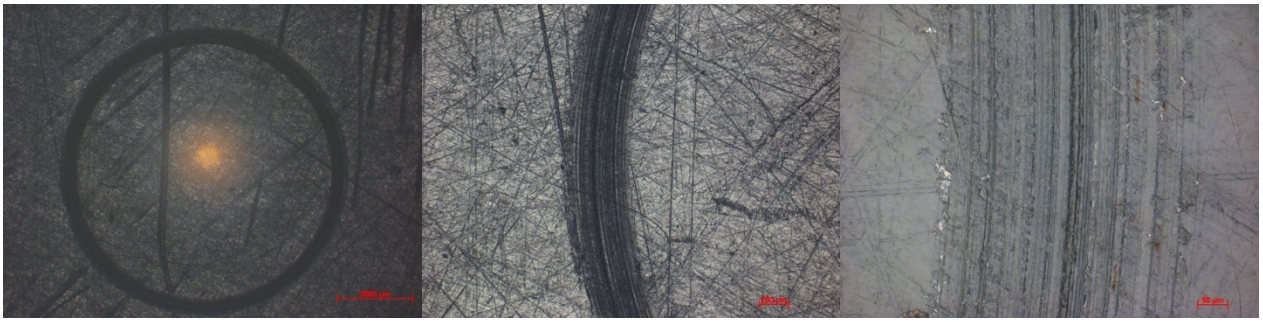

Figure H11. Wear tracks (from 72 hours measurements) for virgin GUR 1050 unirradiated block samples with using 2 N

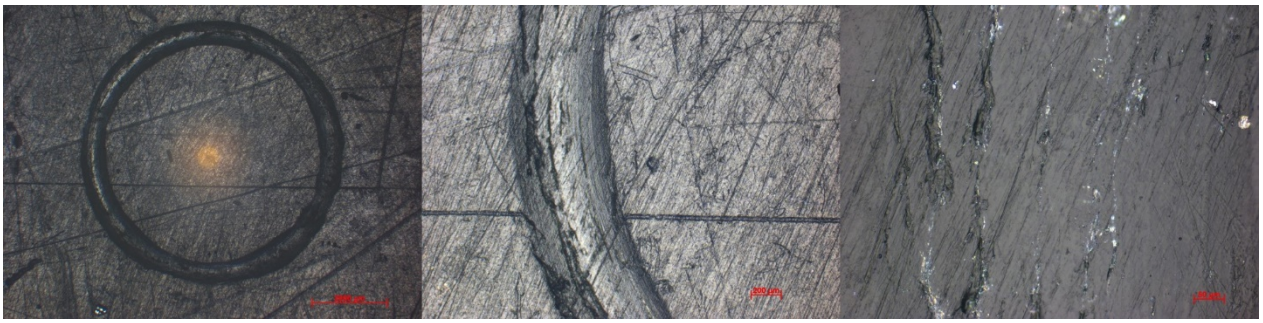

Figure H12. Wear tracks (from 72 hours measurements) for 6 weeks aged GUR 1050 unirradiated block samples with using 2 N

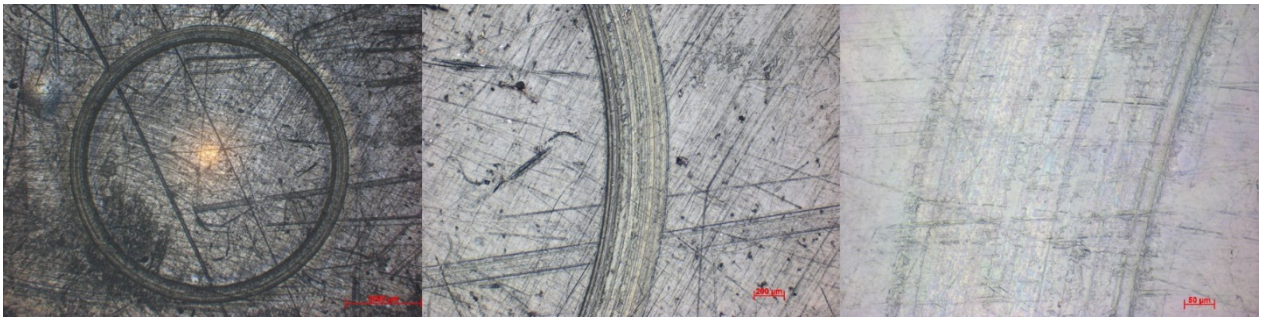

Figure H13. Wear tracks (from 72 hours measurements) for virgin GUR 1020 unirradiated block samples with using 2 N

Die approbierte gedruckte Originalversion dieser Dissertation ist an der TU Wien Bibliothek verfügbar.
The approved original version of this doctoral thesis is available in print at TU Wien Bibliothek.
TU Bibliothek Your knowledge hub WIEN

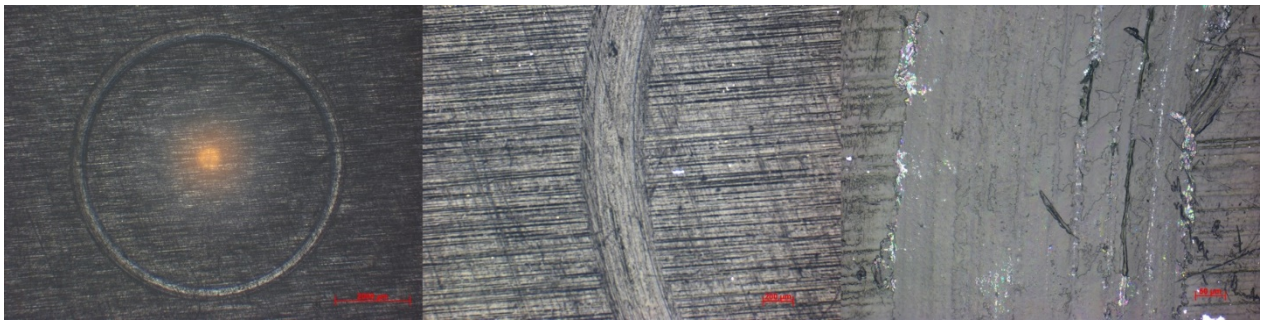

Figure H14. Wear tracks (from 72 hours measurements) for 6 weeks aged GUR 1020 unirradiated block samples with using 2 N

Table H8. Comparison of virgin and extended accelerated aged Dsa/Durasul® and X3™/Stryker explants' morphological and mechanical values

Name	OI	TVI	Hardness (MPa)	E-Modulus (GPa)	Xr (%)
Dsa (virgin)	0.005±0.004	0.053±0.002	40.5±1.7	0.7±15.8	51±1.2
X3 (virgin)	0.047±0.008	0.029±0.002	57.1±1.7	1.074±29.2	60.3±1.4
Dsa (shelf aged)	0.02±0.008	0.054±0.001	41.3±1.56	0.734±0.017	49.6±0.85
X3 (shelf aged)	0.09±0.01	0.028±0.001			62.56±0.76
Dsa 3w aged	0.02±0.003	0.055±0.001	42±1.09	0.729±0.025	49.017±1.93
X3 3w aged	0.23±0.06	0.029±0.002	58.28±1.75	1.04±0.035	66.47±0.23
Dsa 6w aged	0.03±0.01	0.05±0.002	42.25±1.13	0.753±0.034	49.39±2.3
X3 6w aged	1.37±0.32	0.03±0.005	61.64±1.63	1.29±0.062	74.79±2.22

Virgin data (in red color) were taken from: Markut-Kohl. R. (2012). Structure-properties correlations in PE-UHMW: influence of consolidation. crosslinking. sterilization. and in-vivo use on hip implants (PhD/TU Wien).

Die approbierte gedruckte Originalversion dieser Dissertation ist an der TU Wien Bibliothek verfügbar.
The approved original version of this doctoral thesis is available in print at TU Wien Bibliothek.
TU Bibliothek Your knowledge hub WIEN

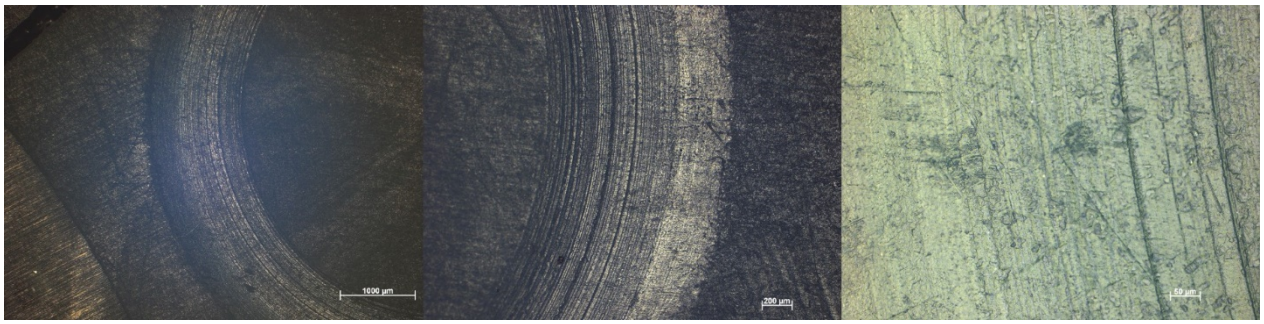

Figure H15. Wear tracks (from 6 hours measurements) for 3 weeks aged X3™ explant samples with using 30 N

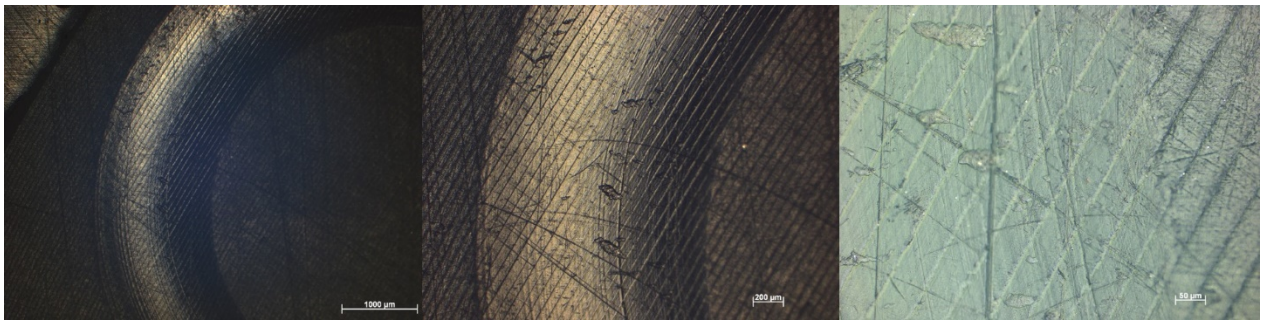

Figure H16. Wear tracks (from 6 hours measurements) for 3 weeks aged Dsa explant samples with using 30 N

Die approbierte gedruckte Originalversion dieser Dissertation ist an der TU Wien Bibliothek verfügbar.
The approved original version of this doctoral thesis is available in print at TU Wien Bibliothek.
TU Bibliothek Your knowledge hub WIEN